UBE3B is a mitochondria-associated E3 ubiquitin ligase whose activity is modulated by its interaction with Calmodulin to respond to oxidative stress

by

Andrea Catherine Braganza

B.S. Biotechnology, Rochester Institute of Technology, 2008

Submitted to the Graduate Faculty of

University of Pittsburgh School of Medicine in partial fulfillment

of the requirements for the degree of

Doctor of Philosophy

University of Pittsburgh

2015

UNIVERSITY OF PITTSBURGH

SCHOOL OF MEDICINE-MOLECULAR PHARMACOLOGY

This dissertation was presented

by

Andrea Catherine Braganza

It was defended on

August 21st, 2015

and approved by

Chairperson: Sruti Shiva, Ph.D., Associate Professor, Department of Pharmacology and Chemical Biology

Bruce Freeman, Ph.D., Professor and Chair, Department of Pharmacology and Chemical Biology

Jing Hu, M.D., Ph.D., Assistant Professor, Department of Pharmacology and Chemical Biology

Jeffrey Brodsky, Ph.D., Professor, Department of Biological Sciences

Sarah Berman, M.D., Ph.D., Assistant Professor, Department of Neurology

Dissertation Advisor: Robert W. Sobol, Ph.D., Associate Professor, Department of Pharmacology and Chemical Biology

UBE3B is a mitochondria-associated E3 ubiquitin ligase whose activity is modulated by its interaction with Calmodulin to respond to oxidative stress

Andrea Catherine Braganza, Ph.D.

University of Pittsburgh, 2015

Recent genome-wide studies found that patients with hypotonia, developmental delay, intellectual disability, congenital anomalies, characteristic facial dysmorphic features, and low cholesterol levels suffer from Kaufman oculocerebrofacial syndrome (also reported as blepharophimosis-ptosis-intellectual disability syndrome). The primary cause of Kaufman oculocerebrofacial syndrome (KOS) is autosomal recessive mutations in the gene UBE3B. However, to date, there are no studies that determine the cellular or enzymatic function of UBE3B. Here we report that UBE3B is a mitochondria-associated protein with HECT E3 ubiquitin ligase activity. Mutating the catalytic cysteine (C1036A) or deleting the entire HECT domain (aa758-1068) results in loss of UBE3B's ubiquitylation activity. Knockdown of UBE3B in human cells results in changes in mitochondrial morphology, a decrease in mitochondria volume and an increase in mitochondrial oxidative stress. We also discovered that UBE3B strongly interacts with calmodulin (CaM) via the N-terminal IQ domain of UBE3B. Deletion of the IQ domain (aa29-58) results in loss of calmodulin binding. We also found that *in vitro* changes in the concentration of calcium resulted in decreased the interaction between UBE3B and CaM. In both these cases we saw an increase in the ubiquitylation activity of UBE3B. These studies are the first to demonstrate that UBE3B is an E3 ubiquitin ligase. Further, the changes in the interaction between UBE3B and calmodulin implicate a role for calcium signaling in mitochondrial protein ubiquitylation and turnover in the cell.

TABLE OF CONTENTS

LIST OF TABLES

LIST OF FIGURES

PREFACE

I have never been one to stop and think about how far I have come and what I have accomplished. I always thought of that as being selfish. So I just went with the motion, because there are always the "What's next?" questions that everyone asked me. But today, as I put the finishing touches to my dissertation, I not only take a step back to appreciate myself, but more importantly, all the people who have helped me get to this point in my life.

Since there are a multitude of people I would like to thank, I am going to use a chronological order. Firstly, I would like to start with my parents, Agnelo and Fatima, because without them, I would not be here writing this acknowledgment. I owe them everything. If it was not for their hard-work and countless sacrifices, I would not have been able to move to USA and pursue my dreams. Letting your Indian teenage daughter move to another country (in a time when Skype did not exist) takes a lot of courage and trust. I thank them for being so open and liberal in their thinking, and not holding onto the notion that a woman's place is in the house. I thank them for sending me to the best schools they could, and always being there for me, even till today. I would also like to thank my brother Floyd. He has always been a great big brother and done everything he could to take care of me. Yes, we did fight, but what siblings didn't? But at the end of it all, he has only wanted the best for me and is still a pillar of strength for me.

Thanks to all my teachers throughout the years. From the ones that supported and developed my talents, to the ones who were hard on me, that only pushed me to do better. I

would like to thank my undergraduate mentor Dr. Dina Newman for giving me my first research experience and answering all my naïve questions. Next, I would like to thank Dr. Nicola Mason for hiring me as her Research Specialist but training me as her graduate student because she knew that was my next step in life.

There are many people in graduate school that have made this journey special. Dr. Robert Sobol has been an exceptional mentor. He started me off with a rotation project that was out of the box for the lab, but was quick to realize its potential and had enough faith in me to let me continue with it as my dissertation project. He has always pushed me to grow, helped me overcome my fear of presenting, and most importantly, taught me to think like a scientist. My thesis committee has been wonderful and instrumental in this journey. Thanks to all of them for keep me on track, while giving me the freedom to test my theories and learn the science. Special thanks to Dr. Bennett Van Houten for allowing me to work in his lab once Dr. Sobol moved, and for being a friend both professional and personally. Thanks to all the members of both the labs who are now not only coworkers but also my friends. They have been vital in my graduate training, keeping the lab atmosphere lively, while helping me build my scientific technique repertoire.

I would like to thank my new family, the Jardini's and Kim Frazier. I thank them for accepting me as one of their own from day one and supporting me through my PhD. Finally, I would like to thank Patrick Jardini, my best friend and my love. Thank you for making every day special and for loving me unconditionally. Thank you for putting up with my stressed ways and showing me that there is a light at the end of the tunnel as I worked on this dissertation. I will never be able to thank you enough for everything you have done for me.

1.0 ABBREVIATIONS

AAA	ATPase associated with diverse cellular activities
Aβ	Amyloid-β
ABAD	Aβ-binding alcohol dehydrogenase
AC-MS	Affinity capture-mass spectrometry
AD	Alzheimer's disease
ALS	Amyotrophic lateral sclerosis
Ank R	Ankyrin repeat
ANKZF1/VMS1	Ankyrin repeat and zinc finger domain containing 1
ANXA7	Annexin 7
apoE	Apolipoprotein E
APP	Amyloid precursor protein
APS	Ammonium persulfate
AS	Angelman Syndrome
ASD	Autism spectrum disorder
A-T	Ataxia-telangiectasia
ATM	Ataxia-telangiectasia mutated
ATP synthase β	Adenosine triphosphate synthase beta
BER	Base-excision repair

BioGRID	The Biological General Repository for Interaction Datasets
BP-ID	Blepharophimosis-Ptosis-Intellectual-Disability syndrome
Ca^{+2}	Calcium
CaM/CALM	Calmodulin
CaMKIV	Ca^{2+}/calmodulin-dependent protein kinase IV
CBI	Center for Biologic Imaging
CC	Coiled-coil region
C.elegans	*Caenorhabditis elegans*
CFTR	Cystic fibrosis transmembrane conductance regulator
COPD	Chronic obstructive pulmonary disease
CUL4B	Cullin 4B
DDR	DNA damage response
Drp1	Dynamin-related protein
DSBs	Double-strand breaks
dsRNA	Double-stranded RNA
DUB	Deubiquitylating enzyme
E1	Ubiquitin-activating enzyme
E2	Ubiquitin-conjugating enzyme
E3	Ubiquitin ligase
E6AP	HPV-E6-associated protein
ENaC	Epithelial sodium channel
ER	Endoplasmic reticulum
ERAD	ER associated degradation

ETC	Electron transport chain
FBS	Fetal bovine serum
Fzo	Fuzzy onion
GAM-HRP	Goat anti-mouse horseradish peroxidase
GAR-HRP	Goat anti-rabbit horseradish peroxidase
GBM	Glioblastoma multiforme
GFP	Green fluorescent protein
GSH	Glutathione
GWAS	Genome-wide association study
H_2O_2	Hydrogen peroxide
HD	Huntington's disease
HECT	Homologous to the E6-AP carboxyl terminus
HKI	Hexokinase I
HPV	Human papilloma virus
HUWE1	HECT, UBA, and WWE domain containing 1 E3 Ubiquitin protein ligase
IBMPFD	Inclusion body myopathy with Paget's disease of bone and frontotemporal dementia
ID	Intellectual disability
IPO4	Importin-4
IQ	Isoleucine-glutamine
IQCB1	IQ motif containing B1
IMM	Inner mitochondrial membrane
IMS	Intermembrane space

JAMM/MPN+	JAB1/MPN/MOV34 metalloenzyme catalytic domain
JBTS	Joubert syndrome
JNK	c-Jun N-terminal kinases
KD	Knocked down or Knockdown
KOS	Kaufman oculocerebrofacial syndrome
LDL	Low density lipoprotein
LigIII	Ligase III
MARCH5	Membrane-associated RING Finger 5
MDM-2	Murine double minute clone 2
Mhtt	Mutant huntingtin
MID1	Midline 1
MKS	Meckel-Gruber syndrome
MM	Mitochondrial matrix
MMP	Mitochondrial membrane potential
MFNs1/2	Mitofusins 1/2
MS	Mass spectrometry
mtBER	Mitochondrial BER
mtDNA	Mitochondrial DNA
miRNA	MicroRNA
MMS	Methyl methanesulfonate
MNNG	*N*′-methyl-*N*′-nitro-*N*-nitrosoguanidine
mPTP	Mitochondrial permeability transition pore
MTS	Mitochondrial targeting sequence

MTS/MTT	3-(4,5-dimethylthiazol-2-yl)-5-(3-carboxymethoxyphenyl)-2-(4-sulfophenyl)-2*H*-tetrazolium
mtSSB	Mitochondrial single-stranded DNA-binding protein
Mulan	Mitochondrial ubiquitin ligase activator of NF-κB
nDNA	Nuclear DNA
NEDD4-2	Neural precursor cell expressed developmentally down-regulated protein 4-2
NES	Nuclear export sequence
NFTs	Neurofibrillary tangles
NHEJ	Nonhomologous end joining
NPHP	Nephronophthisis
NTC	No template control
$O_2^{\cdot -}$	Superoxide
$^1O_2$	Singlet oxygen
O_3	Ozone
$^{\cdot}OH$	Hydroxyl radical
OMM	Outer mitochondrial membrane
OMMAD	OMM associated degradation
OTU	Ovarian tumor
p53	Tumor suppressor cellular tumor antigen p53
PAR	Poly-ADP-ribose
PBS	Phosphate buffered saline
PD	Parkinson’s disease

PINK1	PTEN-induced putative kinase 1
PIRM	Ptosis, Intellectual disability, Retarded growth and Mortality
PKB/Akt	Protein kinase B
Polβ	Polymerase beta
POLRMT	Mitochondrial RNA polymerase
PP2A	Protein serine/threonine phosphatase 2A
PPP2CA	Protein phosphatase 2A, catalytic subunit, alpha isoform
qRT-PCR	Quantitative reverse transcription polymerase chain reaction
RBR	RING-between-RING
RING	Really interesting new gene
RISC	RNA-silencing complex
RNAi	RNA interference
RNF	RING finger
$RO^{\cdot}$	Alkyoxyl radical
$ROO^{\cdot}$	Peroxyl radical
ROS	Reactive oxygen species
RPE	Retinal pigment epithelial
RQ	Relative quantity
scFv	Single chain fragment variable
shRNA	Stable gene knockdown/short hairpin RNA
siRNA	Transient gene knockdown
SNPs	Single-nucleotide polymorphisms
SOD	Superoxide dismutase

SOD2	Manganese superoxide dismutase
SVM	Support Vector Machine
TBT	TBS-Tween 0.3 % buffer
TEMED	*N,N,N′,N′*-Tetramethylethylenediamine
TFAM	Mitochondrial transcription factor A
TFB2M	Mitochondrial transcription factor B2
TMZ	Temozolomide
UBA1	Ubiquitin-like modifier-activating enzyme 1
UBB	Ubiquitin B
UBE3A	Ubiquitin-protein ligase E3A
UBE3B	Ubiquitin-protein ligase E3B
UBE3C	Ubiquitin-protein ligase E3C
U-box	UFD2 homology
UBP	Ubiquitin-specific processing protease
UBR1	Ubiquitin protein ligase E3 component N-Recognin 1
UCH	Ubiquitin C-terminal hydrolases
UFD2	Ubiquitin-fusion degradation 2
UPS	Ubiquitin/proteasome system
USP	Ubiquitin-specific protease
USP5	Ubiquitin carboxyl-terminal hydrolase 5
VCP	Valosin-containing protein
VIM	VCP interacting motif
WCE	Whole cell extracts

WT	Wild type
XPO1	Exportin-1
ZnF	Zinc-finger domain

2.0 INTRODUCTION

2.1 UBIQUITYLATION

In 2004, Aaron Ciechanover, Avram Hershko and Irwin Rose were awarded the Nobel Prize in Chemistry for *"the discovery of ubiquitin-mediated protein degradation"*. This was the first time that the mechanism of protein degradation at the molecular level, as well as its involvement in numerous biological processes, such as activation and deactivation of proteins, subcellular localization, cell cycle control, DNA damage repair, gene transcription and immunity, were revealed (1).

Protein degradation, also referred to as proteolysis, is a major process in the maintenance and perseverance of the cellular structure and function of a cell. It helps to tightly regulate the concentrations of essential proteins within the cell, in addition to enabling the cell to remove damaged and misfolded proteins (2). The main mechanism of proteolysis is through ubiquitylation, wherein, one or more ubiquitin molecules are added to the target protein (3). These targeted proteins are then taken to the 26S proteasome for degradation. This system is known as the ubiquitin/proteasome system (UPS) (4-6).

In the first step of ubiquitylation, the 76-residue, 8.5 kDa ubiquitin protein is adenylated on its C-terminus by the ubiquitin-activating enzyme (E1) using ATP as the energy source (7). This activated ubiquitin is covalently fused via a thioester linkage to a cysteine residue in the E1

(8). This step is crucial for cellular homeostasis because failure to activate ubiquitin, as seen by the chemical inhibition of E1 activity in the cell, results in the almost immediate shutdown of the entire UPS (9). At this point the E1 cannot take the activated ubiquitin straight to the substrate (except for the case of non-ribosomal polypeptide synthesis) (10). Therefore, ubiquitin is transferred from the E1 onto a cysteine residue of an ubiquitin-conjugating enzyme (E2), and then to a lysine residue on protein targets in concert with an ubiquitin ligase (E3) (11). Ubiquitylation can either be the attachment of a single ubiquitin protein (mono-ubiquitylation) or the attachment of a chain of ubiquitins (poly-ubiquitylation). While there is little diversity in E1 and E2 enzymes, the human genome contains >1,000 annotated ubiquitin E3 ligases (12,13). In some cases, members of the E4 ligases can add a poly-ubiquitin chain to a mono-ubiquitylated site. For example, p300 carries out this function on a site monoubiquitylated by Mdm2 on p53 (14). It is, however, the E3 ligases that specify the timing and substrate selection of ubiquitylation reactions (12,13,15-17). E3 ligases only share a few conserved motifs and are, therefore, very specific (18). E3 ligases contain a RING (Really interesting new gene), a HECT (Homologous to the E6-AP Carboxyl Terminus), or an Ubiquitin-Fusion Degradation 2 (UFD2) homology (U-box) domain, which catalyzes covalent addition of ubiquitin to the substrate (19). The process of ubiquitylation has been summarized in **Figure 1**. Therefore, ubiquitin ligases are key regulatory determinants in the ubiquitylation reaction.

Whether a substrate is mono-ubiquitylated or poly-ubiquitylated, the ubiquitylation bonds are always formed with one of the seven lysine residues from the ubiquitin molecule. These 'linking' lysines are represented by a "K" (which is the one-letter amino acid notation of lysine) and a number, referring to its position in the ubiquitin molecule. First, an ubiquitin molecule is bonded by its C-terminus to a specific lysine residue (e.g. K48, K29, K63, etc.) on the target

protein. Poly-ubiquitylation occurs when the C-terminus of another ubiquitin, will be linked again to a lysine residue (for example again K48 or K29) on the previously added U ubiquitin molecule, forming a chain. This process repeats several times, leading to the addition of several ubiquitins (20).

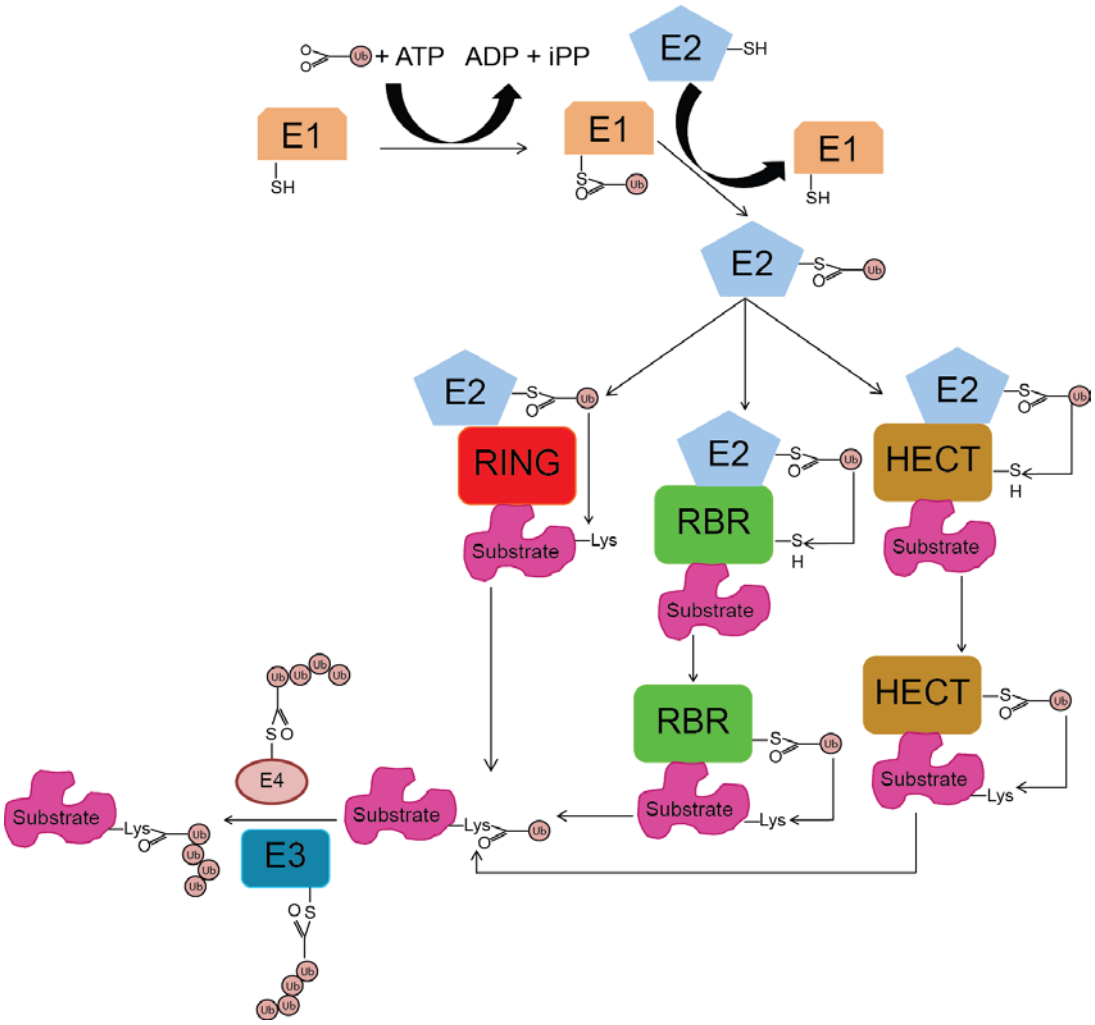

Figure 1. Model of Ubiquitylation.

Ubiquitylation is a post translation modification (PTM) that is mainly associated with protein degradation by the proteasome. It occurs in three steps and involves the protein ubiquitin, ATP, the ubiquitin activating enzyme (E1), an ubiquitin conjugating enzyme (E2), an ubiquitin ligase (E3) and a substrate. In the first step ubiquitin is activated by the E1 using ATP and attached to the active site cysteine on E1. In the next step, ubiquitin is transferred from the E1 to the active site cysteine on an E2 via a trans(thio)esterification reaction. In the final step the E3 binds to the

substrate and the E2-ubiquitin to facilitate the transfer of the ubiquitin to a lysine on the substrate, either directly (as in the case of RING E3 ligases) or through an intermediate self-ubiquitylation step (as in the case of HECT and RBR E3 ligases). The substrate can either be mono-ubiquitylated or poly-ubiquitylated depending on the signal. Sometimes there is a fourth step where an E4 can add an already assembled poly-ubiquitin chain to a mono-ubiquitylated substrate.

As mentioned before, not all ubiquitin-labeled proteins are degraded by the proteasome. Mono-ubiquitylation (or specific cases of poly-ubiquitylation) and different chain linkage types can alter the fate of a protein in a less terminal fashion, by potentially affecting its function, trafficking in multiple pathways or its degradation through lysosomes (21-24). For example, even though sometimes a single K29 or K48-linked poly-ubiquitin (tetra-ubiquitin) chain is sufficient to target a substrate to 26S proteasomes for destruction and recycling (referred to as the “molecular kiss of death”), K63, K11 and K6-linked poly-ubiquitin chains on target proteins are involved in DNA damage tolerance, kinase activation, trafficking, non-proteolytic translation and inflammation (20,24-27). Of all the known lysine linkages, K48-linked chains are the most studied.

The ubiquitylation process is also reversible by deubiquitylating enzymes (DUBs) that catalyze the removal of ubiquitin moieties from proteins as well as disassemble ubiquitin chains to replenish the pool of intracellular ubiquitin (28,29). Deubiquitylation is an important process because it can cancel ubiquitylation signals, serve as a quality control for regulating ubiquitylation, and remove ubiquitin chains from substrate proteins prior to degradation by the proteasome (28). Five subclasses of DUBs have been described with the largest and most diverse being the USP (ubiquitin-specific protease) or UBP (ubiquitin-specific processing protease) subclass (from now on referred to as USP). USPs contain two highly conserved short motifs,

termed the Cys and His boxes, which encompass key catalytic residues. USPs are believed to target specific protein substrates. Ubiquitin C-terminal hydrolases (UCH) constitute the second class of DUBs and are believed generally to function nonspecifically in the cleavage of free ubiquitin chains. Finally, recent studies have identified the ovarian tumor (OTU), Josephin, and JAB1/MPN/MOV34 metalloenzyme catalytic domain (JAMM/MPN+) as three additional families of deubiquitinating enzymes (28-30).

Ubiquitylation plays a critical role in a number of diseases such as Cystic Fibrosis. Ubiquitylation is responsible for the degradation of the mis-folded Cystic fibrosis transmembrane conductance regulator (CFTR) chloride ion channel. In Liddle's syndrome, a mutation in the catalytic HECT domain of the E3 ligase neural precursor cell expressed developmentally down-regulated protein 4-2 (NEDD4-2) prevents the efficient ubiquitin-mediated degradation of the epithelial sodium channel (ENaC), leading to hypertension through excessive sodium and water re-absorption (31-33). In certain cancers, oncogenic targets such as the oncogene c-Myc are mutated so that they are no longer subject to ubiquitylation, and therefore escape degradation and promote cell growth (34). The human papilloma virus (HPV), responsible for certain forms of cervical cancer, relies on its own viral E6 protein to promote ubiquitin-mediated degradation of the tumor suppressor cellular tumor antigen p53 (p53) (35). Other cancers may promote the over-expression of E3 ligases such as Murine Double Minute Clone 2 (MDM-2) leading to inactivation and enhanced degradation of p53 (36,37).

There are still many unresolved questions in the field of ubiquitylation. For example, a majority of the E3 ligases have yet to be characterized, with an even larger number of substrates that have not been defined. Therefore, identifying theses E3s and their substrates as targets for human therapy and cancer treatments make for promising drug discoveries.

2.2 REACTIVE OXYGEN SPECIES (ROS) IN THE MITOCHONDRIA

The human genome is constantly damaged by genotoxins that include endogenous cellular metabolites (such as reactive oxygen species (ROS) and alkylating agents) and exogenous UV light and ionizing radiation. These genetic insults activate oncogenes, inactivate tumor suppressors and change the level or function of 'modifier' proteins, which when left unrepaired can potentially increase an organism's susceptibility to cancer, organ dysfunction, neuro-degeneration and a myriad of other diseases (38,39).

Besides converting energy substrates into ATP, the mitochondria have been found to be very dynamic organelles. Recent advance in imaging technologies have revealed that the mitochondria move rapidly within and between subcellular compartments, undergo rapid fission and fusion, and accumulate damage to their DNA (mtDNA) as they age (40-42). They also respond to changes in electrical activity and growth factor receptors, function as signaling outposts that contain kinases, deacetylases and other signal transduction enzymes, signal apoptosis, and participate in ROS metabolism (43-46).

ROS are natural byproducts of normal metabolism and include superoxide ($O_2^{\bullet -}$), hydrogen peroxide (H_2O_2), hydroxyl radical ($^{\bullet}OH$), peroxyl radical ($ROO^{\bullet}$), alkoxyl radical ($RO^{\bullet}$), ozone (O_3), and singlet oxygen ($^1O_2$) (47). The majority of ROS are generated from complex I (NADH dehydrogenase) and complex III (ubiquinone-cytochrome *c* reductase) of the electron transport chain (ETC) in the mitochondria (47-49). The majority of electrons that enter the ETC are accepted by oxygen to form water in a process that does not yield free radicals (47). However, under basal conditions, 1-3% of electrons escape from respiratory complexes distal to cytochrome *c* oxidase (complex IV) as a side-product of oxidative respiration, and in turn reduce mitochondrial oxygen to produce $O_2^{\bullet -}$ (47,50). For a long time, it was thought that ROS were

exclusively toxic molecules that caused harm and damage to the cells. However, it is now known that low levels of some ROS species have signaling roles and are in fact essential for cell survival (51). Under normal physiological conditions a number of protective mechanisms, which include the amino acid cysteine or the enzymes thioredoxin, glutathione (GSH), catalase and superoxide dismutases (SODs) scavenge ROS and keep the oxidative damage to a minimum (52,53). However ROS can increase dramatically during times of high environmental and metabolic stress, overcome protective mechanisms, and cause a plethora of detrimental effects in the cell. This includes significant damage to cellular organelles, particularly the macromolecules such as lipids, DNA and proteins, as well the progression of pathologies such as ischemia/reperfusion injury and sepsis (54-56). The 'mitochondrial free radical theory of aging' suggests that these oxidatively damaged proteins may become inactivated, lose their proper tertiary structure and potentially form toxic aggregates within the organelle, leading to mitochondrial dysfunction which has been linked with age-related neurological degenerative diseases such as Alzheimer's and Parkinson's disease, among other aliments (57-61). This theory is supported by the inverse correlation between mitochondrial ROS production and lifespan in mammals, and the protective effects of mitochondrially-targeted catalase against cancer, cardiac diseases and insulin resistance in mice (62,63). Unfortunately ROS are not the only aspects of dysfunctional mitochondria. Mutations in mitochondrial DNA (mtDNA), ATP shortage, activation of mitochondrial permeability transition, loss of MMP, altered fusion/fission dynamics, calcium (Ca^{2+}) deregulation, inflammation, and mitochondrial autophagy are all disrupted in many diseases (50,64). Hence understanding the functions of quality control processes to eliminate the damaged mitochondria are critical.

2.3 MITOCHONDRIAL DISEASES

The mitochondria are dynamic organelles that can move along the cytoskeleton, change morphology through fission and fusion events and supply the cell with energy by oxidative phosphorylation, amongst its other important functions. As seen in **Figure 2**, mitochondrial quality control is tightly regulated and involves a large number of players that help with repair or clearance of damaged proteins. Current research suggests that mitochondrial dysfunction plays a key role in a large number of neurodegenerative and age-related diseases such as Alzheimer's disease (AD), Parkinson's disease (PD), intestinal barrier dysfunction, depression, chronic obstructive pulmonary disease (COPD), diabetes, and cancer (65-71). Here I review a few diseases that result from defects in the mitochondria.

In humans, the mitochondria has a circular genome (mtDNA), contains approximately 16,600 base pairs and codes for 37 genes (72). In most species the mtDNA is solely inherited from the mother (73). A vast majority of the proteins present in the mitochondria are coded for by nuclear genes. Those imported into the inner compartments of the mitochondria, that is, inside the outer mitochondrial membrane (OMM), contain a mitochondrial targeting sequence (MTS) (74,75). mtDNA is known to be preferentially damaged (before nuclear DNA) by cellular oxidative stress, especially mitochondrial ROS (76). One key repair gene that is activated by DNA double-strand breaks (DSBs) and oxidative stress is Ataxia telangiectasia mutated (ATM) (77). ATM has been linked to the regulation of mtDNA copy number and mitophagy (78-80). Deficiencies in ATM results in the downregulation of the only DNA ligase in the mitochondria ligase III (ligIII), and lowered mitochondrial base excision repair (mtBER) capacity (81,82). Patients with defects in ATM suffer from an autosomal recessive disease known as ataxia-

telangiectasia (A-T), and are predisposed to cancer, insulin resistance and neurodegeneration (83).

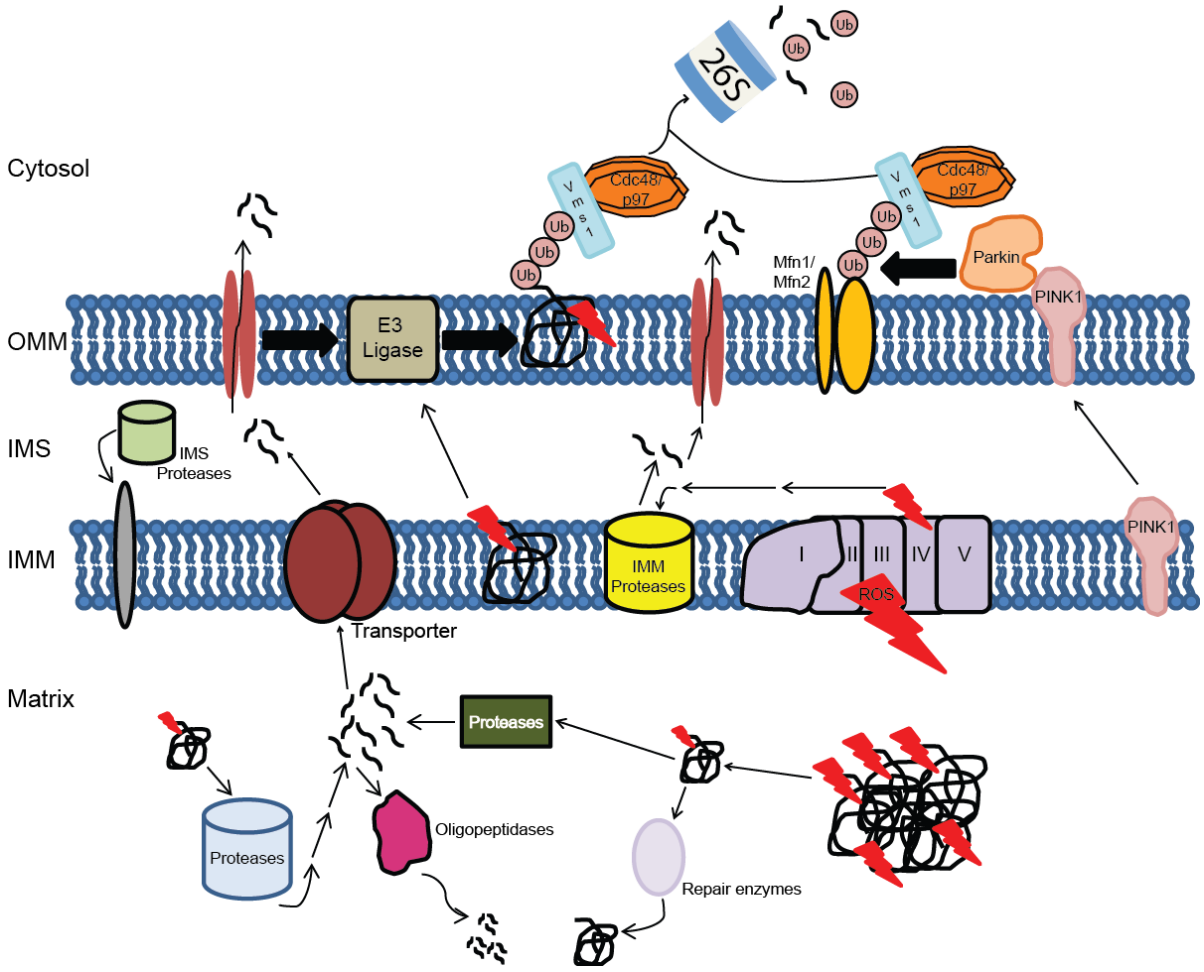

Figure 2. Schematic of mitochondrial quality control pathways.

The mitochondria are divided into two compartments, the intermembrane space (IMS) and the matrix. The outer mitochondrial membrane (OMM) separates the IMS from the cytosol, while the inner mitochondrial membrane (IMM) divides the IMS from the matrix. There are numerous quality control mechanisms in place in, and around the mitochondria to repair and degrade damaged proteins. In the matrix, the mitochondrial matrix repair enzymes, proteases and peptidases control the repair, refolding and degradation of damaged proteins (symbolized by the lightning bolt in the protein chain). Proteins are also damaged by reactive oxygen species (ROS) that are generated from the electron transport chain (ETC) that resides in the IMM. Proteases in the IMM and the IMS process and degrade the proteins in the IMM. The nuclear transcribed kinase PINK1 is imported from the cytosol through the OMM to the IMM under normal conditions. However, when there is a drop in mitochondrial membrane potential,

PINK1 gets stuck on the OMM where it recruits the cytosolic E3 ligase Parkin and participates (with other OMM E3 ligases) in mitochondrial associated degradation (MAD) of proteins by the proteasome. These proteins might retro-translocate to the OMM from different mitochondrial sub-compartments. This figure is modified from (84).

Low-density lipoprotein (LDL) is one of the five major groups of lipoproteins that deliver cholesterol to cells throughout the body via the bloodstream. However when the LDLs leave the vasculature and invade the endothelium, they can be exposed to endothelial cell mitochondrial ROS and become oxidized to form ox-LDL (85,86). In diets high in fat and cholesterol, ox-LDL can accumulate in the arterial wall to induce endothelial dysfunction by impairing the bioactivity of endothelial nitric oxide, promoting leukocyte adhesion, inflammation, thrombosis and smooth muscle cell proliferation to lead to a disease known as atherosclerosis (50,87). The mtDNA in aortic samples from patients suffering from atherosclerosis had greater damage than age-matched non-atherosclerotic aortic samples (88). In murine models there was a correlation between mtDNA damage and the extent of atherosclerotic lesions in apolipoprotein E (apoE) knockout mice, as well as manganese superoxide dismutase (SOD2) deficiency that resulted in mitochondrial dysfunction in apoE knockout mice (87). These results support the notion that an increase in mitochondrial ROS and mtDNA damage is a precursor to the development of atherosclerosis.

A highly studied mitochondrial maintenance pathway is that of the mitochondrial kinase PTEN-induced putative kinase 1 (PINK1) and the cytosolic E3 ubiquitin ligase Parkin, where mutations in both have been found to be associated with early-onset PD (89-93). Under normal cellular conditions, PINK1 is imported into the mitochondria, cleaved by mitochondrial proteases and degraded, while Parkin is in the cytosol in an auto-inhibited state (94-96). When the MMP is depolarized the import of PINK1 is blocked on the outer mitochondrial membrane

(OMM), which leaves its kinase domain facing the cytosol, and triggers the recruitment of Parkin to the mitochondria (97-99). How PINK1 recruits Parkin to the mitochondria is a very complex process with several different proposed mechanisms. In one mechanism, PINK1 can autophosphorylate itself, and directly and indirectly trigger Parkin phosphorylation, which can activate its E3 ligase activity (100-102). Another mechanism suggests that PINK1 transiently recruits Parkin to the mitochondria, which then catalyzes K63-linked ubiquitin chain formation on mitochondrial proteins; which in turn serve as secondary docking sites for activated Parkin proteins and synthesis of additional K63 chains, thus amplifying the signal (103,104). Recently a novel mechanism of Parkin activation involving phosphorylated ubiquitin was identified (105-107). Here, PINK1 phosphorylates ubiquitin at Ser65 and the phosphorylated ubiquitin then interacts with phosphorylated Parkin, thus releasing the E3 ligase's auto-inhibition, allowing Parkin to perform its ubiquitylation function. Since Parkin plays a major role in PD, it is vital that its molecular mechanism in mitochondrial dysfunction is completely understood.

AD is characterized by extracellular amyloid-β (Aβ) aggregates as well as intracellular neurofibrillary tangles (NFTs) consisting of hyperphosphorylated tau protein (50). The amyloid precursor protein (APP) has both an endoplasmic reticulum (ER) signal as well as a MTS (50). In disease conditions, APP is overexpressed and directed to the mitochondria where it can get stuck in the mitochondrial double membrane (108). Here it is cleaved by mitochondrial γ-secretases at the OMM and the mitochondrial protease Omi in the intermembrane space (IMS) and cleared from the mitochondria (109,110). However when Aβ is imported into the mitochondria it complexes heme groups to affect ETC function and inhibits Aβ-binding alcohol dehydrogenase (ABAD), resulting in increased ROS, mitochondria swelling and apoptosis (111-114). In patients with AD the mitochondria are very fragmented (possibly due to increased

fission), the function of various mitochondrial enzymes are impaired, there is an accumulation of oxidation products, and there is a change in the antioxidant levels in brain and fluid samples (113,115-117).

In Huntington's disease (HD) there is an expansion of a trinucleotide repeat in the *Huntingtin* gene leading to the accumulation of mutant huntingtin (mhtt) and formation of inclusions in the striatum (66). Defects in complexes I and II, lowered membrane potential, reduced aconitase activity, abnormal depolarization, and altered structure and number indicate a role of the mitochondria in HD (66,117). Mhtt activates the mitochondrial fission protein dynamin related protein-1 (Drp1), leading to mitochondrial fragmentation (118). This fragmentation results in reduced Ca^{+2}-buffering capacity, changes in Ca^{+2} transport and a decreased Ca^{+2} threshold for the mitochondrial permeability transition pore (mPTP) opening (119,120). In neuronal cells, mhtt aggregates physically block the transit of mitochondria along neuronal processes (121). All these changes result in a decrease in the number of functional mitochondria that may contribute to the neurodegeneration in HD patients.

Mitochondrial Ubiquitin Ligase Activator of NF-κB (Mulan) is a mitochondrial E3 ligase that was previously identified as an activator of NF-κB and is anchored to the OMM through two transmembrane domains such that the RING Finger (RNF) domain is in the cytosol where it can access the UPS components (122,123). The mitochondrial localization signal, as well as the RNF domain, is required for Mulan to function (124). Mulan is important in the regulation of mitochondria trafficking, with changes in Mulan levels leading to altered mitochondrial distribution (123). In addition to its interaction with NF-κB, Mulan also regulates cell growth, apoptosis and mitophagy through c-Jun N-terminal kinases (JNK), p53, protein kinase B (PKB/Akt) and Mitofusin 2 (Mfn2) (123-127). As a substrate, Mulan has been shown to be

regulated by the mitochondrial protease Omi/HtrA2, where inactivation of Omi/HtrA2 results in the accumulation of Mulan and an increase in mitophagy, which in turn could be responsible for the motor neuron disease and premature aging phenotype observed in mice (128).

As seen above, mutations in mitochondrial proteins and any damage that is not repaired can have serious consequences for the organelle and the organism as a whole. Therefore understanding the molecular mechanisms that result in mitochondrial dysfunction is critical in finding a cure to these debilitating diseases.

2.4 CALMODULIN AND CALCIUM SIGNALING

Survival of an organism depends on the communication between and among its cells. This occurs either through direct contact or through signals delivered in the form of electrical impulses or chemical messengers. At the end of a chemical signal is a receiver, usually a protein that senses the arrival of the messenger, interprets the message and regulates the particular downstream activity (129). One such messenger protein is Calmodulin (CaM), a calcium-modulated protein.

In 1883, a British physiologist, Sydney Ringer, first noticed the importance of calcium (Ca^{+2}) ions as a cell regulator in cardiac muscle contraction, and in the 1950's, L.V. Heilbrunn showed that muscle fibers contracted after injection with Ca^{+2} (129). Ca^{+2} ions are now known to affect almost all aspects of cellular physiology, ranging from endocytosis and exocytosis, neurotransmission, cell motility, cell division and chromosome movement, with many of these Ca^{+2}-regulated processes mediated through CaM (130,131).

CaM is the fourth member of the Ca^{+2}-binding protein family, with the other three being parvalbumin, intestinal Ca^{+2}-binding protein and troponin-C (132-135). CaM consists of a single polypeptide with 148 amino acids, has a molecular weight of 16.7 kiloDaltons (kDa), and is highly conserved amongst all vertebrates (136). It is believed that this high degree of amino acid conservation is essential to maintain the interaction of CaM with the diverse family of CaM binding proteins (137). CaM can bind to a target in one of two ways, either in a calcium-bound (holoCaM) or calcium-free (apoCaM) form, and therefore making its interaction with partners either Ca^{+2}-dependent or Ca^{+2}-independent (138). The CaM binding regions of CaM target proteins do not have strong sequence homology. However, there is some conservation between these regions in that they are often found within or near a pseudosubstrate domain, serine/threonine phosphorylation sites, and regions responsible for interaction with other proteins (138). This sequence diversity could contribute to the multiple functions of the CaM receiver proteins. There are three classes of CaM binding motifs that are used to identify CaM binding regions. The first class was initially described in neuromodulin and unconventional myosins and is known as the IQ motif (139). It is ~20-25 amino acids in length, with the core fitting the consensus IQ*XXX*RG*XXX*R (where *X* is any amino acid), and is usually arranged as an amphiphilic α-helical conformation (137,139-141). Frequently these motifs appear in tandem and can bind multiple CaM molecules with the highest affinity in the absence of Ca^{+2} (142). In the case of IQGAP1, CaM can bind to its IQ region both in the presence and absence of Ca^{+2} (143,144). Interestingly, the length of the linker in repeated IQ motif containing proteins is similar between each IQ motif, which suggests the possibility that the linkers might have functions other than just serving as a connection between the different IQ motifs (145). The second and third classes of CaM binding motifs are closely related and are responsible for Ca^{+2}-

dependent binding. They are known as 1-8-14 and 1-5-10 based on the conserved hydrophobic residues within these motifs (138).

CaM is a very stable and abundant molecule that is able to retain its biological activity after exposure to rough laboratory treatment. Because of this it can easily be prepared in its pure form and studied extensively (146). CaM has four calcium-binding domains and in the absence of Ca^{+2} ions it is in its inactive form. The affinity for Ca^{+2} is in the physiological range of micromolar concentration, therefore when the intracellular Ca^{+2} concentration is increased in response to an appropriate stimulus, CaM binds Ca^{+2} ions and assumes a more helical, active conformation (131). From structure-function relationship studies, it has been found that the biological activity of CaM depends greatly on the integrity of the entire molecule. Therefore, a single mutation that results in a gross change of the primary structure of CaM may be lethal to the cell (130). The low 4.3 isoelectric point of CaM is due to the large number (~30%) of its amino acids consisting of acidic aspartate and glutamate residues. CaM contains seven helices, consisting of residues 7-19, 29-39, 46-55, 65-92, 102-112, 119-128 and 138-148 (146). The four Ca^{+2}-binding domains contain 12 amino acids each; with the 1^{st} domain consisting of amino acids 20-31, the 2^{nd} amino acids 56-67, the 3^{rd} amino acids 93-104 and finally the 4^{th} amino acids 129-140 (131). They all have a typical helix-loop-helix conformation, with one major difference in domains 2 and 3; these two domains share the long helix four. Helix four provides the carboxy-terminal helix for domain 2 and the amino-terminal helix for domain 3 and is two to three times longer than any of the other helices in the molecule (146).

The mitochondria are thought to act as a Ca^{+2} buffering organelle to reduce to Ca^{+2} concentrations (147,148). For example, when neuroblastoma cells are induced to differentiate into neuron-like cells, there is an increase in mitochondrial fusion and intra-mitochondrial Ca^{+2}

levels suggesting a link between mitochondria Ca^{+2} handling and neurogenesis (149). Therefore, understanding the molecular mechanisms underlying CaM-dependent systems may lead to the identification of new strategies for therapeutic intervention.

2.5 UBE3B

E3 ubiquitin ligases catalyze the final step in the ubiquitylation reaction where they act as both the molecular matchmaker and the catalyst to specify both timing and substrate selection in the pathway (150). There are more than 1000 known E3 ligases, with 95% of these belonging to the RING family (123). Besides the three E3 ligase families of proteins mentioned before, there is another more recently discovered family known as the RING-between-RING (RBR) family. The RING ligases catalyze the direct transfer of ubiquitin from the E2 to the substrate (150,151). Conversely, the HECT and RBR E3 ligases covalently transfer the ubiquitin from the E2 to itself. The catalytic cysteine on the E3 ligase serves as the site of attachment for a thioester-linked poly-ubiquitin chain, which then is transferred to the substrate (12,152-154). The HECT domain is approximately 350 amino acids in length and is always found at the carboxyl-terminal end of HECT E3 proteins (155). Several studies have shown a critical role of a number of E3 ligases such as, Ubiquitin-protein ligase E3A (UBE3A), Ubiquitin-protein ligase E3B (UBE3B), HECT, UBA, and WWE domain containing 1 E3 Ubiquitin protein ligase (HUWE1), Midline 1 (MID1), Cullin 4B (CUL4B), and Ubiquitin protein ligase E3 component N-Recognin 1(UBR1) in spatial and temporal control of protein turnover in the nervous system. Defects in these proteins results in development, maintenance and regulation anomalies of specialized neuronal structures and neuronal transmission (156-167).

HPV-E6-associated protein (E6AP) (also known as UBE3A) is encoded by the UBE3A gene locus and is the prototype for the HECT E3 ligase family. It is a cytosolic E3 ligase that is best known for the degradation of p53 in papillomavirus infected human cells (168). When UBE3A is mutated in humans it leads to defects in the overall proteasome function of the cell and manifests as a neurodevelopmental disorder known as Angelman syndrome (AS), characterized by motor dysfunction, severe intellectual disability, speech impairment, seizures, hyperactivity and autism spectrum disorder (ASD) (164,169-172). Because of the overlap of AS symptoms with other neurodevelopmental disorders, the progress made towards understanding and treating AS will be broadly applicable.

Another HECT E3 ligase, the ubiquitin-protein ligase 3C (UBE3C, also known as KIAA10 or RAUL) has been implicated in the ubiquitin-proteasome pathway where it regulates physiological and cancer-related processes (173-175). UBE3C is overexpressed in glioma tissues (particularly glioblastoma multiforme; GBM) where it ubiquitylates and degrades the tumor suppressor gene annexin A7 (ANXA7) resulting in the progression of glioma, poor overall survival and early tumor recurrence (176). Inhibition of UBE3C results in a significant decrease in cell migration and invasion *in vitro* (176), therefore it might be a promising therapeutic target for glioma treatment.

E3 enzymes, namely membrane-associated RING Finger 5 (MARCH5/MITOL) (177,178), Mulan/MAPL (179), RNF144B/IBRDC2 (180), RNF185 (181) and Parkin (182) were found to localize to the OMM. Furthermore, ubiquitin-dependent protein degradation was shown to modulate mitochondrial morphology and impact mitophagy (177,183-186). In addition, quality control of mitochondria-localized poly-Q, amyotrophic lateral sclerosis associated mSOD1 and S-nitrosylated proteins are performed by the ubiquitin-proteasome system

(187,188). Analogous to the ER, which is quality controlled by ER associated degradation (ERAD), mitochondria might be considered to be under control of OMM-associated degradation (OMMAD) (189,190).

Kaufman oculocerebrofacial syndrome (KOS), also referred to as Blepharophimosis-Ptosis-Intellectual-Disability Syndrome (BP-ID), is an autosomal recessively inherited disorder that is caused by bi-allelic mutations in the UBE3B gene. It is characterized by intellectual disabilities (ID) and developmental delay, hypotonia, microcephaly, structural eye anomalies and other organ malformations, as well as distinctive facial dysmorphic features (191). Following the identification of the genetic variants that cause KOS, 14 patients from eleven unrelated families have been reported (157,159,191,192). A homozygous mutation in UBE3B in monozygotic twins that results in an arginine to cysteine (R922C) substitution was identified in an Autism genome-wide association study (GWAS) (193). In cattle, a mutation that results in an altered UBE3B protein that lacks 40 amino acids (of which 20 are located in the conserved HECT-domain) leads to a bovine phenotype that resembles human KOS and is known as Ptosis, Intellectual disability, Retarded growth and Mortality (PIRM) syndrome (194). However none of these studies have defined a functional role for UBE3B in cellular protein homeostasis nor have these or any studies demonstrated E3 ubiquitin ligase activity for the UBE3B protein.

Damaged mitochondrial proteins need to be removed and replaced with functional counterparts to maintain mitochondrial function and cellular homeostasis. The UPS is suggested to be a major route of mitochondrial protein turnover. Select proteins from the OMM, the IMS, the inner mitochondrial membrane (IMM) and the mitochondrial matrix (MM) have been shown to be ubiquitylated and degraded by the proteasome. In this dissertation, I propose that UBE3B functions to ubiquitylate damaged mitochondrial proteins for proteasomal degradation in

response to oxidative stress induced an increase in cellular Ca^{+2} levels. Given the suggested role of defective UBE3B in KOS, autism and PIRM, defining the mechanism of action of this E3 ligase and its role in the UPS regarding mitochondrial maintenance will have significant impact in this basic biological mechanism of protein turnover and give insight into multiple neurodegenerative conditions.

3.0 AIMS FOR DISSERTATION

AIM 1: To define the role of UBE3B in response to mitochondrial stress

1) To show that UBE3B is an E3 ligase I will determine the catalytic activity of full length UBE3B, UBE3B missing the catalytic domain (UBE3BΔHECT), or the autism mutant (UBE3B (R922C)) using an *in vitro* ubiquitylation assay.
2) To measure the production of ROS species and visualize changes in the intracellular localization of UBE3B (full length and mutants) at different time points +/- ROS producing agents using live cell imaging. I will also perform subcellular fractionation and immunoblots to confirm the fluorescent microscopy data.

In this dissertation, I was able to complete AIM 1.1 but not AIM 1.2. This is because I had unexpected difficulties showing the ubiquitylation activity of wild type UBE3B. I was able to follow a different hypothesis and showed that the problems I faced might have been due to the role CaM plays in regulating UBE3B's function. Herein I find that when CaM is bound to the IQ domain of UBE3B, UBE3B's activity is suppressed.

AIM 2: To determine the effects of mitochondrial stress on the localization and function of ANKZF1

1) To show the recruitment of ANKZF1-GFP to the mitochondria in response to treatment with mitochondrial stress agents using confocal microscopy. I will also perform

subcellular fractionation and immunoblots to confirm the microscopy data. I will also determine the effects of mitochondrial stressors on cell survival in ANKZF1 knockdown cells.

2) I will make deletions in the three main domains of ANKZF1, i.e. the N-terminus, the mitochondrial targeting domain (MTD) and the VCP interacting motif (VIM), and show how these deletions affect (a) the recruitment of ANKZF1 to the mitochondria; and (b) the cell's ability to cope with mitochondrial ROS.

This AIM is detailed in Appendix 1. I was able to show that wild type ANKZF1 is recruited to the mitochondria after inhibition of proteasomal degradation but not stress caused by Oligomycin or H_2O_2. I was not able to work on AIM 2.1 because of the problems I had with AIM 1.

AIM 3: To identify the binding partners of UBE3B and determine if UBE3B and ANKZF1 interact to remove these damaged mitochondrial proteins after ROS production

1) I will identify the mitochondrial proteins that are ubiquitylated by UBE3B using our HA-UBE3B cell line by co-immunoprecipitation followed by mass spectrometry. Immunoblots will be performed to confirm the mass spectrometry results.
2) To show if the interaction between UBE3B and ANKZF1 changes +/- stress, I will measure the levels of both proteins before and after treatment with mitochondrial stressor by co-immunoprecipitation and immunoblot. I will also show that the UBE3B/ANKZF1 interaction is necessary for mitochondrial protein turnover by over-expressing ANKZF1-GFP and knocking down UBE3B (or the reverse) and by measuring the changes in the levels of the mitochondrial proteins identified in sub-aim Aim 3.1.

I was able to identify that CaM binds to the IQ motif of UBE3B and deletion of this motif abolished this interaction. The mass spectrometry results using cells overexpressing HA-UBE3B and HA-UBE3B(C1036A) protein are detailed in Appendix 2. I also utilized a novel approach known as the proximity biotin ligation assay which utilizes Biotin ligase / UBE3B fusions and biotin to "tag" proteins that come within 10µm of the fusion proteins (195). This method was used to confirm the HA-tag mass spectrometry data we obtained. This project is still ongoing. However I was able to confirm the interaction between wild type UBE3B and CaM.

I was not able to start AIM 3.2 because I was not able to complete AIMS 1.2 and 2.2.

4.0 MATERIALS AND METHODS

4.1 CHEMICALS AND REAGENTS

*Trans*IT®-2020 Transfection reagent (Cat# MIR5400) was from Mirus and the siPORT™ *NeoFX*™ Transfection reagent (Cat# AM4511) was from Life Technologies. The siRNA UBE3B-s40200 (Cat# 4390824) was from Ambion. The Silencer® Negative Control siRNA #2 (Cat# AM4613), TaqMan Primer Probe Set for UBE3B (Cat# 4331182) and β-Actin were from Applied Biosystems. OptiMEM, alpha EMEM and phosphate buffered saline (PBS) were from Invitrogen. FuGENE® Transfection Reagent (Cat# E2311) was from Promega. Puromycin was from Clontech Laboratories, and gentamycin was from Irvine Scientific. All the plastic tissue culture supplies were from Corning and Thermo Fisher Scientific. All PCR primers were from Eurofins MWG Operon. DreamTaq DNA Polymerase (Cat# FEREP0703) was from Thermo Fisher Scientific and dNTPs (Cat# 4303442) were from Life Technologies. The *Pfu* Turbo DNA Polymerase (Cat# 600250) and QuickChange II XL site-Directed Mutagenesis kit (Cat# 200521) were from Agilent Technologies. The TOPO® TA Cloning® Kit for Sequencing, with One Shot® TOP10 Chemically Competent *E.coli* (Cat# K4575-40), Gateway® LR Clonase® II Enzyme Mix (Cat# 11791-100) and T4 DNA Ligase (Cat# EL0011) were from Life Technologies. The plasmid p4054 HA-E6AP isoform II (Cat# 8658) was purchased from Addgene. Restriction enzymes *XbaI*, *Bsu36I* and *BamHI* were from New England Biolabs. The

QIAquick PCR Purification Kit (Cat# 28106) and QIAquick Gel Extraction Kit (Cat# 29706) were from QIAGEN. The TALON® Metal Affinity Resin (Cat# 635501) and HisTALON™ Buffer Set (Cat# 635651) were from Clontech. The Amicon Ultra-15 Centrifugal Filter Units (Cat# UFC900324) were from EMD Millipore and the DC Protein Assay Kit II (Cat# 500-0112EDU) was from Bio-Rad. The Anti-6x-His Epitope Tag Ab, Clone HIS.H8 (Cat# MA121315) was from Thermo Fisher Scientific. FLOAT-A-LYZER G2 (Cat# G235051) was from Spectrum Laboratories. The Anti-HA Affinity Matrix (Cat# 11815016001) was from Roche. The Mitochondria Isolation Kit for Cultured Cells (Cat# 89874) was from Life Technologies. Primary antibodies: UBE3B antibody (Cat# SAB4503523) from Sigma Aldrich, ubiquitin (Ub) antibody (Cat# AUB01) was from Cytoskeleton, α-Tubulin antibody (Cat# CP06) from EMD Millipore, proliferating cell nuclear antigen (PCNA) antibody (Cat# sc-56) from Santa Cruz, cytochrome c oxidase IV (COX IV) antibody (Cat# A21348) from Life Technologies, Turbo-green fluorescent protein (TurboGFP) antibody (Cat# AB513) from Evrogen, adenosine triphosphate synthase beta (ATP synthase β) antibody (Cat# MA1-930) from Thermo Fisher Scientific, and calmodulin (CALM) antibody (Cat# ab45689) from Abcam. The hybridoma cell clone #12CA5, expressing the anti-HA monoclonal antibody, was a generous gift from Kara Bernstein (University of Pittsburgh). The 12CA5 hybridoma cells were used to generate ascites and the resulting Ab was purified using protein-A-agarose and isotyped (IgG2b/Kappa). Secondary antibodies: goat anti-mouse horseradish peroxidase (GAM-HRP) conjugates and goat anti-rabbit horseradish peroxidase (GAR-HRP) conjugates were from Bio-Rad, goat anti-mouse Cy5 (Cat# ab150115) from Abcam and goat anti-rabbit Cy3 (Cat# A-11011) was from Life Technologies. The Novex® NuPAGE® SDS-PAGE gel systems were from Life Technologies. Signal generation substrates were from Bio-Rad and Thermo Fisher

Scientific. All electrophoresis reagents were from Bio-Rad. The ubiquitin activating enzyme (UBE1) (Cat# E-305) and Ubiquitin Aldehyde (Cat# U-201) were from Boston Biochem. The ubiquitin conjugating enzyme (E2) Selection Panels (Cat# UB200) were from Life Sensors. The Magnesium/ATP Cocktail (Cat# 20-113) was from EMD Millipore. The Protease Inhibitor Mini-Tablets (Cat# 88665) and IP Lysis Buffer (Cat# 87788) were from Thermo Fisher Scientific, and the MG-132 (Cat# 474790) was from Calbiochem. Biotin (Cat# BP232-1) was from Thermo Fisher Scientific and Dynabeads MyOne Streptavidin C (Cat# 65001) was from Life Technologies.

4.2 STABLE CELL LINE GENERATION AND CULTURE CONDITIONS

LN428 glioblastoma cells and culture conditions were as previously described (196). Cells were maintained at 37°C in 5% CO_2 and grown in alpha EMEM media containing 10% heat-inactivated fetal bovine serum (FBS), antibiotic/antimycotic, L-glutamine and gentamycin.

Human UBE3B complementary DNA was PCR amplified (using primers purchased from Eurofins MWG Operon) and cloned into the pENTR/D-TOPO plasmid to create the pENTR-UBE3B vector as per standard Topo-cloning methodology (197). With this plasmid as the template, UBE3B tagged proteins or mutants were made, either via standard PCR or with the QuickChange XL Site-Directed Mutagenesis kit. The sequence of each primer is listed in **Table 1**. Briefly, we made HA-UBE3B, UBE3B-HA, HA-UBE3BΔHECT, HA-UBE3B(619-end), HA-UBE3B(757-end), and UBE3B(ΔIQ)-HA using primer pairs HA-UBE3B-F/UBE3B-R, UBE3B-F/UBE3B-HA-R, HA-UBE3B-F/UBE3BΔHECT-R, HA-UBE3B(619-end)-F/UBE3B-R, HA-

UBE3B(757-end)-F/UBE3B-R and UBE3B(ΔIQ)-F/UBE3B-HA-R, respectively (**Figures 3*A*, 4*A*, 5*A*, 6*A* and 7*A*, respectively**).

Table 1. Deoxyoligonucleotides used.

Oligo Name	Sequence (5'-3')*
GFP-UBE3B-F	ACTCTAGAATGTTCACCCTGTCTCAGACCTCG
GFP-UBE3B-R	TAGTCTAGACTAGGAGAGTTCAAAGCCCGTGTTCATGC
UBE3B-GFP-F	ATTCTAGACACCATGTTCACCCTGTCTCAGACCTCG
UBE3B-GFP-R	TAGCTCTAGAATGGAGAGTTCAAAGCCCGTGTTCATGC
UBE3BΔHECT-GFP-R	ATCGGATCCAATCCCCACTGGTTGTCTTGAACAGATT
UBE3B(C1036A)-F	TGCCCACCTCCTCCACC**GCC**TTCAACCTGCTCAAGC
UBE3B(C1036A)-R	GCTTGAGCAGGTTGAA**GGC**GGTGGAGGAGGTGGGCA
UBE3B(R922C)-F	CAACTCCTGAACTGCAG**T**GTCTCATCTCTGGCGACAATGC
UBE3B(R922C)-R	GCATTGTCGCCAGAGATGAGAC**A**CTGCAGTTCAGGAGTTG
HA-UBE3A-F	CACCATGTACCCATACGATGTTCCAGATTACGCTGAGAAGCTG
HA-UBE3A-R	TTACAGCATGCCAAATCCTTTGGCATACGTGATGG
HA-UBE3B-F	CACCATGTACCCATACGATGTTCCAGATTACGCTTTCACCCTGTCTCAGACC
UBE3B-F	CACCATGTTCACCCTGTCTCAGACCTCGAGAGCATGG
UBE3B-R	CTAGGAGAGTTCAAAGCCCGTGTTCATGCTGATGGCG
HA-UBE3B(619-end)-F	CACCATGTACCCATACGATGTTCCAGATTACGCTGAGAGGCTG
HA-UBE3B(757-end)-F	CACCATGTACCCATACGATGTTCCAGATTACGCTAAGGATCTCAAACC
HA-UBE3A(418-end)-F	CACCATGTACCCATACGATGTTCCAGATTACGCTTGTCCCTTTATATTGAATGC
UBE3BΔHECT-R	CTAGGAGAGTTCAAAGCCCGTGTTCATGCTGATGGCG
UBE3B-HA-R	CTAAGCGTAATCTGGAACATCGTATGGGTAGGAGAGTTCAAAGCCCGTG
Ubiquitin-F	CACCCAGATTTTCGTGAAAACCCTTACG
Ubiquitin-R	TTAACCACCACGAAGTCTCAACACAAGATG
UBE3B(ΔIQ)-F	CACCATGGCAGATGACCCTGAGTCCACTAAAAGAAGTGC

*The bold bases indicate the mutated bases.

Using the pENTR-HA-UBE3B plasmid as template, we made the HA-UBE3B(C1036A) and HA-UBE3B(R922C) mutations using primer pairs UBE3B(C1036A)-F/UBE3B(C1036A)-R and UBE3B(R922C)-F/UBE3B(R922C)-R, respectively (**Figures 8*A* and 9*A* respectively**).

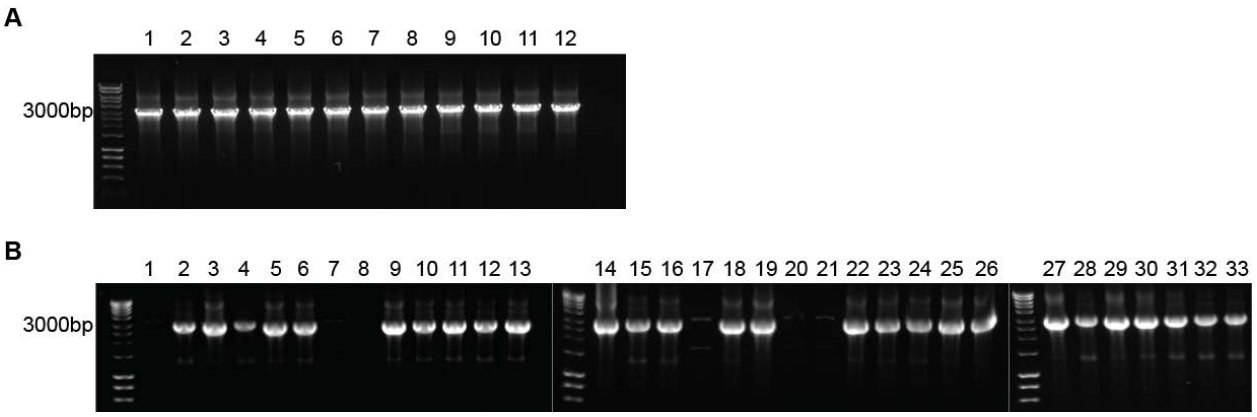

Figure 3. Generation of HA-UBE3B constructs.

(A) Optimization of the primers HA-UBE3B-F and UBE3B-R using Platinum® *Pfx* DNA Polymerase and pENTR-UBE3B in gradient PCR for amplification of HA-UBE3B for pENTR/D-TOPO cloning into pENTR vector. **(B)** PCR amplification screen using *Taq* DNA Polymerase of mini-prep pENTR-HA-UBE3B plasmids from transformed One Shot Top 10 *E.coli* cells.

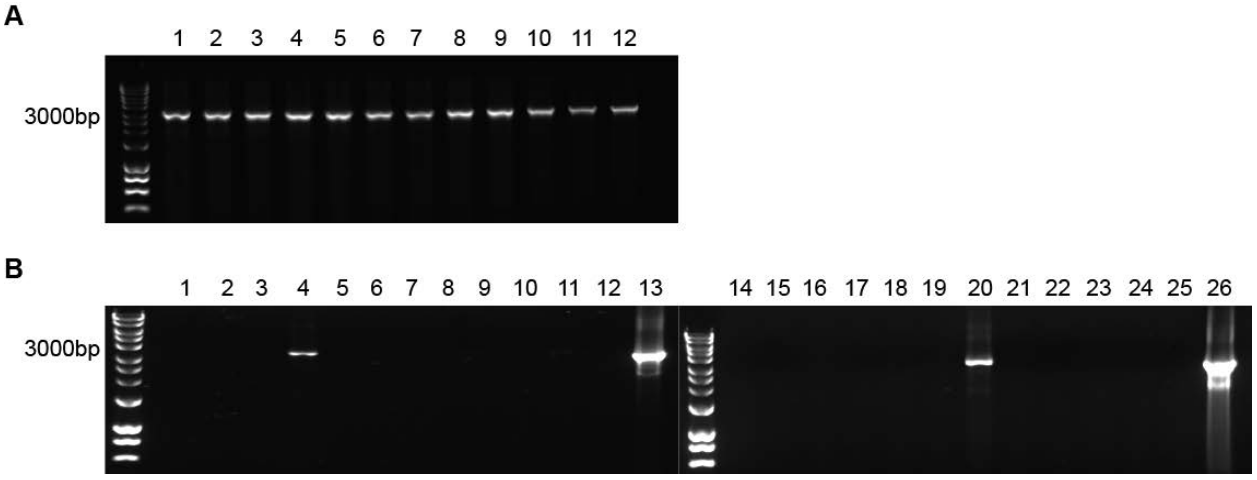

Figure 4. Generation of UBE3B-HA constructs.

(A) Optimization of the primers UBE3B-F and UBE3B-HA-R using Platinum® *Pfx* DNA Polymerase and pENTR-UBE3B in gradient PCR for amplification of UBE3B-HA for pENTR/D-TOPO cloning into pENTR vector. **(B)** PCR amplification screen using *Taq* DNA Polymerase of mini-prep pENTR-UBE3B-HA plasmids from transformed One Shot Top 10 *E.coli* cells. Lanes 13 and 26 were positive control lanes that used PCR purified DNA instead of mini-prep plasmids.

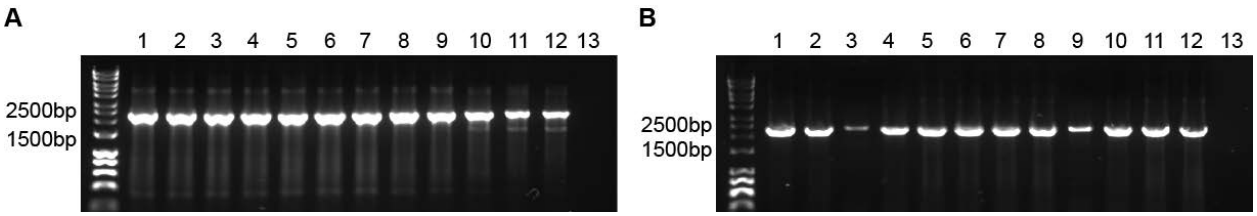

Figure 5. Generation of HA-UBE3BΔHECT constructs.

(A) Optimization of the primers HA-UBE3B-F and UBE3BΔHECT-R using Platinum® *Pfx* DNA Polymerase and pENTR-UBE3B in gradient PCR for amplification of HA-UBE3BΔHECT for pENTR/D-TOPO cloning into pENTR vector. **(B)** PCR amplification screen using *Taq* DNA Polymerase of mini-prep pENTR-HA-UBE3BΔHECT plasmids from transformed One Shot Top 10 *E.coli* cells.

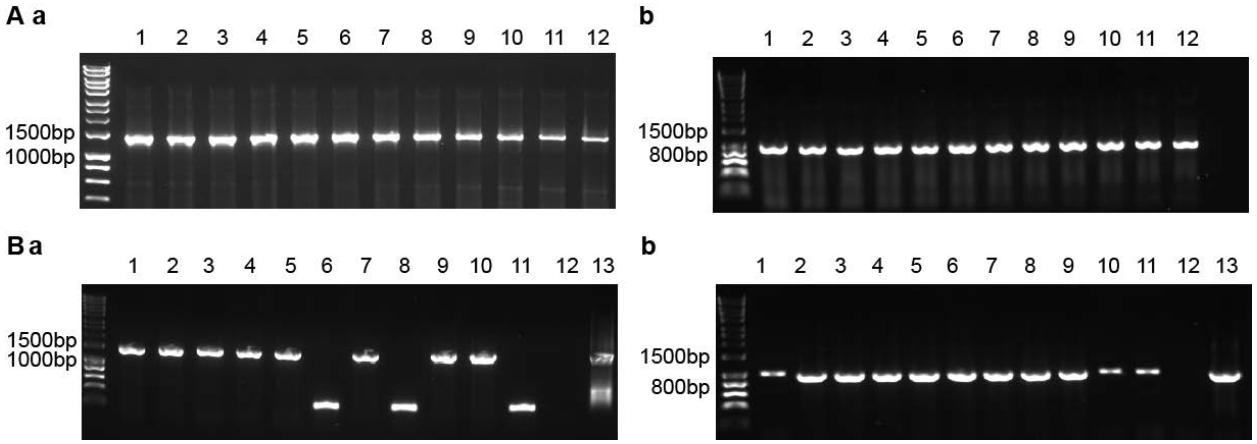

Figure 6. Generation of HA-UBE3B(619-end) and HA-UBE3B(757-end) constructs.

(A) Optimization of the primers **(a)** HA-UBE3B(619-end)-F and UBE3B-R, and (b) HA-UBE3B(757-end)-F and UBE3B-R, using Platinum® *Pfx* DNA Polymerase and pENTR-UBE3B plasmid in gradient PCR for amplification of **(a)** HA-UBE3B(619-end), and **(b)** HA-UBE3B(757-end) respectively, for pENTR/D-TOPO cloning into pENTR vector. **(B)** PCR amplification screen using *Taq* DNA Polymerase of mini-prep **(a)** pENTR-HA-UBE3B(619-end), and **(b)** pENTR-HA-UBE3B(757-end) plasmids from transformed One Shot Top 10 *E.coli* cells.

Using the pENTR-HA-UBE3B(C1036A) plasmid as template, we made HA-UBE3B(619-end)(C1036A) and HA-UBE3B(757-end)(C1036A) using primer pairs HA-UBE3B(619-end)-F/UBE3B-R and HA-UBE3B(757-end)-F/UBE3B-R, respectively (**Figure**

10*A*). Using p4054 HA-E6AP isoform II plasmid (Addgene) as template we made HA-UBE3A and HA-UBE3A(418-end) using primer pairs HA-UBE3A-F/HA-UBE3A-R and HA-UBE3A(418-end)-F/HA-UBE3A-R, respectively (**Figure 11*A***).

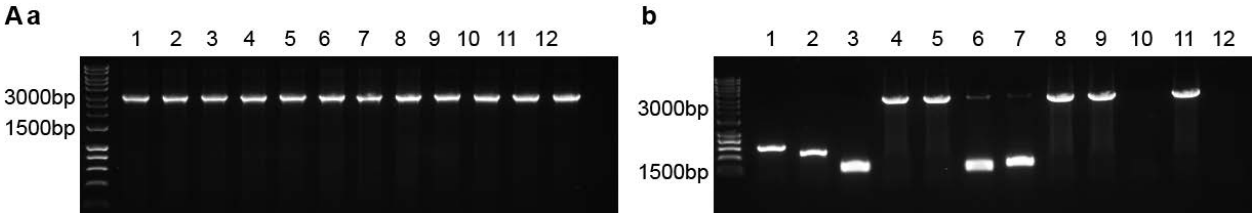

Figure 7. Generation of UBE3BΔIQ-HA constructs.

(A) Optimization of the primers UBE3B(ΔIQ)-F and UBE3B-HA-R using Platinum® *Pfx* DNA Polymerase and pENTR-UBE3B in gradient PCR for amplification of UBE3BΔIQ-HA for pENTR/D-TOPO cloning into pENTR vector. **(B)** PCR amplification screen using *Taq* DNA Polymerase of mini-prep pENTR-UBE3BΔIQ-HA plasmids from transformed One Shot Top 10 *E.coli* cells.

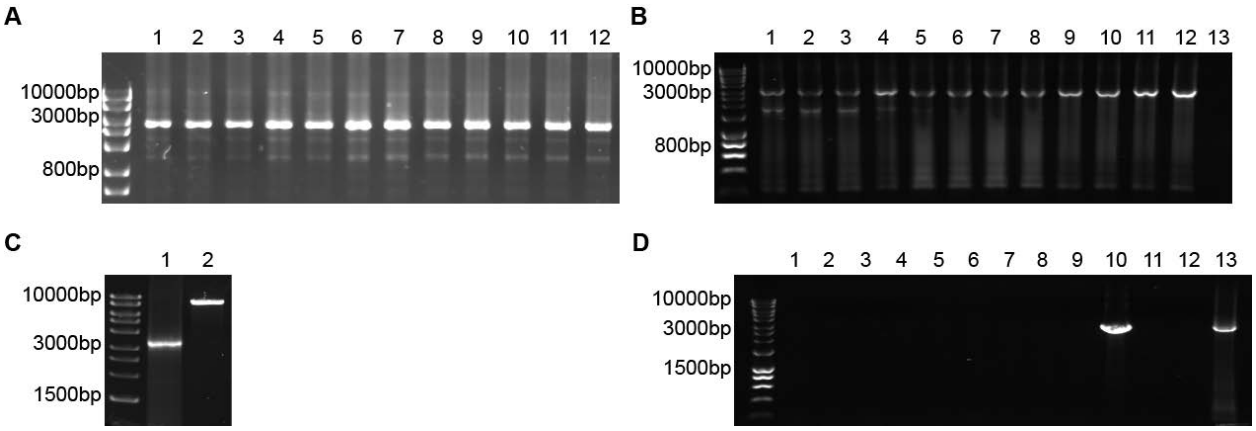

Figure 8. Generation of HA-UBE3B(C1036A) and UBE3B(C1036A)-copGFP constructs.

(A) Site-directed mutagenesis on plasmid pENTR-HA-UBE3B with primers UBE3B(C1036A)-F and UBE3B(C1036A)-R to create pENTR-HA-UBE3B(C1036A) plasmid. **(B)** Optimization of the primers UBE3B-GFP-F and UBE3B-GFP-R using Platinum® *Pfx* DNA Polymerase and plasmid pENTR-HA-UBE3B(C1036A) in gradient PCR for amplification of UBE3B(C1036A) with *XbaI* restriction digest sites for ligation into pCT-CMV-MCS-copGFP-Puro vector. Gradient temperatures: 1: 52°C, 2: 52.5°C, 3: 53.6°C, 4: 54.9°C, 5: 57°C, 6: 59.6°C, 7:

62.6°C, 8: 65.2°C, 9: 67.2°C, 10: 68.6°C, 11: 69.6°C, and 12: 70°C. Best temperature chosen was 70°C. **(C)** *XbaI* restriction digested and gel-purified PCR amplified UBE3B(C1036A) insert and pCT-CMV-MCS-copGFP-Puro vector for ligation using T4 DNA Ligase. **(D)** PCR amplification screen using *Taq* DNA Polymerase of mini-prep pCT-CMV-UBE3B(C1036A)-copGFP-Puro plasmids from transformed One Shot Top 10 *E.coli* cells.

Positive clones were selected and plasmids were extracted with the QIAprep Spin Miniprep Kit (Qiagen) (**Figures 3*B*, 4*B*, 5*B*, 6*B*, 7*B*, 9*B*, 10*B* and 11*B***). Once sequence verified, the open reading frames from each of the plasmids pENTR-HA-UBE3B, pENTR-UBE3B-HA, pENTR-HA-UBE3BΔHECT, pENTR-HA-UBE3B(C1036A), pENTR-HA-UBE3B(R922C), pENTR-HA-UBE3B(619-end), pENTR-HA-UBE3B(619-end)(C1036A), pENTR-HA-UBE3B(757-end), pENTR-HA-UBE3B(757-end)(C1036A), pENTR-UBE3B(ΔIQ)-HA, pENTR-HA-UBE3A and pENTR-HA-UBE3A(418-end) were transferred into a Gateway-modified pLVX-IRES-Puro vector, (Clontech) by the LR reaction using the Gateway LR Clonase II Enzyme Mix (Life Technologies) as per the manufacturer's instruction. Positive clones were selected and plasmids were extracted with the QIAprep Spin Miniprep Kit (Qiagen). For the UBE3B-copGFP, UBE3BΔHECT-copGFP, copGFP-UBE3B and copGFP-UBE3BΔHECT fusion plasmids we used pENTR-UBE3B and either pCT-CMV-MCS-copGFP-EF1-Puro or pCT-CMV-copGFP-MCS-EF1-Puro (System Biosciences) respectively. For the UBE3B(C1036A)-copGFP, UBE3B(R922C)-copGFP, copGFP-UBE3B((R215C/I1059F) and copGFP-UBE3B(R346Q) fusion plasmids we used pENTR-UBE3B(C1036A), pENTR-UBE3B(R922C), pENTR-UBE3B(R215C/I1059F) or pENTR-UBE3B(R346Q), respectively, and either pCT-CMV-MCS-copGFP-EF1-Puro or pCT-CMV-copGFP-MCS-EF1-Puro (System Biosciences) respectively.

We made copGFP-UBE3B, cop-UBE3B(R215C/I1059F) and copGFP-UBE3B(R346Q) using primer pair GFP-UBE3B-F/GFP-UBE3B-R, we made UBE3B-copGFP, UBE3B(C1036A)-copGFP, UBE3B(R922C)-copGFP, UBE3B(R215C/I1059F)-copGFP and UBE3B(R346Q)-copGFP using primer pair UBE3B-GFP-F/UBE3B-GFP-R, while we made UBE3BΔHECT-copGFP using primer pair UBE3B-GFP-F/UBE3BΔHECT-GFP-R (**Figures 8*B*, 12*A*, 13*A* and 14*B***). The UBE3B, UBE3B(C1036A), UBE3B(R922C), UBE3B(R215C/I1059F) and UBE3B(R346Q) open-reading frames were PCR amplified to engineer the restriction enzyme site *XbaI* on both ends, while the UBE3BΔHECT-copGFP open-reading frame was PCR amplified to engineer the restriction enzyme sites *XbaI* and *BamHI* for cloning in-frame with copGFP using standard protocols. After PCR, products were digested with the respective enzymes; purified fragments were ligated into the pCT-CMV-copGFP-MCS-EF1-puro lentiviral vector hydrolysed by *XbaI*, or *XbaI* and *BamHI* (**Figures 8*C*, 12*B*, 13*B* and 14*C***). Positive colonies were selected and sequenced (**Figures 8*D*, 13*C*, 14*D* and 15*A***). To determine if UBE3B was correctly inserted into pCT-CMV-copGFP-MCS-EF1-Puro and pCT-CMV-MCS-copGFP-EF1-Puro, and if UBE3B(R922C), UBE3B(R215C/I1059F) and UBE3B(R346Q) clones were correctly inserted into pCT-CMV-MCS-copGFP-EF1-Puro the plasmids were digested with either *XbaI* or *BamHI*. If the constructs were present, there will be a 300bp band in the digested products. While, if the constructs are present in the correct orientation, there should be a 500bp band and a 10,000bp band in the *BamHI* digested products (**Figures 14*E* and 15*C*, *D*&*E***).

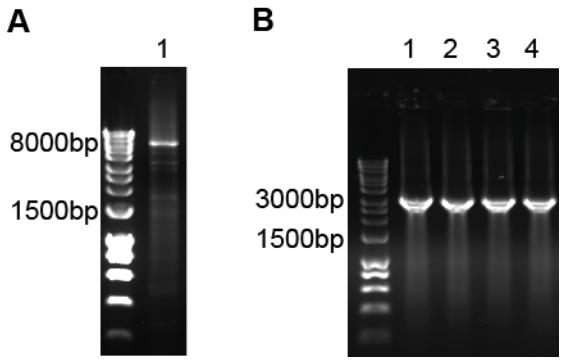

Figure 9. Generation of HA-UBE3B(R922C) constructs.

(A) Site-directed mutagenesis and *DpnI* digestion of plasmid pENTR-HA-UBE3B with primers UBE3B(R922C)-F and UBE3B(R922C)-R to create pENTR-HA-UBE3B(R922C) plasmid. **(B)** PCR amplification screen using *Taq* DNA Polymerase of mini-prep pENTR-HA-UBE3B(R922C) plasmids from transformed One Shot Top 10 *E.coli* cells.

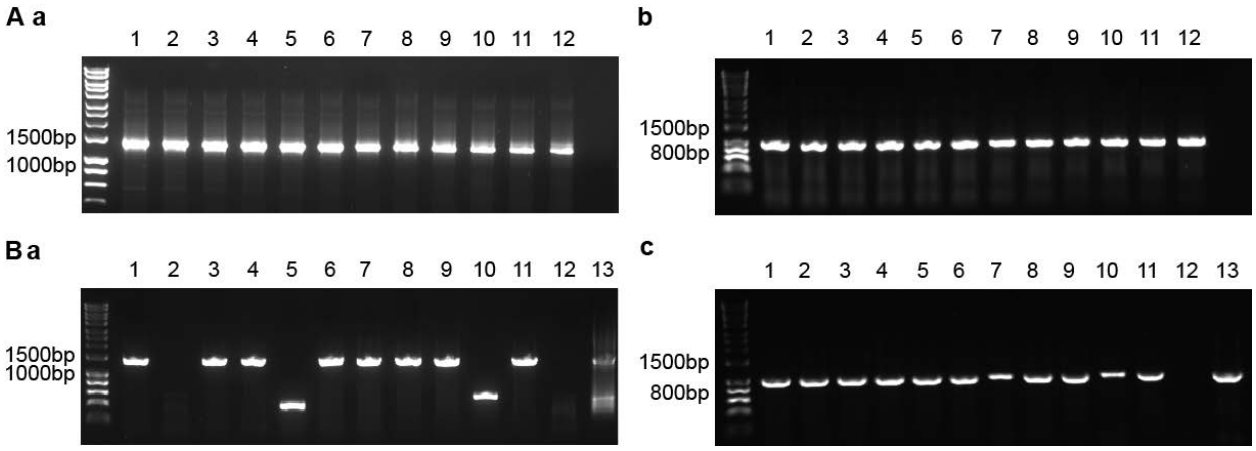

Figure 10. Generation of HA-UBE3B(C1036A)(619-end) and HA-UBE3B(C1036A)(757-end) domain constructs.

(A) Optimization of the primers **(a)** HA-UBE3B(618-end)-F and UBE3B-R, and **(b)** HA-UBE3B(757-end)-F and UBE3B-R using Platinum® *Pfx* DNA Polymerase and pENTR-UBE3B(C1036A) plasmid in gradient PCR for amplification of **(a)** HA-UBE3B(619-end)(C1036A), and **(b)** HA-UBE3B(757-end)(C1036A), respectively, for pENTR/D-TOPO cloning into pENTR vector. **(B)** PCR amplification screen using *Taq* DNA Polymerase of mini-prep **(a)** pENTR-HA-UBE3B(619-end)(C1036A) and **(b)** pENTR-HA-UBE3B(757-end)(C1036A) plasmids from transformed One Shot Top 10 *E.coli* cells.

To determine if UBE3BΔHECT was inserted into pCT-CMV-MCS-copGFP-EF1-Puro, clones were digested with *XbaI* or *BamHI*. If the construct was present, there will be a 2500bp band and an 8000bp band in the digested product (**Figure 13*D***). Sequence-verified plasmids were transiently transfected and lentivirus production was as described below. The pLPC-MYC-BirA plasmid was a kind gift from Dr. Roderick O'Sullivan at the University of Pittsburgh. To create the BirA-UBE3B and UBE3B-BirA fusion plasmids, we had pENTR-BirA-UBE3B and pENTR-UBE3B-BirA plasmids synthesized by GenScript. Once sequence verified, we transferred the open reading frames into the Gateway-modified pLVX-IRES-Puro vector as described above.

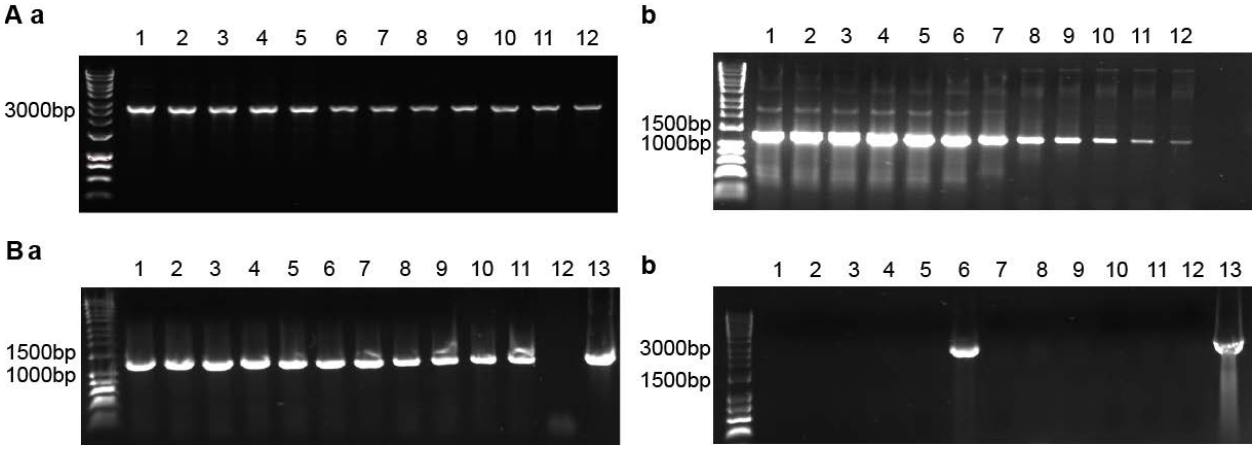

Figure 11. Generation of HA-UBE3A and HA-UBE3A(418-end) constructs.

(A) Optimization of the primers **(a)** HA-UBE3A-F and UBE3A-R, and **(b)** HA-UBE3A(418-end)-F and UBE3A-R using Platinum® *Pfx* DNA Polymerase and p4054 HA-E6AP plasmid in gradient PCR for amplification of **(a)** HA-UBE3A and **(b)** HA-UBE3A(418-end), respectively, for pENTR/D-TOPO cloning into pENTR vector. **(B)** PCR amplification screen using *Taq* DNA Polymerase of mini-prep **(a)** pENTR-HA-UBE3A and **(b)** pENTR-HA-UBE3A(418-end) plasmids from transformed One Shot Top 10 *E.coli* cells.

All the vectors used and developed in this study are listed in **Table 2**, and all the pENTR and pCT-CMV-copGFP-MCS-EF1-Puro/pCT-CMV-MCS-copGFP-EF1-Puro plasmid maps are listed in **Appendix F**.

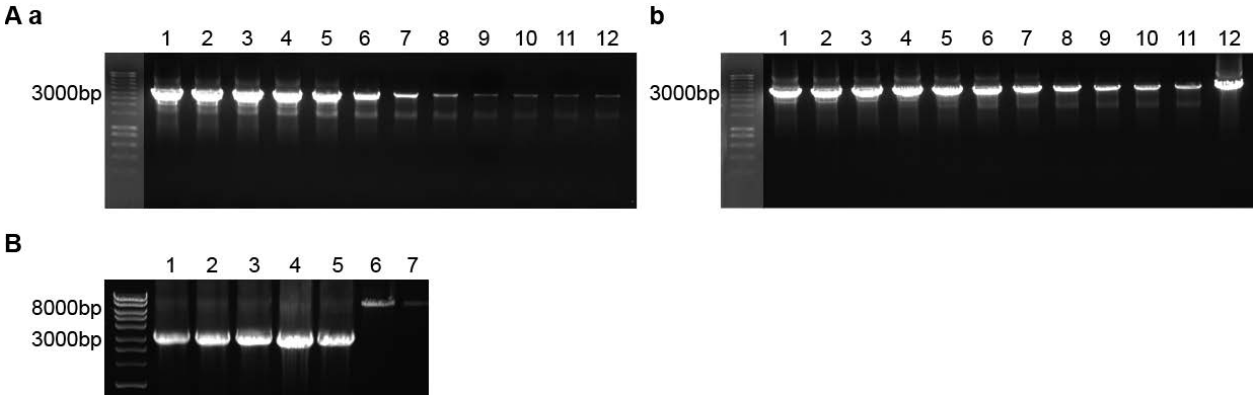

Figure 12. Generation of copGFP-tagged UBE3B wild type and point mutant constructs.

(A)(a) Optimization of the primers GFP-UBE3B-F and GFP-UBE3B-R using Platinum® *Pfx* DNA Polymerase and pENTR-UBE3B in gradient PCR for amplification of UBE3B with *XbaI* restriction digest sites for ligation into pCT-CMV-copGFP-MCS-Puro vector. **(b)** Optimization of the primers UBE3B-GFP-F and UBE3B-GFP-R using Platinum® *Pfx* DNA Polymerase and pENTR-UBE3B in gradient PCR for amplification of UBE3B with *XbaI* restriction digest sites for ligation into pCT-CMV-MCS-copGFP-Puro vector. Gradient temperatures: 1: 52°C, 2: 52.5°C, 3: 53.6°C, 4: 54.9°C, 5: 57°C, 6: 59.6°C, 7: 62.6°C, 8: 65.2°C, 9: 67.2°C, 10: 68.6°C, 11: 69.6°C, and 12: 70°C. Best temperature chosen for (a) primer set was 62.6°C, and for (b) primer set was 70°C. **(B)** Restriction digested and gel-purified PCR amplified constructs and vectors for ligation using T4 DNA Ligase. 1: UBE3B with *XbaI* restriction digested sites for ligation into pCT-CMV-copGFP-MCS-Puro vector, 2: Restriction digested and gel purified constructs and vectors that are ready for ligation. 1: UBE3B with *XbaI* restriction digested sites for ligation into pCT-CMV-MCS-copGFP-Puro vector, 3: UBE3B(R215C/I1059F) with *XbaI* restriction digested sites for ligation into pCT-CMV-copGFP-MCS-Puro vector, 4: UBE3B(R215C/I1059F) with *XbaI* restriction digested sites for ligation into pCT-CMV-MCS-copGFP-Puro vector, 5: UBE3B(R346Q) with *XbaI* restriction digested sites for ligation into pCT-CMV-copGFP-MCS-Puro vector, 6: pCT-CMV-copGFP-MCS-Puro vector with *XbaI* restriction digested sites, and 7: pCT-CMV-MCS-copGFP-Puro vector with *XbaI* restriction digested sites.

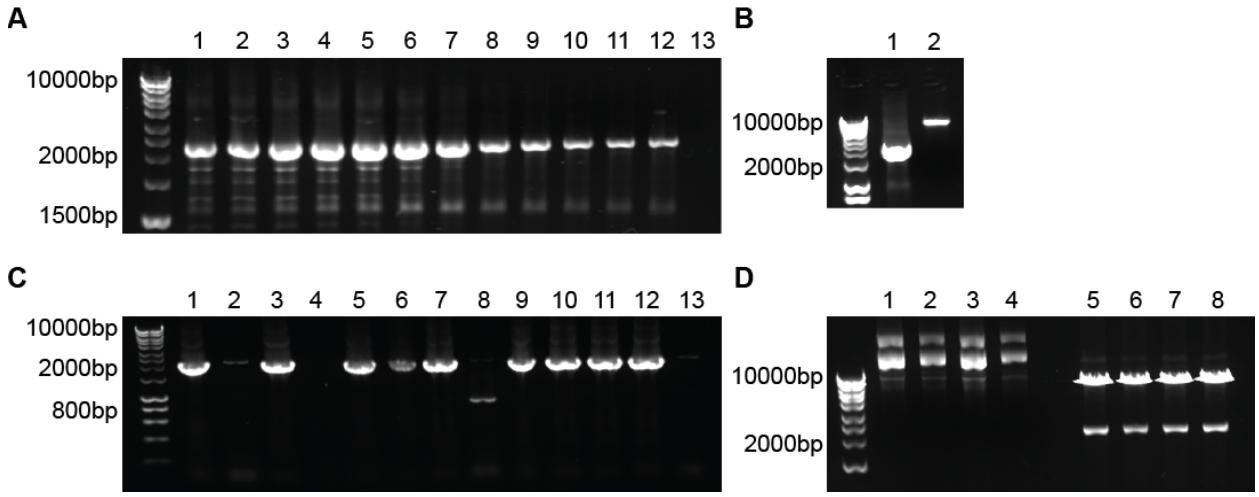

Figure 13. Generation of UBE3BΔHECT-copGFP constructs.

(A) Optimization of the primers UBE3B-GFP-F and UBE3BΔHECT-GFP-R using Platinum® *Pfx* DNA Polymerase and pENTR-UBE3BΔHECT in gradient PCR for amplification of UBE3BΔHECT with *XbaI* and *BamHI* restriction digest sites on the N- and C-terminals respectively, for ligation into pCT-CMV-MCS-copGFP-Puro vector. Gradient temperatures: 1: 52°C, 2: 52.5°C, 3: 53.6°C, 4: 54.9°C, 5: 57°C, 6: 59.6°C, 7: 62.6°C, 8: 65.2°C, 9: 67.2°C, 10: 68.6°C, 11: 69.6°C, and 12: 70°C. Best temperature chosen was 70°C. **(B)** *XbaI* and *BamHI* restriction digested and gel-purified PCR amplified UBE3BΔHECT insert and pCT-CMV-MCS-copGFP-Puro vector for ligation using T4 DNA Ligase. **(C)** PCR amplification screen using *Taq* DNA Polymerase of mini-prep pCT-CMV-UBE3BΔHECT-copGFP-Puro plasmids from transformed One Shot Top 10 *E.coli* cells. **(D)** Lanes 1-4: Undigested mini-prep pCT-CMV-UBE3BΔHECT-copGFP-Puro plasmids, and Lanes 5-9: Mini-prep pCT-CMV-UBE3BΔHECT-copGFP-Puro plasmids digested with *XbaI* and *BamHI*. If insert is present, expected band sizes are ~2500bp and ~8000bp.

Table 2. Vectors developed for and used in this study.

Plasmid name	Insert description	Parental vector
pENTR-UBE3B	UBE3B	pENTR/D-TOPO
pENTR-UBE3BΔHECT	UBE3BΔHECT	pENTR/D-TOPO
pENTR-UBE3B(C1036A)	UBE3B(C1036A)	pENTR/D-TOPO
pENTR-UBE3B(R215C/I1059F)	UBE3B(R215C/I1059F)	pENTR/D-TOPO
pENTR-UBE3B(R346Q)	UBE3B(R346Q)	pENTR/D-TOPO
pENTR-UBE3B(R922C)	UBE3B(R922C)	pENTR/D-TOPO
pENTR-HA-UBE3B	HA-UBE3B	pENTR/D-TOPO
pENTR-UBE3B-HA	UBE3B-HA	pENTR/D-TOPO
pENTR-HA-UBE3BΔHECT	HA- UBE3BΔHECT	pENTR/D-TOPO
pENTR-HA-UBE3B(C1036A)	HA-UBE3B(C1036A)	pENTR/D-TOPO
pENTR-HA-UBE3B(R922C)	HA-UBE3B(R922C)	pENTR/D-TOPO

pENTR-HA-UBE3B(619-end)	HA-UBE3B(619-end)	pENTR/D-TOPO
pENTR-HA-UBE3B(619-end)(C1036A)	HA-UBE3B(619-end)(C1036A)	pENTR/D-TOPO
pENTR-HA-UBE3B(757-end)	HA-UBE3B(757-end)	pENTR/D-TOPO
pENTR-HA-UBE3B(757-end)(C1036A)	HA-UBE3B(757-end)(C1036A)	pENTR/D-TOPO
pENTR-HA-UBE3A	HA-UBE3A	pENTR/D-TOPO
pENTR-HA-UBE3A(418-end)	HA-UBE3A(418-end)	pENTR/D-TOPO
pENTR-UBE3B(ΔIQ)-HA	UBE3B(ΔIQ)-HA	pENTR/D-TOPO
pCT-CMV-UBE3B-copGFP-Puro	UBE3B-copGFP	pCYTO-CMV-MCS-copGFP-EF1-Puro
pCT-CMV-copGFP-UBE3B-Puro	copGFP-UBE3B	pCYTO-CMV-copGFP-MCS-EF1-Puro
pCT-CMV-UBE3BΔHECT-copGFP-Puro	UBE3BΔHECT-copGFP	pCYTO-CMV-MCS-copGFP-EF1-Puro
pCT-CMV-copGFP-UBE3BΔHECT-Puro	copGFP-UBE3BΔHECT	pCYTO-CMV-copGFP-MCS-EF1-Puro
pCT-CMV-UBE3B(C1036A)-copGFP-Puro	UBE3B(C1036A)-copGFP	pCYTO-CMV-MCS-copGFP-EF1-Puro
pCT-CMV-UBE3B(R215C/I1059F)-copGFP-Puro	UBE3B(R215C/I1059F)-copGFP	pCYTO-CMV-MCS-copGFP-EF1-Puro
pCT-CMV-copGFP-UBE3B(R215C/I1059F)-Puro	copGFP-UBE3B(R215C/I1059F)	pCYTO-CMV-copGFP-MCS-EF1-Puro
pCT-CMV-copGFP-UBE3B(R346Q)-Puro	copGFP-UBE3B(R346Q)	pCYTO-CMV-copGFP-MCS-EF1-Puro
pCT-CMV-UBE3B(R346Q)-copGFP-Puro	UBE3B(R346Q)-copGFP	pCYTO-CMV-MCS-copGFP-EF1-Puro
pCT-CMV-UBE3B(R922C)copGFP-Puro	UBE3B(R922C)-copGFP	pCYTO-CMV-MCS-copGFP-EF1-Puro
pLVX-HA-UBE3B-IRES-Puro	HA-UBE3B	pLVX-GW-IRES-Puro
pLVX-UBE3B-HA-IRES-Puro	UBE3B-HA	pLVX-GW-IRES-Puro
pLVX-HA-UBE3BΔHECT-IRES-Puro	HA- UBE3BΔHECT	pLVX-GW-IRES-Puro
pLVX-HA-UBE3B(C1036A)-IRES-Puro	HA-UBE3B(C1036A)	pLVX-GW-IRES-Puro
pLVX-HA-UBE3B(R992C)-IRES-Puro	HA-UBE3B(R922C)	pLVX-GW-IRES-Puro
pLVX-HA-UBE3B(619-end)-IRES-Puro	HA-UBE3B(619-end)	pLVX-GW-IRES-Puro
pLVX-HA-UBE3B(619-end)(C1036A)-IRES-Puro	HA-UBE3B(619-end)(C1036A)	pLVX-GW-IRES-Puro
pLVX-HA-UBE3B(757-end)-IRES-Puro	HA-UBE3B(757-end)	pLVX-GW-IRES-Puro
pLVX-HA-UBE3B(757-end)(C1036A)-IRES-Puro	HA-UBE3B(757-end)(C1036A)	pLVX-GW-IRES-Puro
pLVX-HA-UBE3A-IRES-Puro	HA-UBE3A	pLVX-GW-IRES-Puro
pLVX-HA-UBE3A(418-end)-IRES-Puro	HA-UBE3A(418-end)	pLVX-GW-IRES-Puro
pLVX-UBE3B(ΔIQ)-HA-IRES-Puro	UBE3B(ΔIQ)-HA	pLVX-GW-IRES-Puro
pLVX-BirA-UBE3B-Puro	BirA-UBE3B	pLVX-GW-IRES-Puro
pLVX-UBE3B-BirA-Puro	UBE3B-BirA	pLVX-GW-IRES-Puro

Lentiviruses were prepared in collaboration with the UPCI Lentiviral facility. Lentiviral particles were generated by co-transfection of 4 plasmids [Control plasmid (pLVX-IRES-Puro) or one of the plasmids expressing UBE3B or UBE3B mutants, together with pMD2.g (VSVG), pVSV-REV and pMDLg/pRRE] into 293-FT cells using TransIT®-2020 Transfection reagent. The collection and isolation of lentiviral particles and transduction of LN428 cells were performed as described previously (198,199). Stable cell lines were developed by selection in puromycin (2 µg/mL) for 2 weeks. Overexpression of UBE3B (or the indicated mutants or fusions) was confirmed by immunoblot (**Figure 16**). All the stable cell lines developed and used in this study are listed in **Table 3**.

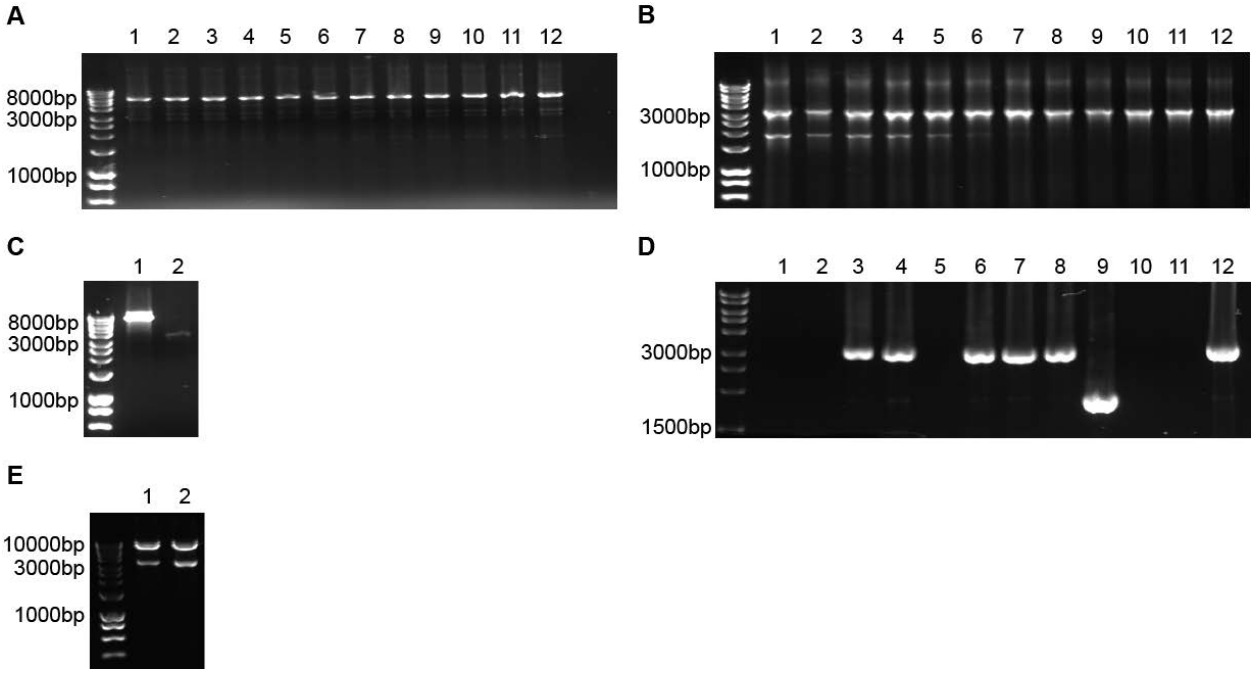

Figure 14. Generation of UBE3B(R922C)-copGFP constructs.

(A) Site-directed mutagenesis and *DpnI* digestion on plasmid pENTR-UBE3B with primers UBE3B(R922C)-F and UBE3B(R922C)-R to create pENTR-UBE3B(R922C) plasmid. **(B)** Optimization of the primers UBE3B-GFP-F and UBE3B-GFP-R using Platinum® *Pfx* DNA Polymerase and pENTR-UBE3B(R922C) in gradient PCR for amplification of UBE3B(R922C) with *XbaI* restriction digest sites for ligation into pCT-CMV-MCS-copGFP-Puro

vector. Gradient temperatures: 1: 52°C, 2: 52.5°C, 3: 53.6°C, 4: 54.9°C, 5: 57°C, 6: 59.6°C, 7: 62.6°C, 8: 65.2°C, 9: 67.2°C, 10: 68.6°C, 11: 69.6°C, and 12: 70°C. Best temperature chosen was 70°C. **(C)** *XbaI* restriction digested pCT-CMV-MCS-copGFP-Puro vector, and digested and gel-purified PCR amplified UBE3B(R922C) insert for ligation using T4 DNA Ligase. **(D)** PCR amplification screen using *Taq* DNA Polymerase of mini-prep pCT-CMV-UBE3B(R922C)-copGFP-Puro plasmids from transformed One Shot Top 10 *E.coli* cells. **(E)** Digestion of mini-prep pCT-CMV-UBE3B(R922C)-copGFP-Puro plasmids with either *XbaI*. If insert (UBE3B(R922C)) is present, expected band sizes with *XbaI* digestion are ~3000bp and ~8000bp.

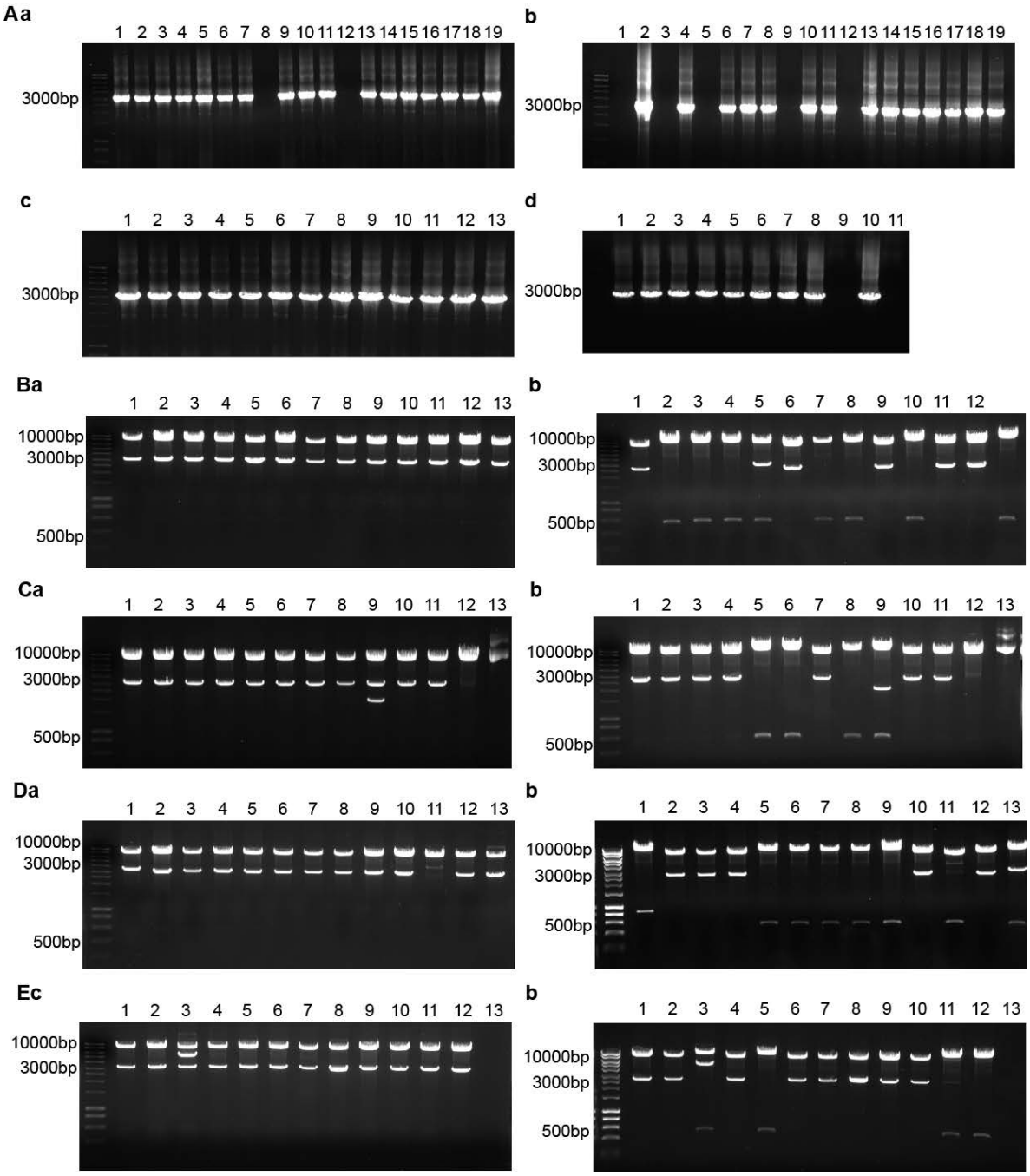

Figure 15. PCR screen and digestion of UBE3B wild type and point mutant plasmids with XbaI and BamHI to determine insert orientation.

(A) PCR amplification using *Taq* DNA Polymerase of mini-prep plasmids from One Shot Top 10 *E.coli* cells after transformation with ligated plasmids **(a)** pCT-CMV-copGFP-UBE3B-Puro, **(b)** pCT-CMV-UBE3B-copGFP-Puro, **(c)** Lanes 1-6 pCT-CMV-copGFP-UBE3B(R215C/I1059F)-Puro, and lanes 7-13 pCT-CMV-UBE3B(R215C/I1059F)-copGFP-Puro, and **(d)** pCT-CMV-copGFP-UBE3B(R346Q)-Puro. **(B)** Digestion of mini-

prep pCT-CMV-copGFP-UBE3B-Puro plasmids with either **(a)** *XbaI* or **(b)** *BamHI*. **(C)** Digestion of mini-prep pCT-CMV-UBE3B-copGFP-Puro plasmids with either (a) *XbaI* or (b) *BamHI*. **(D)** Digestion of mini-prep pCT-CMV-copGFP-UBE3B(R215C/I1059F)-Puro plasmids with either (a) *XbaI* or (b) *BamHI*. **(E)** Digestion of mini-prep pCT-CMV-UBE3B(R215C/I1059F)-copGFP-Puro plasmids with either (a) *XbaI* or (b) *BamHI*. If insert is present, expected band sizes with *XbaI* digestion are ~3000bp and ~8000bp, and with *BamHI* digestion, expected band sizes are ~500bp and ~10,000bp.

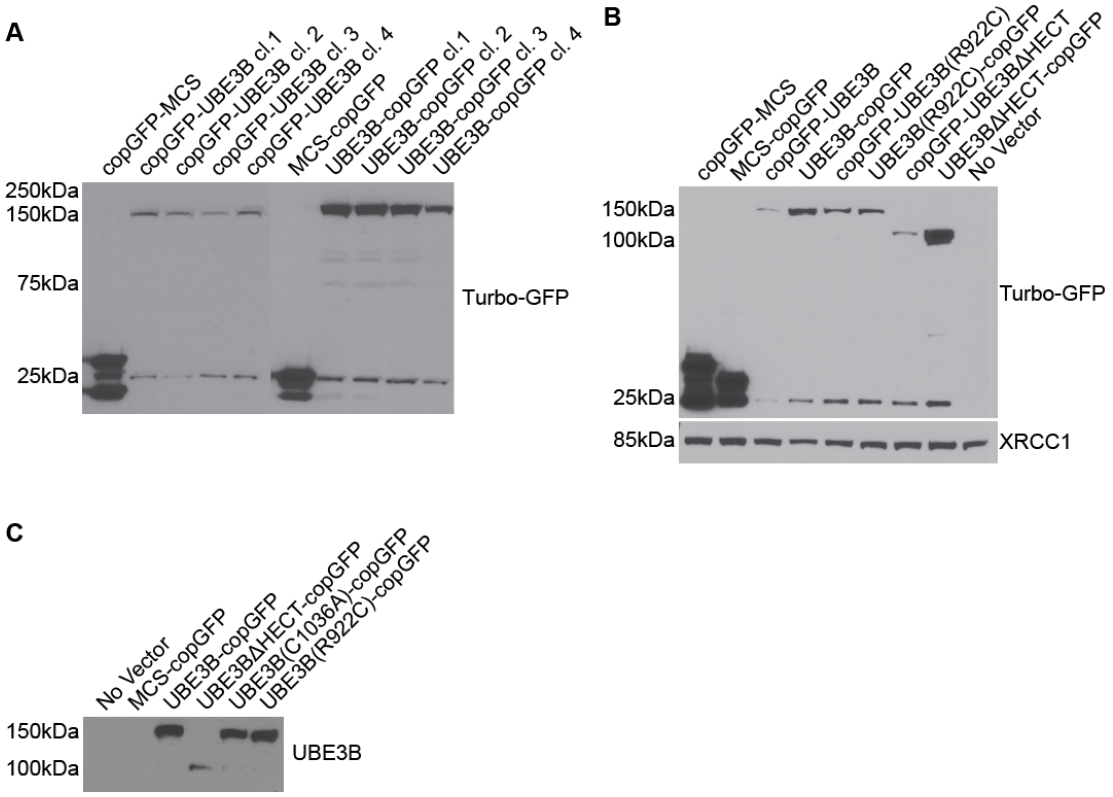

Figure 16. Immunoblot of whole cell extracts (WCE) from LN428 cells stably expressing cop-GFP tagged UBE3B proteins.

(A) Whole cell extracts (WCE) of cells transduced with different clones of wild type UBE3B with either N- or C-terminus copGFP tags. **(B)** WCE of cells transduced with copGFP-UBE3B, UBE3B-copGFP, copGFP-UBE3B(R922C), UBE3B(R922C)-copGFP, copGFP-UBE3BΔHECT or UBE3BΔHECT-copGFP. **(C)** WCE of cells transduced with UBE3B-copGFP, UBE3BΔHECT-copGFP, UBE3B(C1036A)-copGFP or copGFP-UBE3B(R922C). Primary antibodies: Turbo-GFP and UBE3B. Loading control: XRCC1. Expected size of full

length and point mutant fusions: ~150kDa, ΔHECT mutants: ~98kDa. Positive controls: copGFP-MCS and MCS-copGFP, where MCS is the Multiple Cloning Site. Negative control: No vector cells.

Table 3. LN428 cell lines developed and used in this study.

Cell line name	Cell line description	Growth media*
LN428	Human glioblastoma tumor cell line	Media #1
LN428/UBE3B-copGFP	LN428 cells expressing UBE3B-copGFP	Media #2
LN428/copGFP-UBE3B	LN428 cells expressing copGFP-UBE3B	Media #2
LN428/UBE3BΔHECT-copGFP	LN428 cells expressing UBE3BΔHECT- copGFP	Media #2
LN428/UBE3B(C1036A)-copGFP	LN428 cells expressing UBE3B(C1036A)-copGFP	Media #2
LN428/copGFP-UBE3BΔHECT	LN428 cells expressing copGFP-UBE3BΔHECT	Media #2
LN428/UBE3B(R215C/I1059F)-copGFP	LN428 cells expressing UBE3B(R215C/1059F)-copGFP	Media #2
LN428/copGFP-UBE3B(R215C/I1059F)	LN428 cells expressing copGFP-UBE3B(R215C/1059F)	Media #2
LN428/UBE3B(R346Q)-copGFP	LN428 cells expressing UBE3B(R346Q)-copGFP	Media #2
LN428/copGFP-UBE3B(R346Q)	LN428 cells expressing copGFP-UBE3B(R346Q)	Media #2
LN428/UBE3B(R922C)-copGFP	LN428 cells expressing UBE3B(R922C)-copGFP	Media #2
LN428/HA-UBE3B	LN428 cells expressing HA-UBE3B	Media #2

LN428/UBE3B-HA	LN428 cells expressing UBE3B-HA	Media #2
LN428/HA-UBE3BΔHECT	LN428 cells expressing HA-UBE3BΔHECT	Media #2
LN428/HA-UBE3B(C1036A)	LN428 cells expressing HA-UBE3B(C1036A)	Media #2
LN428/HA-UBE3B(R922C)	LN428 cells expressing HA-UBE3B(R922C)	Media #2
LN428/HA-UBE3A	LN428 cells expressing HA-UBE3A	Media #2
LN428/UBE3B(ΔIQ)-HA	LN428 cells expressing UBE3B(ΔIQ)-HA	Media #2
LN428/BirA-UBE3B	LN428 cells expressing BirA-UBE3B	Media #2
LN428/UBE3B-BirA	LN428 cells expressing UBE3B-BirA	Media #2

4.3 TRANSIENT TRANSFECTIONS OF SIRNA

UBE3B was depleted in LN428 cells by transient siRNA transfection, as previously described (200). Briefly, 4 x 10^5 LN428 cells were wet-reverse transfected with either 90nmol/L siRNA UBE3B-s40200 (Ambion) or 90nmol/L Silencer® Negative Control siRNA #2 (Applied Biosystems). The siRNA were prepared with siPORT™ *NeoFX*™ and OptiMEM and the transfections were incubated for 24 hours at 37°C before replacement with fresh media.

4.4 TRANSIENT TRANSFECTION OF PLASMIDS

Proteins were overexpressed in LN428 cells by transient plasmid transfection. 1 x 10^6 cells were transfected with 7µg DNA. The plasmids were prepared with OPTI-MEM media and FuGENE® Transfection Reagent (Promega) for 30 minutes at room temperature before being added to the adherent cells dropwise. The transfections were incubated for 24 hours at 37°C before replacement with fresh media.

4.5 MTS ASSAY

Twenty-four hours after siRNA-mediated UBE3B KD, cells were seeded into 96-well plates at a density of 2,000 cells per well and allowed to grow for 48 hours at 37°C before determining the relative amount of metabolically active cells by an MTS assay. Results are the average of three separate experiments and normalized to the Silencer® Negative Control siRNA #2 cells, with error bars representing the standard error of the mean.

4.6 QUANTITATIVE RT-PCR ANALYSIS

Expression of UBE3B mRNA after siRNA-mediated KD was measured by quantitative RT-PCR (qRT-PCR) using an Applied Biosystems StepOnePlus system as described previously (201). We used the Applied Biosystems TaqMan Gene Expression Assay human UBE3B:

Hs00296200_m1, and normalized gene expression to the expression of human β-actin (Cat# 4333762T).

4.7 CELL EXTRACION, MITOCHONDRIA ISOLATION AND IMMUNOBLOT ANALYSIS

Mitochondria were isolated using the Mitochondria Isolation Kit for Cultured Cells (Life Technologies). Mitochondrial extracts and whole cell extracts (WCE) were prepared using 2X clear Laemmli buffer (2%SDS, 20% glycerol and 63mM Tris-HCl pH 6.8). Protein concentrations were determined by the Bio-Rad Protein Assay Kit II (Cat# 500-0002) according to the manufacturer's instruction. Ten micrograms of protein was loaded on precast 4%-12% Tris-Bis Novex® NuPAGE® SDS-PAGE gels (Life Technologies), run at 200V for an hour at room temperature and the proteins were transferred onto PVDF membrane (Bio-Rad). These membranes were blocked with 5% Milk in TBST for 1 hour shaking at room temperature and probed with respective antibodies overnight shaking at 4°C. Membranes were washed with 1X TBST, three times for 5 minutes each wash and then probed with secondary antibody for 1 hour shaking at room temperature before being washed as before. The membranes were developed using Immun-Star HRP Substrate onto X-Ray film (Thermo Fisher Scientific).

4.8 EXPRESSION AND PURIFICATION OF HIS-UBIQUITIN

Flag-tagged human wild type ubiquitin (pcDNA3.1-Flag-humanUb) and phosphomimetic mutant S65D ubiquitin (pcDNA3.1-Flag-humanUb-S65D) plasmids were a generous gift from Dr. Noriyuki Matsuda at the Tokyo Metropolitan Institute of Medical Science. Complementary DNA was PCR amplified (using primers purchased from Eurofins MWG Operon) with an N-terminus polyhistindine tag (His) and cloned into pENTR/D-TOPO plasmid to create pENTR-Ub-WT and pENTR-Ub-S65D) vectors via a standard Topo-cloning methodology (197) (**Figure 17**). Once sequence verified, the open reading frames from the plasmids pENTR-Ub-WT and pENTR-Ub-S65D were transferred into a pDEST-17 vector (Invitrogen) by an LR reaction using the Gateway LR Clonase II Enzyme Mix (Life Technologies) as per the manufacturer's instruction. Positive clones were selected and plasmids were extracted with the QIAprep Spin Miniprep Kit (Qiagen). The pDEST-17-Ub-WT and pDEST-17-Ub-S65D plasmids were transformed into One-Shot BL21(DE3)pLysS Chemically Competent Cells (Life Technologies). To induce the expression of the His-Ub-WT and His-Ub-S65D proteins, bacterial cultures were allowed to grow at 37°C and 250 rpm to an OD_{600} = 0.5-0.7, before the addition of Isopropyl β-D-1-thiogalactopyranoside (IPTG), for a final concentration of 1μM IPTG. The cultures were allowed to grow for another 3.5 hrs. The bacteria were pelleted at 6000 x g for 15 minutes at 4°C, followed by resuspension of the pellet in Buffer A (50 mM Tris-HCl pH 7.6, 100 mM NaCl, 0.1 mM PMSF and 1 tablet protease inhibitor/20 mL Buffer A). The bacterial suspensions were pelleted at 6000 x g at 4°C for 15 minutes, supernatants discarded and the pellets frozen overnight at -80°C. The recombinant His-Ub-WT and His-Ub-S65D proteins were purified using the TALON® Metal Affinity Resin and HisTALON™ Buffer Set (Clontech) according to the manufacturer's protocol. The purified proteins were dialyzed with Dialysis Buffer (50 mM Tris-

HCl, pH 7.6; 100 mM NaCl, 0.5 mM EDTA and 5 mM DTT), changing the buffer four times, every 6-8 hours. The dialyzed proteins were concentrated using Amicon Ultra Centrifugal Filter Devices (EMD Millipore) and the protein concentrations were measured using the DC™ Protein Assay (Bio-Rad) (**Figure 18**).

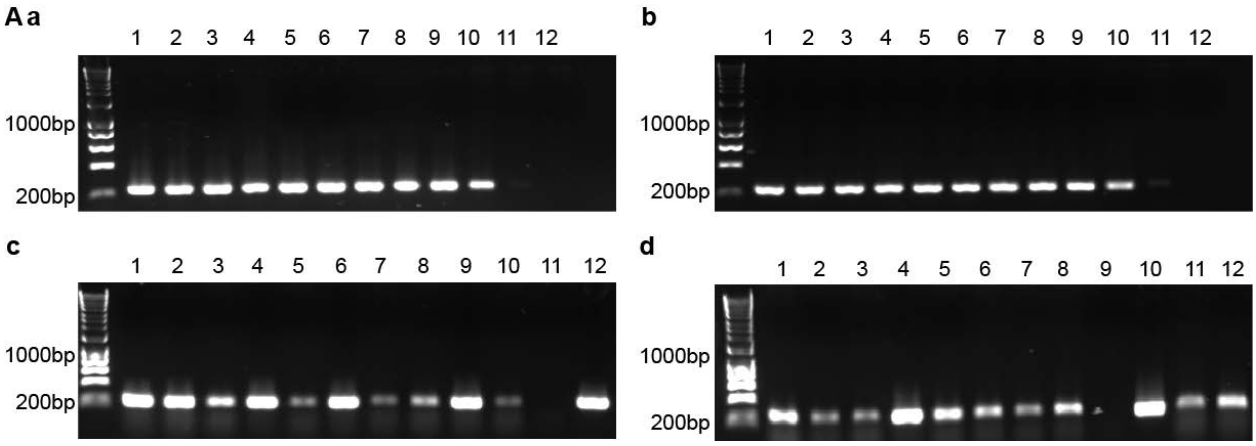

Figure 17. Generation of Ubiquitin(WT) and Ubiquitin(S65D) constructs.

(A) Optimization of the primers Ubiquitin-F and Ubiquitin-R using Platinum® *Pfx* DNA Polymerase and **(a)** pcDNA3.1-Flag-Ubiquitin(WT), or **(b)** pcDNA3.1-Flag-Ubiquitin(S65D), in gradient PCR for amplification of **(a)** His-Ubiquitin(WT) or **(b)** His-Ubiquitin(S65D) respectively, for pENTR/D-TOPO cloning into pENTR vector. **(B)** PCR amplification screen using *Taq* DNA Polymerase of mini-prep **(a)** pENTR-His-Ubiquitin(WT), or **(b)** pENTR-His-Ubiquitin(S65D) plasmids from transformed One Shot Top 10 *E.coli* cells.

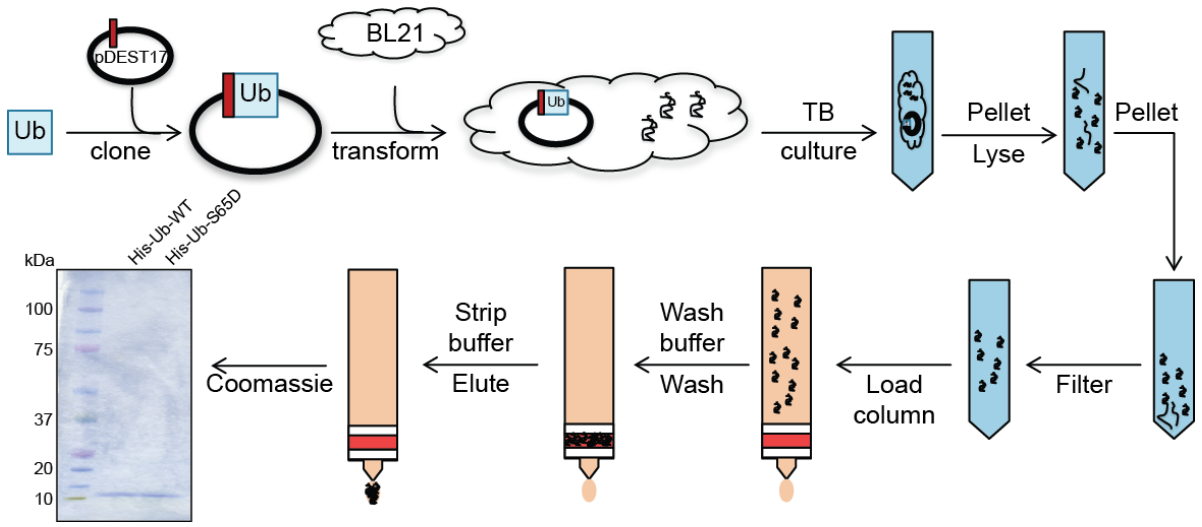

Figure 18. Purification process for His-tagged Ubiquitin constructs.

Schematic of the workflow used to create purified His-tagged ubiquitin wild type and S65D mutant and the coomassie stain of the purified His-ubiquitin proteins. Ubiquitin(WT) and Ubiquitin(S65D) was cloned into pENTR/D-TOPO vector and then transferred into the His-tag containing pDEST17 vector. BL21 cells were transformed with the pDEST17 vectors, cultured and induced to produce the proteins. The proteins were lysed, pelleted and purified following the ClonTech Talon His-column purification process. The eluate were dialyzed and concentrated to remove the purification salts and impurities, run on a SDS-PAGE gel, and coomassie stained.

4.9 IMMUNOPRECIPITATION AND UBIQUITYLATION ACTIVITY ASSAY

LN428 cells expressing HA-tagged UBE3B WT or mutant proteins (and HA-UBE3A as a positive control) were grown to 90% confluence in 100mm dishes and harvested using IP Lysis Buffer supplemented with Protease Inhibitor (both from Thermo Fisher Scientific). The lysates were rotated for 1 hour at 4°C before pelleting the cell debris. The supernatant was incubated by rotating overnight at 4°C with Anti-HA Affinity Matrix (Roche). The beads were washed with Binding Buffer (10mM $Na_2H_2PO_2$, 10mM Na_2HPO_4 and 150µM NaCl; pH 7.0), followed by washes with Ubiquitylation Assay Buffer (10 mM Tris-HCl, pH 7.5, 100 mM NaCl, and 0.5 mM

DTT). The ubiquitylation assay was performed on the beads for 2 hours at 30°C in a volume of 30µL containing 0.1µM E1 (Boston Biochem), 0.25µM of each of the E2s (UBE2A/UBE2D1/UBE2D3/UBE2G2/UBE2L3/UBE2N/UBE2S/UBE2Z) (Life Sensors), 1µM ubiquitin aldehyde (Boston Biochem), 0.75µg/µL purified His-ubiquitin (see below) and 1X Magnesium/ATP cocktail (EMD Millipore). The ubiquitylation assays were stopped by adding 2X blue Laemmli (plus β-Mercaptoethanol) and heating the samples at 70°C for 15 minutes. Ubiquitylation activity was measured by immunoblot.

4.10 AFFINITY CAPTURE OF BIOTINYLATED PROTEINS

LN428 cells that stably express BirA-UBE3B or UBE3B-BirA proteins were grown to 80% confluence in 150mm dishes and incubated in complete media supplemented with 50µM biotin to allow for biotin labeling of proteins as previous described (195). Briefly, 24 hours after biotin addition, the cells were washed three times with PBS and lysed at 25°C in 1 mL Lysis Buffer (50 mM Tris, pH 7.4, 500 mM NaCl, 0.4% SDS, 5 mM EDTA, 1 mM DTT, and protease inhibitor; Thermo Fisher Scientific) and sonicated. Triton X-100 was added to 2% final concentration. After further sonication, an equal volume of 4°C 50 mM Tris (pH 7.4) was added before additional sonication (subsequent steps at 4°C) and centrifugation at 16,000 relative centrifugal force. Supernatants were incubated with 100µl Dynabeads MyOne Steptavadin C1 (Life Technologies) overnight. Beads were collected and washed twice for 8 min at 25°C (all subsequent steps at 25°C) in 1 ml Wash Buffer 1 (2% SDS in dH_2O). This was repeated once with Wash Buffer 2 (0.1% deoxycholate, 1% Triton X-100, 500 mM NaCl, 1 mM EDTA, and 50 mM Hepes, pH 7.5), once with Wash Buffer 3 (250 mM LiCl, 0.5% NP-40, 0.5% deoxycholate,

1 mM EDTA, and 10 mM Tris, pH 8.1) and twice with Wash Buffer 4 (50 mM Tris, pH 7.4, and 50 mM NaCl). Bound proteins were removed from the magnetic beads with 50µl of Laemmli SDS-sample buffer at 95°C.

4.11 IMMUNOFLUORESCENCE AND CONFOCAL IMAGING

Cells were cultured on glass coverslips for 24 hours before being fixed with 2% paraformaldehyde for 20 minutes, permeabilized with 0.1% Triton X-100 for 15 minutes, and blocked with 2% bovine serum albumin for 45 minutes, all at room temperature. Anti-ATP Synthase β antibody (Thermo Fisher Scientific) at 1:250 dilution was incubated for 1 hour, followed by goat anti-mouse Alexa Fluor 647 (Abcam) at 1:1000 for 1 hour and DAPI stain for 30 seconds, all at room temperature. Slides were mounted and imaged on the Nikon A1 confocal microscope in the University of Pittsburgh Center for Biologic Imaging (CBI) and on the Nikon N-SIM super-resolution microscope at the USA Mitchell Cancer Institute Cellular and Biomolecular Imaging Facility.

4.12 PMITO-TIMER TRANSFECTION AND ANALYSIS

Cells were simultaneously transfected with siRNA specific to UBE3B and the plasmid encoding for the Mito-Timer reporter (Addgene). Transfection was performed as described above with the addition of pMito-Timer DNA to the transfection mixture. Cells were then plated on Fluorodish glass-bottomed dishes (World Precision Instruments), and imaged (live) 72 hours after

transfection with the Nikon A1rsi confocal microscope at the USA Mitchell Cancer Institute Cellular and Biomolecular Imaging Facility.

4.13 LIQUID CHROMATOGRAPHY TANDEM MASS SPECTROMETRY (LC-MS/MS) ANALYSIS

Immunoprecipitated samples were separated on SDS-PAGE gels (Bolt® 4-12% Bis-Tris Plus Gel, Life Technologies, Grand Island, NY) to about 1cm (150v for 10min) and stained with Simply Blue™ SafeStain (Life Technologies, Grand Island, NY). After washing with Milli-Q water, the whole stained regions were excised, washed with HPLC water and destained with 50% acetonitrile/25mM ammonium bicarbonate until no visible blue staining. Gel pieces were dehydrated with 100% acetonitrile, reduced with 10mM dithiothreitol (DTT) at 56°C for 1 hour, followed by alkylation with 55mM iodoacetamide (IAA) at room temperature for 45min in the dark. Gel pieces were then again dehydrated with 100% acetonitrile to remove excess DTT and IAA, and rehydrated with 20ng/µl trypsin in 25mM ammonium bicarbonate and digested overnight at 37°C. The resultant tryptic peptides were extracted with 70% acetonitrile/5% formic acid, speed-vac dried and re-constituted in 18µl 0.1% formic acid.

Tryptic digests were analyzed using a high-resolution liquid chromatography tandem mass spectrometer as previously described (199,202). In brief, samples were loaded with a nanoAcquity autosampler (Waters, Waltham MA) onto a capillary sample trap column, separated using a reverse phase gradient on a commercial PicoChip™C18 column and electrospray ionization source (New Objective, Inc. Woburn MA). Mass analysis was performed on a hybrid LTQ/Orbitrap Velos mass spectrometer (Thermo Fisher, Waltham MA). Data dependent

acquisition was used to acquire one high resolution full scan mass spectrum followed by 13 low resolution tandem mass spectra in the linear ion trap, with dynamic exclusion setting enabled to minimize redundant selection of precursor ions.

MS/MS spectra were searched by COMET against an indexed human database build from a non-redundant NCBI human database with the following modifications: static modification of cysteine (carboxyamidomethylation, +57.02Da) and variable modification of methionine (oxidation, +15.99Da). The mass tolerance was set to 20ppm for precursor ions and 0.8Da for fragment ions. Custom differential mass spectrometry software (dMS 1.0, InfoClinika, Seattle WA) was used to align, integrate, and link the high resolution peak areas data to the protein identification results from a COMET sequence database search (203). Relative quantitation is achieved by comparing the sum of all isotopes of particular defined peptides. Each resulting feature is defined by its particular m/z, elution time, charge state, and intensity.

5.0 RESULTS

5.1 UBE3B'S PREDICTED STRUCTURE IS HOMOLOGOUS TO THE FAMILY OF HECT E3 LIGASES

Previous reports have proposed that UBE3B belongs to the HECT subfamily of E3 ubiquitin ligases (204). However, there are no reports on the predicted structure or function of UBE3B. Therefore we used the software packages **P**rotein **H**omology/analog**Y** **R**ecognition **E**ngine (Phyre^2) and CLUSTALW2 to identify and align homologous proteins to UBE3B, and predict the three-dimensional structure of the different domains of UBE3B (205-207). As shown in **Figure 19*A***, the N-terminus of UBE3B is predicted to contain the calmodulin-binding (IQ) motif and the substrate binding domain. The C-terminus of UBE3B is the HECT domain, which is comprised of two lobes, the N-lobe that is predicted to bind to the E2(s), and the C-lobe that is predicted to contain the catalytic cysteine, which forms a covalent thioester bond with ubiquitin. The N- and C- lobes are connected via a flexible linker. To evaluate the conserved IQ motif and HECT domain of UBE3B, we aligned each with other homology motifs/domains (**Figures 19*B* and *C***). Details of the alignment of either the IQ motif or the HECT domain with the top seven sequences as ranked by Phyre^2 are given in **Tables 4 and 5**.

A

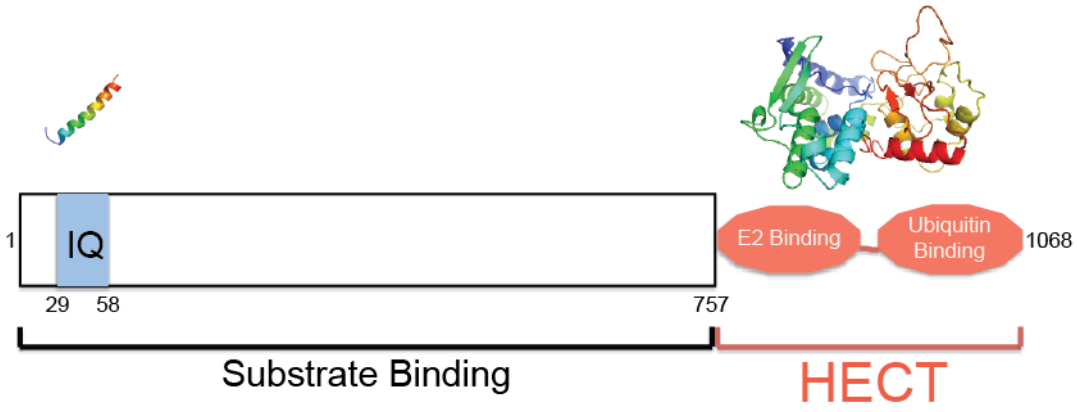

B

```
UBE3B                          RERAAVVIQAHVRSFLCRSRLQRDIRREID  58
Myosin-5A                      -RAACIRIQKTIRGWLLRKRYLCMQRAAI- 794
Myosin Va                      --AACIRIQKTIRGWLMRKKYMRMRRGD-- 794
Myosin IC                      RQSLATKIQAAWRGFHWRQKFLR------- 721
Myosin                         --DVIIAFQAQCRGYLARKAFAK------- 814
SM Myosin Heavy Chain          --DVIIAFQAQCRGYLARKAFAKRQQQLE- 820
Muscle Myosin Heavy Chain      --KIMSWMQAWARGYLSRKGFKK------- 802
Myosin Heavy Chain             --KIISMFQAHIRGYLIRKAYKKLQDQRI- 806
                                       :*   *.:  *.
```

C

```
UBE3B VEVSDDQDTGDTLGSVLRGFFTIRKREPGGRLPTSSTCFNLLKLPNYSKKSVLREKLRYA 1058
UBE3C G-----------------------GSDLERLPTASTCMNLLKLPEFYDETLLRSKLLYA 1073
Huwe1 F-------------------QIHRDDRSTDRLPSAHTCFNQLDLPAYESFEKLRHMLLLA 4363
Nedd4 F-------------------TVEQWG-TPEKLPRAHTCFNRLDLPPYESFEELWDKLQMA 1308
Itch  F-------------------CIEKVG-KENWLPRSHTCFNRLDLPPYKSYEQLKEKLLFA 893
HACE1 F-------------------TIAAVPYTPNLLPTSSTCINMLKLPEYPSKEILKDRLLVA 898
HECW2 F-------------------CVEKWG-KITALPRAHTCFNRLDLPPYPSFSMLYEKLLTA 1562
                                    ** : **:* *.** : .   *   *  *
```

Figure 19. Alignment of HECT E3 ligases with UBE3B.

(A) Schematic of UBE3B showing the IQ domain (amino acids 29-58) and the HECT domain (amino acids 757-1068). The proposed 3-D structures of the IQ and HECT domains using Phyre[2] are shown above the schematic. The N-terminus of HECT domains are known to bind to substrate. The HECT domain is composed of two lobes; the N-lobe binds the E2(s), while the C-lobe contains the catalytic cysteine that binds ubiquitin. **(B)** Alignment of UBE3B with calmodulin binding domains as predicted by Phyre[2] and using CLUSTALW2. **(C)** Alignment of UBE3B with HECT E3 ligase domains as predicted by Phyre[2] and using CLUSTALW2. The conserved catalytic cysteine is highlighted in red. "*' denotes a single fully conserved residue, ":" denotes conservation between groups of strongly similar properties, and "." denotes conservation between groups of weakly similar properties.

Table 4. Details of the top seven sequence alignments with the IQ motif of UBE3B using Phyre[2].

Rank	Template	Alignment Coverage %	Confidence	%ID
1	Myosin-5a	90	86.7	32
2	Myosin Va	83	79.0	31
3	Unconventional Myosin-1C	73	77.4	39
4	Myosin	66	77.0	24
5	Smooth muscle myosin heavy chain	86	74.9	19
6	Myosin heavy chain, muscle	66	74.3	30
7	Myosin heavy chain	86	74.3	30

The Alignment Coverage, Confidence and % ID for the IQ motif are shown. The Alignment Coverage gives the percentage of alignment between the query sequence and the template, the Confidence represents the probability (from 0-100) that the match between the query sequence and the template is a true homology, and the % ID is the likelihood the model is accurate. For extremely high accuracy models the % ID should be above 30-40% however, if the confidence is high even very low % ID (<15%) can be very useful.

Table 5. Details of the top seven sequence alignments with the HECT domain of UBE3B using Phyre[2].

Rank	Template	Alignment Coverage %	Confidence	%ID
1	Rsp5	97	100.0	34
2	Huwe1	97	100.0	37
3	HECT, E3 ligase	97	100.0	34
4	Nedd4-like	96	100.0	36
5	Smad	96	100.0	33

6	HECT, E3 ligase	97	100.0	30
7	Ubr5	38	100.0	30

The Alignment Coverage, Confidence and % ID for the HECT domain are shown. The Alignment Coverage gives the percentage of alignment between the query sequence and the template, the Confidence represents the probability (from 0-100) that the match between the query sequence and the template is a true homology, and the % ID is the likelihood the model is accurate. For extremely high accuracy models the % ID should be above 30-40% however, if the confidence is high even very low % ID (<15%) can be very useful.

5.2 KNOWN MUTATIONS IN UBE3B

From GWAS studies in humans, fourteen patients from 11 different families were found with homozygous mutations in *UBE3B* that resulted in KOS (157,159,191,192). One pair of monozygotic twins was found to carry a homozygous missense mutation in *UBE3B* that resulted in the amino acid R922 to C mutation and gave rise to autism and not KOS (193). All the known human UBE3B mutations so far are summarized in **Figure 20**. It is important to note that patients with homozygous missense mutations before the catalytic HECT domain presented with milder craniofacial dysmorphisms and no blepharophismosis, suggesting the importance of the HECT domain for the proper functioning of UBE3B (157,159,191,192).

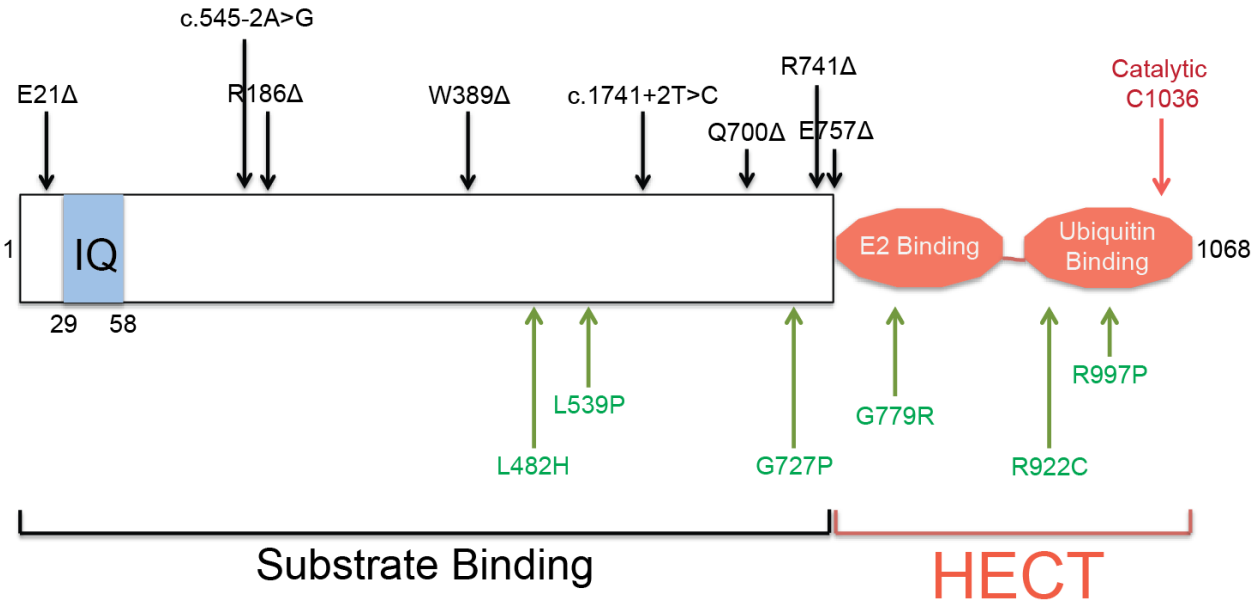

Figure 20. Schematic of UBE3B with known mutations.

UBE3B is 1068 amino acids long and consists of an IQ motif (denoted in blue) and a HECT domain (denoted in peach). Above the protein schematic (in black) are truncating mutations, while below the schematic (in green) are missense mutations. The N-terminus of HECT E3 ligases contain the substrate binding sites. The C-terminus consists of two lobes, the N-lobe contains the E2 binding sites, and the C-lobe contains the ubiquitin binding site and the catalytic cysteine. Amino acid 1036 is proposed to be the catalytic cysteine of UBE3B.

5.3 UBE3B ASSOCIATES WITH THE MITOCHONDRIA

To determine the subcellular localization of UBE3B and if the HECT domain affected localization, we created glioblastoma (LN428) cell lines that stably overexpress the different UBE3B constructs with copGFP tags (Schematic of constructs are shown in **Figure 21 and 22**). Using confocal microscopy on fixed cells, we determined that a majority of wild type UBE3B, UBE3B(C1036A), UBE3B(R922C), UBE3B(R215C/I1059F) and UBE3B(R346Q) co-localized

with the mitochondrial marker ATP Synthase β, while UBE3BΔHECT is significantly more cytosolic (**Figures 23 and 24**).

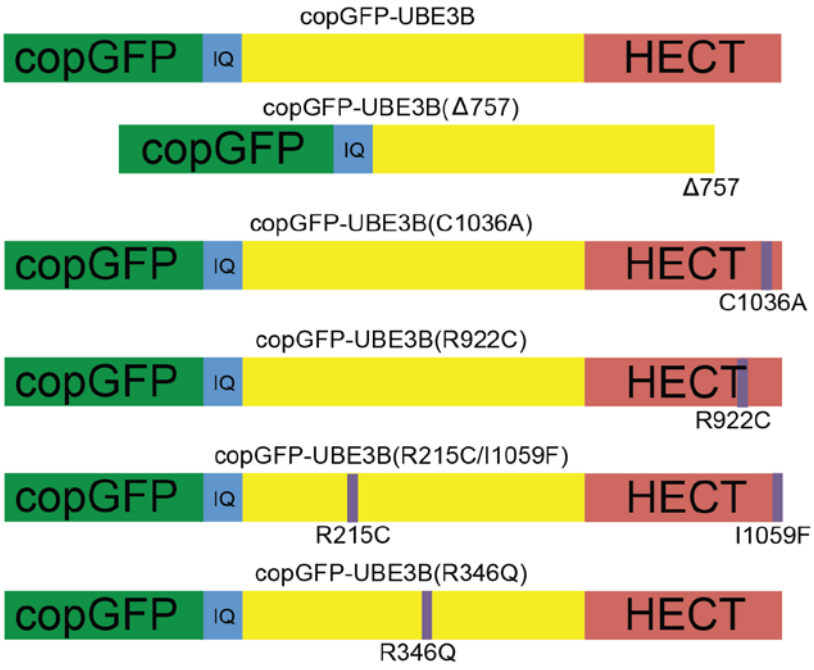

Figure 21. Schematic of copGFP-UBE3B constructs.

Schematic depicting the UBE3B wild type and mutant constructs with N-terminus copGFP tag that were stably overexpressed in LN428 cells. The copGFP tag is in green, UBE3B is in yellow, the IQ motif is in blue, the HECT domain is a pink, and the position of the point mutants are in purple.

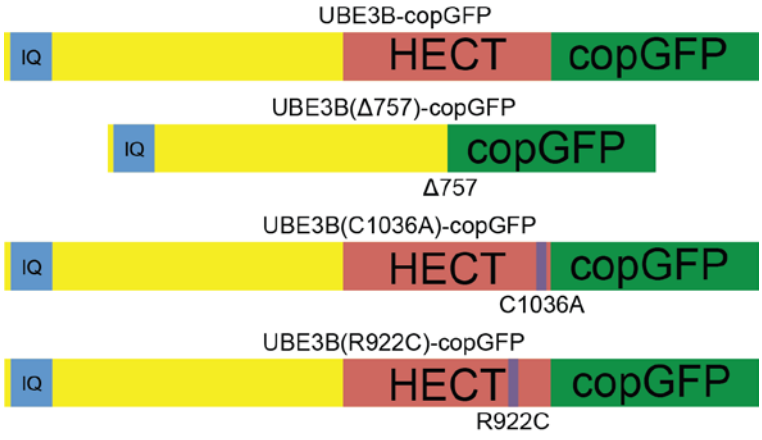

Figure 22. Schematic of UBE3B-copGFP constructs.

Schematic depicting the UBE3B wild type and mutant constructs with C-terminus copGFP tag, that were stably overexpressed in LN428 cells. The copGFP tag is in green, UBE3B is in yellow, the IQ motif is in blue, the HECT domain is a pink, and the position of the point mutants are in purple.

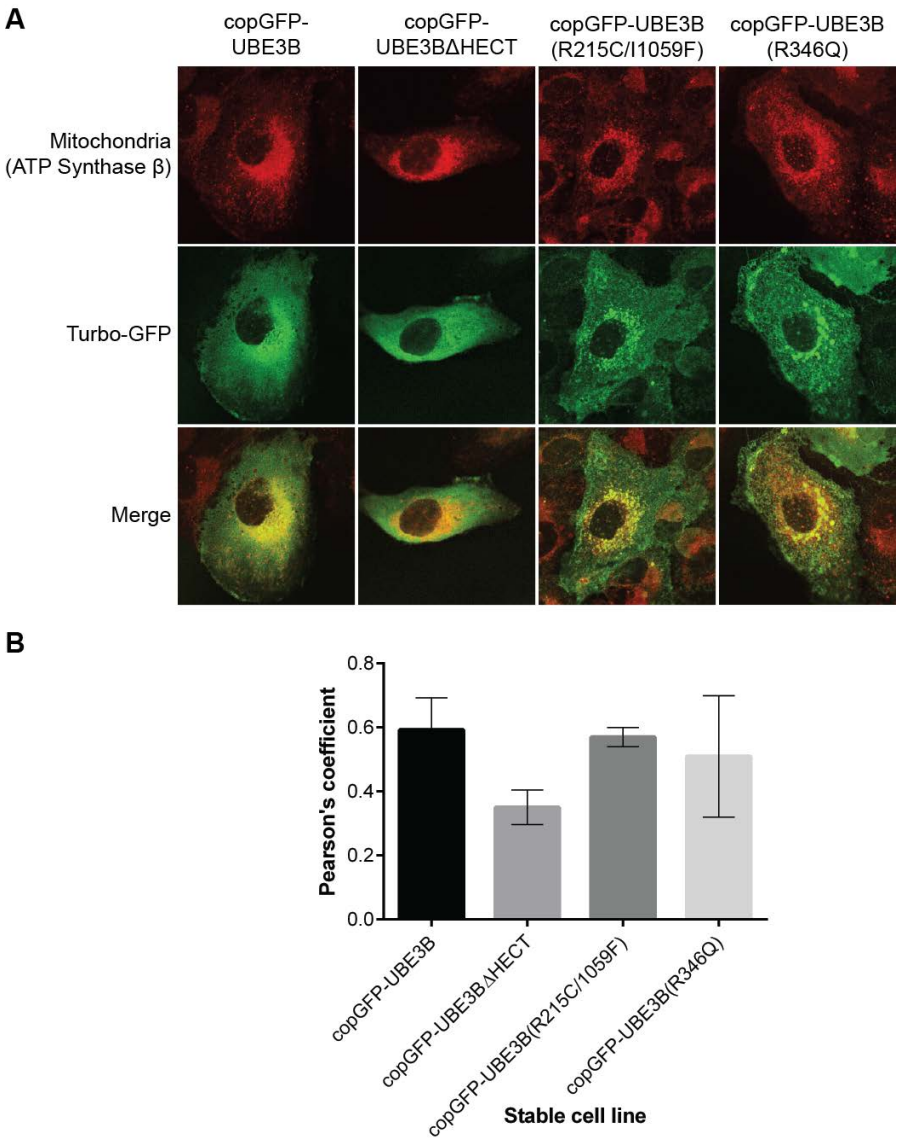

Figure 23. Immunofluorescence showing the association of copGFP-UBE3B wild type and mutants with the mitochondria.

(A) LN428 cells were transduced with lentiviral particles to create stable cell lines that expressed copGFP-UBE3B, copGFP-UBE3BΔHECT, copGFP-UBE3B(R215C/I1059F) or copGFP-UBE3B(R346Q) protein. The mitochondria were stained with ATP Synthase β as a marker, fixed and imaged using the Confocal A1 Nikon Microscope. **(B)**

Quantification of the co-localization of UBE3B with the mitochondrial marker ATP Synthase β, using NIS Element software and PRISM.

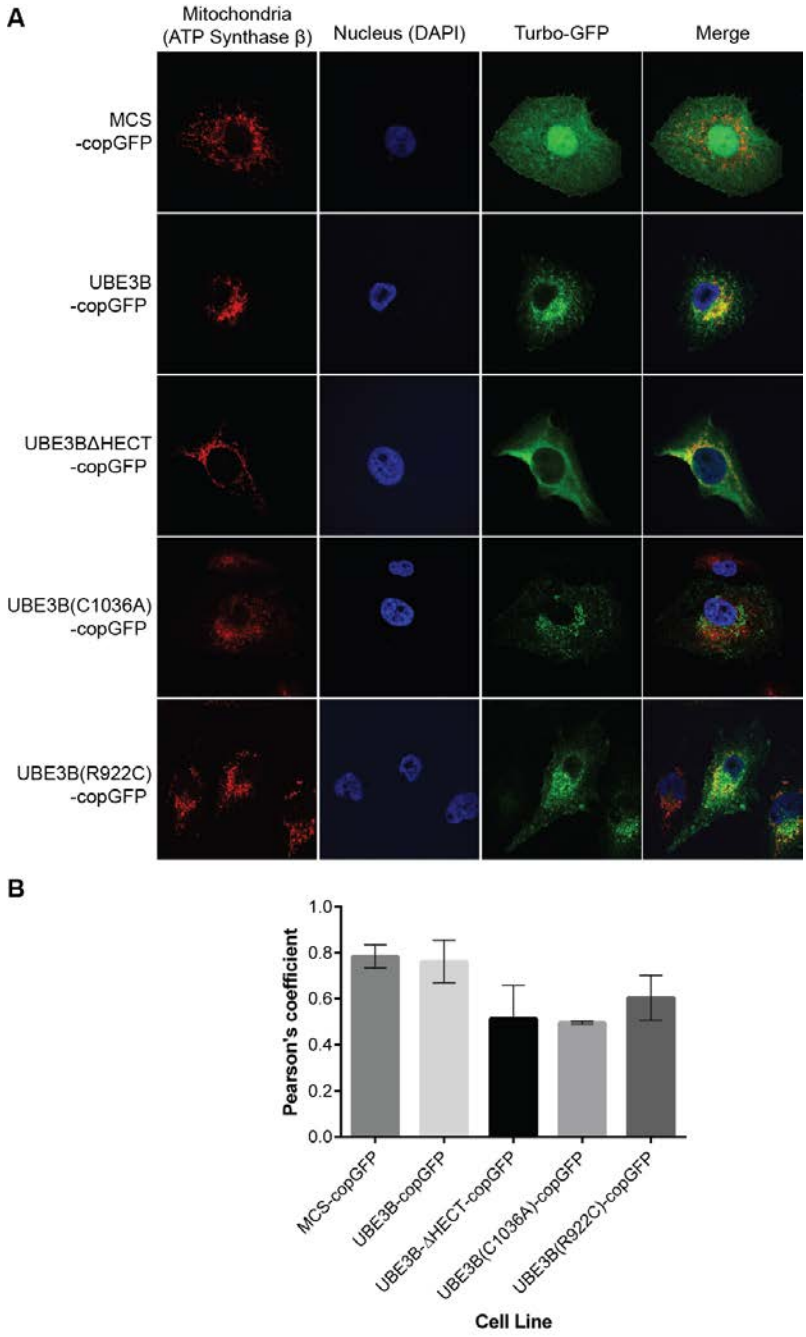

Figure 24. Immunofluorescence showing the co-localization of UBE3B-copGFP wild type and mutants with the mitochondria.

(A) LN428 cells were transduced with lentiviral particles to create stable cell lines that expressed copGFP, UBE3B-copGFP, UBE3BΔHECT-copGFP, UBE3B(C1036A)-copGFP or UBE3B(R922C)-copGFP protein. copGFP was used as a positive GFP control. The mitochondria were stained with ATP Synthase β and the nucleus with DAPI, fixed and imaged using the Confocal A1 Nikon Microscope. **(B)** Quantification of the co-localization of UBE3B with the mitochondrial marker ATP Synthase β, using NIS Element software and PRISM.

At this point we decided to continue the project only with the C-terminus copGFP constructs, namely, UBE3B-copGFP, UBE3BΔHECT-copGFP and UBE3B(C1036A)-copGFP because the location of the copGFP tag does not seem to affect the subcellular localization of UBE3B.

We confirmed the immunofluorescence results by subcellular fractionation, where we isolated the mitochondria from the stable expressing cell lines, followed by immunoblot analysis (**Figure 25*A***). To confirm that UBE3B's subcellular recruitment to the mitochondria was not an artifact of the overexpression of the tagged proteins, we isolated mitochondria from the control LN428 cells and showed the presence of endogenous UBE3B in the mitochondrial fraction (**Figure 25*B***).

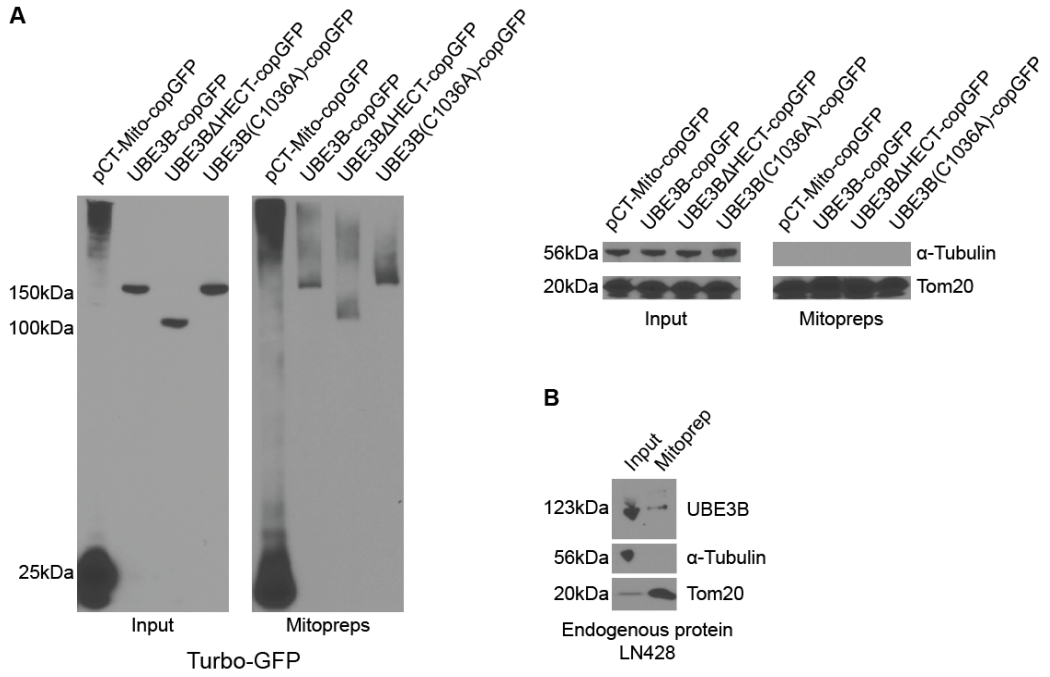

Figure 25. Subcellular fractionation of UBE3B-copGFP wild type and mutants confirm the immunofluorescence co-localization of UBE3B with the mitochondria.

(A) To confirm the immunofluorescence results, subcellular fractionation of the stable cell lines was performed, and the mitochondria were isolated. Immunoblots to compare the whole cell lysates (input) and mitochondrial preps (mitopreps) were performed. Ab specific to TurboGFP was used to detect UBE3B-copGFP proteins, α-Tubulin was used as a cytosolic marker, and Tom20 was used as a mitochondrial marker. **(B)** To show that endogenous UBE3B is on the mitochondria and the immunofluorescence and subcellular fractionation results in *A* and *B* are not an artifact of overexpression, we performed subcellular fractionation and immunoblot for endogenous UBE3B in LN428 cells.

5.4 KNOCKDOWN OF UBE3B DECREASES MITOCHONDRIAL FUNCTION AND CHANGES THE MORPHOLOGY OF THE MITOCHONDRIA

Since we found that UBE3B associates with the mitochondria, we wanted to identify if changes in UBE3B protein expression levels affected mitochondrial morphology. To do this UBE3B was

depleted (knocked down; KD) in LN428 cells using siRNA from Ambion (**Figure 26*A***). Via MTS Assay, it was determined that loss of UBE3B resulted in decreased NAD(P)H-dependent cellular oxidoreductase enzyme activity, an indicator of decreased cellular survival and mitochondrial function (**Figure 26*B***). Using fixed cell confocal microscopy we saw that the mitochondria of UBE3B-KD cells were more punctate-like, instead of the more linear and reticular network observed in the scrambled siRNA (negative control) cells (**Figure 26*C***). To confirm that the fragmented phenotype of the mitochondria in the UBE3B-KD was due to the loss of mitochondria, we measured the total number of mitochondrial voxels, and found that it was significantly decreased in the UBE3B-KD cells as compared to the healthy control cells (**Figure 26*D***).

A novel methodology to study mitochondrial function and biogenesis in cells uses the fluorescent probe, pMitoTimer (208-211). The pMitoTimer vector expresses a mitochondrially-targeted green fluorescent protein whose emission spectrum shifts irreversibly towards the red when oxidized (209). Seventy-two (72) hours after co-transfection of pMitoTimer and either UBE3B siRNA or scrambled siRNA, the cells were imaged using live cell confocal microscopy. We saw a significantly higher red to green ratio in the UBE3B-KD cells, thus supporting our results that mitochondrial function and turnover are affected when UBE3B is depleted from the cells (**Figure 26*E***). It is important to note that since pMitoTimer is a dual-emission probe and a number of factors can affect its readout, follow-up experiments need to be performed to confirm these results.

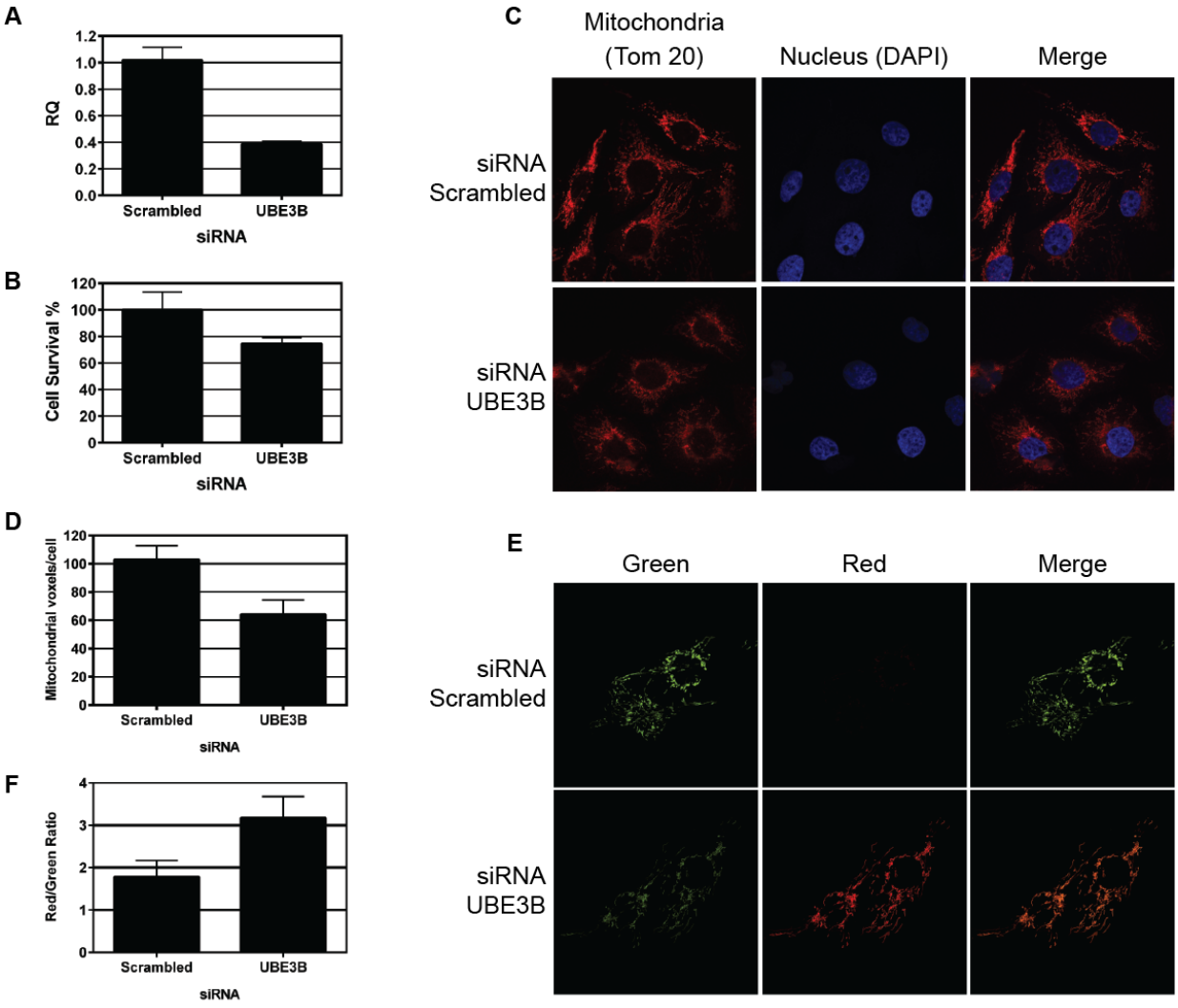

Figure 26. Knockdown of UBE3B results in changes in mitochondrial morphology and a decrease in mitochondrial function.

LN428 cells were transfected with 90nM (final concentration) siRNA UBE3B or scrambled siRNA for 72 hours before being used for subsequent experiments. **(A)** qRT-PCR was performed to measure the knockdown of UBE3B mRNA expression levels. β-Actin was used as the endogenous control and mRNA expression was normalized to siRNA untreated cells. **(B)** To determine cellular survival, 2000 cells/well were plated 24 hours after siRNA transfection. After 48 hours incubation, an MTS Assay was performed. **(C)** To determine if there are changes to the mitochondrial morphology after depletion of UBE3B protein, confocal imaging was performed on fixed cells, 72 hours after knockdown (transfection of siRNA). ATP Synthase beta is the mitochondrial marker (excitation wavelength: 647 nm, emission wavelength: 666 nm). **(D)** Z-stacking using the confocal microscope on the fixed

cells from (C) was performed to determine the changes in mitochondrial voxels in UBE3B-KD cells as compared to scrambled treated cells. **(E)** To determine if UBE3B knockdown affected mitochondrial biogenesis, cells were co-transfected with UBE3B siRNA and the ratiometric reporter vector pMito-Timer. Confocal imaging was performed 72 hours after transfection. **(F)** Quantitation of collected images from (E) show a decrease in mitochondrial biogenesis in knockdown cells.

5.5 UBE3B CAN SELF-UBIQUITYLATE USING ITS HECT-DOMAIN CATALYTIC CYSTEINE

HECT E3 ligases have been shown to form poly-ubiquitylation chains on their catalytic HECT domains before the transfer of the ubiquitin chain to their substrates (152,212). Therefore, the ubiquitylation activity of these ligase proteins can be determined in *in vitro* ubiquitylation assays even without a known substrate. Recent publications have shown a novel activation mechanism for Parkin wherein phospho-mimic ubiquitin (Ub-S65D) can activate Parkin and increase the poly-ubiquitin chain formation on Parkin as opposed to wild type ubiquitin (Ub-WT) (101,105,106). We expressed and purified recombinant His-tagged wild type ubiquitin (His-Ub-WT) or His-tagged phospho-mimic ubiquitin (His-Ub-S65D) (**Figures 17 and 18**) and used these to determine if UBE3B's E3 ligase function is activated in the same way as Parkin in cells. We performed an *in vitro* ubiquitylation activity assay using either His-Ub-WT or His-Ub-S65D and immunoprecipitated N-terminus HA-tagged UBE3B (HA-UBE3B) (**Figure 27*A***). We did not see a difference in the formation of poly-ubiquitin chains on UBE3B between the two forms of ubiquitin. Next, we wanted to determine if poly-ubiquitylation on UBE3B was time dependent. For this we measured the *in vitro* ubiquitylation activity on UBE3B at 30 minute

intervals from 0 hours up to 3 hours (**Figure 27*B***). An increase in the poly-ubiquitin chain formation is seen with the increase in time, with a plateau at 2 hours.

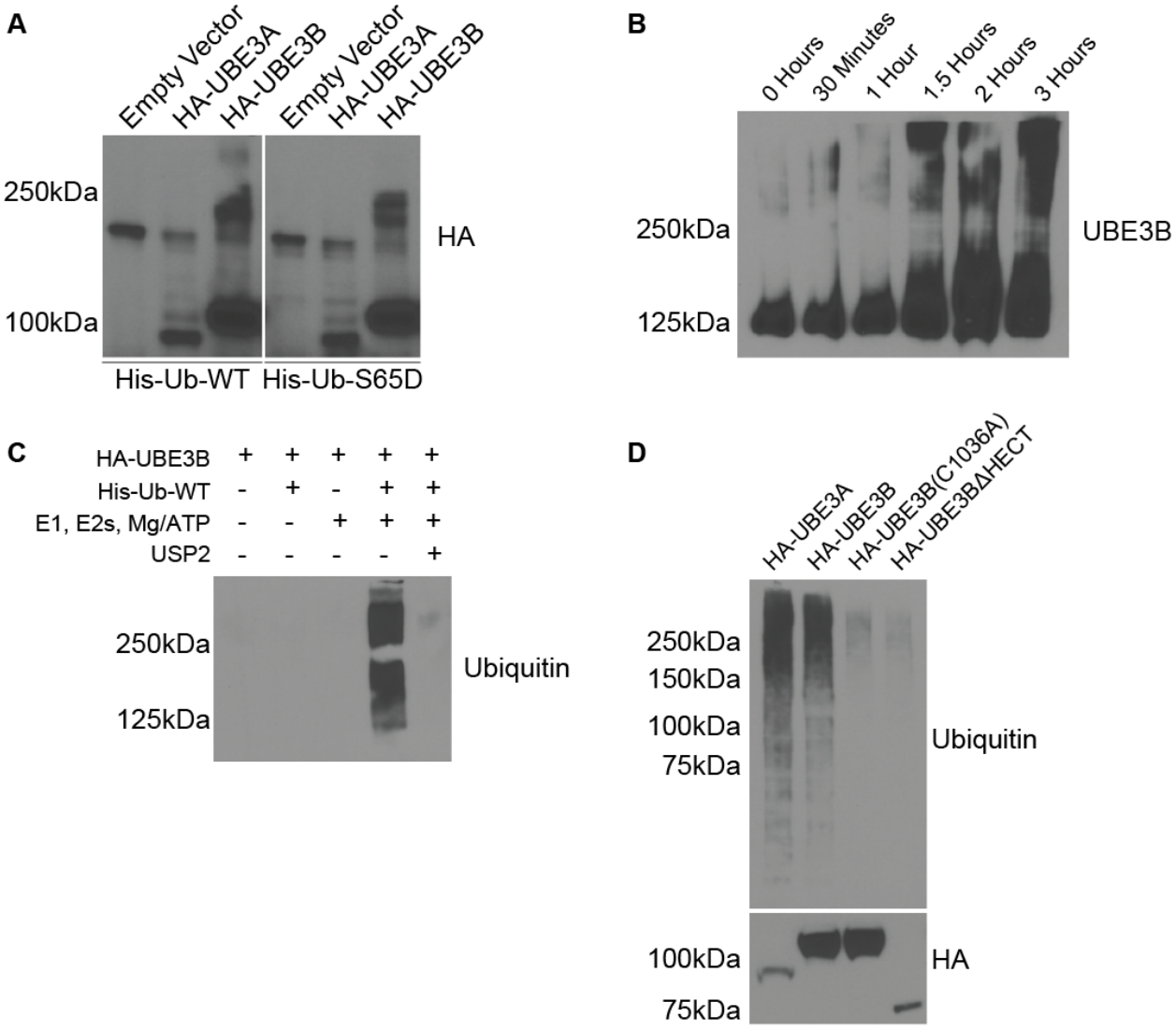

Figure 27. UBE3B is a HECT E3 ligase that can self-ubiquitylate its catalytic cysteine C1036 *in vitro*.

Cell lysates from LN428 cells that stably express UBE3A, UBE3B, UBE3BΔHECT or UBE3B(C1036A), all with N-terminal HA tags were immunoprecipitated (IPed) using Anti-HA Affinity Matrix and subjected to ubiquitylation activity assays. The ubiquitylation assays were carried out in 30µL reactions with 0.1µM E1, 0.25µM of each of the E2s (UBE2A/UBE2D1/UBE2D3/UBE2G2/UBE2L3/UBE2N/UBE2S/UBE2Z), 1µM ubiquitin aldehyde, 0.75µg/µL His-ubiquitin and 1X Magnesium/ATP cocktail, unless otherwise stated. The HECT E3 ligase, UBE3A was used as a positive control. **(A)** Ubiquitylation activity assay was performed *in vitro* using His-tagged wild type ubiquitin

(His-Ub-WT) or phosphomimetic ubiquitin (His-Ub-S65D). **(B)** Time dependent increase in poly-ubiquitin chain formation was seen in the ubiquitylation assay. **(C)** Polyubiquitin chain formation was lost when ubiquitin, or E1, E2s and ATP were removed from the reaction mix, or after 20 µg of the catalytic core of the deubiquitinating enzyme USP2 was added to a completed reaction for 30 minutes at 37°C. **(D)** Polyubiquitin chains were not formed in the reactions containing the catalytic inactive (HA-UBE3B(C1036A)) and HECT delete (HA-UBE3BΔHECT) mutants of UBE3B. Completed reactions were applied to immunoblot for analysis of ubiquitylation with hemagglutinin (HA), UBE3B or Ubiquitin (Ub) antibodies. Bottom panel shows comparable loading of the immunoprecipitated proteins. Representative immunoblots from three independent experiments are shown. Antibodies used for each of the immunoblots are listed on the side of the panels.

To show that this ubiquitylation activity was specific to UBE3B and not a reaction between the cocktail of E1, E2s, ubiquitin and Mg^{2+}/ATP, a drop-out ubiquitylation assay was performed. Here, one enzyme/set of enzymes was missing from each reaction. As a control to show that the smear seen was indeed ubiquitylation, the catalytic core of the deubiquitylating (DUB) enzyme USP2 was added to the *in vitro* ubiquitylation assay that contained all the enzymes after 2 hours (**Figure 27*C***) (210). Lastly, to show that the HECT domain of UBE3B, specifically the proposed catalytic cysteine in the HECT domain, catalyzes the formation of the poly-ubiquitylation chains observed, the ubiquitylation activity was performed using UBE3B with an inactive catalytic cysteine (HA-UBE3B(C1036A)) or UBE3BΔHECT (HA-UBE3BΔHECT) (**Figure 27*D***). As shown, the mutation of C1036 or the deletion of the HECT domain eliminated the ubiquitylation activity.

5.6 UBE3B INTERACTS WITH CALMODULIN VIA ITS IQ MOTIF

As seen from **Figure 19*B*,** UBE3B contains a proposed IQ motif near its N-terminus, suggesting an interaction between UBE3B and calmodulin (213-215). Thus far, there are no known E3 ligases that interact with calmodulin. Therefore, determining if calmodulin binds to and/or regulates UBE3B will be a novel finding. Since HA-tagged UBE3B (HA-UBE3B) is readily immunoprecipitated from stable LN428/HA-UBE3B cells, we analyzed the immunoprecipitated proteins by mass spectrometry. Quantification results for two proteotypic CaM peptides showed a significant increase in signal for both peptides bound to either HA-UBE3B or HA-UBE3B(C1036A), with only a background-level signal in the control cells (**Figure 28*A***). The interaction between UBE3B and calmodulin was also confirmed by immunoprecipitation of HA-UBE3B followed by immunoblot for calmodulin (**Figure 28*B***). These results were also confirmed when calmodulin (eGFP-HA-His-CALM1) was overexpressed in UBE3B-copGFP cells, immunoprecipitated and the isolated proteins were probed for UBE3B by immunoblot (**Figure 28*C***).

To more elegantly determine if the UBE3B and calmodulin interaction is observed in cells and not limited to a protein-protein interaction in cell lysates, we developed the Bio-ID system to validate UBE3B interacting proteins by fusing the promiscuous *E. coli* biotin ligase BirA-R118G to either the N- or C-terminus of UBE3B and developed stable cell lines expressing each (**Figure 29**). These cells were then pulsed with biotin (50 µM; 24 hrs) and the resulting biotinylated proteins represent those ‘in proximity’ of UBE3B, within 10 nm (195,216). In support of the mass spectrometry and IP/IB results above, we find that calmodulin is strongly biotinylated in cells expressing either BirA-UBE3B or UBE3B-BirA but not in control cells and only when biotin is added to the cells 24 hrs prior to lysate preparation (**Figure 28*D***). This

supports our contention that UBE3B and calmodulin interact and is in-line with earlier reports that the resulting biotinylated proteins are within 10 nm of the BirA-fusion protein in cells (216).

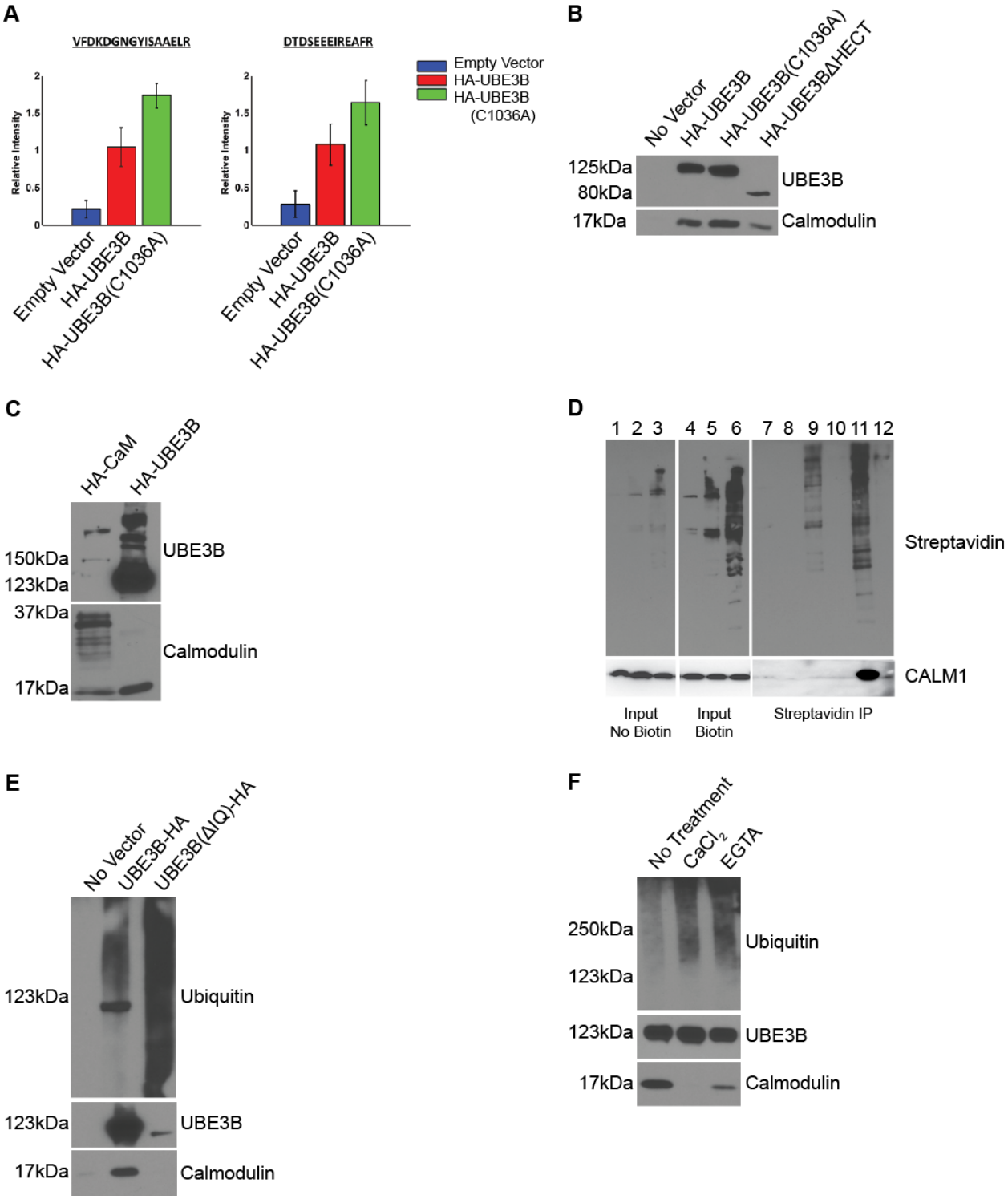

Figure 28. UBE3B associates with Calmodulin through its IQ motif and the interaction is calcium-dependent.

(A) Quantification results for two proteotypic calmodulin peptides, VFDKDGNGYISAAELR and DTDSEEEIREAFR. Bar graphs of mean and SEM following affinity purification and high resolution LC-MS analysis of LN428 cells expressing an empty vector, wild type HA-tag UBE3B (HA-UBE3B), and the catalytic inactive UBE3B with an HA-tag (HA-UBE3B(C1036A)). **(B)** Immunoblot to confirm the interaction of CaM to UBE3B as seen by LC-MS. **(C)** To confirm that the interaction between CaM and UBE3B is specific, we performed reverse IPs, where eGFP-HA-His-CALM1 was overexpressed in UBE3B-copGFP cells and lysates were HA-IPed. Immunoblots were probed against CaM and UBE3B antibodies. We used HA-UBE3B as a positive control for the IPs, and the expected size of UBE3B-copGFP is 150kDa. **(D)** BioID expression of BirA-UBE3B and UBE3B-BirA with Streptavidin IP to confirm the HA-UBE3B and CaM interaction. Lanes 1-6 are Input and Lanes 7-12 are Streptavidin IP samples. Lanes 1-3 and 7-9 were not treated with Biotin; and Lanes 4-6 and 10-12 were treated with 5 μM Biotin for 24 hours before harvest. Lanes 1, 4, 7 and 10 are cells with no vector; Lanes 2, 5, 8 and 11 are cells that stably express BirA-UBE3B protein; and Lanes 3, 6, 9 and 12 are cells that stably express UBE3B-BirA protein. **(E)** LN428 cells were transiently transfected with UBE3BΔIQ-HA plasmid followed by immunoprecipitation with HA-Affinity Matrix beads after 24 hours. Ubiquitylation assay as described in Figure 26 was performed on the beads and immunoblots were performed on the reaction using Ubiquitin, HA and CaM antibodies. **(F)** CaM interaction with UBE3B is lost when IP beads are washed with $CaCl_2$. Ubiquitylation is increased when CaM is not bound to UBE3B.

To show that the interaction between calmodulin and UBE3B is indeed through the IQ motif, we created UBE3B(ΔIQ)-HA, where the IQ motif of UBE3B was deleted (amino acids 1-63) (**Figure 28*E***). Immunoblot confirmed the loss of this CaM-UBE3B interaction after immunoprecipitation. Interestingly, we also saw an increase in poly-ubiquitin chains with UBE3B(ΔIQ) compared with wild type UBE3B in the *in vitro* ubiquitylation assays (**Figure 28*E***).

Lastly, we wanted to determine if the CaM-UBE3B binding was calcium dependent or independent. To do this, we washed the immunoprecipitation HA-Affinity Matrix beads with

Binding and Ubiquitylation Buffers supplemented with either 5mM $CaCl_2$ or 1mM EGTA (a calcium specific chelator) before the *in vitro* ubiquitylation assays. CaM binding is lost with the $CaCl_2$ washes, while the ubiquitylation activity of UBE3B is increased (**Figure 28*F***).

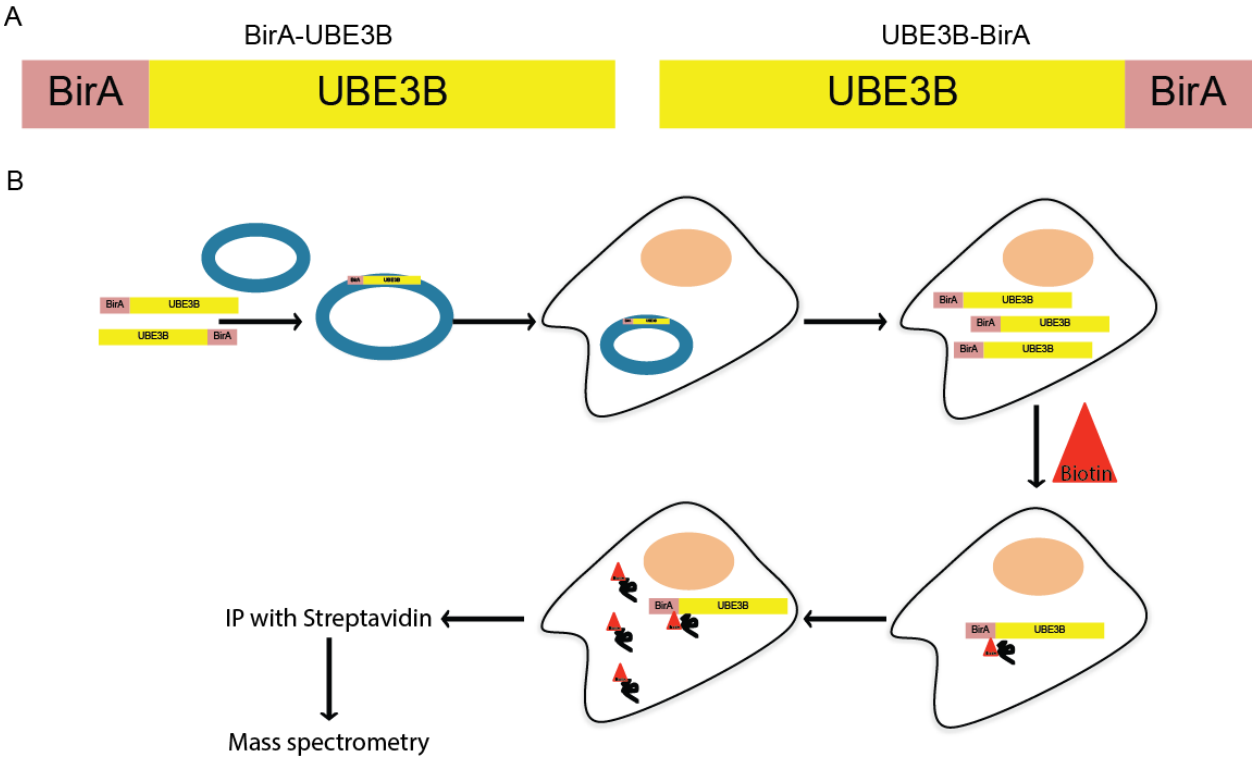

Figure 29. Schematic of BirA and UBE3B fusions and expression process.

(A) Schematic of the two Biotin Ligase (BirA) and UBE3B constructs used. One has BirA on the N-terminus of UBE3B, and the other has BirA on the C-terminus of UBE3B. **(B)** Schematic for the creation of stable cell lines expressing either BirA-UBE3B or UBE3B-BirA proteins. The fusions were inserted into a lentivirus vector and stable cell lines were created. Cells were treated with 50 nM Biotin for 24 hours, harvested, immunoprecipitated with Streptavidin beads and the biotinylated proteins were analyzed using LC-MS.

6.0 DISCUSSION

Ubiquitylation is a well-controlled, tightly regulated three step post translational process that controls the fate of its target protein. The third step involves an E3 ligase that controls the substrate specificity and timing of ubiquitylation with every E3 ligase interacting with only specific substrate proteins. HECT E3 ligases are the second most abundant family of E3 ligases (123,217). It is important to note that HECT E3 ligases retain the decision of ubiquitylation type because of their distinctive mode of action while RING E3 ligases are more promiscuous in the type of ubiquitylation they perform and depend on their E2 partner to define the type of ubiquitylation (218). Here we focus on defining the function and identifying the interactors of the novel HECT E3 ligase UBE3B in glioblastoma cells.

We had previously performed a synthetic lethal siRNA screen in glioblastoma cells and determined that knockdown of UBE3B resulted in sensitization of the cells to Temozolomide (TMZ) treatment (200). In the same study we also found that within 30 minutes of treatment with TMZ, ROS was produced in the cell, specifically in the mitochondria. Besides the GWAS studies that identified homozygous mutations in UBE3B as the cause of KOS, no studies have been published about the cellular function of UBE3B. From our Phyre^2 and CLUSTALW2 alignments, UBE3B is proposed to be a HECT E3 ligase with an IQ motif at its N-terminus and a C-terminus HECT domain, with the region around the catalytic cysteine being highly conserved and homologous to other well-studied E3 ligases such as UBE3C, Huwe1, Nedd4, Itch and

Hace1. Our first goal was to determine the subcellular localization of UBE3B. From the stable cell lines that expressed UBE3B with a copGFP tag, we saw that UBE3B associates with the mitochondria. However, when the HECT domain of UBE3B is deleted, we see a more cytosolic expression of the protein. Since the copGFP tag did not affect mitochondria localization, we decided to only use the C-terminus cop-GFP cell lines for the subcellular fractionation experiments. Here we confirmed the results of the immunofluorescence where we see a reduction of UBE3BΔHECT protein compared to UBE3B wild type and UBE3B(C1036A) proteins in the mitochondria fraction.

Next we wanted to determine if knocking down UBE3B would impact the cell, especially the mitochondria. It has been shown that the *C.elegans* ortholog of UBE3B, *oxi-1*, was required for proteasomal degradation after oxidative stress (157). We found that knocking down UBE3B using siRNA resulted in a more fragmented, punctate-like mitochondrial network compared to the tubular mitochondria of the control siRNA cells. Interestingly, mitochondrial biogenesis in UBE3B-KD cells was decreased when compared with the control. These results suggest that UBE3B might play an important role in regulating morphology and oxidative stress levels in mitochondria. We were unable to generate stable cell lines depleted of UBE3B suggesting a critical role of UBE3B in cellular survival.

From our results using the *in vitro* ubiquitylation assays, we have demonstrated that UBE3B is indeed a HECT E3 ligase that uses its catalytic cysteine to bind to ubiquitin and form poly-ubiquitin chains. Deletion of the HECT domain and inactivation of the catalytic cysteine results in loss of UBE3B's ability to form poly-ubiquitin chains. Unlike the RING-in-between-RING (RBR) E3 ligase Parkin, UBE3B's ubiquitylation activity is not enhanced by the binding of phosphomimetic ubiquitin (Ub-S65D) (105,106,219,220). HECT E3 ligases are involved in a

large number of cellular processes, from UBE3C promoting growth and metastasis of renal cell carcinoma, to Nedd4 enhancing cell proliferation and autophagy, to Itch inhibiting skin inflammation (221-223). Amongst the reported disease-associated mutations in UBE3B that cause Kaufman oculocerebrofacial syndrome (KOS), the seven different nonsense, frame-shift and splice site mutations that are predicted to cause protein truncation before or at the beginning of the HECT domain, and therefore abolish UBE3B's ligase activity, have the most severe phenotypic effects (157,159,191,192). Therefore, our results defining that the HECT domain of UBE3B is the active E3 ubiquitin ligase domain are consistent with these clinical findings.

Identifying E3 ligase substrates is extremely difficult as the interaction between the E3 ligase and substrates are generally weak and transient. One novel approach is proximity-dependent biotin labeling (BioID), a novel, semi-quantitative mass spectrometry method that is used to identify interacting proteins in cells. A recent study combined 26S proteasome inhibitor (MG132) treatment with BioID labeling to identify the interacting partners of the beta transducin repeat-containing polypeptides β-TrCP1 (FBXW1) and β-TrCP2 (FBXW11), which are part of the E3 ligase SCF complex (224). In combination with mass spectrometry, we used two different labeling methods to identify the interacting partners of UBE3B, HA-UBE3B and BirA/UBE3B fusions. CaM was one of the proteins that were identified in both the mass spectrometry experiments (**Figure 28**). From the literature, the IQ motif of proteins has been known to interact with calmodulin, the universal calcium sensor in eukaryotes (214,225-227). Calcium binding to calmodulin has been shown to induce major conformational changes in the IQ motifs and to increase the flexibility of the myosin-1c tail (228). Therefore, we believe that calmodulin might be a regulatory factor, rather than a substrate for UBE3B's function. From studies on auto-inhibition of HECT E3 ligases, one study performed by Wang et al showed that calcium binds to,

and activates the E3 ligase Nedd4 by releasing the C2 domain auto-inhibition (229). From our studies, we found that deletion of UBE3B's IQ motif abolishes the interaction with CaM and results in a significant increase of UBE3B's ability to form poly-ubiquitin chains *in vitro*. We also found that increasing the calcium concentration in the reaction releases the CaM binding with wild type UBE3B followed by an increase in UBE3B's ubiquitylation activity. Therefore we propose that an increase in calcium signaling within the cell results in the disassociation of the calmodulin interaction with UBE3B, which activates UBE3B and enhances its ubiquitylation activity.

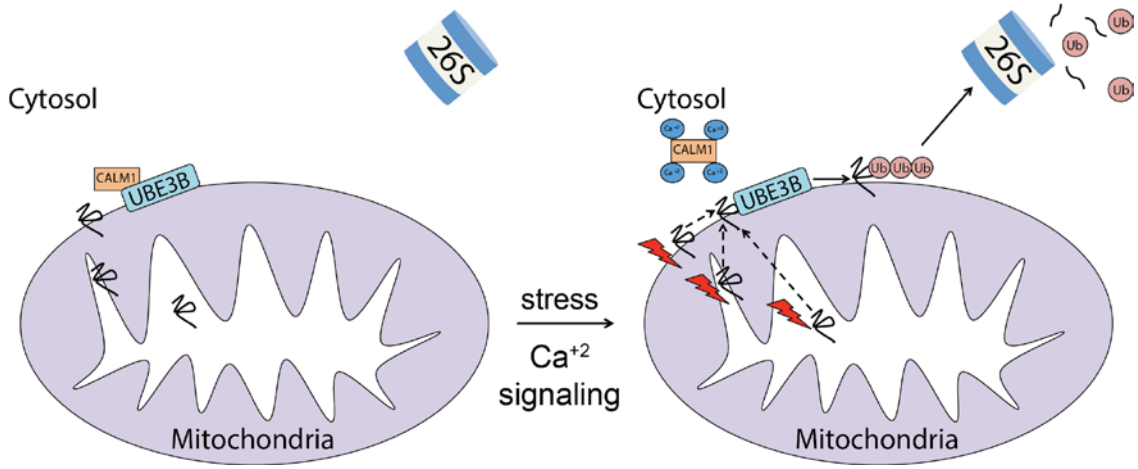

Figure 30. Schematic of UBE3B's activation in response to calcium signaling/mitochondrial stress.

We propose that the E3 ligase UBE3B associates with the mitochondria. Under normal cellular conditions, UBE3B is bound to calmodulin through its N-terminus IQ motif in a calcium-dependent manner. However, in response to mitochondrial stress the intracellular calcium levels increase thereby activating CaM and releasing it from UBE3B. CaM-free UBE3B can now bind to its substrates (potentially damaged mitochondrial proteins) and ubiquitylate substrates for degradation by the UPS.

We propose a dynamic model for the regulation of mitochondrial structure and ubiquitylation that comprises the secondary messenger calmodulin, the HECT E3 ligase UBE3B and damaged mitochondrial proteins (**Figure 30**). We hypothesize that CaM inhibits UBE3B's

E3 ligase activity. When there is an increase in calcium signaling after mitochondrial stress, CaM is activated. Activated calmodulin in turn is released from UBE3B thus allowing for its ubiquitylation activity to ubiquitylate damaged mitochondrial proteins for proteasomal degradation. Thus, identifying the substrates of UBE3B will be important to determine the clinical significance of UBE3B mutations and determine a therapeutic strategy for patients who suffer from KOS.

7.0 FUTURE DIRECTIONS

The findings during this dissertation are novel and exciting for the field of ubiquitylation. This is the first study, which we know of, that shows CaM directly interacting with and modulating the function of an E3 ligase. However this is only the beginning in the long road of discoveries for the function of, and role played by UBE3B. I would like to outline a few of these potential future directions for this project.

7.1 STUDYING THE ROLE OF CALMODULIN BINDING TO UBE3B

The interaction between UBE3B and CaM is turning out to be an exciting discovery. We saw two important results, (i) CaM binding is lost when there is an excess of Ca^{+2}, and reduced when the Ca^{+2} levels are chelated by EGTA, and (ii) UBE3B's ubiquitylation activity is increased in both these cases compared to when CaM is strongly bound. This leads us to believe that any perturbations to the intracellular Ca^{+2} levels in the cell (which could be because of an increase in ROS in the cell, or an influx of Ca^{+2} from extracellular sources) activates UBE3B's E3 ligase activity to ubiquitylate damaged proteins, thus reducing the harmful effects they can have on the overall survival of the cell. It is important to note that we were unable to create stable cell lines that expressed UBE3BΔIQ-HA protein, and transient transfection of the construct lead to the death of a high number of cells compared with the control. Therefore the next step would be to

develop an inducible system to control the expression of UBE3BΔIQ-HA protein in our cells. This way we can try and determine the death pathways that are activated when UBE3BΔIQ is overexpressed, evaluate the impact on mitochondrial morphology and function and determine the sub-cellular localization of UBE3B when not bound to CaM, among many other possible endpoints.

As seen from our mass spectrometry results in **Appendix B**, PP2A is one potential protein that is associated with UBE3B. Therefore, we can determine how the phosphorylation occurs (explained in greater detail in **Appendix B**), and if PP2A phosphorylation and CaM binding working agonistically or antagonistically to effect the function of UBE3B.

We can use the wide array of newly synthesized fluorescent protein (FP) chimeras that modulate their fluorescence in response to intracellular Ca^{+2} changes (230). Thus we can use live cell imaging to see if there are changes in the sub cellular localization of UBE3B (more recruitment to the mitochondria, perhaps?), see if there are differences between varied expression levels of UBE3B (overexpressed, normal and KD) after calcium signaling over time, or determine a good time to harvest the cells for the *in vitro* ubiquitylation assay.

We now know that the IQ motif of UBE3B is required for binding to CaM. To determine the amino acids critical for this association we can start by mutating each of the key IQ residues IQAHVRSFLCR individually to alanine. We can start combining two-three mutations at a time to determine if multiple residues are required for this interaction.

Therefore, there are a large number of experiments that can be conducted to study how the UBE3B-CaM interaction occurs and how it affects the cell.

7.2 VALIDATION OF THE INTERACTION BETWEEN UBE3B AND THE MASS SPECTROMETRY IDENTIFIED PROTEINS

The proteins identified during our mass spectrometry experiments (detailed in **Appendix B**) provide a large number of directions we can follow for this project. We are currently in the process of using the new BirA/UBE3B fusion constructs followed by mass spectrometry to confirm the HA-UBE3B results and/or identify other potential UBE3B interacting proteins. Once we have narrowed our list to highly probable hits, we can start to validate those one-by-one using methods similar to the ones we will use to study the UBE3B-CaM interaction stated above (**Section 7.1**).

7.3 EFFECTS OF DISEASE ALLELES ON UBE3B'S ACTIVITY

To date, fourteen patients with homozygous mutations in UBE3B are known to suffer from the disease KOS. These mutations are listed in **Figure 20**. It will be very interesting to study how each of these clinically relevant mutations affect the subcellular localization and activity of UBE3B in cells. Methods such as (i) ubiquitylation activity assay to determine if UBE3B's activity is affected, (ii) MTS assay to determine changes in mitochondrial function and cell survival, (iii) Cell proliferation assays such as CellTiter GLO and crystal violet, (iv) JC-1 as a marker for changes in mitochondrial membrane potential, and (v) live and fixed-cell imaging assays to determine the changes in the expression of mitofusion and mitofission markers (MFNs and Drp1), can be employed. It will also be of interest to see how/if the interaction between UBE3B and calmodulin is affected by these mutations.

7.4 E2(S) THAT BIND TO UBE3B

Recent studies have found that specific E2(s) bind different E3s and control their activity in the ubiquitylation reaction (231,232). In this dissertation we used eight E2s in the *in vitro* ubiquitylation activity assays for UBE3B. To determine which E2(s) are specific for UBE3B from this array, we will have to repeat the ubiquitylation activity assays with each E2 individually, or a combination of E2s. From the Phyre^2 results, it is predicted that the E2 binding sites are at positions F826, N829, L830, S832, I833, Y836, L843, L845, Y849, D850, D852, L857, L862, Y879 and M883. Therefore, once we identify the E2(s) that bind to UBE3B, we can mutates these amino acids and determine which residue is important for the interaction. In the case of Parkin, it was seen that UBE2D, UBE2L3 and UBE2N all resulted positively regulated its activation, translocation and enzymatic function (233). Interestingly, UBE2R1 functions antagonistically to these three E2s, wherein it inhibits the translocation of Parkin to the mitochondria and prevents Parkin from ubiquitylating its target proteins (233). Therefore, it will be interesting to see if there are E2(s) that perform a similar antagonist effect on the function of UBE3B.

7.5 IS THE FUNCTION OF UBE3B DIFFERENT IN OTHER CELL LINES

The studies on UBE3B we have performed so far are all using the glioblastoma cell line, LN428. It will be interesting to know if UBE3B functions in the same way in other high energy cell lines such as the heart and muscle, where its mRNA expression levels are high, as well as cells that have a lower mRNA expression level, such as the breast and pituitary cells (for more information

please visit http://www.genecards.org/cgi-bin/carddisp.pl?gene=UBE3B and http://www.gtexportal.org) (234-238). We will need to perform similar experiments as we did using the different LN428 cell lines we developed and compare the results to determine if the enzymatic function and associated proteins of UBE3B are similar between the different cell lines.

7.6 CRYSTAL STRUCTURE OF UBE3B

There are a vast number of programs available today that predict the three dimensional structure of proteins. However, having the crystal structure of a protein is invaluable. Not only will you be able to know the unique tertiary structure of the protein, but you can also determine regions of high flexibility, and how proteins change their spatial arrangement to modulate their function during protein-protein interactions, to name a few. Therefore, we will be able to learn a lot more about UBE3B once we are able to solve its crystal structure. We will also be able to then determine how the clinical mutations affect this structure and its interactions, thus helping us understand the causes of the diseases we observe.

APPENDIX A

STUDY OF THE FUNCTION OF ANKZF1 IN THE MITOCHONDRIA

A.1 INTRODUCTION

Fuzzy onion (Fzo) is an outer mitochondrial membrane (OMM) protein that mediates mitochondrial fusion and is the best characterized mitochondrial target of ubiquitin-proteasome system (UPS) dependent degradation in yeast (184,239). The human homologs are known as mitofusin 1 and mitofusin 2 (MFN1, MFN2). After mitochondrial stress, the E3 ubiquitin ligase Parkin is recruited and ubiquitylates damaged mitochondrial proteins such as MFNs1/2 and hexokinase I (HKI) (240,241). Until the characterization of the ubiquitin-dependent molecular chaperone, p97, it was not known how the UPS removed damaged proteins from the OMM (242). p97, also known as valosin-containing protein (VCP) or Cdc48 in yeast and *Caenorhabditis elegans* (*C.elegans*), is an ATPase Associated with diverse cellular Activities (AAA). In addition to the mitochondrial UPS, p97 also participates in endoplasmic reticulum (ER) proteostasis, autophagy and membrane remodeling (242-246), with mutations in p97 being associated with a wide spectrum of degenerative diseases from inclusion body myopathy with Paget's disease of bone and frontotemporal dementia (IBMPFD) to Parkinson's disease (PD) (247-249). Thus p97 plays a key role in the two main degradation systems in a cell: the

proteasome and the autophagy pathways (250). The p97 protein is composed of a N-terminal domain, an unstructured C-terminal domain and two ATPase cassettes (D1 and D2). The ATPase cassettes are required to extract polyubiquitylated proteins from the mitochondria and present them for proteasomal degradation (251-253). Therefore, ubiquitin serves as a major determinant of p97 function (254).

Since p97 is involved in diverse, unrelated cellular functions and pathways, it relies on different adaptor proteins (also known as p97 cofactors) to determine its specificity (255-257). Cofactors of p97 cofactors are defined as proteins that contain p97-interacting domains or motifs such as the ubiquitin binding and ubiquitin interacting motifs. Recently, studies performed in yeast identified a new Cdc48/p97-binding cofactor, Vms1 (258-260). Under normal growth conditions the Vms1 complex resides in the cytosol. However, on treatment with mitochondrial toxicants Vms1 recruits Cdc48/p97 and Npl4 (another Cdc48 cofactor), to the mitochondria to extract ubiquitylated proteins for proteasomal degradation (258). Deletion of *VMS1* caused an increase in polyubiquitylated mitochondrial proteins, a decrease in the rate of Fzo1 degradation (a known substrate of the mitochondrial E3 ligase Mdm30), biochemical defects and respiratory failure. Knockdown of Vms1 in *C.elegans* resulted in hypersensitivity to H_2O_2 (259,261). High levels of the loss-of-function variant of ubiquitin B (UBB) UBB^{+1} impairs the UPS to overcome the mechanisms that would eliminate the proteins, which in turn affects mitochondrial dynamics and triggers cell death (262-267). A recent study has found that the cell cytotoxicity of UBB^{+1} is antagonized by Cdc48/Vms1 complexes (268). Thus, in yeast and *C. elegans* Vms1 is critical at the mitochondria for cellular and organismal viability under conditions of mitochondrial stress. However, the cellular function of the human analog of Vms1, Ankyrin repeat and zinc finger domain containing 1 (ANKZF1) (also referred to as VMS1) is currently unknown and

identification of its function will be critical to developing therapeutic agents for mammalian diseases.

A.2 METHODS AND MATERIALS

A.2.1 Chemicals and Reagents

OptiMEM, alpha EMEM and phosphate buffered saline (PBS) were from Invitrogen. FuGENE® Transfection Reagent (Cat# E2311) was from Promega. Puromycin was from Clontech Laboratories, and gentamycin was from Irvine Scientific. All the plastic tissue culture supplies were from Corning and Thermo Fisher Scientific. All PCR primers were from Eurofins MWG Operon. DreamTaq DNA Polymerase (Cat# FEREP0703) was from Thermo Fisher Scientific and dNTPs (Cat# 4303442) were from Life Technologies. The *Pfu* Turbo DNA Polymerase (Cat# 600250) and QuickChange II XL site-Directed Mutagenesis kit (Cat# 200521) were from Agilent Technologies. The TOPO® TA Cloning® Kit for Sequencing, with One Shot® TOP10 Chemically Competent *E.coli* (Cat# K4575-40), Gateway® LR Clonase® II Enzyme Mix (Cat# 11791-100) and T4 DNA Ligase (Cat# EL0011) were from Life Technologies. Restriction enzymes *XbaI, EcoRI* and *Bsu36I* were from New England Biolabs. The QIAquick PCR Purification Kit (Cat# 28106) and QIAquick Gel Extraction Kit (Cat# 29706) were from QIAGEN. Oligomycin (Cat# O4876), Rotenone (Cat# R8875), H_2O_2 (Cat# H1009) and MG132 (Cat# C2211) were from Sigma. Primary antibodies: β-actin antibody (Cat# A1978) from Sigma, Turbo-green fluorescent protein (TurboGFP) antibody (Cat# AB513) from Evrogen, adenosine triphosphate synthase beta (ATP synthase β) antibody (Cat# MA1-930) from Thermo Fisher

Scientific. Secondary antibodies: goat anti-mouse horseradish peroxidase (GAM-HRP) conjugates and goat anti-rabbit horseradish peroxidase (GAR-HRP) conjugates were from Bio-Rad, goat anti-mouse Cy5 (Cat# ab150115) from Abcam and goat anti-rabbit Cy3 (Cat# A-11011) was from Life Technologies. The Novex® NuPAGE® SDS-PAGE gel systems were from Life Technologies. Signal generation substrates were from Bio-Rad and Thermo Fisher Scientific.

A.2.2 Stable Cell line generation and culture conditions

LN428 glioblastoma cells and culture conditions were as previously described (196). Cells were maintained at 37°C in 5% CO2 and grown in alpha EMEM media containing 10% heat-inactivated fetal bovine serum (FBS), antibiotic/antimycotic, L-glutamine and gentamycin.

Human pRS425-ANKZF1 complementary DNA was a kind gift from Jeffrey Brodsky (University of Pittsburgh). With this plasmid as the template, ANKZF1-copGFP protein was made, either via standard PCR. The sequence of each primer is listed in Table 1. Briefly, we used pRS425-ANKZF1 and pCT-CMV-MCS-copGFP-EF1-Puro vector (System Biosciences), and primer pair ANKZF1-XbaI-F and ANKZF1-EcoRI-R (**Figure 31*A***). The open reading frame was PCR amplified to engineer the restriction enzyme sites *XbaI* and *EcoRI* for cloning in-frame with copGFP using standard protocols. After PCR, products were digested with the enzymes; purified fragments were ligated into the pCT-CMV-MCS-copGFP-EF1-puro lentiviral vector also hydrolysed by *XbaI* and *EcoRI* (**Figure 31*B***). Positive clones were selected; plasmids were extracted with the QIAprep Spin Miniprep Kit (Qiagen), and sequenced (**Figure 31*C***). To determine if ANKZF1 was correctly inserted into the pCT-CMV-copGFP-MCS-EF1-Puro vector, the clones were digested with *Bsu36I*. If the constructs were present in the correct

orientation, there was a 2000bp and an 8000bp band (**Figure 31*D***). Sequence-verified plasmids were transiently transfected and lentivirus production was as described below.

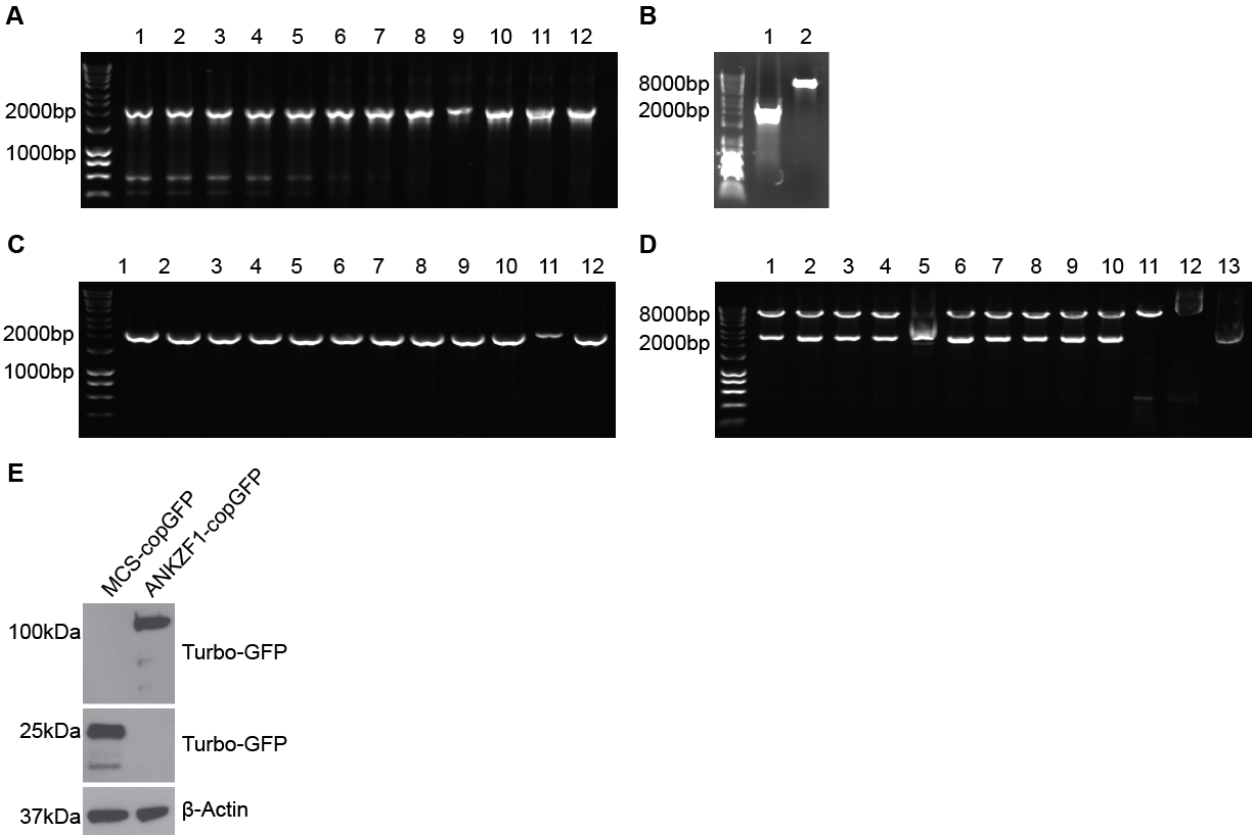

Figure 31. Generation of ANKZF1-copGFP stable cell lines.

(A) Optimization of the primers ANKZF1-XbaI-F and ANKZF1-EcoRI-R using Platinum® *Pfx* DNA Polymerase and plasmid pRS426-ANKZF1 in gradient PCR for amplification of ANKZF1 with *XbaI* and *EcoRI* restriction digest sites for ligation into pCT-CMV-MCS-copGFP-Puro vector. Gradient temperatures: 1: 52°C, 2: 52.5°C, 3: 53.6°C, 4: 54.9°C, 5: 57°C, 6: 59.6°C, 7: 62.6°C, 8: 65.2°C, 9: 67.2°C, 10: 68.6°C, 11: 69.6°C, and 12: 70°C. Best temperature chosen was 70°C. **(B)** *XbaI* and *EcoRI* restriction digested and gel-purified PCR amplified ANKZF1 insert and pCT-CMV-MCS-copGFP-Puro vector for ligation using T4 DNA Ligase. **(C)** PCR amplification screen using *Taq* DNA Polymerase of mini-prep pCT-CMV-ANKZF1-copGFP-Puro plasmids from transformed One Shot Top 10 *E.coli* cells. **(D)** Digestion of mini-prep pCT-CMV-ANKZF1-copGFP-Puro plasmids with *Bsu36I* enzyme. LN428 cells were transduced with lentiviral particles to create stable cell lines expressing ANKZF1-copGFP protein **(E)** lysed to make whole cell extracts (WCE) and immunoblotted, or **(F)** fixed and imaged using the Confocal A1 Nikon Microscope. The mitochondria were stained with ATP Synthase β as a marker.

Lentiviruses were prepared in collaboration with the UPCI Lentiviral facility. Lentiviral particles were generated by co-transfection of 4 plasmids [Control plasmid (pLVX-IRES-Puro) or one of the plasmids expressing UBE3B or UBE3B mutants, together with pMD2.g (VSVG), pVSV-REV and pMDLg/pRRE] into 293-FT cells using TransIT®-2020 Transfection reagent. The collection and isolation of lentiviral particles and transduction of LN428 cells were performed as described previously (198,199). Stable cell lines were developed by selection in puromycin (2 µg/mL) for 2 weeks. Overexpression of ANKZF1-copGFP was confirmed by immunoblot (**Figure 31*E***).

A.2.3 Transient Transfections of Plasmids

Proteins were overexpressed in LN428 cells by transient plasmid transfection. 1 x 10^6 cells were transfected with 7µg DNA. The plasmids were prepared with OPTI-MEM media and FuGENE® Transfection Reagent (Promega) for 30 minutes at room temperature before being added to the adherent cells dropwise. The transfections were incubated for 24 hours at 37°C before replacement with fresh media.

A.2.4 Cell Extract

Whole cell extracts (WCE) were prepared using 2X clear Laemmli buffer (2%SDS, 20% glycerol and 63mM Tris-HCl pH 6.8), and the protein concentrations were determined by the Bio-Rad Protein Assay Kit II (Cat# 500-0002), according to the manufacturer's instruction. Ten micrograms of protein was loaded on precast 4%-12% Tris-Bis Novex® NuPAGE® SDS-PAGE gels (Life Technologies), run at 200V for an hour at room temperature and the proteins were

transferred onto PVDF membrane (Bio-Rad). These membranes were blocked with 5% Milk in TBST for 1 hour shaking at room temperature and probed with respective antibodies overnight shaking at 4°C. Membranes were washed with 1X TBST, three times for 5 minutes each wash and then probed with secondary antibody for 1 hour shaking at room temperature before being washed as before. The membranes were developed using Immun-Star HRP Substrate onto X-Ray film (Thermo Fisher Scientific).

A.2.5 Treatment with Oligomycin, Rotenone and MG132

5 x 10^4 cells were plated on coverslips and allowed to attach overnight at 37°C, 5% CO_2. The next day the media was removed and fresh media containing either no drug, 2µM Oligomycin (Sigma), 2µM Rotenone (Sigma), or 25µM or 50µM MG132 (Sigma) was added and any changes in the cells was observed for up to 2 hours. The cells were fixed and imaged following the Immunofluorescence and Confocal Imaging Protocol.

A.2.6 Treatment with H_2O_2

5 x 10^4 cells that stably overexpressed either ANKZF1-copGFP or Mito-copGFP were plated on coverslips and allowed to attach overnight at 37°C, 5% CO_2. The next day the media was removed and fresh media containing either no drug or 0.25mM or 0.5mM H_2O_2 (Sigma) was added to the cell for 3 hours. The cells were fixed and imaged following the Immunofluorescence and Confocal Imaging Protocol.

A.2.7 Immunofluorescence and Confocal Imaging

Cells were cultured on glass coverslips for 24 hours before treatment. The treated cells were fixed with 2% paraformaldehyde for 20 minutes, permeabilized with 0.1% Triton X-100 for 15 minutes, and blocked with 2% bovine serum albumin for 45 minutes, all at room temperature. Anti-ATP Synthase β antibody (Thermo Fisher Scientific) at 1:250 dilution was incubated for 1 hour, followed by goat anti-mouse Alexa Fluor 647 (Abcam) at 1:1000 for 1 hour and DAPI stain for 30 seconds, all at room temperature. Slides were mounted and imaged on the Nikon A1 confocal microscope in the University of Pittsburgh Center for Biologic Imaging (CBI).

A.3 ANKZF1 RESULTS AND DISCUSSION

The current model for mitochondrial protein degradation suggests that (i) damaged mitochondrial proteins are presented on the surface of the outer mitochondrial membrane (OMM), (ii) Parkin is recruited from the cytosol to the mitochondria in response to the change in mitochondrial membrane potential, (iii) the damaged proteins are ubiquitylated by Parkin and additional E3 ligases, and (iv) the ubiquitylation recruits the Vms1/Cdc48 complex to degrade the proteins via the proteasomal degradation pathway (269-271). In studies performed by *Heo et al.* they found that under normal log phase growth, the levels of Fzo1 are identical in wild-type and the Vms1 deletion mutant (*vms1*Δ), however, the *vms1*Δ mutant exhibited elevated levels of Fzo1 protein at day 2.5 of culture (261). Therefore, they concluded that Vms1 is required for mitochondrial protein degradation.

In this project we wanted to study the function of the human homology of Vms1, ANKZF1. Using the data available from the Vms1 studies, we predict the domain structure of ANKZF1 as detailed in **Figure 32**.

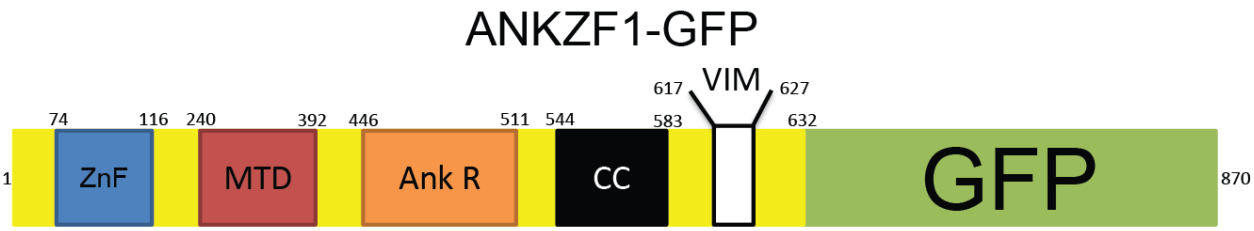

Figure 32. Schematic representation of the domain structure of full-length ANKZF1 with C-terminus GFP Tag.

Full-length ANKZF1 contains a zinc-finger domain (ZnF), a mitochondrial targeting domain (MTD), an ankyrin repeat (Ank R), a predicted coiled-coil region (CC), and a VCP (Valosin-containing protein) interacting motif (VIM). Adapted from (258).

To study ANKZF1, we generated stable cells that overexpressed ANKZF1 with a C-terminus copGFP. Using confocal microscopy we were able to show that ANKZF1, just like its yeast homolog Vms1, is cytosolic under normal growing conditions (**Figure 33**). It was found that Vms1 was recruited to the mitochondria after treatment with H_2O_2 and depletion of Vms1 in *C.elegans* resulted in hypersensitivity to H_2O_2 (259,261). We wanted to determine the effects of H_2O_2 on ANKZF1. We treated our stable overexpressing cell lines with 0.25mM and 0.5mM H_2O_2 and observed the changes in the subcellular localization of ANKZF1 over 3 hours. As seen in **Figure 33**, ANZKF1 is recruited from the cytosol to the perinuclear region. However, this recruitment does not coincide with the mitochondria, therefore suggesting that ANKZF1 is recruited to another organelle besides the mitochondria. From the study performed by *Tran et al.*, they found that the *Saccharomyces cerevisiae* homolog of ANKZF1, Vms1p, is involved in the

ERAD pathway (259). Therefore, ANKZF1 might also play a similar function in the post-ubiquitylation step in ERAD and the recruitment of ANKZF1 we see after H_2O_2 treatment could be to the ER.

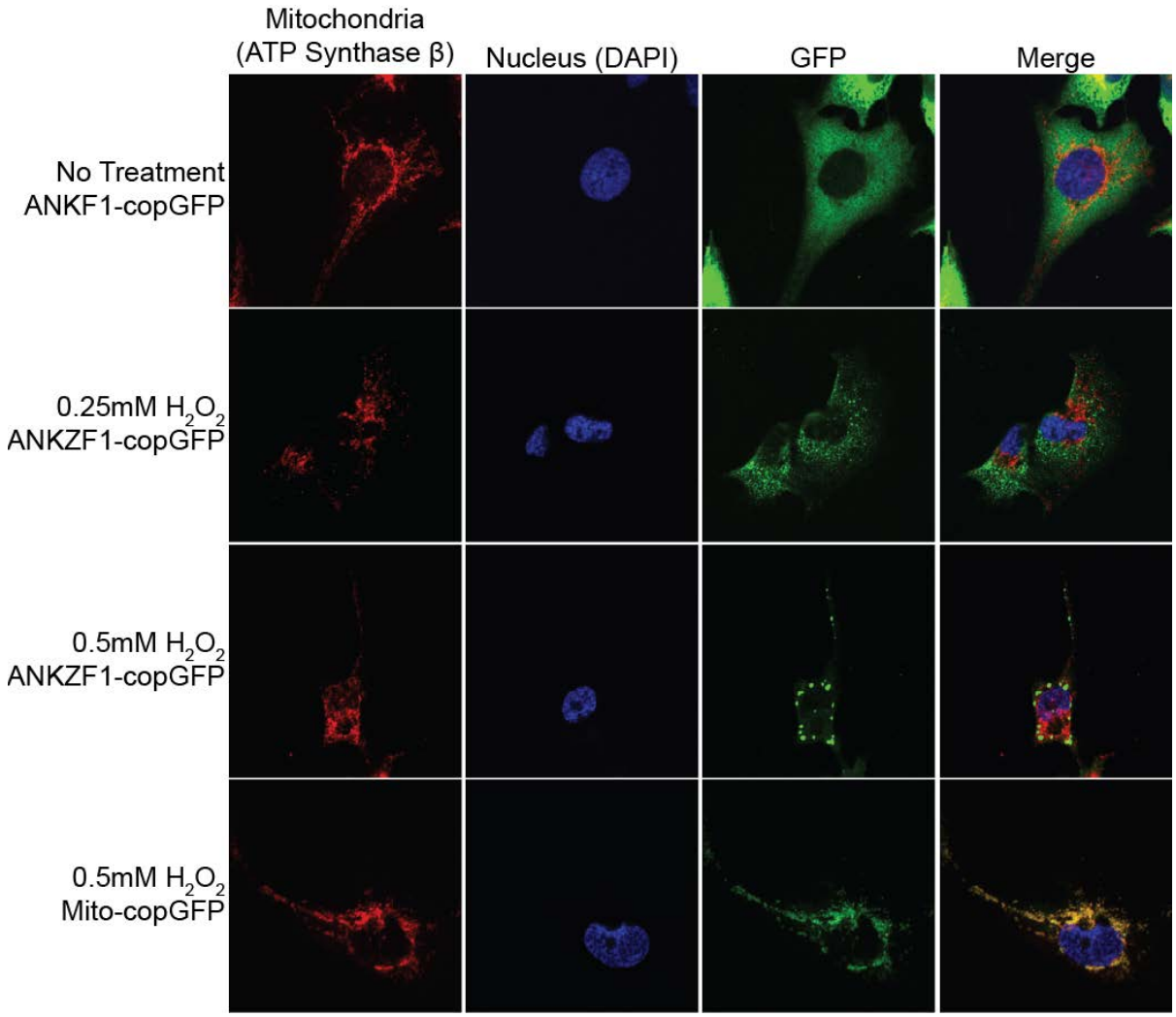

Figure 33. Treatment with H2O2 recruits ANKZF1 to the perinuclear region, but not the mitochondria.

LN428 cells were transduced with lentiviral particles to create stable cell lines that express either ANKZF1-copGFP or Mito-copGFP proteins. The cells were treated with no drug, 0.25mM H_2O_2, or 0.5mM H_2O_2 for 3 hours, washed fixed and imaged using the Confocal A1 Nikon Microscope. The mitochondria were stained with ATP Synthase β and the nucleus with DAPI.

Lastly we treated the cells with 2µM Oligomycin, 2µM Rotenone, or two concentrations of MG132 (25µM or 50µM) to determine if the subcellular localization of ANKZF1 changes in the cell. We noticed that after 2 hours of treatment with MG132, ANKZF1 is recruited to the mitochondria (**Figure 34**). However, this mitochondrial recruitment is not observed with the treatment of Oligomycin. It is important to note that treatment with Rotenone completely killed the cells, even after only a 10 minute treatment with the drug (data not shown).

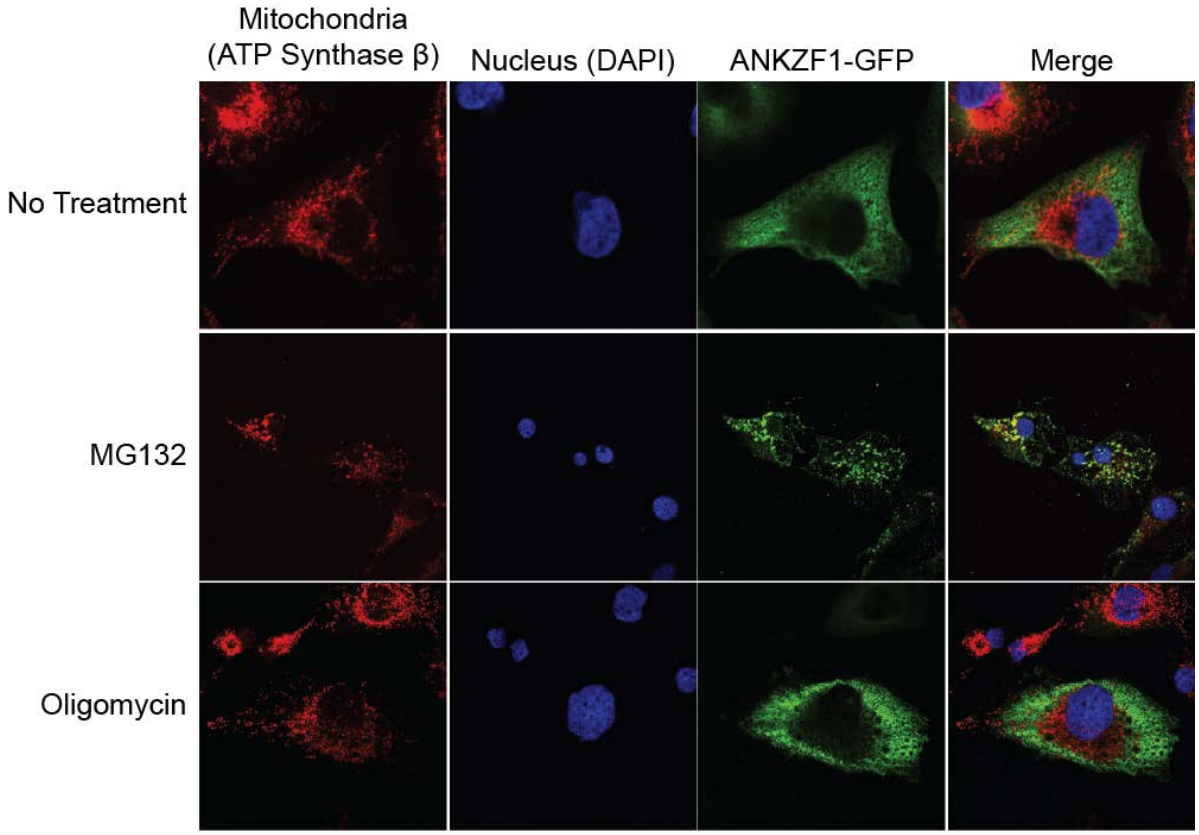

Figure 34. ANKZF1 is recruited to the mitochondria after treatment with MG132 but not Oligomycin.

LN428 cells were transduced with lentiviral particles to create stable cell lines that express ANKZF1-copGFP proteins. The cells were treated with no drug, 50µM MG132 or 2µM Oligomycin for 2 hours, washed fixed and imaged using the Confocal A1 Nikon Microscope. The mitochondria were stained with ATP Synthase β and the nucleus with DAPI.

Identification of the function of ANKZF1 in mammalian cells will be important because of the crucial role its homologs play in the yeast and *C.elegans* UPS system. Even though we could not study this pathway in the detail we had proposed, continued efforts will be made to finish the proposed aims by the lab.

APPENDIX B

MASS SPECTROMETRY ANALYSIS OF UBE3B BINDING PROTEINS

B.1 INTRODUCTION

Mass spectrometry (MS) is a very useful technique that is now widely used to identify the amount and type of chemicals present in a compound by measuring the mass-to-charge ratio and the abundance of gas-phase ions (272). Briefly, the atoms or molecules are first charged (ionized) by removing electrons to yield a positive ion. Next, the ions are accelerated and deflected by a magnetic field based on their masses, such that, the lighter the ion, the more they deflect. Lastly, these ions are passed through a machine that detects them electronically (272).

In our research we wanted to identify the proteins that associate with UBE3B. Therefore, we used Affinity Capture – MS (AC-MS) where a bait protein (here it is UBE3B) is affinity captured from cell extracts by either polyclonal antibody or, in our case, epitope tag and the associated interaction partner(s) are then identified by MS methods.

B.2 RESULTS AND DISCUSSION

There is no prior report in the literature describing the isolation of proteins associated with UBE3B. Therefore, to identify proteins that are associated with UBE3B *in vivo* we used the LC-MS/MS approach and HA-UBE3B and HA-UBE3B(C1036A) as the bait proteins. Our experiments identified 40 proteins that we deem specifically associated with UBE3B (**Figure 35)**.

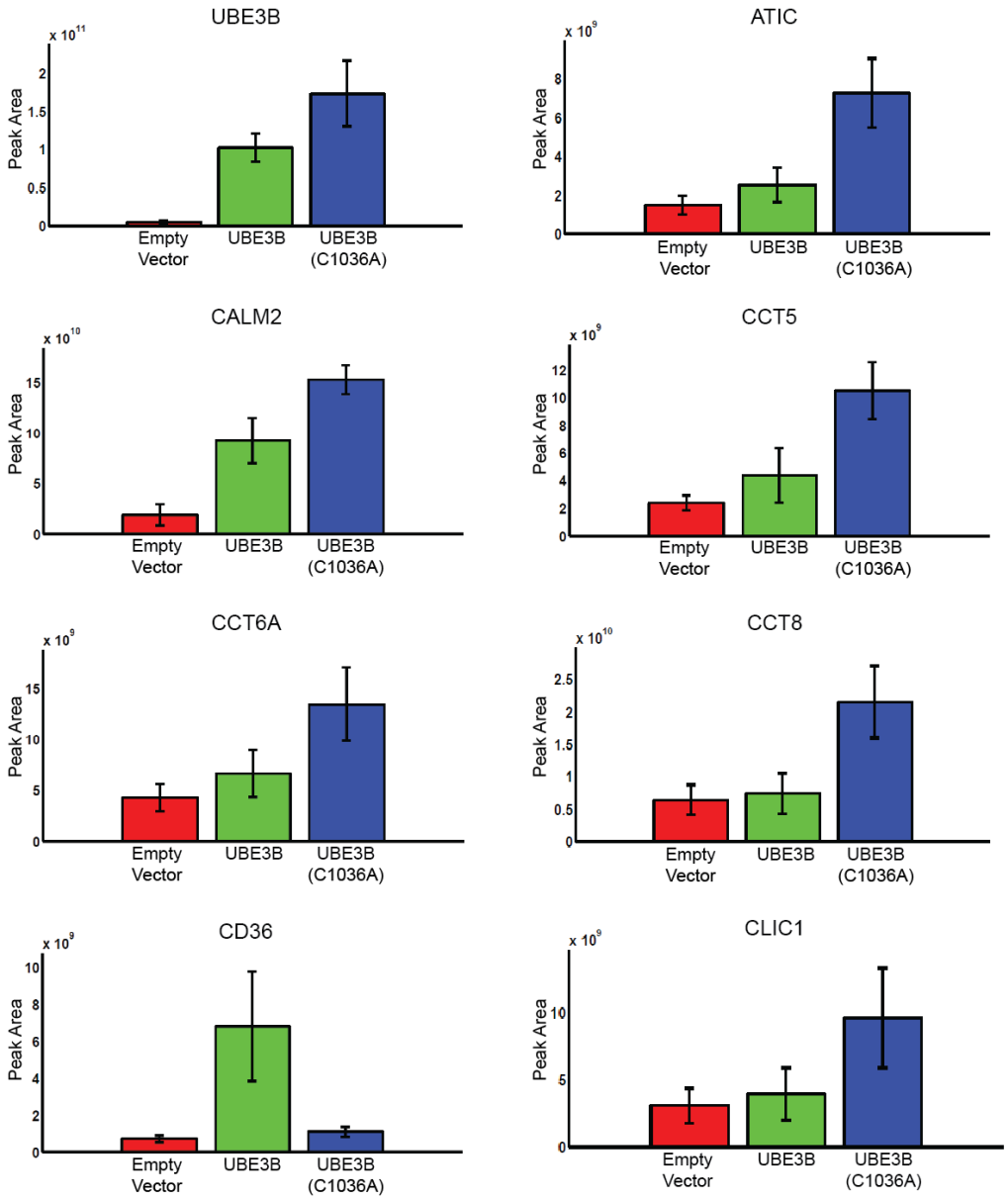

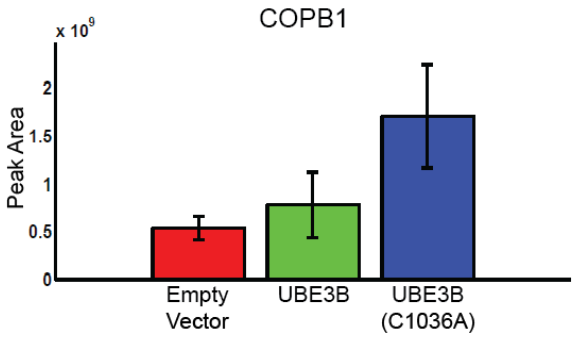
COPB1
x 10^9
Peak Area
2
1.5
1
0.5
0
Empty Vector
UBE3B
UBE3B (C1036A)

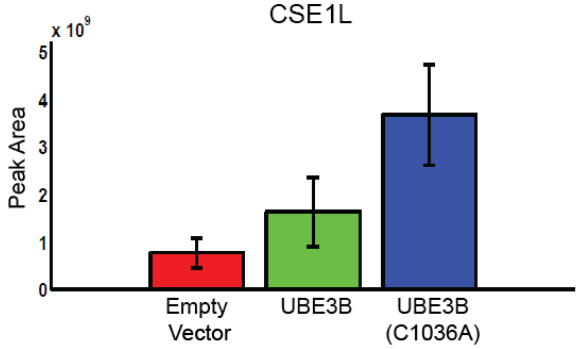
CSE1L
x 10^9
Peak Area
5
4
3
2
1
0
Empty Vector
UBE3B
UBE3B (C1036A)

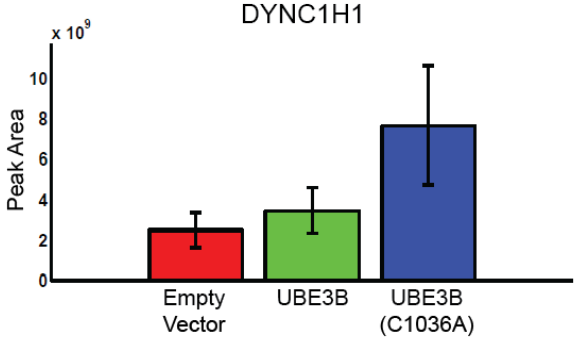
DYNC1H1
x 10^9
Peak Area
10
8
6
4
2
0
Empty Vector
UBE3B
UBE3B (C1036A)

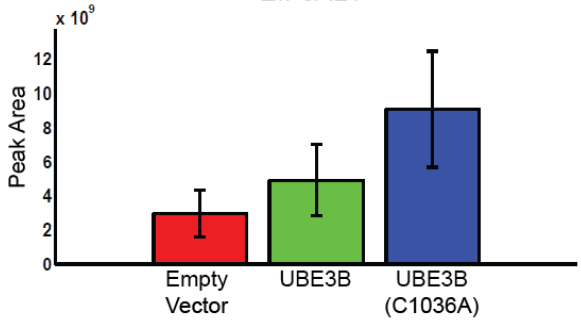
EIF5AL1
x 10^9
Peak Area
12
10
8
6
4
2
0
Empty Vector
UBE3B
UBE3B (C1036A)

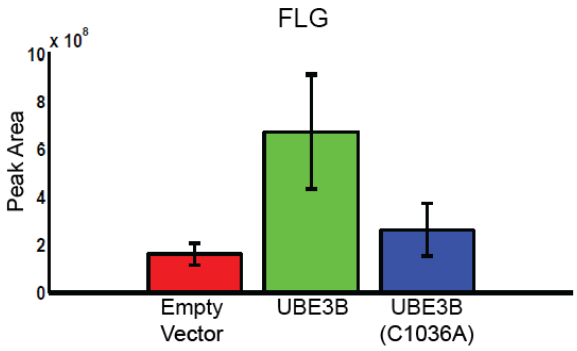
FLG
x 10^8
Peak Area
10
8
6
4
2
0
Empty Vector
UBE3B
UBE3B (C1036A)

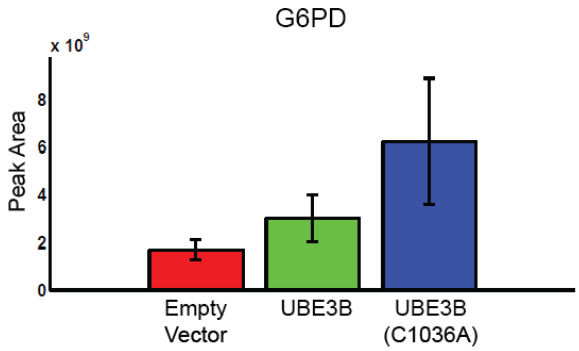
G6PD
x 10^9
Peak Area
8
6
4
2
0
Empty Vector
UBE3B
UBE3B (C1036A)

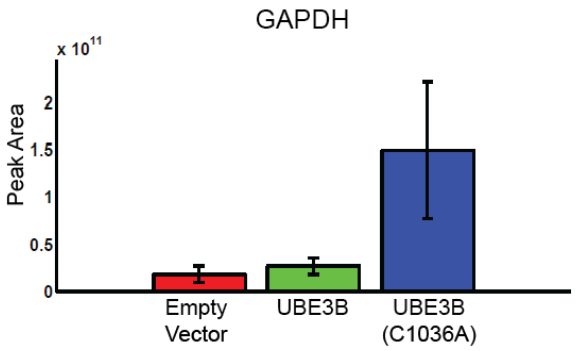
GAPDH
x 10^11
Peak Area
2
1.5
1
0.5
0
Empty Vector
UBE3B
UBE3B (C1036A)

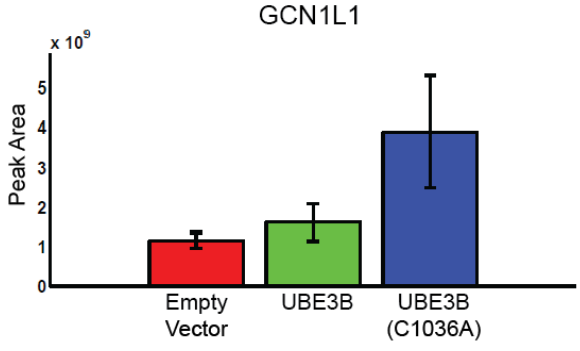
GCN1L1
x 10^9
Peak Area
5
4
3
2
1
0
Empty Vector
UBE3B
UBE3B (C1036A)

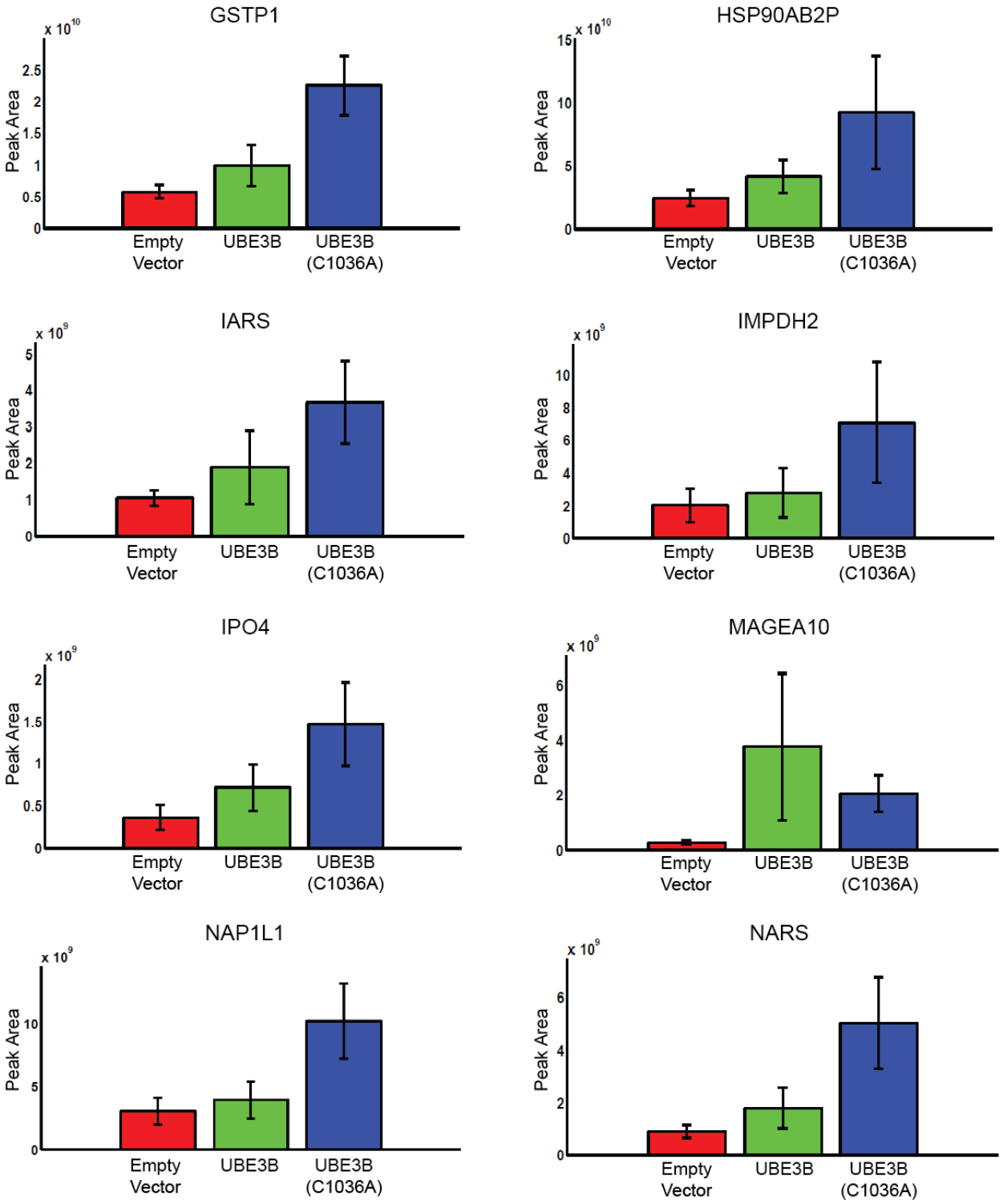
GSTP1
x 10^10
Peak Area
2.5
2
1.5
1
0.5
0
Empty Vector
UBE3B
UBE3B (C1036A)
HSP90AB2P
x 10^10
15
10
5
0
IARS
x 10^9
5
4
3
2
1
IMPDH2
x 10^9
10
8
6
4
2
IPO4
x 10^9
2
1.5
1
0.5
MAGEA10
x 10^9
6
4
2
NAP1L1
x 10^9
10
5
NARS
x 10^9
6
4
2

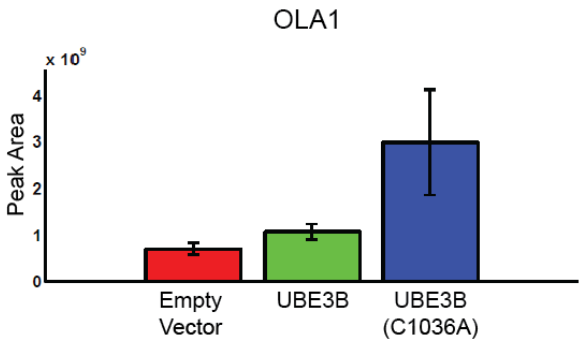
OLA1
x 10^9
Peak Area
0
1
2
3
4
Empty Vector
UBE3B
UBE3B (C1036A)

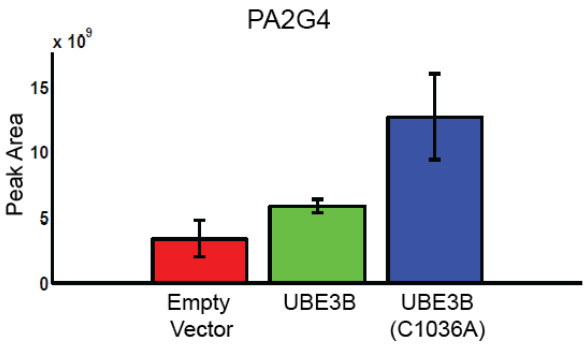
PA2G4
x 10^9
Peak Area
0
5
10
15
Empty Vector
UBE3B
UBE3B (C1036A)

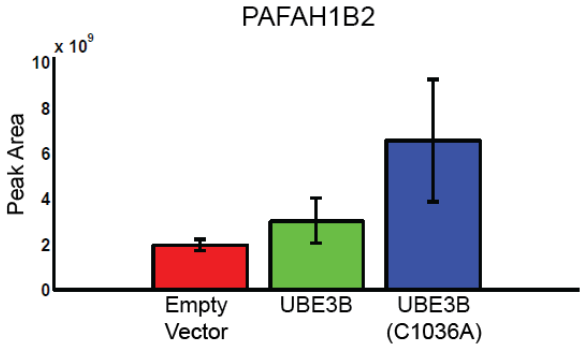
PAFAH1B2
x 10^9
Peak Area
0
2
4
6
8
10
Empty Vector
UBE3B
UBE3B (C1036A)

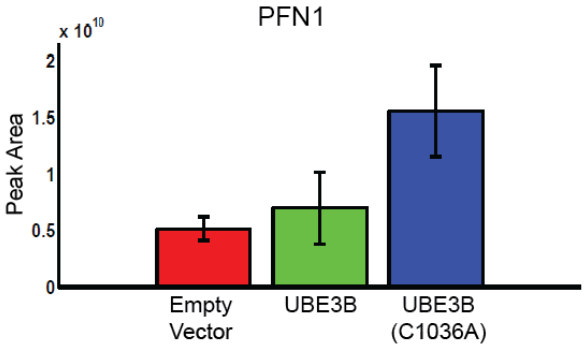
PFN1
x 10^10
Peak Area
0
0.5
1
1.5
2
Empty Vector
UBE3B
UBE3B (C1036A)

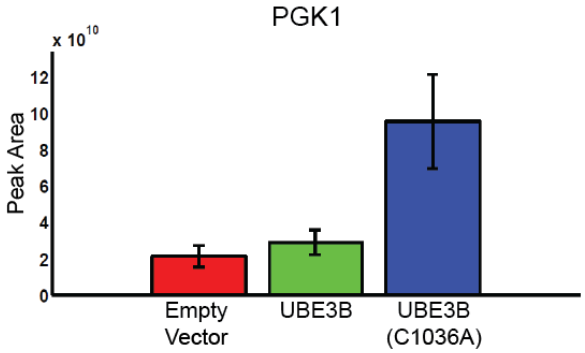
PGK1
x 10^10
Peak Area
0
2
4
6
8
10
12
Empty Vector
UBE3B
UBE3B (C1036A)

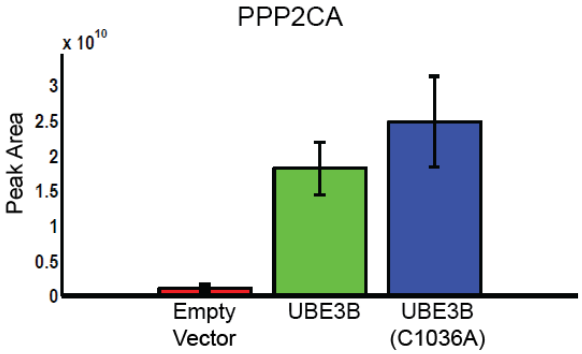
PPP2CA
x 10^10
Peak Area
0
0.5
1
1.5
2
2.5
3
Empty Vector
UBE3B
UBE3B (C1036A)

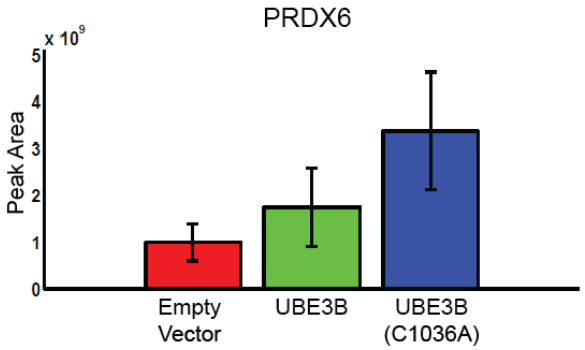
PRDX6
x 10^9
Peak Area
0
1
2
3
4
5
Empty Vector
UBE3B
UBE3B (C1036A)

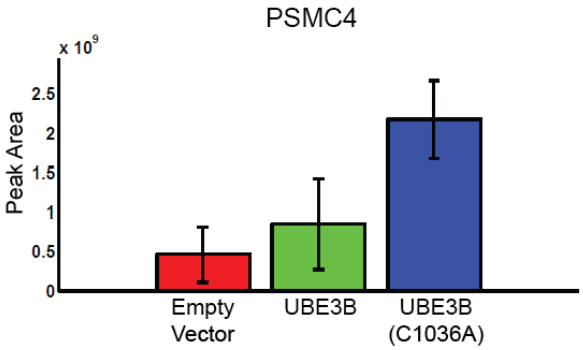
PSMC4
x 10^9
Peak Area
0
0.5
1
1.5
2
2.5
Empty Vector
UBE3B
UBE3B (C1036A)

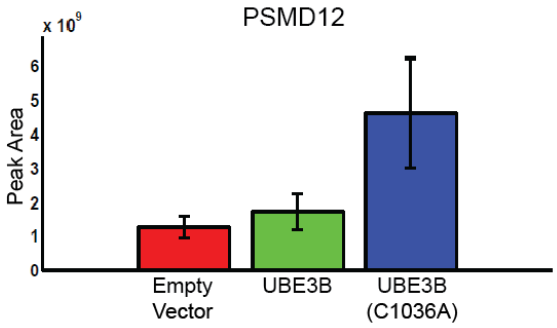
PSMD12
x 10^9
Peak Area
0
1
2
3
4
5
6
Empty Vector
UBE3B
UBE3B (C1036A)

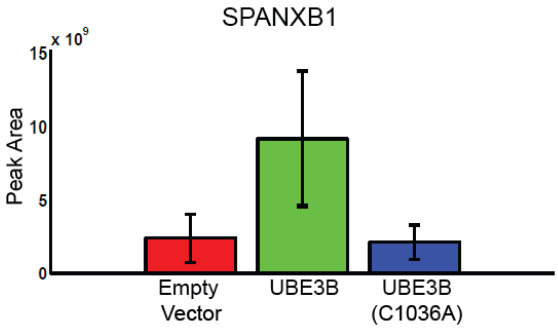
SPANXB1
x 10^9
Peak Area
0
5
10
15
Empty Vector
UBE3B
UBE3B (C1036A)

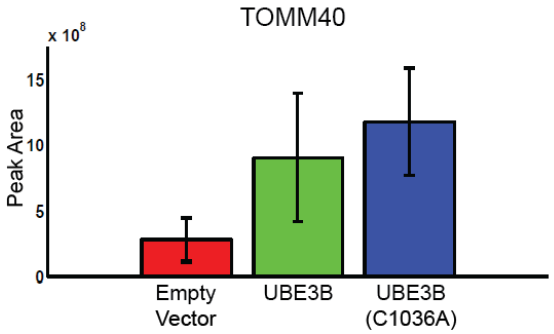
TOMM40
x 10^8
Peak Area
0
5
10
15
Empty Vector
UBE3B
UBE3B (C1036A)

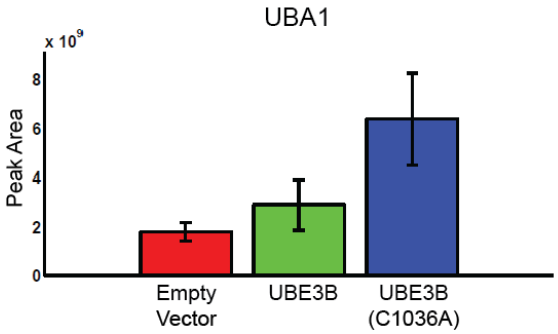
UBA1
x 10^9
Peak Area
0
2
4
6
8
Empty Vector
UBE3B
UBE3B (C1036A)

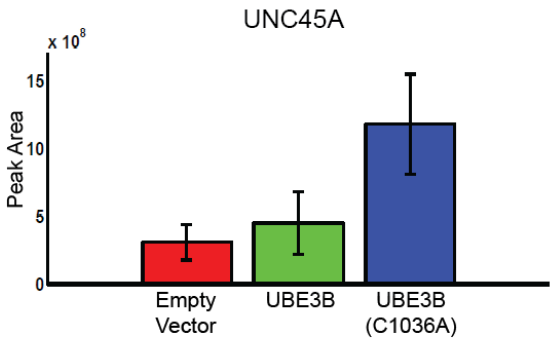
UNC45A
x 10^8
Peak Area
0
5
10
15
Empty Vector
UBE3B
UBE3B (C1036A)

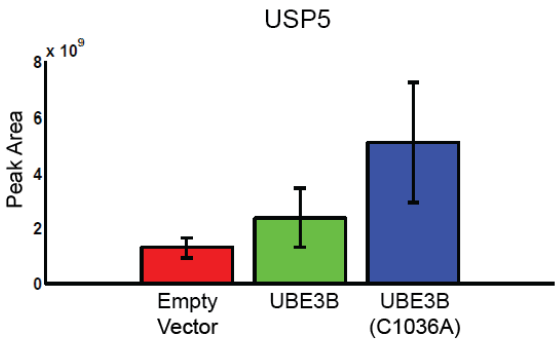
USP5
x 10^9
Peak Area
0
2
4
6
8
Empty Vector
UBE3B
UBE3B (C1036A)

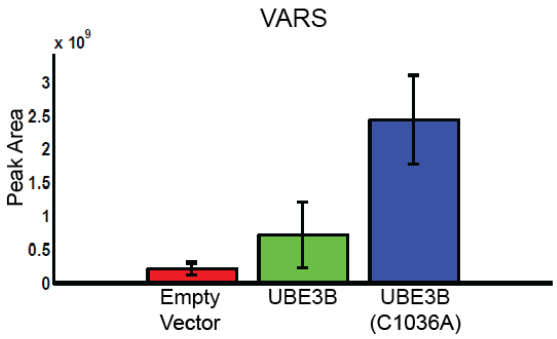
VARS
x 10^9
Peak Area
0
0.5
1
1.5
2
2.5
3
Empty Vector
UBE3B
UBE3B (C1036A)

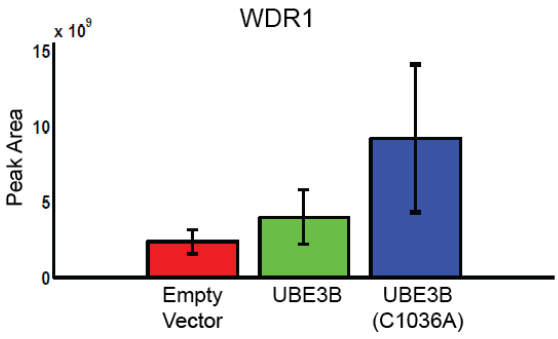
WDR1
x 10^9
Peak Area
0
5
10
15
Empty Vector
UBE3B
UBE3B (C1036A)

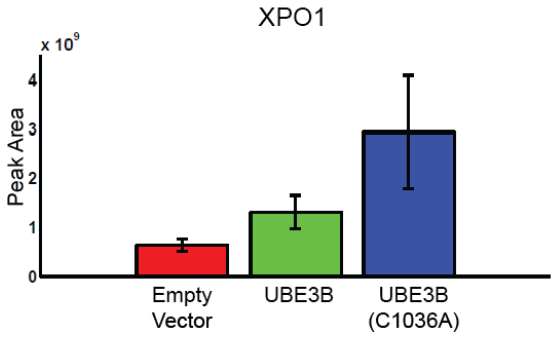
XPO1
x 10^9
Peak Area
0
1
2
3
4
Empty Vector
UBE3B
UBE3B (C1036A)

Figure 35. Peptides identified from LC-MS/MS of proteins associated with UBE3B.

40 potential peptides that associate with UBE3B were identified. Bar graphs of mean and SEM following affinity purification and high resolution LC-MS analysis of LN428 cells expressing an empty vector, wild type HA-tag UBE3B (HA-UBE3B), and the catalytic inactive UBE3B with an HA-tag (HA-UBE3B(C1036A)).

Amongst them are the E1 activating enzyme ubiquitin-like modifier-activating enzyme 1 (UBA1), and a deubiquitylating enzyme ubiquitin carboxyl-terminal hydrolase 5 (USP5), which fits with our main results that UBE3B is an E3 ligase that participates in ubiquitylation. Interestingly, we also identified the nuclear import and export proteins Importin-4 (IPO4) and exportin-1 (XPO1). Given these findings we ran a nuclear export sequence (NES) test on UBE3B using LocNES (http://prodata.swmed.edu/LocNES/LocNES.php), an online Support Vector Machine (SVM) predictor that locates classical nuclear export signals (NESs) in CRM1 cargoes. We found five potential NES sequences (**Table 6**). It is important to note that we did not see any nuclear localization in our overexpression cell lines. Therefore, the interactions between UBE3B and IPO4 and/or XPO1 will need to be validated further to confirm the mass spectrometry data.

Table 6. There are five potential NES of UBE3B as predicted by LocNES.

Position	Sequence	Score
29-43	RERAAVVIQAHVRSF	0.006
71-85	RSALCIFKIARKLLF	0.032
72-86	SALCIFKIARKLLFL	0.038
73-87	ALCIFKIARKLLFLF	0.021
75-89	CIFKIARKLLFLFRI	0.044
151-165	**EILQDSRLITLYLTM**	**0.313**
153-167	LQDSRLITLYLTMLV	0.096
155-169	DSRLITLYLTMLVTF	0.105
199-213	HLNQHGFYSVLQILL	0.010
223-237	CLSKGTLTAAFSLAL	0.080
226-240	KGTLTAAFSLALRPV	0.012
241-255	IAAQFSDNLIRPFLI	0.005
246-260	SDNLIRPFLIHIMSV	0.010

253-267	FLIHIMSVPALVTHL	0.018
256-270	HIMSVPALVTHLSTV	0.072
263-277	LVTHLSTVTPERLTV	0.120
305-319	**EGCHTLCLMGNLLHL**	**0.189**
323-337	SPRVLEEETDGFVSL	0.108
366-380	FSQSVDYGLNESMHL	0.011
373-387	GLNESMHLITKQLQF	0.037
374-388	LNESMHLITKQLQFL	0.014
382-396	TKQLQFLWGVPLIRI	0.015
384-398	QLQFLWGVPLIRIFF	0.031
387-401	FLWGVPLIRIFFCDI	0.064
451-465	RVDSAEVQKVCNICV	0.008
465-479	VLYQTSLTTLTQIRL	0.022
467-481	YQTSLTTLTQIRLQI	0.087
481-495	ILTGLTYLDDLLPKL	0.040
488-502	LDDLLPKLWAFICEL	0.043
518-532	DTEESKQLLAMLMLF	0.078
534-548	**DCSRHLITILDDIEV**	**0.188**
549-563	YEEQISFKLEELVTI	0.030
556-570	**KLEELVTISSFLNSF**	**0.251**
558-572	EELVTISSFLNSFVF	0.038
613-627	EDHWLRKDLKPSVLF	0.004
633-647	DRKRAQLILQYIPHV	0.010
671-685	VETSSASPHVTHITI	0.007
700-714	QLSQHAMKGVIRVKF	0.015
706-720	MKGVIRVKFVNDLGV	0.015
735-749	LEEIIKRVFDPALNL	0.067
778-792	VGKMLGKAVYEGIVV	0.000
782-796	LGKAVYEGIVVDVPF	0.003
787-801	YEGIVVDVPFASFFL	0.019
790-804	IVVDVPFASFFLSQL	0.012
874-888	ENKISYIHLMAHFRM	0.023
892-906	IKNQTAALISGFRSI	0.057
982-996	PPLLGFAYLKPPFSI	0.009
987-1001	FAYLKPPFSIRCVEV	0.005
1007-1021	**TGDTLGSVLRGFFTI**	**0.312**
1028-1042	GRLPTSSTCFNLLKL	0.094
1047-1061	KKSVLREKLRYAISM	0.045
1053-1067	EKLRYAISMNTGFEL	0.039

All predicted NES sequences on UBE3B with the predicted scores. The top five significant NES sequences were identified on UBE3B and are in bold. The first column is location of the NES candidate, the second column is the sequence of the NES candidate, and the last column is the probability of the candidate being a real NES. Cross-validation showed that a cutoff of 0.1 gives 68% recall rate with 26% precision. Recall is defined as the fraction of real NESs whose probability score is higher than the cutoff value. Precision measures the percentage of real NESs among NES candidates with probability score higher than a cutoff.

The protein kinase, Ca^{2+}/calmodulin-dependent protein kinase IV (CaMKIV) functions as a potent stimulator of Ca^{+2}-dependent gene expression and has also been shown to stably associate with protein serine/threonine phosphatase 2A (PP2A) (273-275). However, the timing and mechanism of binding of these two complexes to CaMKIV was unknown. Recently, it was found that the Ca^{2+}/CaM binding-autoinhibitory domain of CaMKIV is required for association of the kinase with PP2A and that binding of PP2A and Ca^{2+}/CaM appears to be mutually exclusive (276). Therefore it is proposed that CaMKIV is activated when intracellular Ca^{+2} levels are increased, and dephosphorylation of CaMKIV by PP2A terminates this activation (276). In our MS analysis, we found CaM and Protein Phosphatase 2A, Catalytic subunit, Alpha isoform (PPP2CA) as potential interactors of UBE3B. PPP2CA is a subunit of PP2A. PPP2CA and γ-H2AX co-immunoprecipitated and co-localized at DNA double-strand break foci, with PPP2CA dephosphorylating γ-H2AX *in vitro*. When PPP2CA was inhibited by RNA interference γ-H2AX foci persisted, there was an inefficiency of DNA repair, and the cells were hypersensitive to DNA damage (277). Therefore, we hypothesize that CaM and PPP2CA function antagonistically as the activator and deactivator of UBE3B, respectively, just as Ca^{+2}/CaM and PP2A regulate the function of CaMKIV.

The website The Biological General Repository for Interaction Datasets (BioGRID) (http://thebiogrid.org) is an open access database that archives and disseminates genetic and protein interaction data from model organisms and humans (278). One of the four proteins predicted to interact with UBE3B is IQ motif containing B1 (IQCB1), which was isolated in a high-throughput proteomic study using human retinal pigment epithelial (RPE) cells (279). The IQCB1 protein is linked to the ciliopathic group of disorders which includes Nephronophthisis (NPHP), Joubert syndrome (JBTS), and Meckel-Gruber syndrome (MKS), and manifests

clinically as cystic kidney disease, cerebellar/neural tube malformation, retinal degeneration, cerebellar vermis aplasia (a significant malformation of the cerebellum that is linked to ataxia), and occipital encephalcele (279-282). It is important to note that we did not isolate this peptide in our mass spectrometry analysis of UBE3B binding proteins. A possible explanation for this discrepancy could be because the interaction between UBE3B and IQCB1 occurs only under certain cellular conditions, ones that did not occur in our cells before harvest. Also, it is highly possible that UBE3B interacts with different proteins in different cells.

$Ca_v3.2$ is a T-type Ca^{+2} channels that transmits nociceptive signals in the primary afferent pain pathway and is ubiquitylated by the E3 ligase WWP1 (283). The deubiquitylating enzyme USP5 was found to interact with $Ca_v3.2$ and knockdown of USP5 increased $Ca_v3.2$ ubiquitylation, thereby decreasing $Ca_v3.2$ protein levels and reducing the whole cell current. As mentioned before, USP5 was found to be associated with UBE3B during our mass spectrometry analysis. Therefore, it will be very interesting to validate this interaction, and see if the UBE3B/USP5 complex acts as a dynamic pair that ubiquitylate/deubiquityate proteins to maintain cellular homeostasis, or if USP5 is a deubiqutylating enzyme that controls the function of UBE3B and prevents it from ubiquityating undamaged target proteins.

The results from this section are novel and exciting for the study of UBE3B. The next steps would be to validate the identified peptides, and then uncover the mechanisms that govern their interaction(s) with UBE3B and the entire UPS to maintain proper functioning of the cell.

APPENDIX C

DEVELOPMENT AND ANALYSIS OF MITOCHONDRIAL-TARGETED, ROS-INDUCING DNA DAMAGING PROTEINS

C.1 INTRODUCTION

Replication of mtDNA is independent of cellular division with only a few enzymes that are known to participate in this process, all of which are encoded by the nuclear DNA (nDNA) and imported into the mitochondria (284). mtDNA is organized in dynamic structures which consists of mitochondrial proteins and the mtDNA, and are known as nucleoids. The proteins that are involved in mtDNA transcription and packaging, such as mitochondrial RNA polymerase (POLRMT), Twinkle, mitochondrial single-stranded DNA-binding protein (mtSSB), and mitochondrial transcription factor B2 and A (TFB2M and TFAM) are localized in the nucleoids and are essential for the replication process (284-286). TFAM is the most abundant protein and functions in packaging and compaction of mtDNA (287-289). Because mtDNA replication is cell cycle independent, its replication rates are higher than that of nDNA, thus increasing the possibility of mutations and increased sensitivity to damage (290).

Complex I and III of the ETC in the mitochondria are important sources of ROS, particularly the superoxide anion, and during non-replicative phases, oxidative damage

represents one of the main types of DNA damage in aerobic organisms (291,292). A novel approach to study oxidative damage in the different organelles of a cell uses a fluorescent dependent signal that relies on the interaction between a reporter polypeptide and a small chemical label (the fluorogen) that is only fluorescent when bound to the reporter (293). These reporter polypeptides are selected from a library of single chain antibodies (scFv's), improved by directed evolution to increase their specificity, and renamed to fluorogen activating proteins (FAPs) (293). Therefore, each FAP is now specific to a particular fluorogen.

Here we endeavored to create FAPs that are targeted to the mitochondria via a TFAM sequence. Using different FAPs, we want to generate different constructs that, when bound to a fluorogen, will generate different types of ROS in the mitochondria, thus allowing us to study the differences in mitochondrial damage based on that particular oxidative stress.

C.2 METHODS AND MATERIALS

C.2.1 Chemicals and Reagents

OptiMEM, alpha EMEM and phosphate buffered saline (PBS) were from Invitrogen. FuGENE® Transfection Reagent (Cat# E2311) was from Promega. Puromycin was from Clontech Laboratories, and gentamycin was from Irvine Scientific. All the plastic tissue culture supplies were from Corning and Thermo Fisher Scientific. All PCR primers were from Eurofins MWG Operon. DreamTaq DNA Polymerase (Cat# FEREP0703) was from Thermo Fisher Scientific and dNTPs (Cat# 4303442) were from Life Technologies. The *Pfu* Turbo DNA Polymerase (Cat# 600250) and QuickChange II XL site-Directed Mutagenesis kit (Cat# 200521) were from

Agilent Technologies. The TOPO® TA Cloning® Kit for Sequencing, with One Shot® TOP10 Chemically Competent *E.coli* (Cat# K4575-40), Gateway® LR Clonase® II Enzyme Mix (Cat# 11791-100) and T4 DNA Ligase (Cat# EL0011) were from Life Technologies. Restriction enzymes *XbaI*, *EcoRI* and *Bsu36I* were from New England Biolabs. The QIAquick PCR Purification Kit (Cat# 28106) and QIAquick Gel Extraction Kit (Cat# 29706) were from QIAGEN. Primary antibody: adenosine triphosphate synthase beta (ATP synthase β) antibody (Cat# MA1-930). Secondary antibodies: goat anti-mouse Cy3 (Cat# ab97035) from Abcam and DRAQ5 (Cat# 62254) were from Thermo Fisher Scientific.

C.2.2 Stable Cell line generation and culture conditions

LN428 glioblastoma cells and culture conditions were as previously described (196). Cells were maintained at 37°C in 5% CO2 and grown in alpha EMEM media containing 10% heat-inactivated fetal bovine serum (FBS), antibiotic/antimycotic, L-glutamine and gentamycin.

Human pCMV6-TFAM-TurboGFP, pBABE-NLS-HA-mCer3, pBABE-NLS-myc-Charlie-G4S-mCer3, pBABE-NLS-myc-dH6-2XG4S-mCer3, pBABE-NLS-myc-dL5-2XG4S-mCer3, pLVX-GFP-LC3-P2A-Luc-T2A-FP635-IRES-Puro, pLVX-TRE3G-TagRFP/TRF1 and pLVX-TRE3G-KR/TRF1 complementary DNA was a kind gift from Marcel Bruchez (Carnegie Mellon University/University of Pittsburgh). With these plasmids as template, we amplified Human TFAM, mCer3, Charlie-mCer3, dH6-mCer3, dL5-mCer3, TagRFP and KillerRed via standard PCR. The sequence of each primer is listed in **Table 1**. Briefly, we made TFAM with different C-terminus joining ends using primer pair TFAM-F/TFAM-mCer3-R, TFAM-F/TFAM-Charlie-R, TFAM-F/TFAM-dH6-R, TFAM-F/TFAM-dL5-R, TFAM-F/TFAM-FP635-R, TFAM-F/TFAM-TagRFP-R, TFAM-F/TFAM-KR-R, mCer3 using primer pair TFAM-

mCer3-R/mCer3-R, Charlie-mCer3 using primer pair TFAM-Charlie-F/mCer3-R, dH6-mCer3 using primer pair TFAM-dH6-F/mCer3-R, dL5-mCer3 using primer pair TFAM-dL5-R/mCer3-R, FP635 using primer pair TFAM-FP635-F/FP635-R, TagRFP using primer pair TFAM-TagRFP-F/TagRFP-R, and KillerRed using primer pair TFAM-KR-F/KR-R.

Table 7. Oligodeoxynucleotides used.

Oligo Name	Sequence (5'-3')*
TFAM-F	CACCATGGCGTTTCTCCGAAGCATGTGGGGCG
TFAM-mCer3-R	CCTTGCTCACACACTCCTCAGCACCATATTTTCG
TFAM-mCer3-F	AGGAGTGTGTGAGCAAGGGCGAGGAGC
mCer3-R	TTACTTGTACAGCTCGTCCATGCCGAGAGTG
TFAM-Charlie-R	GCTGCACCTGACACTCCTCAGCACCATATTTTCG
TFAM-Charlie-F	AGGAGTGTCAGGTGCAGCTGGTGGAGTCTG
TFAM-dH6-R	CTGGACTTGACACTCCTCAGCACCATATTTTCG
TFAM-dH6-F	AGGAGTGTCAAGTCCAGTTGCAAGAATCTGGACC
TFAM-dL5-R	CGACGGCCTGACACTCCTCAGCACCATATTTTCG
TFAM-dL5-F	AGGAGTGTCAGGCCGTCGTTACCCAAGAACC
TFAM-FP635-R	CCTTAGACACACACTCCTCAGCACCATATTTTCG
TFAM-FP635-F	AGGAGTGTGTGTCTAAGGGCGAAGAGCTGATTAAGG
FP635-R	CTATTCTTTCCCCTGCACTGTACCCCCCAATC
TFAM-TagRFP-R	AGCTCTTCGCCCTTAGACACACACTCCTCAGCACCATATTTTCG
TFAM-TagRFP-F	ATGGTGCTGAGGAGTGTGTGTCTAAGGGCGAAGAGCTGATTAAGG
TagRFP-R	CTAATTAAGTTTGTGCCCCAGTTTGCTAGGGAGGTC
TFAM-KR-R	CCTCTGAACCACACTCCTCAGCACCATATTTTCG
TFAM-KR-F	AGGAGTGTGGTTCAGAGGGCGGCCCCGCCCTG
KR-R	CTAGATCTCGTCGTGGCTACCGATGGCGCTGG

TFAM was fused on the N-terminus of the different FAPs. The mCer3 and TagRFP tags were used as a subcellular fluorescent marker for the proteins and can be used as a negative control when a fluorogen is added.

The open reading frames of mCer3, Charlie-mCer3, dH6-mCer3, dL5-mCer3, TagRFP and KillerRed were engineered to include 10 base pairs (bp) of TFAM on their N-terminus for PCR joining with respective TFAM, which was also engineered to include between 19-28 bp of each of the FAPs on its C-terminus. Joining PCR was carried out with PCR purified products for

10 cycles without polymerase to join the respective products, and then used in standard PCR with polymerase (**Figure 36*A***). PCR purified complementary DNA was cloned into pENTR/D-TOPO plasmid to create the pENTR-UBE3B vector as per standard Topo-cloning methodology (197). Positive clones were selected and plasmids were extracted with the QIAprep Spin Miniprep Kit (Qiagen) (**Figures 36*B***).

Once sequenced verified, the open reading frames from each of the plasmids, pENTR-TFAM-mCer3, pENTR-TFAM-mCer3-Charlie, pENTR-TFAM-mCer3-dH6, pENTR-TFAM-mCer3-dL5, pENTR-TFAM-KillerRed, pENTR-TFAM-FP635 and pENTR-TFAM-TagRFP were transferred into a Gateway-modified pLVX-IRES-Neo vector, (Clontech) by the LR reaction using the Gateway LR Clonase II Enzyme Mix (Life Technologies) as per the manufacturer's instruction. Positive clones were selected and plasmids were extracted with the QIAprep Spin Miniprep Kit (Qiagen). All the vectors developed for this project are listed in **Table 8**.

Table 8. Vectors developed for and used in this study.

Plasmid name	Insert description	Parental vector
pENTR-TFAM-mCer3	TFAM-mCer3	pENTR/D-TOPO
pENTR-TFAM-mCer3-Charlie	TFAM-mCer3-Charlie	pENTR/D-TOPO
pENTR-TFAM-mCer3-dH6	TFAM-mCer3-dH6	pENTR/D-TOPO
pENTR-TFAM-mCer3-dL5	TFAM-mCer3-dL5	pENTR/D-TOPO
pENTR-TFAM-FP635	TFAM-FP635	pENTR/D-TOPO
pENTR-TFAM-TagRFP	TFAM-TagRFP	pENTR/D-TOPO
pENTR-TFAM-KillerRed	TFAM-KillerRed	pENTR/D-TOPO
pLVX-TFAM-mCer3-IRES-Neo	HA-mCer3	pLVX-GW-IRES-Neo
pLVX-TFAM-mCer3-Charlie-IRES-Neo	TFAM-mCer3-Charlie	pLVX-GW-IRES-Neo
pLVX-TFAM-mCer3-dH6-IRES-Neo	TFAM-mCer3-dH6	pLVX-GW-IRES-Neo
pLVX-TFAM-mCer3-dL5-IRES-Neo	TFAM-mCer3-dL5	pLVX-GW-IRES-Neo
pLVX-TFAM-FP635-IRES-Neo	TFAM-FP635	pLVX-GW-IRES-Neo
pLVX-TFAM-TagRFP-IRES-Neo	TFAM-TagRFP	pLVX-GW-IRES-Neo
pLVX-TFAM-KillerRed-IRES-Neo	TFAM-KillerRed	pLVX-GW-IRES-Neo

Lentiviruses were prepared in collaboration with the UPCI Lentiviral facility. Lentiviral particles were generated by co-transfection of 4 plasmids [Control plasmid (pLVX-IRES-Neomycin) or one of the plasmids, together with pMD2.g (VSVG), pVSV-REV and pMDLg/pRRE] into 293-FT cells using TransIT®-2020 Transfection reagent. The collection and isolation of lentiviral particles and transduction of LN428 cells were performed as described previously (198,199). Stable cell lines were developed by selection in neomycin (2 µg/mL) for 2 weeks.

Table 9. LN428 cell lines developed and used in this study.

Cell line name	Cell line description	Growth media*
LN428	Human glioblastoma tumor cell line	Media #1
LN428/TFAM-mCer3	LN428 cells expressing TFAM-mCer3	Media #2
LN428/TFAM-mCer3-Charlie	LN428 cells expressing TFAM-mCer3-Charlie	Media #2
LN428/TFAM-mCer3-dH6	LN428 cells expressing TFAM-mCer3-dH6	Media #2
LN428/TFAM-mCer3-dL5	LN428 cells expressing TFAM-mCer3-dL5	Media #2
LN428/TFAM-FP635	LN428 cells expressing TFAM-FP635	Media #2
LN428/TFAM-TagRFP	LN428 cells expressing TFAM-TagRFP	Media #2
LN428/TFAM-KillerRed	LN428 cells expressing TFAM-KillerRed	Media #2

*Media #1: α-MEM with 10% heat inactivated FBS, 5µg/ml Gentamycin, 80µg Penicillin/80µg Streptomycin/0.32µg Amphotericin per ml, 2mM L-Glutamine.

*Media #2: Media #1 supplemented with Neomycin (1.0 µg/ml).

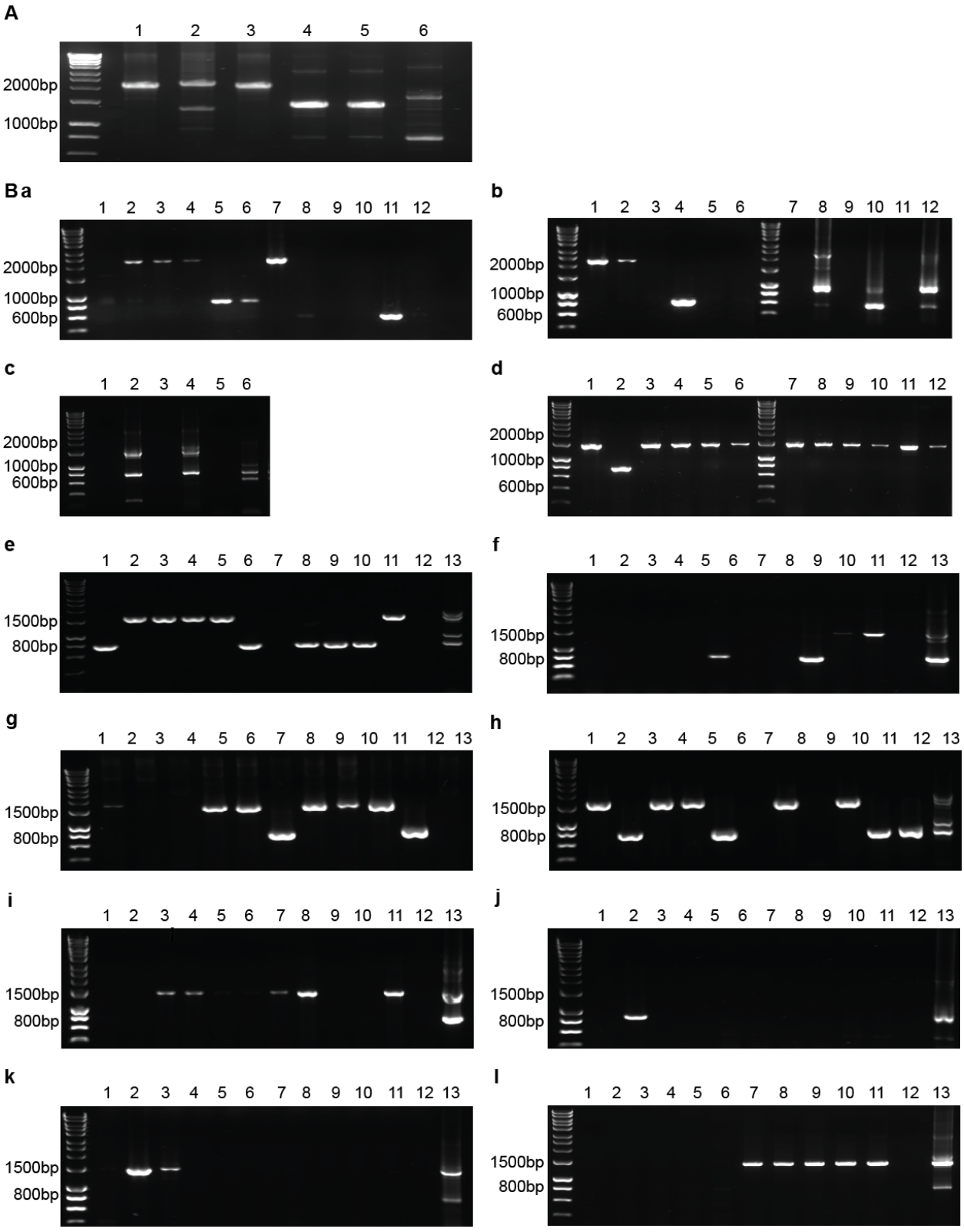

Figure 36. Generation of TFAM-fusion constructs.

After primer pairs were optimized using Platinum® *Pfx* DNA Polymerase and respective plasmids (refer to Tables 1 and 2 respectively) and PCR purified, the PCR products were used in **(A)** Joining PCR using 72°C as the best annealing temperature for primers **(B)** PCR amplification screen using *Taq* DNA Polymerase of mini-prep **(a)** Lanes 1-6: pENTR-TFAM-Charlie and Lanes 7-12: pENTR-TFAM-dH6, **(b)** Lanes 1-6: pENTR-TFAM-dL5 and Lanes 7-12 : for controls for TFAM-Charlie, TFAM-dH6 and TFAM-dL5 **(c)** Lanes 1-4: pENTR-TFAM-FP635 and Lanes 5 and 6: Controls for FP635, **(d)** Lanes 1-6: pENTR-TFAM-KillerRed and Lanes 7-12: pENTR-TFAM-mCer3 (e) pENTR-TFAM-FP635, (f) pENTR-TFAM-TagRFP, (g) pENTR-TFAM-FP635, (h) pENTR-TFAM-FP635, (i) pENTR-TFAM-TagRFP, (j) pENTR-TFAM-Charlie, (k) pENTR-TFAM-KillerRed, and (l) pENTR-TFAM-mCer3, plasmids from transformed One Shot Top 10 *E.coli* cells. Only plasmids with correct size inserts were sequenced verified and used in LR reactions to transfer the open reading frame inserts into pLVX-GW-IRES-Neo vector.

C.3 RESULTS AND DISCUSSION

In this project we utilized a novel system of organelle specific (in this case, the mitochondria) oxidative damage that utilizes genetically encoded and small-molecule activated photosensitizer proteins. These proteins are directed to the mitochondria via fusion with TFAM. Upon visible light-stimulation and/or small-molecule binding (fluorogen activating proteins or HaloTag), ROS is produced only in the mitochondria, thus allowing us to study its damaging effects on the mitochondria, specifically the damaged mitochondrial proteins.

We generated seven different constructs fused to the TFAM sequence (**Figure 37**). Three were controls (TFAM-mCer3, TFAM-FP635 and TFAM-TagRFP), to determine transfection efficiently or select for cells stably expressing the fusions, and to show that the tag itself was generating oxidative stress itself in the cells (**Figure 38**).

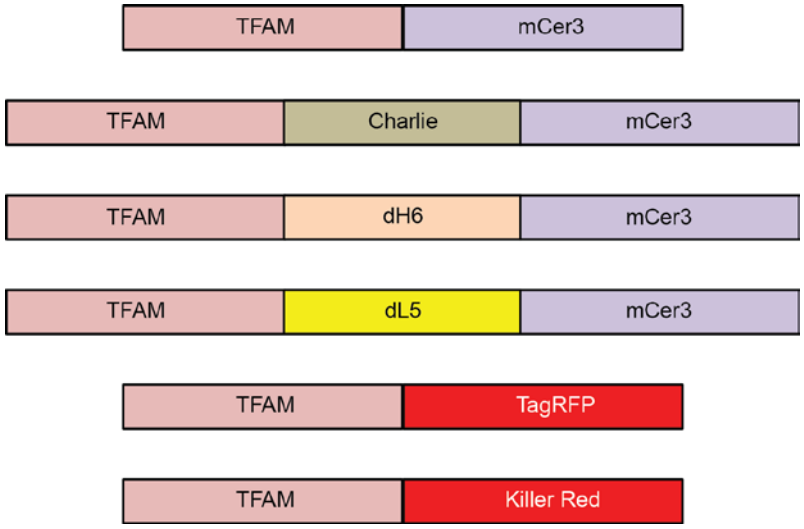

Figure 37. Schematic for the TFAM-fusions.

TFAM was fused on the N-terminus of the different FAPs. The mCer3 and TagRFP tags were used as a subcellular fluorescent marker for the proteins and can be used as a negative control when a fluorogen is added.

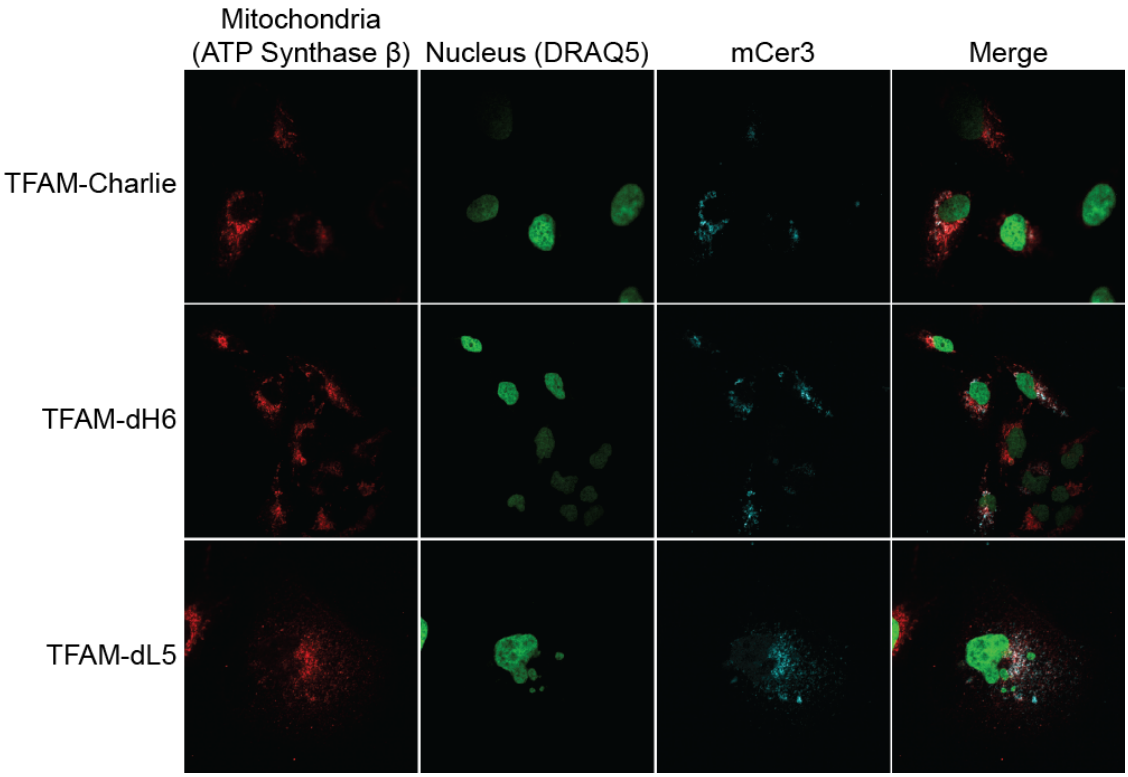

Figure 38. : Immunofluorescence for LN428 cells stably expressing the TFAM-fusion proteins.

LN428 cells were transduced with lentiviral particles to create stable cell lines that expressed TFAM-mCer3, TFAM-mCer3-Charlie, TFAM-mCer3-dH6, TFAM-mCer3-dL5, TFAM-KillerRed, TFAM-FP635 and TFAM-

TagRFP protein. The mitochondria were stained with ATP Synthase β as a marker, fixed and imaged using the Confocal A1 Nikon Microscope.

This novel system has the advantage of selectively directing the ROS generating complex to the mitochondrial genome and will provide insight into the source of ROS needed to activate the UBE3B response, this identifying the degradation pathway(s) that lead to disruption of mitochondrial homeostasis and disease.

APPENDIX D

$CACL_2$ TREATMENT IN CELLS

We performed these experiments to determine if we would see similar changes in the UBE3B/CaM interaction after $CaCl_2$ treatment of cells.

LN428 cells expressing HA-tagged UBE3B WT or were grown to 90% confluence in 100mm dishes. Serum-free media was added to the cells for 12 hours. The cells were treated with growth media, 1.25 mM $CaCl_2$, 1.25 mM $CaCl_2$ + 1µM Ionomycin, 1.25 mM $CaCl_2$ + 10µM MG-132, 1.25 mM $CaCl_2$ + 1µM Ionomycin + 10µM MG-132, or 0.25mM EGTA for 6 hours in normal growth media. The treated cells were harvested using IP Lysis Buffer supplemented with Protease Inhibitor (both from Thermo Fisher Scientific). The lysates were rotated for 1 hour at 4°C before pelleting the cell debris. The supernatant was incubated by rotating overnight at 4°C with Anti-HA Affinity Matrix (Roche). The beads were washed with Binding Buffer (10mM $Na_2H_2PO_2$, 10mM Na_2HPO_4 and 150µM NaCl; pH 7.0), followed by washes with Ubiquitylation Assay Buffer (10 mM Tris-HCl, pH 7.5, 100 mM NaCl, and 0.5 mM DTT). The ubiquitylation assay was performed on the beads for 2 hours at 30°C in a volume of 30µL containing 0.1µM E1 (Boston Biochem), 0.25µM of each of the E2s (UBE2A/UBE2D1/UBE2D3/UBE2G2/UBE2L3/UBE2N/UBE2S/UBE2Z) (Life Sensors), 1µM

ubiquitin aldehyde (Boston Biochem), 0.75µg/µL purified His-ubiquitin (see below) and 1X Magnesium/ATP cocktail (EMD Millipore). The ubiquitylation assays were stopped by adding 2X blue Laemmli (plus β-Mercaptoethanol) and heating the samples at 70°C for 15 minutes. Ubiquitylation activity and the presence of CaM were measured by immunoblot (**Figure 39**).

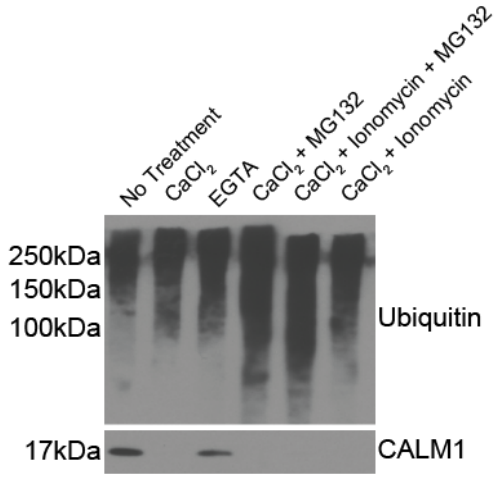

Figure 39. *In vivo* treatment of HA-UBE3B with $CaCl_2$.

HA-UBE3B overexpressing cells were serum starved for 12 hours. They were treated with No Treatment, 1.25 mM $CaCl_2$, 0.25 mM EGTA, 1.25 mM $CaCl_2$ + 10µM MG132, 1.25 mM $CaCl_2$ + 1µM Ionomycin + 10µM MG132, or 1.25 mM $CaCl_2$ + 1µM Ionomycin for 6 hours. The cells were lyzed, immunoprecipitated (IPed) using Anti-HA Affinity Matrix and subjected to ubiquitylation activity assays. The ubiquitylation assays were carried out in 30µL reactions with 0.1µM E1, 0.25µM of each of the E2s (UBE2A/UBE2D1/UBE2D3/UBE2G2/UBE2L3/UBE2N/UBE2S/UBE2Z), 1µM ubiquitin aldehyde, 0.75µg/µL His-ubiquitin and 1X Magnesium/ATP cocktail. Completed reactions were applied to immunoblot for analysis of ubiquitylation with Ubiquitin (Ub), and CaM binding with Calmodulin (CALM1) antibodies. Representative immunoblots from three independent experiments are shown. Antibodies used for each of the immunoblots are listed on the side of the panels.

APPENDIX E

The book chapter was published in *Genotoxicity and DNA Repair: A Practical Approach*, Methods in Pharmacology and Toxicology, and compiled below.

USE OF RNA INTERFERENCE TO STUDY DNA REPAIR

Elise Fouquerel, Jianfeng Li, Andrea Braganza, Zhongxun Yu, Ashley R. Brown, Xiao-Hong Wang, Sandy Schamus, David Svilar, Qingming Fang, and Robert W. Sobol

E.1 ABSTRACT

DNA repair pathways maintain the integrity of the genome and thereby help prevent the onset of cancer, disease, and aging phenotypes (294). As such, the critical requirement for DNA repair proteins and pathways in response to radiation and genotoxic chemotherapeutics implicates DNA repair proteins as prime targets for improving response to currently available anticancer regimens. Although defects in critical DNA repair pathways or proteins can predispose to cancer onset (295), such cancer-specific DNA repair defects offer novel approaches for tumor-selective therapy.

To effectively evaluate the functional role of a specific DNA repair protein with regard to cell survival, response to genotoxins, and genome stability, it has become standard practice to employ select genetic tools to alter expression of the gene of interest and/or reexpress a mutant transgene (196,201,296). A useful approach to reduce or suppress a specific gene of interest in cells is RNA interference. Briefly, RNA interference is a posttranscriptional gene-silencing biological mechanism whereby RNA molecules inhibit gene expression either by translational suppression or by the targeted degradation of specific mRNA molecules. Once the gene of interest is suppressed in this manner and validated for gene expression loss, the resulting knockdown (KD) cells can be used for functional analysis to define the cellular impact of gene loss and provide a resource for evaluating mutants of the gene, such as somatic or germ-line mutations, for impact on function (297). Herein, we describe methods to modify human cells via RNA interference as well as methods to validate gene KD and some measures of cellular response to genotoxins to uncover functional DNA repair defects in the absence of the gene.

Key words RNA interference, siRNA, shRNA, Lentivirus, Knockdown, qRT-PCR, PARP, DNA damage response, Cell survival

E.2 INTRODUCTION

In this chapter, we describe several methods we have employed for regulating gene expression in human cells via RNA interference. We present approaches for both transient (siRNA) and stable (shRNA) gene knockdown (KD) as well as the details for several procedures routinely used for validation of gene expression loss (**Figure 40**). Finally, we describe numerous functional

endpoints useful in characterizing the impact of the targeted gene depletion with regard to DNA repair and the cellular response to genotoxins.

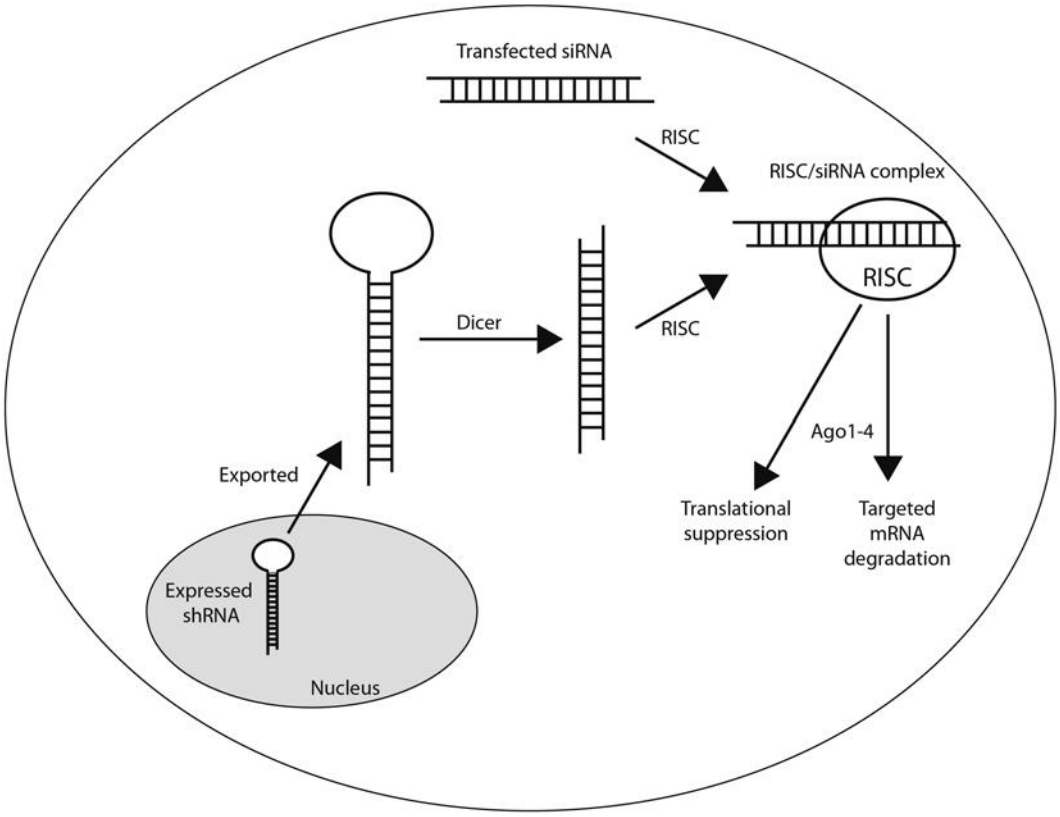

Figure 40. Simplified diagram of siRNA and shRNA processing to facilitate gene knockdown.
The transduced shRNA is exported from the nucleus to the cytoplasm and processed by Dicer to yield a siRNA-like molecule similar to the transfected siRNA. These are bound with the RISC complex and the Ago proteins to trigger translational suppression or target mRNA degradation.

E.2.1 RNA Interference in Human Cells Using siRNA

RNA interference (RNAi) is a highly specific posttranscriptional gene-silencing mechanism that is mediated by the introduction of double-stranded (ds) RNA molecules 21 bp in length, referred to as short interfering RNA or siRNA (**Figure 40**). One strand of the siRNA is then incorporated into an RNA-silencing complex (RISC) to target the complementary RNA for destruction by a

second nuclease, Ago2 (298-300). Note that there are multiple Ago family proteins (Ago1–Ago4) involved in siRNA and microRNA (miRNA) processing (301). Molecules of siRNA are now routinely used to transiently silence gene expression in a gene- and sequence-specific manner (302-304). Molecules such as siRNAs are important tools to investigate DNA repair pathways because the expression of select DNA repair factors can be transiently suppressed (knocked down; KD) with high specificity and selectivity using these complementary oligoribonucleotide molecules. This method of gene regulation has become invaluable to identify gene function, validate anticancer gene targets, and is currently being evaluated for clinical potential (305). The utility of RNAi as a genetic tool for the study of biological pathways and stress responses in mammalian cells has made significant strides since the first demonstration of RNAi in mammalian cells in 2001 (303).

The siRNA can be delivered directly to cells using multiple approaches, including microinjection, electroporation, and transfection (306). Currently there are two variations of siRNA transfection procedures being used: forward transfection and reverse transfection. They differ in the order and timing of the addition of the three necessary components for transfection: (1) the siRNA molecules, (2) the lipid-based transfection reagent, and (3) the cells to be targeted. In the forward (standard) transfection proto-col, the siRNA and lipid are complexed together and then added to pre-plated cells (e.g., normally the cells are seeded to the wells of a plate 24 h before addition of the siRNA/lipid complex). In the reverse transfection protocol, the siRNA/lipid mixture is added to the wells of the plate first and then the cells are added subsequently. Reverse transfection offers the flexibility of testing siRNA reagents at various concentrations or utilizing existing siRNA library resources to perform large-scale screens (200). To demonstrate the utility of siRNA, we will focus on the reverse transfection procedure

optimized in our lab and will provide detailed information on the procedures and expected outcomes using siRNA to knock down the DNA repair gene UNG (200).

E.2.2 RNA Interference in Human Cells Using shRNA

RNAi-mediated knockdown can also be achieved via the expression of double-stranded RNA (dsRNA) hairpins of 21–23 bp in length (**Figure 40**), referred to as small hairpin RNA or short hairpin RNA (shRNA). The expressed shRNA is transported from the nuclease to the cytoplasm and cleaved by a nuclease (Dicer) into dsRNAs of 21–23 bp in length to yield the desired siRNA and is processed as indicated above. Stable expression of shRNAs can mediate effective gene knockdown (307-309). Most recently, expression of shRNA in cells is typically accomplished using retroviral or lentiviral vectors although lentiviral vectors have become the most routinely used and are the most commonly available resource. To prepare HIV-based lentivirus particles, the shuttle vector (encoded to express the shRNA and a selection cassette such as puromycin, G418, or EGFP) is co-transfected with the required lentiviral packaging vectors into a packaging cell line such as 293FT (310), a clonal derivative of the human kidney 293T cell line (Invitrogen). Complete libraries of shRNA shuttle vectors specific to any human or mouse gene are available from a number of commercial sources, including Sigma, Thermo Scientific, System Biosciences, among many others. Numerous packaging systems have been reported and most are commercially available or available from Addgene (http://www.addgene.org). We routinely use the so-called “third-generation” packaging system in which the gene-specific shRNA plasmids are co-transfected into 293FT cells together with the packaging plasmids pMD2.g(VSVG), pRSV-REV, and pMDLg/ pRRE to generate replication-defective viral particles capable of

transducing numerous cell types (201,311). Virus particles are isolated from the cell culture supernatant and may be stored at −80 °C or used immediately for transduction of the target cell. With the proper selection, a stable gene silenced or KD mammalian or human cell line can be readily established (196,200,201,312).

E.2.3 Validating Gene Knockdown by qRT-PCR

A critical and essential aspect of any RNAi experiment is validation of gene knockdown. This is most readily accomplished by a quantitative reverse transcription polymerase chain reaction (qRT-PCR) analysis using a real-time qRT-PCR protocol (313). Although the specificity of siRNA is normally very precise (314), it is essential to also test the expression of other relevant genes to most effectively conduct your study. For example, when studying the role of DNA polymerase β (Polβ) in response to chemotherapeutic agents (197), we routinely test the expression of several of the relevant base excision repair (BER) genes such as MPG, APE1, and PARP1 (296). An advantage of analysis by qRT-PCR is the ready availability of specific reagents. Material for RNA isolation or qRT-PCR-ready cell lysates are readily available, and validated primers and probes for real-time qRT-PCR are available for any gene. In general, we routinely analyze a transfected (siRNA) or transduced (shRNA) cell line for gene knockdown using RNA from three separate samples, comparing expression to a control such as the same cell line transfected with a control siRNA or transduced with a GFP-expressing or scrambled shRNA-expressing lentivirus. Analysis across samples is normalized to the expression of β-actin, measured for each sample. As expected, the goal is to achieve complete gene expression knock-down. In practice, knockdown greater than 75 % is likely to yield a significant loss of steady-

state protein levels and result in a functional impact from the loss of the expressed mRNA (196,201,296).

E.2.4 Validating Gene Knockdown by Immunoblot

The ultimate and most stringent validation to demonstrate that you have succeeded in "knocking down" your gene is to show a loss or suppression of protein expression (315). We routinely use immunoblotting to validate the loss of gene expression and in some cases, complement this analysis with a functional test (296). However, the loss of protein, as determined by immunoblotting, is a highly reliable method for validating gene expression loss. This standard laboratory analytical procedure is only limited by the availability of the antibody.

E.2.5 PARP Activation in Response to DNA-Damaging Agents

Genomic DNA damage from genotoxins must be repaired to prevent gene mutations, aneuploidy, senescence, or cell death that can contribute to cancer, early-onset aging, and/or degenerative diseases (294). There are multiple overlapping mechanisms and processes in human cells that govern and orchestrate the response to genotoxins, collectively referred to as the DNA damage response (DDR) (316). The initial DDR of a cell involves the recognition of the DNA damage followed by the propagation of a series of signals ranging from alterations in RNA or protein expression and modification of protein function or stability through posttranslational modification, among other signals. The cell's defense to genotoxic lesions is triggered and

accomplished by a series of events that mediate and regulate proliferation, cell death, or DNA repair crucial to its survival (317,318).

PARP1 is a major response protein in the DDR pathway and binds to and is activated by damaged DNA (strand breaks) to initiate a signal cascade by utilization of NAD^+ to modify numerous proteins with poly-ADP-ribose (PAR), including histones, polymerases, topoisomerases, and PARP1 itself (319). PARP1 (as well as PARP2 and PARP3) (320,321) acts as sensors of DNA damage such as DNA single-strand or double-strand breaks and becomes activated, consuming NAD^+ to synthesize PAR (201). It is clear that activated PARP1 (together with PARP2 and PARG) facilitates DNA repair via roles in BER (322) and nonhomologous end joining (NHEJ) (320,323-330), the latter also involving PARP3 (320). In this context, being able to detect PAR levels in cells is an effective method to define the sensitivity of a cell to a DNA-damaging agent and its capacity to repair such damage. In this chapter, we describe two standard approaches to detect and quantify PAR, either by immunoblot or immunofluorescence.

E.2.6 Complementing Gene KD Cells and Evaluating Cell Survival in Response to DNA-Damaging Agents

One of the advantages of developing a stable KD cell line, deficient in the expression of the endogenous gene, is the capacity to then complement the cell line by reexpression of the cDNA, for example, with the wild-type (WT) cDNA or encoding a mutation (**Figure 41**). By analysis of normal and cancer tissues, it has been found that most of the 150–200 genes among the DNA repair pathways harbor germ-line or somatic mutations. For example, there are numerous mutations for the BER gene Polβ found to have either protein-altering germ-line single-nucleotide polymorphisms (SNPs) or functionally altering somatic mutations when isolated from

tumor tissue (297). In fact, it was recently described that "… we can expect all cancer cells to be defective in some aspect of DNA repair … There are at least 150 different proteins that catalyze DNA repair … To seed new therapies, geneticists and molecular biologists are needed to explore the detailed consequences of an alteration in each of these repair pathways…" (331).

To facilitate effective complementation and expression of the transgene while reducing endogenous expression by RNAi, one must either mutate the cDNA to eliminate the RNAi target sequence or use an shRNA specific for the 3′untranslated region of the target gene (**Figure 41**). Once accomplished, the utilization of an RNAi-resistant expression system is a robust method to reexpress or complement a KD cell line. Following gene knockdown, we routinely develop lentiviral-based cDNA expression vectors to complement the KD cells. With such a system, the investigator is open to effectively study KD phenotype rescue, the functional role of specific amino acid residues such as those in the enzyme active site, those implicated in protein-protein interactions, or those that may be a target for posttranslational modification. Once in hand, these modified cell lines are then valuable resources to evaluate the role of these proteins (and mutants) in response to genotoxins.

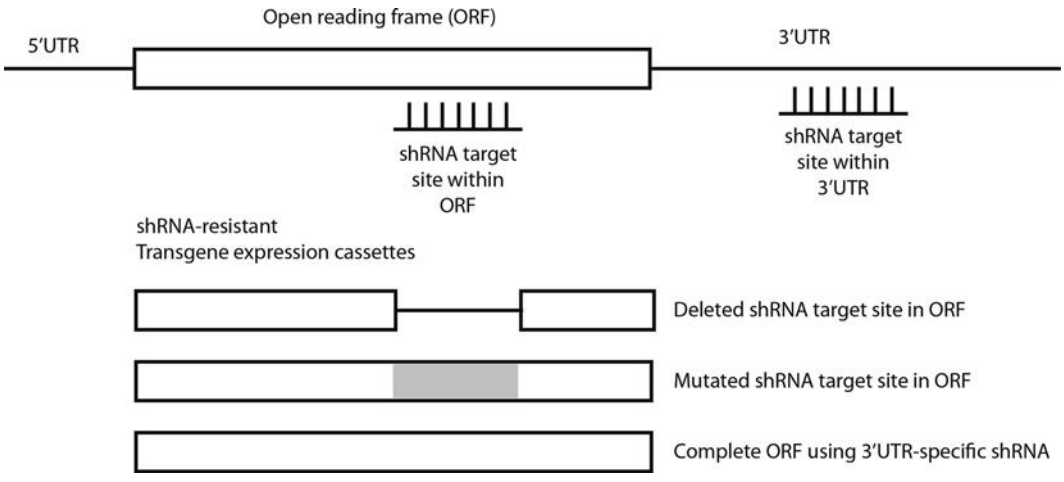

Figure 41. Scheme for transgene complementation after gene knockdown.
The target for RNA interference can be within the open reading frame (ORF) of the target mRNA or specific to the

3′untranslated region (3′UTR). As indicated, effective transgene design for shRNA-resistant expression of your target gene requires either deletion of the shRNA target site within the ORF, mutation of the shRNA target site within the ORF, or expression of the transgene in cells targeted with a 3′UTR-specific shRNA

Cells treated with cytotoxic compounds will respond differently depending on the DNA repair capacity of the cell. For example, cells expressing the protein MGMT are highly resistant to the cytotoxic effects of the alkylating agent-induced DNA lesion O ^{6}-methyl-dG, but in the absence of MGMT expression, the lesion is highly toxic (296). There are many methods to measure cytotoxicity. Here, we will focus on the MTS assay and the CyQUANT assay that are used to monitor the cytotoxicity of a genotoxin after short-term or long-term exposure to the agent, respectively.

The MTS assay measures the reducing potential of the cell using a colorimetric reaction. Viable cells can reduce the agent 3-(4,5-dimethylthiazol-2-yl)-5-(3-carboxymethoxyphenyl)-2-(4-sulfophenyl)-2*H*-tetrazolium (MTS) to produce a formazan product that has an absorbance maximum at 490–500 nm in phosphate-buffered saline (PBS), in the presence of phenazine methosulfate (332). The MTS assay is more convenient than the MTT assay, since the reagent can be added to the cells directly without the intermittent steps required in the MTT assay. However, this convenience makes the MTS assay susceptible to colorimetric interference (333). In general, one needs to take caution when using this assay, depending on the cell type, the DNA-damaging agent, and the experiment as a whole. Since the assay measures cellular reducing potential (mitochondrial function), a resting cell may have a lower overall level of reducing potential, whereas a highly proliferative cell is likely to have a high reducing potential. In that regard, treatments that induce senescence but not cell death may appear in this assay to reduce cell number. To avoid such potential problems, we routinely test cells using the MTS assay as well as a second assay, as described below.

The CyQUANT assay is based on a cell-permeable DNA-binding dye in combination with a background suppression reagent to estimate cell number (334). We routinely use this assay to evaluate genotoxic response 8–12 days after exposure to the agent. As DNA content is highly regulated, cell number estimates are very accurate. The masking dye blocks staining of dead cells and cells with compromised cell membranes, causing only healthy cells to be stained. Recent studies using diverse sets of cytotoxic compounds and assay types have shown that cell number (proliferation) is among the most sensitive indicators of cytotoxicity (335). In our hands, this assay yields cell survival or proliferation outcomes similar to that of a clonogenic assay if control cells are allowed to undergo seven or more doublings before analysis. Therefore, the CyQUANT assay provides a highly accurate measure of cell number, allowing for the evaluation of proliferation as well as cytotoxicity in response to genotoxin exposure.

E.3 MATERIALS

E.3.1 RNA Interference in Human Cells Using siRNA

- siRNA specific for human UNG (Ambion; cat# 4390824; siRNA ID: s14679)
- Silencer® Negative Control #2 siRNA (50 μM) (Ambion; AM4613)
- siPORT™ NeoFX™ Transfection Agent (Applied Biosystems; AM4511)
- Opti-MEM® 1 Reduced-Serum Medium (1×), liquid (Invitrogen; 31985-070)

- Trypsin, 0.25 % (1×) with EDTA, liquid (Invitrogen; 25200-114)
- PBS (Invitrogen; 14190-250)

All the listed reagents are stored according to the manufactures' instructions.

E.3.2 RNA Interference in Human Cells Using shRNA

- The three lentiviral packaging plasmids (pMD2.g(VSVG), pRSV-REV, and pMDLg/pRRE), available from Addgene (cat# 12259, #12253, and cat #12251, respectively)
- The 293FT cell line (cat# R700-07), available from Life Technologies
- TransIT-293 (cat# MIR-2704, 2700, 2705, or 2706), avail-able from Mirus
- Millipore Steriflip vacuum filters (cat# SE1M003M00), avail-able from Fisher Scientific (Fisher Scientific cat# SC50 FL0 25)
- Lenti-X Concentrators (cat# 631231), available from Clontech
- Ultracentrifuge tubes (Beckman Ultra-Clear tubes, cat# 344058), available from Fisher Scientific (Fisher Scientific cat# NC9146666)

E.3.3 Validating Gene Knockdown by qRT-PCR

- TaqMan® Gene Expression Cells-to-CT™ Kit (cat# AM1728), available from Life Technologies.
- PBS (cat# 14190-250), available from Invitrogen.
- DNase and RNase-free H_2O.
- Two heat blocks set to 37 and 95 °C or a PCR thermocycler.

- Applied Biosystems StepOnePlus™ Real-Time PCR System.
- Applied Biosystems StepOne™ Software.
- TaqMan® Gene Expression Assays (the specific assay will depend on the gene you are targeting) are available from Life Technologies.
- TaqMan® Gene Expression Master Mix is available from Life Technologies.

E.3.4 Validating Gene Knockdown by Immunoblot

Cell extracts diluted twice in the sample buffer (2×). For cell extracts prepared for detection of PAR, *see* Sect. 2.5.

Note: *Alternatively and depending on the molecular weight of the protein of interest, a higher or lower concentration of Acryl/ Bis 30 % can be used.*

- Sample buffer (2×) (LaemmLi blue 2×: 2 % SDS, 20 % glyc-erol, 62.5 mM Tris-HCl, pH 6.8, 0.01 % Bromophenol blue).
- Stacking gel buffer (Tris-HCl 0.5 M, pH 6.8, SDS 0.4 %) - also sold as a ready-to-use solution by Bio-Rad (cat# 161-0799) (stable at room temperature).
- Separating gel buffer (Tris-HCl 1.5 M, pH 8.8, SDS 0.4 %) - also sold as a ready-to-use solution by Bio-Rad (cat# 161-0798) (stable at room temperature).
- Isopropanol (100 %).
- Acryl/Bis 30 %; ratio 37.5/1 (Bio-Rad cat#) (keep at 4 °C).
- Ammonium persulfate (APS).
- *N*,*N*,*N*′,*N*′-Tetramethylethylenediamine (TEMED) (Bio-Rad cat# 161-0800) kept at 4 °C.

- Running buffer, 5× (30 g/L Tris-base, 144 g/L glycine, 0.5 % SDS) stored at room temperature. A 1× solution is prepared by mixing 200 mL of a 5× stock solution and 800 mL of dH_2O. This solution can be used up to five times and is kept at room temperature.
- Vertical electrophoresis system, 1.0 mm gel thickness (e.g., Mini-PROTEAN® Tetra Cell, Bio-Rad).
- Prestained protein molecular weight markers—for example, Precision Plus Protein Kaleidoscope™ from Bio-Rad (cat# 161-0375).
- Blotting transfer buffer, 10× (30 g/L Tris-base, 144 g/L glycine, 1 % SDS). The stock solution can be stored at room temperature. Before the transfer, prepare a 1× solution by diluting 100 mL of the 10× stock solution in 615 mL of dH_2O and adding 285 mL of 70 % ethanol. This solution can be reused up to five times if stored at 4 °C.
- Blotting transfer system (Mini Trans-Blot Electrophoretic Transfer Cell, Bio-Rad).
- Nitrocellulose transfer membrane (Bio-Rad Nitrocellulose Membranes 0.45 μm; cat# 162-0115).
- TBS-Tween 0.3 % buffer (TBT): prepared by diluting Tris-buffered saline, pH 7.4 (10×; Boston BioProducts; cat# BM-300), in 900 mL dH_2O and adding 3 mL of 100 % Tween 20. The TBS is also available in powder format (Sigma-Aldrich; cat# D5773).
- Blocking powder (Blotting-Grade Blocker; cat# 170-6404) or low-fat dry milk.

  Note: *BSA can be used for special antibodies if speciÞed by the company.*
- Primary antibody against the protein of interest.
- Secondary antibody (we use goat anti-mouse or goat anti-rabbit horseradish peroxidase (HRP) conjugate from Bio-Rad; an alternate secondary antibody can be used depending on the primary antibody species).

- *Detection reagents*: For expected normal-to-strong signals, we use Immun-Star™ HRP from Bio-Rad (cat# 170-5040). If the signal is expected to be weak or low, a more sensitive product can be used such as SuperSignal ® West Femto Maximum Sensitivity Substrate from Thermo Fischer (cat# 34095).
- *Detection system*: The HRP signal can be detected using X-ray film. We use Premium X-ray Film from Phenix (#EBA45) or a Bio-Rad Molecular Imager® Chemidoc™ XRS+ system.

E.3.5 PARP Activation in Response to DNA-Damaging Agents

Poly-ADP-ribose Detection by Immunoblot

- DNA-damaging agents specific to your experiment (MNNG, methyl methanesulfonate (MMS), H_2O_2, ionizing radiation, etc). In the example shown here, we use MNNG, *N*′-methyl-N′-nitro-*N*-nitrosoguanidine (prepared as a 10 mM stock solution in DMSO), available from TCI America (# N0527; Portland, OR).
- Plated cells.
- Ice-cold PBS (cat# 14190-250), available from Invitrogen.
- Sample buffer 2× (*see* Sect. 2.4).
- Materials for SDS-PAGE and immunoblot as described in Sect. 2.4.
- Mouse monoclonal PAR antibody 10H (196,201).
- Secondary antibody; goat anti-mouse Ab conjugated with HRP.

Poly-ADP-ribose Detection by Immunofluorescence

- Coverslips washed in 5 mL 70 % ethanol
- Microscope slides

- DNA-damaging agents specific to your experiment (MNNG, MMS, H_2O_2, ionizing radiation, etc)
- Methanol and acetone (100 %), stored at −20 °C
- PBS-Triton X-100, 0.1 % (alternatively, PBS-Tween 0.3 % can be used)
- PBS-BSA, 0.5 %
- PBS-BSA, 2 %
- Primary antibody mouse; monoclonal anti-PAR, clone 10H (196,201)
- Secondary antibody; goat anti-mouse Ab conjugated with Alexa Fluor 488
- Mounting solution containing DAPI (ProLong® Gold Antifade Reagent with DAPI; Life technologies cat# P-36931).

E.3.6 Complementing Gene KD Cells and Evaluating Cell Survival in Response to DNA-Damaging Agents

Complementation or reexpression of the protein of interest after gene KD can be accomplished using any plasmid- or viral-based transgene expression system. We have found success with lentiviral vectors (e.g., from Clontech), allowing expression of DNA polymerase β (Polβ) with numerous selection agents such as hygromycin, G418, or EGFP. Most of the shRNA lentiviral vectors we have used employ a puromycin cassette for selection. Therefore, using separate selection agents for complementation is critical. We find no difficulty with transducing a cell multiple times, for example, to express shRNA for gene KD followed by transduction with a cDNA expression vector to reexpress the gene of interest or to express mutants of the cDNA

(332). Once stable cell lines are developed, they yield a valuable resource for analysis of cell survival in response to DNA-damaging agents (200,296,336).

MTS Assay

- Cell culture medium (depends on which cell used).
- PBS (cat# 14190-250), available from Invitrogen.
- MNNG, *N*′-methyl-*N*′-nitro-*N*-nitrosoguanidine (prepared as a 10 mM stock solution in DMSO), available from TCI America (# N0527; Portland, OR).
- Promega CellTiter 96 AQueous One, available from Promega (Catalogue No. G356B), aliquot and store at −30 °C.
- Hemocytometer, CASY counter, or similar cell counting device.
- Multi-well aspirator.
- Multichannel pipettor.
- Cell culture medium (depends on which cell used).
- PBS (cat# 14190-250), available from Invitrogen.
- MNNG, *N*′-methyl-*N*′-nitro-*N*-nitrosoguanidine (prepared as a 10 mM stock solution in DMSO), available from TCI America (# N0527; Portland, OR).
- CyQUANT GR reagent (Catalogue No. C7026, Life technol-ogies), store at −30 °C.
- Lysis buffer, store at 4 °C.
- Parafilm.
- Hemocytometer, CASY counter, or similar cell counting device.
- Multi-well aspirator.
- Multichannel pipettor.

E.4 METHODS

E.4.1 RNA Interference in Human Cells Using siRNA

Validated siRNAs are available from a number of sources and are generally available as individual siRNAs or a gene-specific pool. Further, libraries can be obtained for the entire genome or those that are limited to specific functional biological pathways or other subgroups such as the druggable genome (200).

The siRNA provided by Ambion is supplied as a lyophilized powder. The user is advised to centrifuge briefly at the highest speed and resuspend the powder with nuclease-free water to a final concentration of 2 μM. All the pipette tips should also be nuclease-free. The siRNA stock solutions can be stored at −20 °C for up to 3 months. For each transfection condition, include three replicate transfections. Remember to include a Negative Control (scrambled) siRNA and a non-transfected control (cells that are mock-transfected with Opti-MEM 1 Medium but no transfection reagent and no siRNA). When possible, prepare master mixes to minimize variability.

For this procedure, cells are seeded in each well of a 6-well plate at 3×10^5 cells for each well.

Note: *The amount of cells for transfection could range from 2×10^5 to 3×10^5, depending on the cell type.*

For this specific gene (UNG), we used 135 nM siRNA (final concentration after transfection) for transfection.

Note: The final concentration should be modified according to the specific siRNA. The recommended concentration ranges from 10 to 150 nM.

These conditions generally result in effective gene knockdown, with loss of UNG mRNA as much as 65 % in this example (**Figure 42**), sufficient to reduce UNG protein levels below detection and to suppress UNG enzymatic activity to background levels (200).

1. On the day of transfection, aspirate the growth media from the cells.
2. Wash cells twice with 1× PBS.
3. Aspirate the PBS.
4. Add enough trypsin to cover the cells (0.5 mL) and place the plate in the incubator for 5 min to allow the cells to detach.
5. After 5 min, gently tap the plate/dish to detach any unbound cells from the surface and suspend the cells in Opti-MEM 1 Media (2.5 mL).

Note: In practice, if you cannot prepare the cell solution as quickly as possible, we recommend using normal growth media (with serum) to neutralize the trypsin. Then prepare the cell solution with Opti-MEM 1 Medium. This helps to prevent cell death caused by trypsin.

6. Count cells using either a hemocytometer or an automated cell counter.

Make the required dilution of cells to yield a final suspension of 3×10^5 cells per well in a volume of 2 mL per well.

7. Store the cell suspension on ice while you quickly prepare the transfection reagent and siRNAs.

Note: *Here, the cell solution volume is 1.4 mL and the siRNA transfection reagent complex is 0.6 mL. The total volume for each well is 2 mL.*

8. For each well, dilute the 5 μL of siPORT NeoFX in 295 μL Opti-MEM 1 Medium and incubate the diluted siPORT NeoFX for 10 min at room temperature.

Note: *The 10 min incubation time should be controlled precisely and you can dilute your siRNA with Opti-MEM 1 Medium dur-ing this period of time. In addition, you can prepare the master mixes in a 15 mL falcon tube.*

9. For each well, dilute 135 μL of 2 μM siRNA in 165 μL Opti-MEM 1 Medium.

10. After the 10 min incubation, mix the diluted siRNA with the diluted siPORT NeoFX in a 1:1 ratio.

11. Incubate at room temperature for 10 min.

12. Dispense 600 μL of the siRNA/siPORT NeoFX complex into the wells of a 6-well culture plate and set up the non-transfected controls (i.e., add only OPTI-MEM 1 Medium to the negative control wells).

13. Overlay 1.4mL of the cells (3 x 105 cells) per well into each well and mix gently by tilting back and forth to distribute evenly. DO NOT swirl the plate.

14. Incubate plate at 37 °C for 24 h.

Note: *If you observe cytotoxicity caused by transfection, we recommend changing the media back to normal growth media 8-10 h after transfection instead of 24 h as indicated.*

15. After 24 h, wash cells with fresh growth media.

16. Gene expression can be measured by qRT-PCR 24 h after transfection or by immunoblot 48 h after transfection.

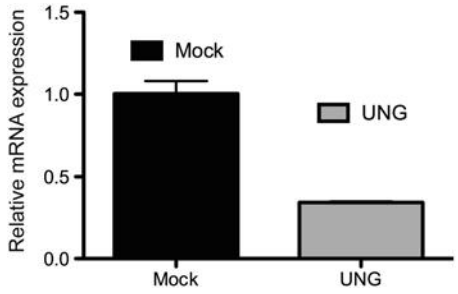

Figure 42. Relative mRNA expression as measured by qRT-PCR after siRNA to knock-down UNG.
Quantification of siRNA-mediated UNG knockdown as determined by qRT-PCR. TaqMan probes were used to quantify mRNA levels on an Applied Biosystems StepOnePlus machine. The qRT-PCR data was analyzed using the Ct method and was normalized to a mock-transfected control. Expression of UNG was normalized to the expression of human ß-actin. The mean of three independent experiments is plotted ± SEM

E.4.2 RNA Interference in Human Cells Using shRNA

Lentivirus production and cell transduction are essentially as we have described previously (196,200,201,296). The method is a classical procedure for virus production. The shuttle or transfer vector (the shRNA-expressing plasmid) is co-transfected into 293FT cells together with the packaging plasmids pMD2.g(VSVG), pRSV-REV, and pMDLg/pRRE to generate replication-defective viral particles capable of transducing numerous cell types (201,311). Importantly, the cells should be sub-confluent when transfected (**Figure 43*A***). Virus particles can be isolated after 48 h. If the transfection efficiency is low or if not transfected, the cells will reach confluence by 48 h (**Figure 43*B***). However, if transfection is successful, virus production leads to a suppression of cell growth (**Figure 43*C***). Effective virus preparation should allow for a high level of transduction, approaching 100 %, as shown here for cells transduced with an EGFP-expressing lentivirus (**Figure 43*D***).

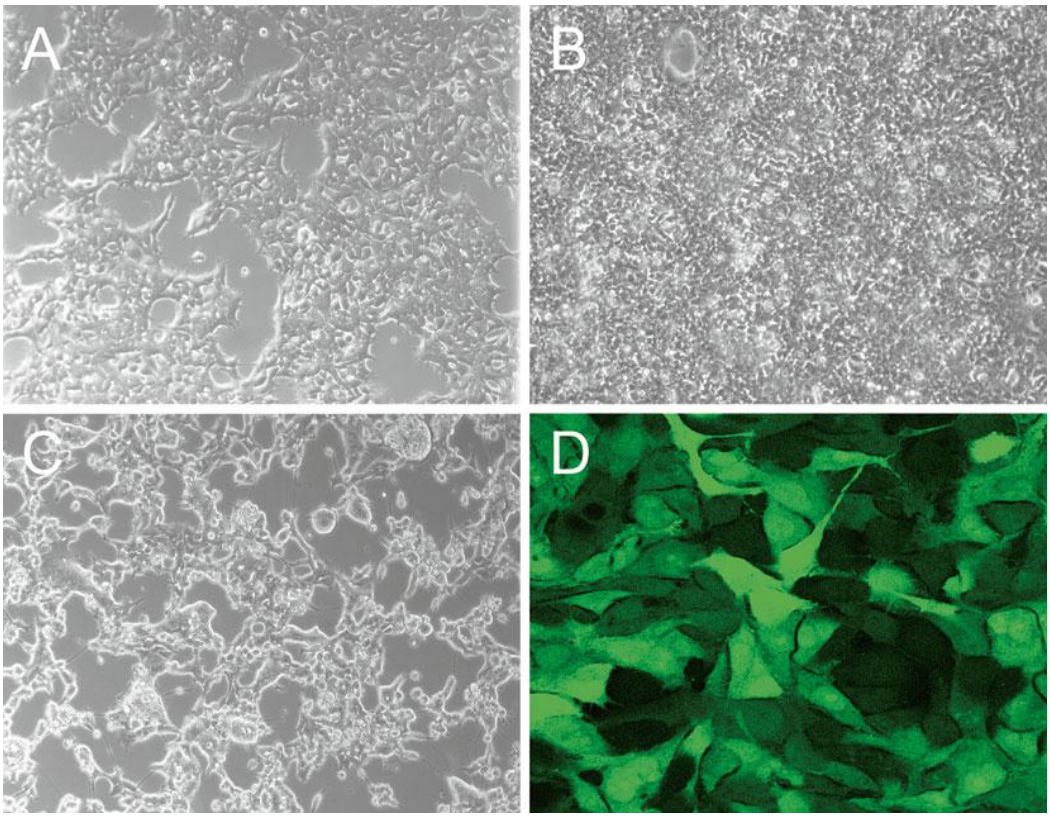

Figure 43. Demonstration of lentivirus production and transduction.
Panels **a**–**c** are white light images of 293FT cells before transfection (Panel **a**) or 48 h after transfection in the absence of plasmid (Panel **b**) or in the pres-ence of the viral vectors (Panel **c**). Panel **d** is a fluorescent image of cells after transduction with an EGFP-expressing lentivirus.

Lentivirus Preparation

We utilize this procedure for the preparation of five different lentiviral preparations:

1. *Small-scale, low titer*: Seed 1.7 × 106 293FT cells (less than 2 weeks old) in a 60 mm dish with 5.5 mL complete growth media and culture the cells at 37 °C, 5 % CO 2 overnight.

Transfect as indicated below (**Table 10**). The final yield of the lentiviral particle suspension is 4 mL and the virus titer is approximately 1×10^6 transforming units per mL (TU/mL).

2. *Medium-scale, low titer*: Seed 1.2×10^7 293FT cells (less than 2 weeks old) in a 150 mm dish with 27 mL complete growth media and culture the cells at 37 °C, 5 % CO_2 overnight.

Transfect as indicated below (**Table 11**). The final yield of the lentiviral particle suspension is 25 mL and the virus titer is approximately 1×10^6 transforming units per mL (TU/mL).

3. *Large-scale, low titer*: Seed 1.2×10^7 293FT cells (less than 2 weeks old) in each of three (295) 150 mm dishes with 27 mL complete growth media each and culture the cells at 37 °C, 5 % CO_2 overnight. Transfect as indicated below (**Table 11**). The final volume of the lentiviral particle suspension is 75 mL and the virus titer is approximately 1×10^6 transforming units per mL (TU/mL).
4. *Medium-scale, medium titer*: Seed 1.2×10^7 293FT cells (less than 2 weeks old) in a 150 mm dish with 27 mL complete growth media and culture the cells at 37 °C, 5 % CO_2 overnight. Transfect and concentrate as indicated below (**Table 11**). The virus titer is approximately 1×10^8 transforming units per milliliter (TU/mL). An aliquot of 10 μL would normally yield ~100 % transduction efficiency when infecting a 100 mm dish of cells.
5. *Large-scale, high titer*: Seed 1.2×10^7 293FT cells (less than 2 weeks old) in three (295) 150 mm dishes with 27 mL complete growth media and culture the cells at 37 °C, 5 % CO_2 overnight. Transfect and concentrate as indicated below (**Table 11**). The final volume of the lentiviral particle suspension is 30 μL and the virus titer is approximately 1×10^9 TU/mL.

Protocol

1. Seed 293FT cells as indicated above.
2. On the second day, prepare the transfection mix according to the materials listed in **Table 10** for transfection of cells in a 60 mm dish or as in **Table 11** for transfection of cells in a 150 mm dish.
3. Add the plasmids, media, and transfection reagent to a tube in this order: (1) media, (2) TransIT-293, and (3) plasmids.

4. Tap gently to mix (do not vortex) and incubate at room temperature for 15–30 min.
5. Add the transfection mix to each dish (do not remove the old media), dropwise.
6. After incubation at 37 °C for 48 h, collect culture media containing viral particles from transfected cells and filter the collection through a 0.45 μm Steriflip vacuum filter.

Table 10. Transfection mix recipe for a 60 mm dish.

Plate (60mm)	Cell Line	Plasmid	Plasmid (0.5μg/μL)	Serum and antibiotic-free media	TransIT-293 (Mirus)
For each plate	293FT	Transfer vector such as pLLox3.7, pLVX-IRES, or pLKO.1-puro	8 μL	0.375 mL	10μL
		pMD2-g(VSVG)	4 μL		
		pRSV-REV	4 μL		
		pMDLg/pRRE	4 μL		

Table 11. Transfection mix recipe for a 150 mm dish.

Plate (150mm)	Cell Line	Plasmid	Plasmid (0.5μg/μL)	Serum and antibiotic-free media	TransIT-293 (Mirus)
For each plate	293FT	Transfer vector such as pLLox3.7, pLVX-IRES, or pLKO.1-puro	56 μL	2.7 mL	70μL
		pMD2-g(VSVG)	28 μL		
		pRSV-REV	28 μL		
		pMDLg/pRRE	28 μL		

7. For the low titer preps, aliquot (1.0 mL per tube) into sterile vials and store at −80 °C.
8. For the medium titer and high titer concentration procedures, *see below*.

Medium Titer Lentivirus Concentration

1. After filtering the viral particles, mix 1 vol of Lenti-X Concentrator with 3 volumes of the filtered viral particles (simply measure the amount of viral supernatant to be

concentrated, divide by 3, and add the resulting amount of Lenti-X Concentrator to your viral supernatant).

2. Mix by gentle inversion. Larger volumes may be accommodated through the use of larger (i.e., 250 or 500 mL) centrifuge tubes.
3. Incubate mixture at 4 °C for 30 min (can be up to overnight and larger volumes (>100 mL) may require longer incubation times).
4. Centrifuge sample at 1,500 × *g* for 45 min at 4 °C. After centrifugation, an off-white pellet will be visible.
5. Carefully remove the supernatant, taking care not to disturb the pellet. Residual supernatant can be removed with either a pipette tip or by brief centrifugation at 1500 × *g*.
6. Gently resuspend the pellet in 25 μL 1× PBS at 4 °C and keep it at 4 °C overnight. The pellet can be somewhat sticky at first, but will go into suspension quickly. The final volume after the overnight incubation will be just over 100 μL.
7. Aliquot (10 μL per tube) into sterile vials. Determine titer of sample immediately or store at −80 °C in single-use aliquots (ten aliquots).
8. An aliquot of 10 μL would normally yield ~100 % transduction efficiency when infecting a 100 mm dish of cells (50 % confluent).

High Titer Lentivirus Concentration

1. After filtering the viral particles, add 36 mL of filtered supernatant to each of two ultracentrifuge tubes and balance the two tubes with additional media or supernatant. It may be useful to titer some of the leftover supernatant to determine if there is a loss of virus during concentration.

2. Cover tubes with a small piece of Parafilm and spin tubes using an SW-28 rotor at 25,000 rpm for 90 min at 4 °C.

3. Decant liquid and leave tube upside down on KimWipe for 10 min in the tissue culture hood. Aspirate remaining media being careful not to touch the bottom of the tube.

4. Add 12.5 μL cold, sterile tissue culture grade PBS to each tube and cover the tubes with Parafilm and then keep those tubes at 4 °C overnight without shaking.

5. To resuspend the pelleted virus, hold the tube at an angle and pipette fluid (the PBS that was added last night) over the pellet 20 times, being careful not to touch the pellet with the pipette tip. It is expected that the pellet will not be resuspended after this is completed. This pellet does not contain virus and can be discarded.

6. Combine the two virus suspensions and aliquot at 5 μL per tube (six tubes), flash-freeze in liquid nitrogen, and store at −80 °C. There should be no change in titer with freezing concentrated virus. Avoid multiple freeze-thaws.

E.4.3 Viral Titer Analysis

1. For a rapid titer determination, the Lenti-X qRT-PCR Titration Kit (Clontech Cat. No. 632165) directly quantifies the viral genomes in your virus stock, which is much faster and often more useful than antibiotic selection since it exploits conserved regions contained in most lentiviral preps.

2. Lenti-X GoStix (Clontech Cat. No. 631244) can also be used for a quick viral titer determination if the viral titer measurement does not need to be highly accurate. It only takes about 30 min.

E.4.4 Lentiviral Transduction Protocol

This protocol is based on a procedure optimized for transduction of the human glioma cell line LN428 (196,201,296) but should be applicable to most other cell lines with minimal alteration.

Table 12. Virus dilution recipe for lentiviral transduction.

Well	Virus	Vol. media (mL)	Vol. virus (mL)	Vol. polybrene (µL) Stock = 8mg/mL)
1	Negative control (no virus)	2.0	0	2
2	Target shRNA virus	1.0	1.0	2
3	Nontarget shRNA control or GFP control	1.0	1.0	2

Cell Seeding

1. Thaw a vial of cells and culture the cells until they are 80 % confluent.

2. Passage the cells and culture the cells until they are 50 % confluent.

3. Trypsinize, count, and then seed 1×10^5 cells per well in a 6-well plate with 2 mL growth medium.

4. Incubate at 37 °C, 5 % CO_2 overnight.

Transduction

1. On the second day, prepare the virus dilutions on ice in sterile tubes, according to **Table 12**.

2. Remove the growth media from each well.

3. Add the lentivirus preparation to each well.

4. Incubate at 32 °C, 5 % CO_2 overnight (16–18 h).

Second Transduction (Optional)

1. In the morning, replace the lentivirus preparation with 2 mL fresh growth media and incubate at 37 °C, 5 % CO_2 for 6–7 h.

2. In the late afternoon, remove the growth media from each well and add the lentivirus preparation (new prep but identical to the first transduction) to each well, according to **Table 12**.

3. Incubate at 32 °C, 5 % CO_2 overnight (16–18 h).

4. The next morning, replace the lentivirus preparation with 2 mL fresh growth media and incubate at 37 °C, 5 % CO_2 for 24 h.

Selection of Transduced Cells

1. Prepare selection medium by adding the proper concentration of selection antibiotic to the growth medium. The concentration of the antibiotic (puromycin, G418, hygromycin) is usually determined empirically. It is recommended that a selection antibiotic titration be performed to determine the lowest concentration of the selection antibiotic needed to efficiently select transduced cells and kill all non-transduced cells.
2. For LN428 cells, the final puromycin concentration is 1 μg/mL.
3. In the morning, remove the growth media and wash the cells in each well with 1 mL pre-warmed PBS.
4. Add 300 μL trypsin and keep the plate in a 37 °C incubator for 5 min.
5. Add 1 mL selection media with the proper concentration of selection antibiotic to each well and pipette up and down to prepare a single cell suspension.

6. Transfer the cell suspension of each well to a freshly prepared 100 mm cell culture dish containing 9 mL of selection medium.
7. Incubate at 37 °C, 5 % CO_2 until the cells reach 90 % confluence. Change medium with the selection medium every 3–4 days.
8. When the cells reach approximately 90 % confluent, remove the growth media and wash the cells in each dish with 3 mL pre-warmed PBS.
9. Add 1 mL trypsin and keep the plate in 37 °C incubator for 5 min and then add 4 mL selection medium and pipette up and down to make a single cell suspension.
10. Transfer 1 mL single cell suspension from each dish to a freshly prepared 100 mm dish with 9 mL selection medium.
11. Keep culturing the cells until the cells in the negative dish (mock transduction) without virus are 100 % dead.
12. Check the knockdown level via qRT-PCR (*see below*).
13. Freeze three vials of cells and passage the remaining cells for the designed experiment.

E.4.5 Validating Gene Knockdown by qRT-PCR

Cell Lysis and Reverse Transcription

TaqMan® Gene Expression Cells-to-CT™ Kit (cat #AM1728).

Note: *There are many different kits available to prepare cDNA. We prefer the Cells-to-C_t Kit due to convenience. It is the fastest method as it only takes about 1.5-2 h to go from cells to* cDNA. *However, you can choose any RNA extraction and RT kit.*

1. This protocol is designed for use with the Applied Biosystems

2. Prepare cells for lysis (two options).

3. *Option #1*: Prepare a cell pellet of 800,000 cells (pellet can be frozen at −80 °C or used immediately); resuspend cell pellet in 50 µL of PBS making a cell suspension of 16,000 cells/µL; distribute 5 µL of the cell suspension to a 1.5 mL tube and place on ice until continuing with the lysis.

Note: *You can use less than 800,000 cells if you do not have a lot of cells to work with. This number was chosen so you can see the cell pellet in the tube. If you use less, adjust the amount of PBS to resuspend the cells.*

4. *Option #2*: At least 24 h prior to lysis, seed enough cells into a well of a 96-well plate to yield around 80,000 cells/well at harvest (this will depend on the growth rate of your cell line); the following day, aspirate the media from each well, add 100 µL of PBS to wash, aspirate PBS and repeat to wash a second time, remove as much PBS as possible, and place on ice for immediate use or freeze at −80 °C to use at a later date.

Note: The 96-well plate method is going to be easier if you are working with a lot of different cell lines. You will lyse directly in the plate so you do nÕt have to worry about opening and closing a lot of tubes. If you use this method, DO NOT seed too many cell lines in the 96-well plate at one time. They will all have to be lysed at the same time and there are time points you have to hit. I usually do not seed more than 18Ð20 wells on each plate. Also, we usually prepare two or three replicates for each sample.

Cell Lysis

1. Prepare a master mix for the lysis consisting of 49.5 µL of lysis solution and 0.5 µL of DNase I (both supplied in the kit) for each sample. Add 0.5× excess to make sure you will not run out of the mix.

Note: For example, if you have ten samples (10.5×), prepare a master mix of 519.75 µL of lysis solution and 5.5 µL of DNase I.

2. Add 50 µL of the lysis master mix (prepared above) to each sample.

3. Mix the lysis reaction by pipetting up and down five times (avoid bubble formation).

4. Incubate the lysis reaction for 5 min at room temperature.

Note: IMPORTANT! Do not allow reaction to exceed 5 min.

5. Add 5 µL of stop solution (supplied in the kit) to each sample.

6. Mix the reaction by pipetting up and down five times (avoid bubble formation).

7. Incubate at least 2 min at room temperature.

Note: IMPORTANT! DO NOT allow reaction to remain at room temperature longer than 20 min; lysates can be stored on ice for up to 2 h or at −20 ¡C for up to 5 months.

Reverse Transcription

1. Prepare a master mix for the RT reaction consisting of 25 µL of 2× RT buffer, 2.5 µL of 20× RT enzyme mix, and 12.5 µL of nuclease-free water (RT buffer and enzyme mix supplied in the kit) for each sample. Add 0.5× excess to make sure you will not run out of the mix. Mix the components gently, but thoroughly.

Note: *For example, if you have ten samples, prepare a 10.5× mas-ter mix of 262.5 µL of 2× RT buffer, 26.25 µL of 20× RT enzyme mix, and 131.25 µL of* H_2O.

2. Distribute 40 µL of the master mix prepared above to a nuclease-free tube for each reaction.

3. Add 10 µL of the sample lysate (or nuclease-free water as a control) to each tube for a final volume of 50 µL.

4. Mix reactions gently, and then centrifuge briefly (assembled reactions can be stored at 4 °C for up to 4 h).

5. Run RT reaction (two options).

6. Option #1: Distribute reactions into a PCR tube or multi-well plate and run on a thermocycler—step 1, 37 °C for 60 min; step 2, 95 °C for 5 min; and step 3, 4 °C for forever.

7. Option #2: Distribute reactions into a 1.5 mL tube and run reaction in a 37 °C heat block for 60 min, immediately transferring to a 95 °C heat block for 5 min and then placing tubes on ice for at least 5 min.

8. Store reactions at −20 °C or immediately proceed with qRT-PCR analysis.

Quantitative RT-PCR

1. This protocol is designed for use with the Applied Biosystems StepOnePlus™ Real-Time PCR System, StepOne™ Software, and TaqMan® Gene Expression Reagents. It is important to thoroughly plan out your experiment before beginning.

Note: *The advantage to using the TaqMan® Assays and Reagents vs. SYBR Green is time. There are hundreds of predesigned TaqMan® Assays and each assay is designed for the same PCR con-ditions. This means there is no need for optimization on your part.*

2. For each sample, you will run your gene(s) of interest plus one or more endogenous controls. You do not need to measure the concentrations of the cDNA before running the PCR. The endogenous controls will help account for differences in concentration between samples. When choosing your endogenous control, be sure to choose one that is not modified by your experiments.

3. For each plate you run, you will need a “wild-type” control sample to compare to the rest of your samples. This is important. Your final value is relative, based on your “wild-type” control. Your control will automatically be set to 1 (or 100 % expression), and all other samples will have

an RQ (relative quantity) value compared to the control (e.g., sample 2 has an RQ value of 0.5; this means sample 2 has 50 %, or half, the expression of your control sample).

4. For each sample, it is recommended to run three reactions/ assay. The software will average these replicates together in your final calculations. This will help eliminate pipetting errors across the wells.

5. The StepOnePlus™ system is designed to read up to 4 dyes/ well. This gives you the ability to add more than one TaqMan® assay/well. However, there is some optimization required with multiplexing. It is a great option if you have limited sample available and will save on reagents, but you have to optimize to ensure you are not getting false results.

6. It is recommended to have an NTC (no template control) for each assay. We usually use water or you can use the water control from the Cells-to-CT reaction. This will allow the software to account for any background signal in the calculations.

7. Plan your plate layout and figure out how many wells you will be using for each assay. Then, prepare your master mixes as follows:

(a) A "1×" master mix for each assay.

(b) 10 µL of 2× TaqMan Universal PCR Mix.

Note: *Here, you can use either the Fast or Standard Mix. It is important to pay attention to which one you are using. The Fast Mix will allow you to run your entire reaction in about 40 min. The Standard takes about 2 h. They both will provide the same results; the Fast Mix is just more convenient.*

(c) 1 µL of 20× TaqMan Gene Expression Assay (some assays will come as a 40× stock; you must dilute these to 20× before use).

(d) 5 µL of nuclease-free water.

8. When preparing your mix, add 0.5× excess so you will not run out of your master mix.

9. Keep master mixes on ice until ready for use.

10. Distribute 4 µL of cDNA from the Cells-to-CT™ reaction to each well.

11. Add 16 µL of your master mix to each well.

Note: *Between each of the two steps above, inspect the wells by eye to make sure each well has approximately the same amount of either cDNA or master mix added. It works best to add the cDNA followed by the master mix. This way you can tell the difference in amounts of liquid in each well. It is difficult to see by eye the difference between 16 µL and 20 µL, but a lot easier to see the difference between 4 µL and 20 µL.*

12. Cover the plate or tubes, mix gently, and centrifuge briefly (mixed reactions can be stored at 4 °C for 1 h).

13. Place plate or tubes in the StepOne™ PCR machine, follow the prompts on the StepOne software to set up your experiment, and run the PCR.

Analysis

1. When analyzing data, ensure the three replicate wells have a similar CT (cycle time) values.

2. The AB software will calculate the RQ (relative quantity) value for you, taking into consideration the endogenous controls and sample replicates and comparing all your samples to the "wild-type" control.

3. Make sure the correct sample is selected as the "wild-type" control and the correct assay is selected as the endogenous control in the experimental setup stage (these can be changed as many times as needed after the PCR has run).

4. Multiply the RQ values by 100 to find the percentage of mRNA expression in relation to your "wild-type" control (e.g., wild type has an RQ value of 1.0 = 100 % expression; sample 1 has an RQ value of 0.56 = 56 % expression). *see* **Figure 44** for an example.

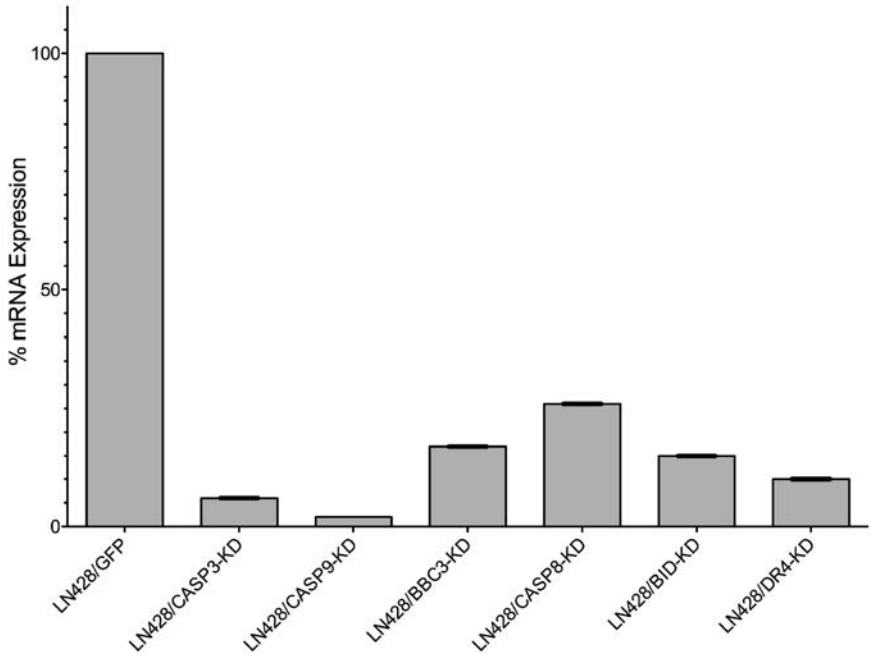

Figure 44. Relative mRNA expression as measured by qRT-PCR after shRNA to knock down several different genes involved in apoptosis signaling.
Quantification of shRNA-mediated knockdown of the apoptosis genes CASP3, CASP9, BBC3, CASP8, BID, and DR4 as determined by qRT-PCR following lentiviral transduction and stable cell line development. TaqMan probes were used to quantify mRNA levels on an Applied Biosystems StepOnePlus machine. The qRT-PCR data was analyzed using the Ct method and was normalized to GFP-transduced control cells. Expression for each was normalized to the expression of human ß-actin. The mean of three independent experiments is plotted ± SEM.

E.4.6 Validating Gene Knockdown by Immunoblot

The goal of any RNAi experiment is to reduce expression of the protein, preferably below detection or at least 75–90 % below the level of the control, such as we have described (196,197,200,201). In this example, we show an example of loss of expression of the protein pRb, suggested to play a role in the cellular response to DNA damage (337). As shown, protein lysates were prepared from cells transduced with a control shRNA (lane 1) and an shRNA

specific to pRb (lane 2), resulting in greater than 90 % loss of the expression of the protein (**Figure 45**).

The following describes the procedures required to validate gene knockdown by immunoblot although it is expected that most labs will have some general knowledge of the immunoblot procedure (338). While precast SDS-PAGE gels are available (e.g., Bio-Rad, Life Technologies), SDS-PAGE gels prepared in the lab are inexpensive and easy to prepare. However, the reliability of the assay is of course dependent on the specificity and effectiveness of the antibody.

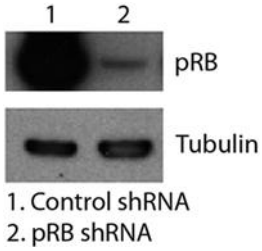

Figure 45. Demonstration of shRNA-mediated gene (pRb) knockdown by immunoblot. Depletion of pRb protein expression following lentiviral transduction and stable cell line development.
Cell extracts from control and pRb-KD cell lines were resolved on a 4–20 % SDS-PAGE gel and immunoblotted for pRb. The blot was stripped and re-probed for tubulin, which was used as a loading control

1. Assemble the spacer plate with a short plate in the casting frame and squeeze the system into the casting stand.

2. Prepare the 10 % separating gel mixing using 4.5 mL H_2O, 3 mL Acryl/Bis (30 %), and 2.5 mL of the separating buffer. Mix by inverting the tube two to three times and then add 68 μL APS and 14 μL TEMED. Mix and pour approximately 8 mL, leaving enough space for the stacking gel.

Note: *Alternatively and depending on the molecular weight of the protein of interest, a higher or lower concentration of Acryl/ Bis 30 % can be used.*

3. Pour 200 μL of isopropanol carefully onto the gel solution. The polymerization can take greater than 10 min.

4. Remove the isopropanol by inverting the plates and wash with now solidified gel with dH_2O.

5. Prepare the stacking gel by mixing 3.04 mL H2O, 660 μL Acryl/Bis 30 %, 1.25 mL of the stacking buffer, 40 μL APS, and 8 μL of TEMED. Mix, pour, and insert the comb. Leave to polymerize approximately 10 min.

6. Gently remove the comb and wash the wells with dH_2O before inserting the gel into the electrophoresis unit.

7. Prepare the 1× running buffer and pour into the unit, avoiding bubbles under the plates to allow better protein migration.

8. Mix the cell extract and the 2× sample buffer at a 1:1 ratio and heat 10 min at 95 °C and load into the wells.

Note: *A 10-well gel can only contain up to 40 μL of sample per well.*

9. Load 5 μL of the prestained protein molecular weight marker in one well.

10. Close the unit with the lead containing the power cables and connect to a power supply.

11. Run the gel at 90 V for 30 min, time enough for the samples to get through the stacking gel and then increase the voltage to 130 V for approximately 1.5 h or until the dye front reaches the bottom of the gel.

12. Carefully disassemble the plates using the gel releaser and soak the gel in a tray containing the 1× transfer buffer prechilled at 4 °C, two foam pads, two pieces of Whatman™ 3MM paper, and the nitrocellulose membrane cut to the size of the gel.

13. Set up the transfer sandwich in a gel holder cassette as shown in **Figure 46**: one foam pad, one piece of Whatman paper, the sheet of nitrocellulose membrane, and the gel. Remove any bubbles that might be trapped between the gel and the membrane by gently rolling a pipette on the gel. Then add the second piece of Whatman paper and the foam pad. Place the sandwich in the tray ensuring that the membrane is close to the anode (+) and the gel on the cathode side (−). Fill the tray with the cold transfer buffer and connect it to the power supply. The transfer is performed at 4 °C (or at RT with a cooling unit inserted in the tank) at 230 mA for 2 h.

10.

Note: *Here, you can use either the Fast or Standard Mix. It is important to pay attention to which one you are using. The Fast Mix will allow you to run your entire reaction in about 40 min. The Standard takes about 2 h. They both will provide the same results; the Fast Mix is just more convenient.*

14. At the end of the transfer, remove the membrane from the sandwich and verify the presence of the prestained molecular weight marker proteins.
15. Wash the membrane briefly in PBT buffer and incubate (30 min to 1 h) in TBT containing 5 % (w/v) Blotting-Grade Blocker, at room temperature, on a rocking platform.
16. Replace the blocking buffer with 10 mL blocking buffer containing the primary antibody diluted at the desired concentration. Incubate for 2 h at room temperature or overnight at 4 °C on a rocking platform.
17. Wash the membrane three times with PBT (10 min) at room temperature.
18. Incubate the membrane for 1 h in 10 mL blocking buffer containing the HRP-conjugated secondary antibody corresponding to the species of the primary antibody.
19. Wash the membrane three times with PBT (10 min each) at room temperature.

20. Place the membrane on a glass plate (proteins facing up) and add 1 mL of detection reagent freshly prepared by mixing an equal amount of each solution. Incubate in the dark for 2 min and detect with film or with the Bio-Rad Molecular Imager® Chemidoc™ XRS+.

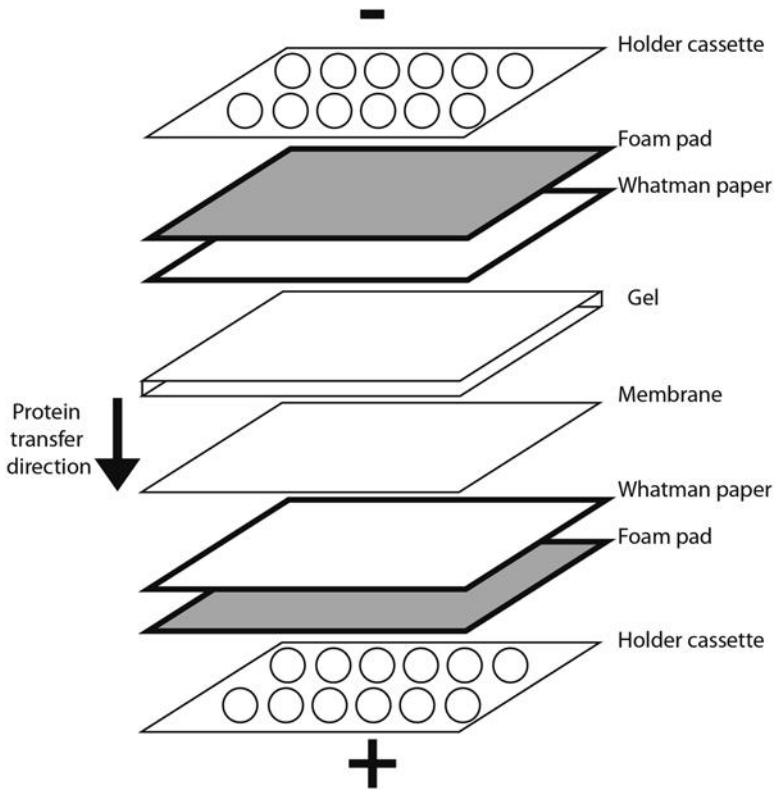

Figure 46. Cartoon diagram demonstrating the preparation of the gel-membrane sandwich for transfer from SDS-PAGE to nitrocellulose in preparation for an immunoblot.

E.4.7 PARP Activation in Response to DNA-Damaging Agents

PAR Detection by Immunoblot

PAR can be detected by immunoblot using one of several poly-clonal or monoclonal antibodies. We routinely use the monoclonal Ab 10H (196,201,296). Care must be taken not only for the analysis but also in the lysate preparation, as detailed below. No signal should be observed in samples isolated from an untreated cell, unless the cell is defective in homologous recombination (339) or defective in expression of the PAR-degrading enzyme PARG (296). As shown (**Figure 47**), PAR production is followed by loss of signal due to PAR hydrolysis mediated by PARG, as we have shown (296). Note also that a more quantitative analysis using these anti-PAR antibodies is available by ELISA, as we have described elsewhere (196).

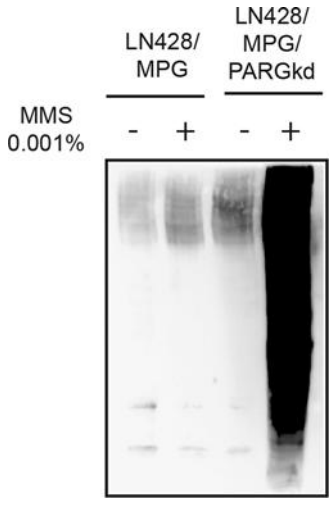

Figure 47. PARP1 activation as measured by immunoblot.
PAR production in LN428/ MPG cells or when depleted for PARG by shRNA (LN428/MPG/PARG-KD) detected by immunoblot with the 10H anti-PAR Ab after 1 h treatment with media or MMS (0.01 %).

1. Seed 10^5 to 5×10^5 cells in a 60 mm dish and incubate for 24 h.

2. When cells reach approximately 80 % confluence, treat the cells to trigger PAR production. The time of treatment may have to be adjusted depending on the damaging agent, its concentration, and the cell sensitivity.

3. After treatment (note above that the treatment time varies depending on the genotoxin), wash cells two times with ice-cold PBS.

4. Remove excess PBS and add 60–100 μL of sample buffer (2×) directly to the plate.

5. Scrape the cells, collect the sample, and transfer to a 1.5 mL microcentrifuge tube.

6. Incubate for 10 min at 95 °C (boiling water bath).

7. Load 30 μL of the sample on an SDS-PAGE gel and transfer to the nitrocellulose membrane as described in Sect. 3.4. We have found that an overnight transfer at 0.08 mA (16 h) gives a better signal when probing for PAR.

8. Discard the blocking buffer and add TBT containing the monoclonal mouse anti-PAR antibody (clone 10H) diluted 1–1,000. Incubate 2 h at RT or overnight at 4 °C on a rocking platform.

9. Wash the membrane three times (10 min each) with PBT and incubate 1 h at RT with TBT containing the HRP-conjugated goat anti-mouse Ab diluted 1–5,000.

10. Detect signal as described in Sect. 3.4. An example of the expected result is shown in **Figure 47**. Here we show the accumu-lation of PAR after MMS treatment of LN428/MPG cells (201) that have been depleted of the PAR-degrading enzyme PARG, essentially as we have shown (296).

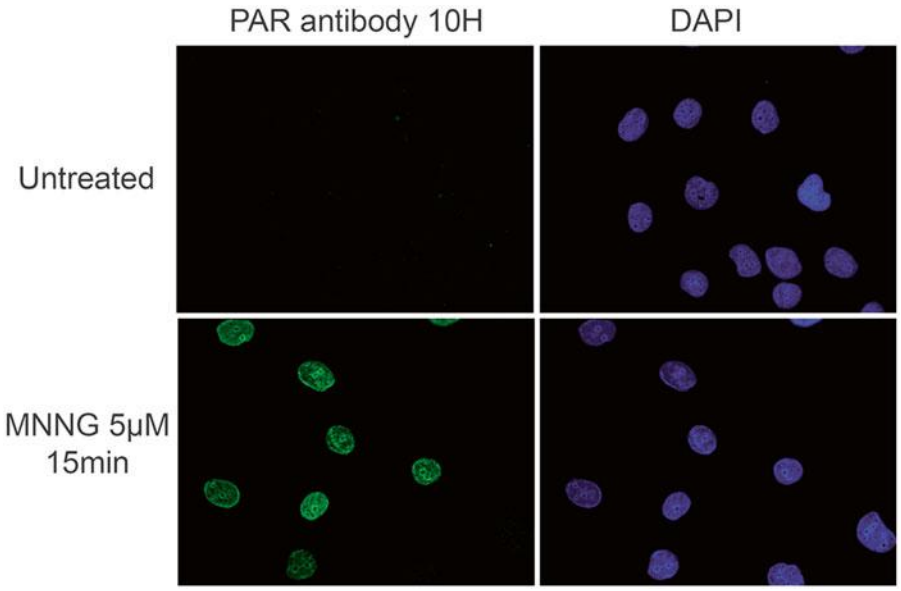

Figure 48. PARP1 activation as measured by immunofluorescence.
PAR production in cells after 0 or 15 min of MNNG treatment (5 μM). PAR is shown in cells exposed to MNNG (5 μM) using the anti-PAR 10H antibody (*left*) and the nucleus is visualized using DAPI (*right*).

PAR Detection by Immunofluorescence

The monoclonal Ab 10H can also be used to detect PAR in cells by immunofluorescence (340). To perform this assay, cells must be cultured and grown on glass coverslips. This is readily accomplished by introducing a coverslip into the wells of a 6- or 12-well plate, depending on the number of cells needed. The diameter of the coverslip is chosen to fit the wells of the plate selected. An example is shown in **Figure 48**, in which LN428/MPG cells (201) were treated with media or with media supplemented with MNNG (5 μM, 15 min). As indicated, no PAR is detectable in the untreated cells, but after treatment with the alkylating agent MNNG, the PAR signal is evident and coincides with nuclear staining by DAPI.

1. Sterilize coverslips in 70 % ethanol and let them dry on the edge of the wells.

2. Seed cells (around 5×10^4 cells/well for a 6-well plate) and incubate for 24 h at 37 °C.

3. Wash cells once with pre-warmed PBS and replace with fresh media containing the DNA-damaging agent.

4. Place the plate on ice and wash cells twice with ice-cold PBS.

5. Fix the cells by adding 3 mL of methanol-acetone (1:1) freshly prepared and stored at −20 °C. Incubate for 20 min on ice.

6. Wash three times with PBS.

7. Permeabilize the cells by treating with PBS-Triton X-100 (0.1 %) for 15 min.

8. Wash three times with PBS followed by five washes with PBS-BSA (0.5 %).

9. Block with PBS-BSA (2 %) for 30–45 min.

10. Wash three times with PBS-BSA (0.5 %).

11. Dilute the monoclonal mouse anti-PAR antibody (clone 10H) to 1/500 in PBS-BSA (0.5 %) and gently drop 50–100 μL on each coverslip. Incubate for 1.5 h at room temperature or overnight at 4 °C in a box containing a wet tissue to keep the slides humid and to avoid dehydration.

12. Wash three times in PBS-BSA (0.5 %) and incubate for 1 h with 50–100 μL of secondary antibody (goat anti-mouse Alexa Fluor 488) at room temperature in the dark.

13. Wash two times in PBS-BSA (0.5 %) and three times in PBS.

14. Drop 25 μL of ProLong® Gold Antifade Reagent with DAPI on a microscope slide. Carefully pick up each coverslip with tweezers and dip in water to remove excess of salts from the PBS. Place the coverslip on the SuperGold with the face con-taining the cells down.

Note: *We use a ready-to-use mounting reagent containing DAPI to stain the nucleus. But it is also possible, prior to mounting, to incubate the cells for 20 min with 0.05 ng/μL DAPI (Sigma-Aldrich) in PBS or for 30 s with Hoechst (Sigma-Aldrich cat# B-2883) diluted in* dH_2O *at 1*

mg/100 mL. The cells are then washed with PBS, rinsed in dH_2O, and mounted with a drop of anti-fading reagent (Mowiol/Dabco or Gelvatol).

15. Let dry overnight at room temperature in the dark (**Figure 48**).

E.4.8 Complementing Gene KD Cells and Evaluating Cell Survival in Response to DNA-Damaging Agents

As described earlier, we routinely complement cells after gene KD with either the WT transgene or a mutant transgene, depending on the focus of the investigation (196,197,201,296,341). We use standard molecular biology procedures for the development of these expression vectors and so we will not detail these here. Importantly, as pointed out in **Figure 41**, care must be taken to ensure that the transgene is not a target of the transfected siRNA or the transduced shRNA.

Evaluating cell survival in response to DNA-damaging agents after gene KD and/or after transgene complementation can be performed using transiently transfected cells, but unless the transfection efficiency is high or the measureable effect is strong, a stable gene KD is preferred for such assays. Examples of the results from either an MTS assay (**Panel a**) or a CyQUANT assay (**Panel b**) are shown in **Figure 49**. Here, we show the cellular response to the DNA alkylating agent MNNG. In the MTS assay, the cells are exposed to MNNG for 48 h and analyzed as detailed below. The LN428 cell line used here has reduced Polβ levels, and as expected, complementation with the WT Flag-Polβ transgene confers MNNG resistance (**Figure 49, Panel a**). Note that complementation with the mutant (K72A) Flag-Polβ transgene has reduced MNNG resistance, owing to its defect in the dRP lyase activity of Polβ (201). Similarly, the T98G cell line is sensitive to MNNG in a long-term assay as shown in **Panel b** (**Figure 49**)

in a Polβ-dependent manner, as complementation with the WT transgene also confers resistance. The following provides details on each of these assays.

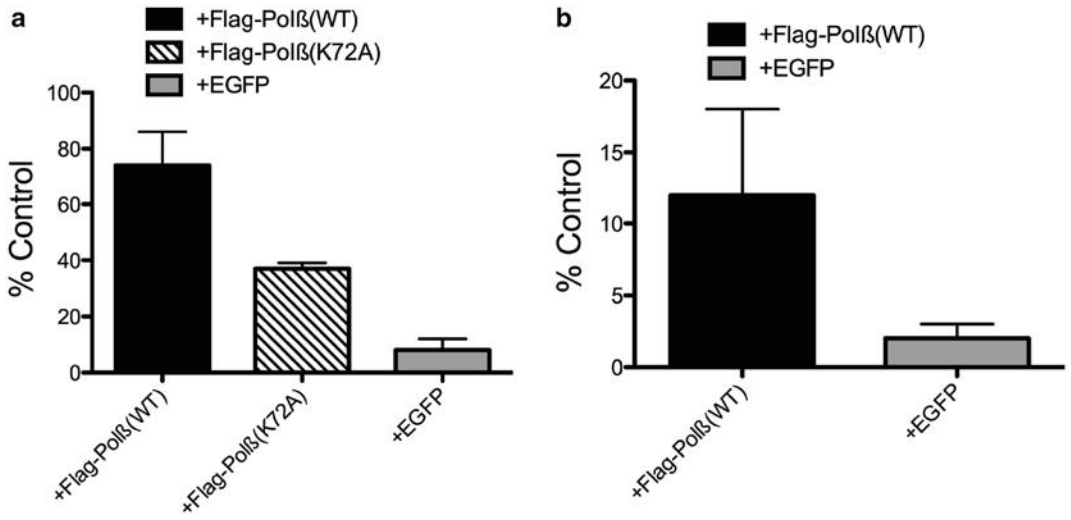

Figure 49. Cell survival analysis in response to MNNG.
(**a**) Cell viability of LN428 cells expressing Flag-Polß(WT), Flag-Polß(K72A), or EGFP (as indicated) after MNNG treatment (3 μM), as measured by the MTS assay 48 h after exposure. Plots show the relative surviving fraction as compared to untreated (control) cells. Means are calculated from triplicate values in each experiment. Results indicate the mean ± S.D. of three independent experiments. (**b**) Cell viability of T98G cells expressing Flag-Polß(WT) or EGFP (as indicated) after MNNG treat-ment (2 μM), as measured by the CyQUANT assay 10 days after exposure. T98G cells or those modified to express Flag-Polß(WT) or EGFP (control) were treated with MNNG and evaluated for cell viability. The plot shows the % viable cells as compared to untreated (control) cells. Results indicate the mean ± S.D. of three independent experiments.

MTS Assay

The MTS assay is performed as we have described previously (197). Before starting the MTS assay, seed 1,000–10,000 cells/well into a 96-well plate and let the cells grow for 48 h. Then add MTS dye to the wells, incubate 3 h at 37 °C, and then measure absorbance at 490 nm. This step is to determine how many cells are needed to obtain the best result. In general, the seeded cell number depends on the duplication time and the size of the cells. You need to determine the number of cells that yield a robust signal but also yield ½ signal strength when ½ of the cells

were seeded (to ensure linearity). After you know how many cells are needed, then you can begin to prepare cells for the MTS assay. For LN428 cells, we suggest seeding 2,000 cells/well.

1. After your desired cells reach 70–80 % confluence, wash the cells with PBS, then trypsinize cells, and resuspend cells with media.

2. Take 100 μL of the cell suspension of the cells and count using a hemocytometer or an automated cell counter.

3. Dilute the cells and seed 200 μL of the required number of cells/well in 96-well plates from column 2 to 11 (eight rows per drug dose) and add media in column 1 and column 12.

4. Incubate seeded cells for 24 h at 37 °C.

5. Twenty-four (24) hours after seeding the cells, remove media from each well of the plate with a multi-well aspirator but leave medium in column 1.

Note: *This step of the MTS assay should be performed very care-fully. Otherwise, you may remove cells and that will lead to unre-liable data*.

6. After mixing the medium with compound thoroughly, add 200 μL mixture with different concentrations of compound to each 8-well row using a multichannel pipettor. We prepare MNNG as a 10 mM stock solution in DMSO and store at −80°C. Here, we dilute the 10 mM MNNG (10 mM) to 10 μM with media. In this example, we treated cells with 0 or 3 μM MNNG.

7. Incubate the treated cells for 48 h at 37 °C.

8. Remove the media very carefully and rinse each well with 200 μL fresh media.

Note: *This step of the MTS assay should be performed very care-fully. Otherwise, you may remove cells and that will lead to unre-liable data*.

9. Prepare CellTiter Solution (Promega CellTiter 96 AQueous One, #G356B) as suggested by the manufacturer.

10. Place 120 μL of fresh medium mixed with CellTiter in each well including column 12 (control well) and incubate for 3 h at 37 °C.

11. Place microplate in the microplate reader to measure absorbance at 490 nm.

12. Calculate the result and plot the result as % control vs. com-pound concentration (**Figure 49, Panel a**).

CyQUANT Assay

The CyQUANT assay is performed as we have described previously (200). Similar to the MTS assay, the seeding cell number depends on the duplication time and the size of the cells. For the CyQUANT assay, the cells need to be cultured for a minimum of six duplication cycles. As such, different cells may require different culture times. For example, for HCT116 cells, we incubate for 5 days after drug treatment, whereas for LN428 or T98G cells, we incubate for 10–12 days after drug treatment. Determining the proper cell number for seeding is very important for this assay. Usually we seed 50–400 cells/well and let the cells grow for 5–10 days to determine how many cells we need to seed per well to obtain the optimal result. For T98G or LN428 cells, we suggest to seed 50–70 cells/well; for HCT116 cells, we suggest to seed 150–200 cells/well.

1. After your cells reach 70–80 % confluence, wash the cells with PBS, then trypsinize cells, and resuspend cells with 5–10 mL media and pass the cell suspension through 0.7 μm filter to obtain a single cell suspension.

2. Take 100 μL of the cell suspension of the cells and count using a hemocytometer or an automated cell counter.

3. Dilute the cells and seed 100 μL of the proper number of cells/well in a 96-well plate to columns 3–11 but seed half the number of cells in column 2. Add media only in column 1 and column 12.

4. Incubate seeded cells for 24 h at 37 °C.

5. Twenty-four (24) hours after seeding cells, remove media from the plate with a multi-well aspirator and leave media in column 1 and column 12.

6. After mixing the media with compound thoroughly, add 200 μL of the mixture with different concentrations of compound to the appropriate column using a multichannel pipettor. Before this step we need to calculate the volume of genotoxin, in this case MNNG, needed. We suggest to calculate the volume of the stock compound used and the volume of final mixture needed.

7. Incubate the treated cells for six duplication cycles at 37 °C.

8. After six duplication cycles, remove the media and rinse each well with 200 μL PBS. Remove the PBS completely.

Note: *This step should be performed very carefully. Otherwise, you may remove cells and that will lead to unreliable data*.

9. Seal edges of the plate with Parafilm to prevent water leaving or entering plate.

10. Freeze plates at −80 °C overnight.

11. Prepare the lysis/dye solution. Remember this dye is light sensitive, so keep it in the dark and add to the plate in a dark environment.

12. Follow dilution shown in **Table 13** to prepare lysis solution.

13. Remove the plates from the freezer and add 200 μL of cell lysis solution with dye to each well being tested.

14. Seal the edges of the plate with Parafilm and cover the plates with aluminum foil to keep the plate protected from the light.

15. Shake the plates for 1 h at room temperature and then incubate overnight at −30°C.

16. Remove the plates from the freezer and thaw the plates slowly at room temperature. Remember to keep them from the light at all times. This process takes approximately 2 h.

Note: *Remember to wait for the solution to be thawed completely*.

17. Read the plates on a fluorescent plate reader.

18. Calculate the result and plot result as % control vs. compound concentration (**Figure 49, Panel b**).

Table 13. Dilutions needed for the CyQUANT assay.

No. wells/plate	No. plates	Milli-Q water/well (mL)	Cell lysis buffer/well (mL)	CyQUANT dye/well (μL)	Total Milli-Q water (mL)	Total cell lysis buffer (mL)	Total CyQUANT dye (μL)
80	4	0.1895	0.01	0.5	60.64	3.2	160
15? Overhead added on at this step					Milli-Q Water/well (mL)	Total cell lysis buffer for all cells (μL)	Total CyQUANT dye for all cells (μL)
					69.736	3.68	184

Note: *CyQUANT reagent is light sensitive. Avoid light exposure for CyQUANT reagent. After lysis buffer with* CyQUANT, *dye is added to the plates*; *remember to cover plates with aluminum foil.*

E.5 ACKNOWLEDGMENTS

This work was supported by grants from the National Institute of Health (NIH) (CA148629, GM087798, and GM099213) to R.W.S. Support for the UPCI Lentiviral Facility was provided by the Cancer Center Support Grant from the National Institutes of Health (CA047904).

APPENDIX F

PLASMID MAPS FOR PENTR AND PCT-COPGFP-MCS-EF1-PURO/PCT-MCS-COPGFP-EF1-PURO VECTORS

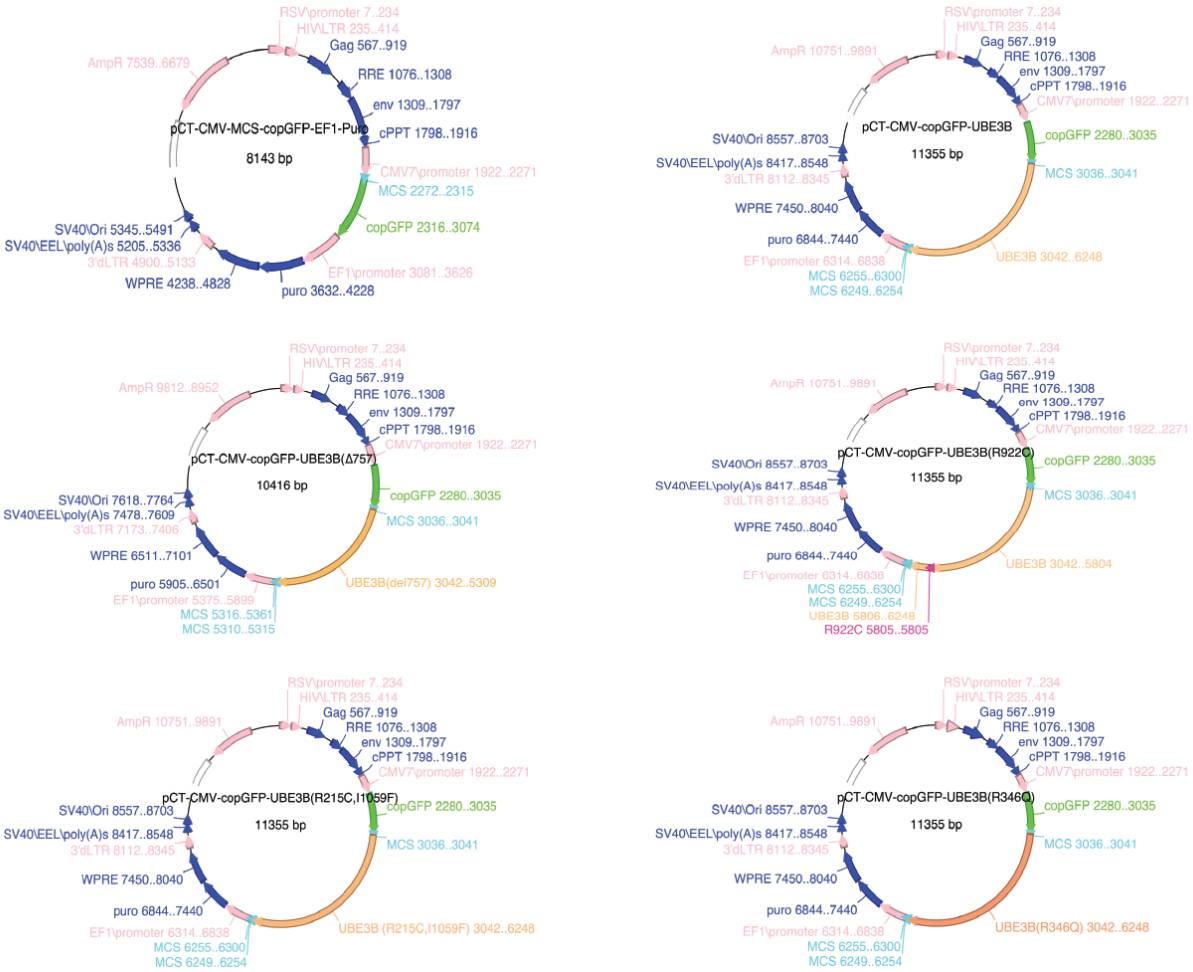

Figure 50. Plasmid maps for copGFP-tagged UBE3B constructs.

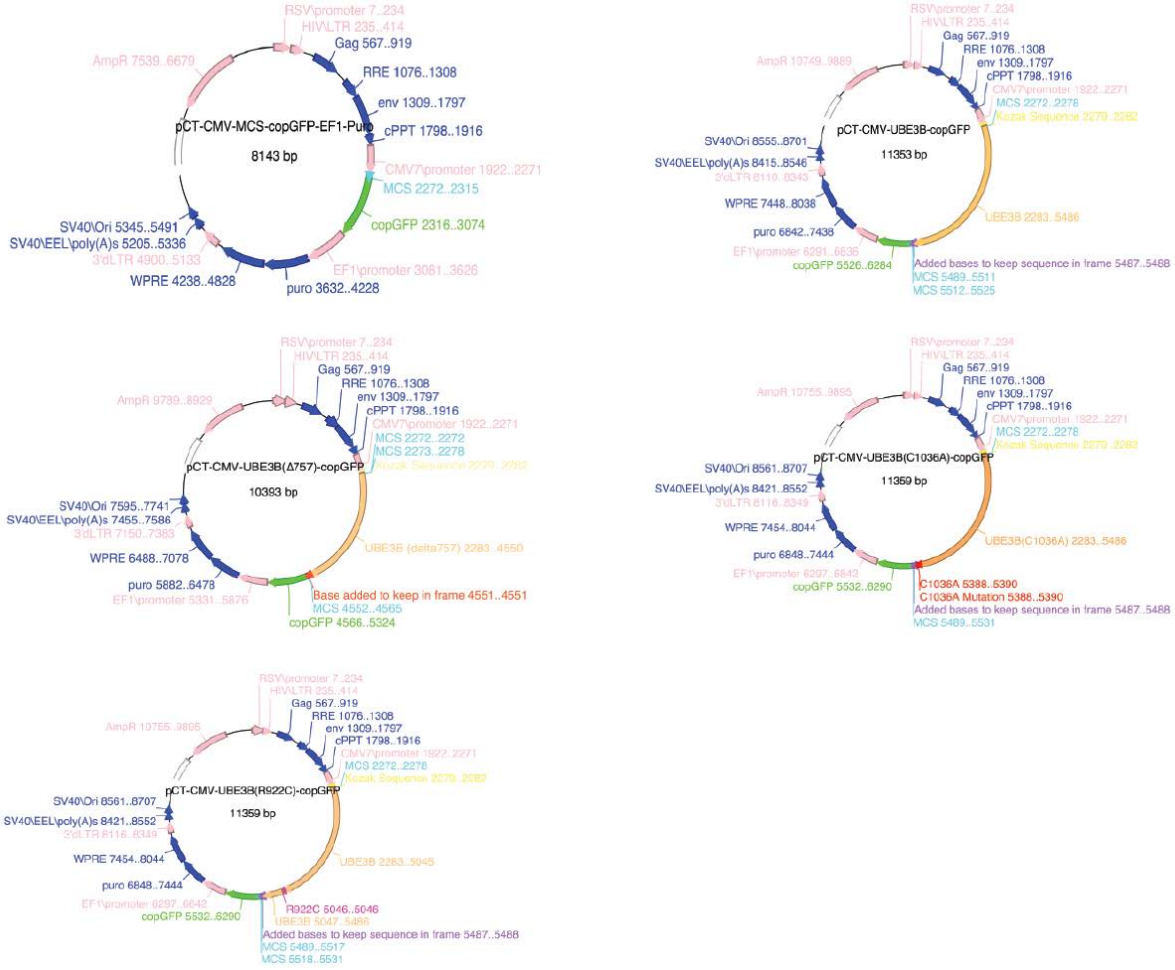

Figure 51. Plasmid maps for UBE3B-copGFP constructs.

Figure 52. Plasmid maps for pENTR-D/TOPO HA-tagged UBE3A and UBE3B constructs.

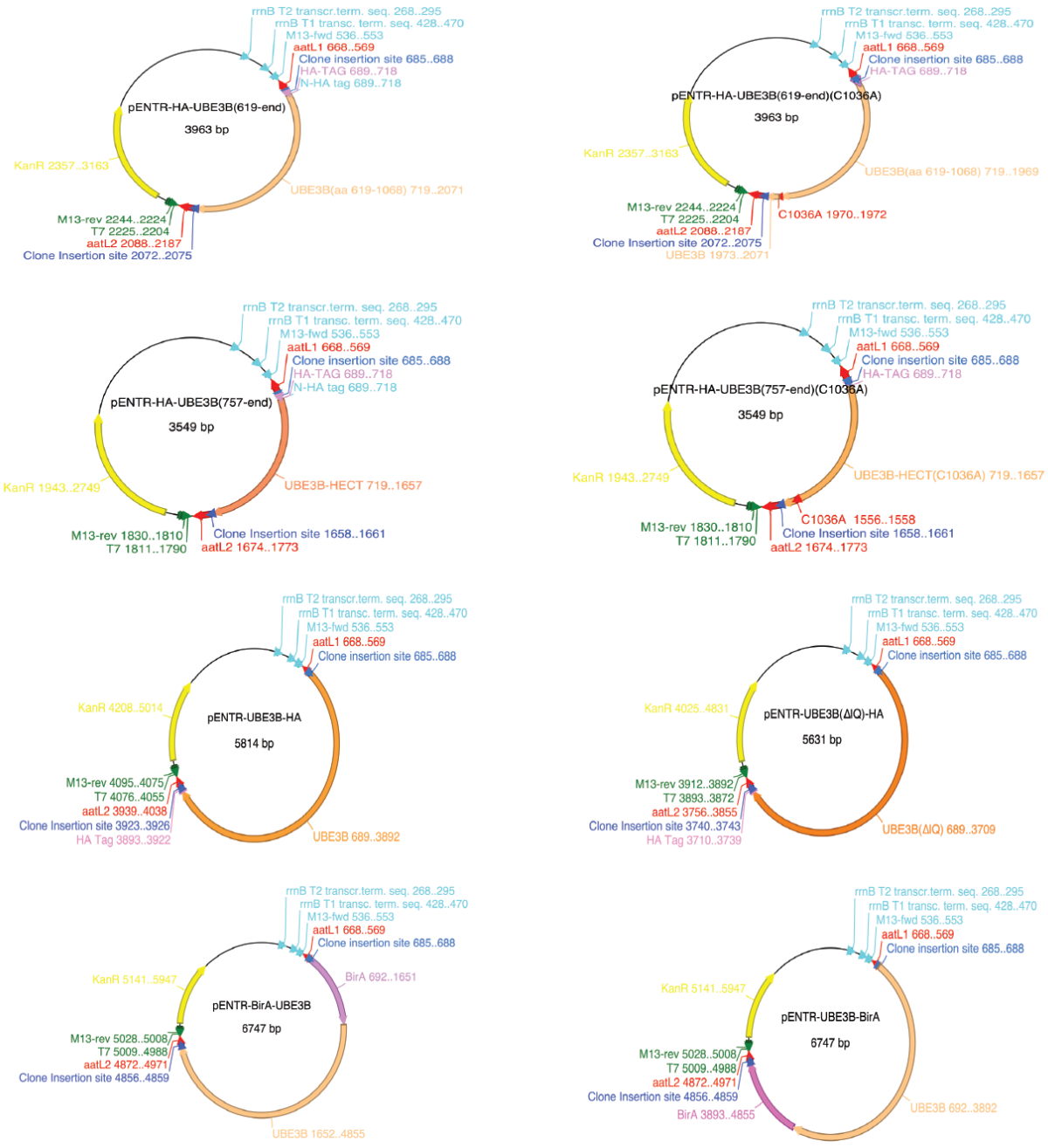

Figure 53. Plasmid maps for pENTR/D-TOPO HA-tagged UBE3B and BirA/UBE3B fusion constructs.

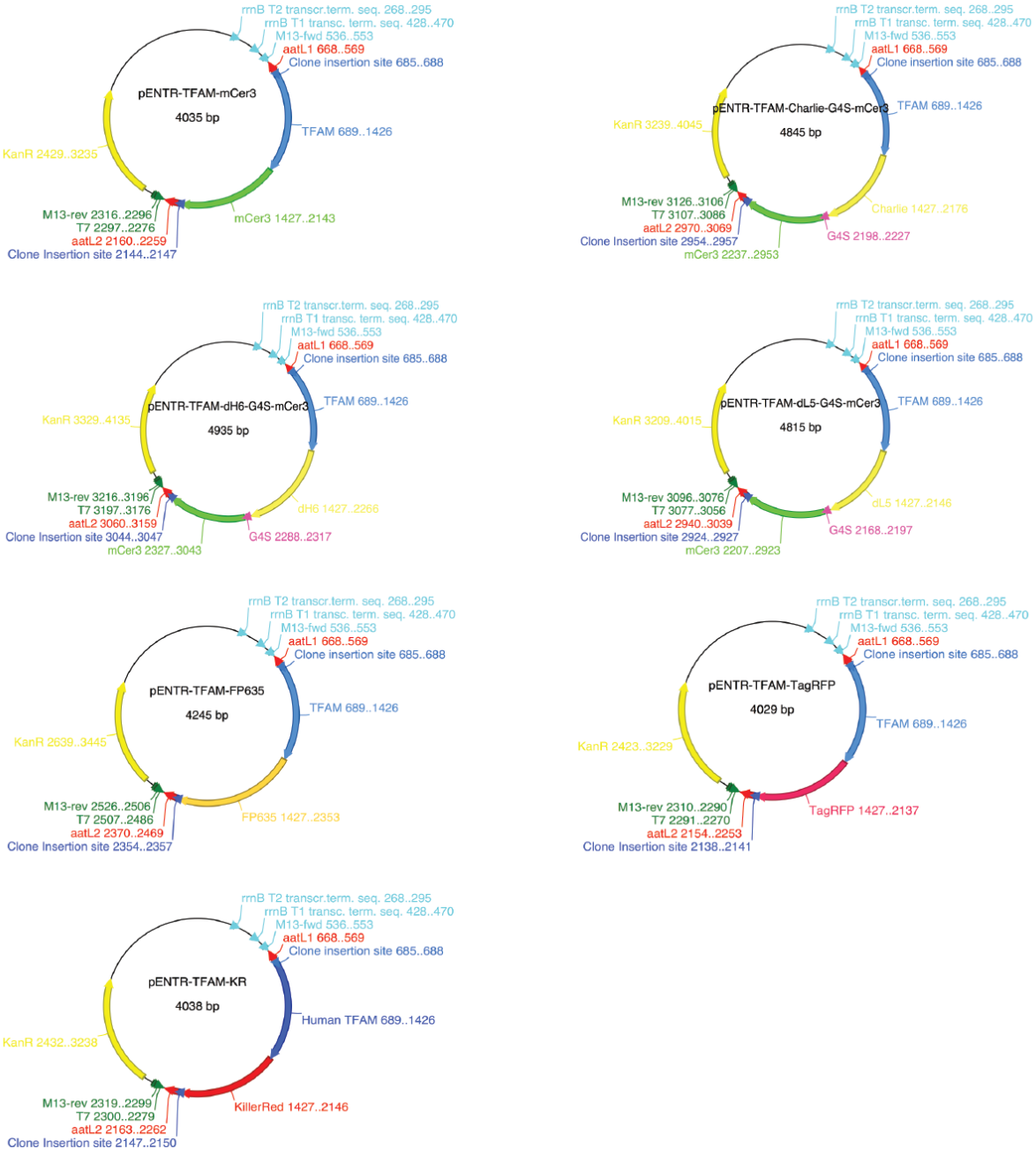

Figure 54. Plasmid maps for pENTR/D-TOPO TFAM fluoro-fusion constructs.

BIBLIOGRAPHY

1. Kerscher, O., Felberbaum, R., and Hochstrasser, M. (2006) *Annual review of cell and developmental biology* **22**, 159-180

2. Hershko, A., and Ciechanover, A. (1998) *Annual review of biochemistry* **67**, 425-479

3. Metzger, M. B., Hristova, V. A., and Weissman, A. M. (2012) *Journal of cell science* **125**, 531-537

4. Komander, D. (2009) *Biochemical Society transactions* **37**, 937-953

5. Tai, H. C., and Schuman, E. M. (2008) *Nature reviews. Neuroscience* **9**, 826-838

6. Kawabe, H., and Brose, N. (2011) *Nature reviews. Neuroscience* **12**, 251-268

7. Hershko, A., Ciechanover, A., and Rose, I. A. (1981) *The Journal of biological chemistry* **256**, 1525-1528

8. Ciechanover, A., Heller, H., Katz-Etzion, R., and Hershko, A. (1981) *Proceedings of the National Academy of Sciences of the United States of America* **78**, 761-765

9. Kleiger, G., and Mayor, T. (2014) *Trends in cell biology* **24**, 352-359

10. Cane, D. E., and Walsh, C. T. (1999) *Chemistry & biology* **6**, R319-325

11. Wu, P. Y., Hanlon, M., Eddins, M., Tsui, C., Rogers, R. S., Jensen, J. P., Matunis, M. J., Weissman, A. M., Wolberger, C., and Pickart, C. M. (2003) *The EMBO journal* **22**, 5241-5250

12. Huibregtse, J. M., Scheffner, M., Beaudenon, S., and Howley, P. M. (1995) *Proceedings of the National Academy of Sciences of the United States of America* **92**, 5249

13. Jackson, P. K., Eldridge, A. G., Freed, E., Furstenthal, L., Hsu, J. Y., Kaiser, B. K., and Reimann, J. D. (2000) *Trends in cell biology* **10**, 429-439

14. Grossman, S. R., Deato, M. E., Brignone, C., Chan, H. M., Kung, A. L., Tagami, H., Nakatani, Y., and Livingston, D. M. (2003) *Science* **300**, 342-344

15. Hershko, A. (1988) *The Journal of biological chemistry* **263**, 15237-15240

16. King, R. W., Peters, J. M., Tugendreich, S., Rolfe, M., Hieter, P., and Kirschner, M. W. (1995) *Cell* **81**, 279-288

17. Sudakin, V., Ganoth, D., Dahan, A., Heller, H., Hershko, J., Luca, F. C., Ruderman, J. V., and Hershko, A. (1995) *Molecular biology of the cell* **6**, 185-197

18. Ciechanover, A. (2004) *Nobel Lecture*

19. Kar, G., Keskin, O., Nussinov, R., and Gursoy, A. (2012) *J Proteome Res* **11**, 1196-1207

20. Miranda, M., and Sorkin, A. (2007) *Molecular interventions* **7**, 157-167

21. Hicke, L., and Dunn, R. (2003) *Annual review of cell and developmental biology* **19**, 141-172

22. Hicke, L. (2001) *Nature reviews. Molecular cell biology* **2**, 195-201

23. Sigismund, S., Polo, S., and Di Fiore, P. P. (2004) *Current topics in microbiology and immunology* **286**, 149-185

24. Komander, D., and Rape, M. (2012) *Annual review of biochemistry* **81**, 203-229

25. Chau, V., Tobias, J. W., Bachmair, A., Marriott, D., Ecker, D. J., Gonda, D. K., and Varshavsky, A. (1989) *Science* **243**, 1576-1583

26. Pickart, C. M., and Fushman, D. (2004) *Current opinion in chemical biology* **8**, 610-616

27. Thrower, J. S., Hoffman, L., Rechsteiner, M., and Pickart, C. M. (2000) *The EMBO journal* **19**, 94-102

28. Amerik, A. Y., and Hochstrasser, M. (2004) *Biochimica et biophysica acta* **1695**, 189-207

29. Wing, S. S. (2003) *The international journal of biochemistry & cell biology* **35**, 590-605

30. Sahtoe, D. D., and Sixma, T. K. (2015) *Trends in biochemical sciences*

31. Henry, K. R., Lee, S., Walker, D., and Zeitlin, P. L. (2015) *Physiological reports* **3**

32. El Khouri, E., Le Pavec, G., Toledano, M. B., and Delaunay-Moisan, A. (2013) *The Journal of biological chemistry* **288**, 31177-31191

33. Zhou, R., Patel, S. V., and Snyder, P. M. (2007) *The Journal of biological chemistry* **282**, 20207-20212

34. Mei, Z., Zhang, D., Hu, B., Wang, J., Shen, X., and Xiao, W. (2015) *The Journal of biological chemistry*

35. Scheffner, M., Werness, B. A., Huibregtse, J. M., Levine, A. J., and Howley, P. M. (1990) *Cell* **63**, 1129-1136

36. Ciechanover, A., and Schwartz, A. L. (2004) *Biochimica et biophysica acta* **1695**, 3-17

37. Momand, J., Zambetti, G. P., Olson, D. C., George, D., and Levine, A. J. (1992) *Cell* **69**, 1237-1245

38. Zhou, B. B., and Elledge, S. J. (2000) *Nature* **408**, 433-439

39. Bassing, C. H., and Alt, F. W. (2004) *DNA repair* **3**, 781-796

40. Liesa, M., Palacin, M., and Zorzano, A. (2009) *Physiological reviews* **89**, 799-845

41. Zinsmaier, K. E., Babic, M., and Russo, G. J. (2009) *Results and problems in cell differentiation* **48**, 107-139

42. Chistiakov, D. A., Sobenin, I. A., Revin, V. V., Orekhov, A. N., and Bobryshev, Y. V. (2014) *BioMed research international* **2014**, 238463

43. Mattson, M. P. (2008) *Annals of the New York Academy of Sciences* **1144**, 97-112

44. Stowe, D. F., and Camara, A. K. (2009) *Antioxidants & redox signaling* **11**, 1373-1414

45. Macaskill, A. F., Rinholm, J. E., Twelvetrees, A. E., Arancibia-Carcamo, I. L., Muir, J., Fransson, A., Aspenstrom, P., Attwell, D., and Kittler, J. T. (2009) *Neuron* **61**, 541-555

46. Kang, M. A., So, E. Y., Simons, A. L., Spitz, D. R., and Ouchi, T. (2012) *Cell death & disease* **3**, e249

47. Al Ghouleh, I., Khoo, N. K., Knaus, U. G., Griendling, K. K., Touyz, R. M., Thannickal, V. J., Barchowsky, A., Nauseef, W. M., Kelley, E. E., Bauer, P. M., Darley-Usmar, V., Shiva, S., Cifuentes-Pagano, E., Freeman, B. A., Gladwin, M. T., and Pagano, P. J. (2011) *Free radical biology & medicine* **51**, 1271-1288

48. Kudin, A. P., Bimpong-Buta, N. Y., Vielhaber, S., Elger, C. E., and Kunz, W. S. (2004) *The Journal of biological chemistry* **279**, 4127-4135

49. Turrens, J. F. (2003) *The Journal of physiology* **552**, 335-344

50. Lane, R. K., Hilsabeck, T., and Rea, S. L. (2015) *Biochimica et biophysica acta*

51. Figueira, T. R., Barros, M. H., Camargo, A. A., Castilho, R. F., Ferreira, J. C., Kowaltowski, A. J., Sluse, F. E., Souza-Pinto, N. C., and Vercesi, A. E. (2013) *Antioxidants & redox signaling* **18**, 2029-2074

52. Magder, S. (2006) *Critical care* **10**, 208

53. Droge, W. (2002) *Physiological reviews* **82**, 47-95

54. Devasagayam, T. T. J., Boloor KK, Sane Ketaki S, Ghaskadbi Saroj S, Lele RD. (October 2004) *Journal of Association of Physicians of India (JAPI)* **52:796**

55. Lionaki, E., and Tavernarakis, N. (2013) *Journal of proteomics*

56. Carreras, M. C., Franco, M. C., Peralta, J. G., and Poderoso, J. J. (2004) *Molecular aspects of medicine* **25**, 125-139

57. Harman, D. (1972) *Journal of the American Geriatrics Society* **20**, 145-147

58. M.-E. Harper, L. Bevilacqua, K. Hagopian, R. Weindruch, and Ramsey, J. J. (2004) *Acta Physiologica Scandinavica* **182**, 321-331

59. Chan, C. B., and Harper, M. E. (2006) *Current diabetes reviews* **2**, 271-283

60. Ando, K., and Fujita, T. (2009) *Free radical biology & medicine* **47**, 213-218

61. Patten, D. A., Germain, M., Kelly, M. A., and Slack, R. S. (2010) *Journal of Alzheimer's disease : JAD* **20 Suppl 2**, S357-367

62. Ku, H. H., Brunk, U. T., and Sohal, R. S. (1993) *Free radical biology & medicine* **15**, 621-627

63. Wanagat, J., Dai, D. F., and Rabinovitch, P. (2010) *Mechanisms of ageing and development* **131**, 527-535

64. Elmore, S. P., Qian, T., Grissom, S. F., and Lemasters, J. J. (2001) *FASEB journal : official publication of the Federation of American Societies for Experimental Biology* **15**, 2286-2287

65. Nunomura, A., Honda, K., Takeda, A., Hirai, K., Zhu, X., Smith, M. A., and Perry, G. (2006) *Journal of biomedicine & biotechnology* **2006**, 82323

66. Schon, E. A., and Manfredi, G. (2003) *The Journal of clinical investigation* **111**, 303-312

67. Ahmad, T., Sundar, I. K., Lerner, C. A., Gerloff, J., Tormos, A. M., Yao, H., and Rahman, I. (2015) *FASEB journal : official publication of the Federation of American Societies for Experimental Biology*

68. Anderson, G., and Maes, M. (2014) *Current pharmaceutical design* **20**, 3812-3847

69. Boland, M. L., Chourasia, A. H., and Macleod, K. F. (2013) *Frontiers in oncology* **3**, 292

70. Montgomery, M. K., and Turner, N. (2015) *Endocrine connections* **4**, R1-R15

71. Rera, M., Clark, R. I., and Walker, D. W. (2012) *Proceedings of the National Academy of Sciences of the United States of America* **109**, 21528-21533

72. Wiesner, R. J., Ruegg, J. C., and Morano, I. (1992) *Biochemical and biophysical research communications* **183**, 553-559

73. Fundation, B. (November 2012) *Bradshaw Foundation*

74. Duhl, D. M., Powell, T., and Poyton, R. O. (1990) *The Journal of biological chemistry* **265**, 7273-7277

75. Amaya, Y., Arakawa, H., Takiguchi, M., Ebina, Y., Yokota, S., and Mori, M. (1988) *The Journal of biological chemistry* **263**, 14463-14470

76. Santos, J. H., Meyer, J. N., and Van Houten, B. (2006) *Human molecular genetics* **15**, 1757-1768

77. Guo, Z., Kozlov, S., Lavin, M. F., Person, M. D., and Paull, T. T. (2010) *Science* **330**, 517-521

78. Valentin-Vega, Y. A., Maclean, K. H., Tait-Mulder, J., Milasta, S., Steeves, M., Dorsey, F. C., Cleveland, J. L., Green, D. R., and Kastan, M. B. (2012) *Blood* **119**, 1490-1500

79. Ambrose, M., Goldstine, J. V., and Gatti, R. A. (2007) *Human molecular genetics* **16**, 2154-2164

80. Eaton, J. S., Lin, Z. P., Sartorelli, A. C., Bonawitz, N. D., and Shadel, G. S. (2007) *The Journal of clinical investigation* **117**, 2723-2734

81. Sharma, N. K., Lebedeva, M., Thomas, T., Kovalenko, O. A., Stumpf, J. D., Shadel, G. S., and Santos, J. H. (2014) *DNA repair* **13**, 22-31

82. Akbari, M., Keijzers, G., Maynard, S., Scheibye-Knudsen, M., Desler, C., Hickson, I. D., and Bohr, V. A. (2014) *DNA repair* **16**, 44-53

83. Akbari, M., Morevati, M., Croteau, D., and Bohr, V. A. (2015) *DNA repair*

84. Osiewacz, H. D., and Bernhardt, D. (2013) *Gerontology* **59**, 413-420

85. Insull, W., Jr. (2009) *The American journal of medicine* **122**, S3-S14

86. Li, J. M., and Shah, A. M. (2004) *American journal of physiology. Regulatory, integrative and comparative physiology* **287**, R1014-1030

87. Madamanchi, N. R., and Runge, M. S. (2007) *Circulation research* **100**, 460-473

88. Ballinger, S. W., Patterson, C., Knight-Lozano, C. A., Burow, D. L., Conklin, C. A., Hu, Z., Reuf, J., Horaist, C., Lebovitz, R., Hunter, G. C., McIntyre, K., and Runge, M. S. (2002) *Circulation* **106**, 544-549

89. Youle, R. J., and Narendra, D. P. (2011) *Nature reviews. Molecular cell biology* **12**, 9-14

90. de Moura, M. B., dos Santos, L. S., and Van Houten, B. (2010) *Environmental and molecular mutagenesis* **51**, 391-405

91. Burchell, V. S., Gandhi, S., Deas, E., Wood, N. W., Abramov, A. Y., and Plun-Favreau, H. (2010) *Expert opinion on therapeutic targets* **14**, 369-385

92. Burchell, V. S., Gandhi, S., Deas, E., Wood, N. W., Abramov, A. Y., and Plun-Favreau, H. (2010) *Expert opinion on therapeutic targets* **14**, 497-511

93. Fitzgerald, J. C., and Plun-Favreau, H. (2008) *The FEBS journal* **275**, 5758-5766

94. Jin, S. M., Lazarou, M., Wang, C., Kane, L. A., Narendra, D. P., and Youle, R. J. (2010) *The Journal of cell biology* **191**, 933-942

95. Matsuda, N., Sato, S., Shiba, K., Okatsu, K., Saisho, K., Gautier, C. A., Sou, Y. S., Saiki, S., Kawajiri, S., Sato, F., Kimura, M., Komatsu, M., Hattori, N., and Tanaka, K. (2010) *The Journal of cell biology* **189**, 211-221

96. Chaugule, V. K., Burchell, L., Barber, K. R., Sidhu, A., Leslie, S. J., Shaw, G. S., and Walden, H. (2011) *The EMBO journal* **30**, 2853-2867

97. Dzamko, N., Zhou, J., Huang, Y., and Halliday, G. M. (2014) *Frontiers in molecular neuroscience* **7**, 57

98. Lazarou, M., Jin, S. M., Kane, L. A., and Youle, R. J. (2012) *Developmental cell* **22**, 320-333

99. Xiong, H., Wang, D., Chen, L., Choo, Y. S., Ma, H., Tang, C., Xia, K., Jiang, W., Ronai, Z., Zhuang, X., and Zhang, Z. (2009) *The Journal of clinical investigation* **119**, 650-660

100. Kondapalli, C., Kazlauskaite, A., Zhang, N., Woodroof, H. I., Campbell, D. G., Gourlay, R., Burchell, L., Walden, H., Macartney, T. J., Deak, M., Knebel, A., Alessi, D. R., and Muqit, M. M. (2012) *Open biology* **2**, 120080

101. Shiba-Fukushima, K., Inoshita, T., Hattori, N., and Imai, Y. (2014) *PLoS genetics* **10**, e1004391

102. Okatsu, K., Oka, T., Iguchi, M., Imamura, K., Kosako, H., Tani, N., Kimura, M., Go, E., Koyano, F., Funayama, M., Shiba-Fukushima, K., Sato, S., Shimizu, H., Fukunaga, Y., Taniguchi, H., Komatsu, M., Hattori, N., Mihara, K., Tanaka, K., and Matsuda, N. (2012) *Nature communications* **3**, 1016

103. Lazarou, M., Narendra, D. P., Jin, S. M., Tekle, E., Banerjee, S., and Youle, R. J. (2013) *The Journal of cell biology* **200**, 163-172

104. Zheng, X., and Hunter, T. (2013) *Cell research* **23**, 886-897

105. Koyano, F., Okatsu, K., Kosako, H., Tamura, Y., Go, E., Kimura, M., Kimura, Y., Tsuchiya, H., Yoshihara, H., Hirokawa, T., Endo, T., Fon, E. A., Trempe, J. F., Saeki, Y., Tanaka, K., and Matsuda, N. (2014) *Nature* **510**, 162-166

106. Kane, L. A., Lazarou, M., Fogel, A. I., Li, Y., Yamano, K., Sarraf, S. A., Banerjee, S., and Youle, R. J. (2014) *The Journal of cell biology* **205**, 143-153

107. Shaw, G. S. (2014) *The Biochemical journal* **460**, e1-3

108. Lin, M. T., and Beal, M. F. (2006) *Nature medicine* **12**, 1241-1243

109. Pinho, C. M., Teixeira, P. F., and Glaser, E. (2014) *Biochimica et biophysica acta* **1837**, 1069-1074

110. Pavlov, P. F., Wiehager, B., Sakai, J., Frykman, S., Behbahani, H., Winblad, B., and Ankarcrona, M. (2011) *FASEB journal : official publication of the Federation of American Societies for Experimental Biology* **25**, 78-88

111. Yan, S. D., Fu, J., Soto, C., Chen, X., Zhu, H., Al-Mohanna, F., Collison, K., Zhu, A., Stern, E., Saido, T., Tohyama, M., Ogawa, S., Roher, A., and Stern, D. (1997) *Nature* **389**, 689-695

112. Lustbader, J. W., Cirilli, M., Lin, C., Xu, H. W., Takuma, K., Wang, N., Caspersen, C., Chen, X., Pollak, S., Chaney, M., Trinchese, F., Liu, S., Gunn-Moore, F., Lue, L. F., Walker, D. G., Kuppusamy, P., Zewier, Z. L., Arancio, O., Stern, D., Yan, S. S., and Wu, H. (2004) *Science* **304**, 448-452

113. Santos, R. X., Correia, S. C., Wang, X., Perry, G., Smith, M. A., Moreira, P. I., and Zhu, X. (2010) *Journal of Alzheimer's disease : JAD* **20 Suppl 2**, S401-412

114. Kim, H. S., Lee, J. H., Lee, J. P., Kim, E. M., Chang, K. A., Park, C. H., Jeong, S. J., Wittendorp, M. C., Seo, J. H., Choi, S. H., and Suh, Y. H. (2002) *Neuroreport* **13**, 1989-1993

115. Nunomura, A., Castellani, R. J., Zhu, X., Moreira, P. I., Perry, G., and Smith, M. A. (2006) *J Neuropathol Exp Neurol* **65**, 631-641

116. Santos, R. X., Correia, S. C., Zhu, X., Smith, M. A., Moreira, P. I., Castellani, R. J., Nunomura, A., and Perry, G. (2013) *Antioxidants & redox signaling* **18**, 2444-2457

117. Johri, A., and Beal, M. F. (2012) *The Journal of pharmacology and experimental therapeutics* **342**, 619-630

118. Song, W., Chen, J., Petrilli, A., Liot, G., Klinglmayr, E., Zhou, Y., Poquiz, P., Tjong, J., Pouladi, M. A., Hayden, M. R., Masliah, E., Ellisman, M., Rouiller, I., Schwarzenbacher, R., Bossy, B., Perkins, G., and Bossy-Wetzel, E. (2011) *Nature medicine* **17**, 377-382

119. Panov, A. V., Gutekunst, C. A., Leavitt, B. R., Hayden, M. R., Burke, J. R., Strittmatter, W. J., and Greenamyre, J. T. (2002) *Nature neuroscience* **5**, 731-736

120. Gellerich, F. N., Gizatullina, Z., Nguyen, H. P., Trumbeckaite, S., Vielhaber, S., Seppet, E., Zierz, S., Landwehrmeyer, B., Riess, O., von Horsten, S., and Striggow, F. (2008) *The Journal of biological chemistry* **283**, 30715-30724

121. Chang, D. T., Rintoul, G. L., Pandipati, S., and Reynolds, I. J. (2006) *Neurobiology of disease* **22**, 388-400

122. Matsuda, A., Suzuki, Y., Honda, G., Muramatsu, S., Matsuzaki, O., Nagano, Y., Doi, T., Shimotohno, K., Harada, T., Nishida, E., Hayashi, H., and Sugano, S. (2003) *Oncogene* **22**, 3307-3318

123. Li, W., Bengtson, M. H., Ulbrich, A., Matsuda, A., Reddy, V. A., Orth, A., Chanda, S. K., Batalov, S., and Joazeiro, C. A. (2008) *PloS one* **3**, e1487

124. Zhang, B., Huang, J., Li, H. L., Liu, T., Wang, Y. Y., Waterman, P., Mao, A. P., Xu, L. G., Zhai, Z., Liu, D., Marrack, P., and Shu, H. B. (2008) *Cell research* **18**, 900-910

125. Lokireddy, S., Wijesoma, I. W., Teng, S., Bonala, S., Gluckman, P. D., McFarlane, C., Sharma, M., and Kambadur, R. (2012) *Cell metabolism* **16**, 613-624

126. Jung, J. H., Bae, S., Lee, J. Y., Woo, S. R., Cha, H. J., Yoon, Y., Suh, K. S., Lee, S. J., Park, I. C., Jin, Y. W., Lee, K. H., An, S., and Lee, J. H. (2011) *Cell death and differentiation* **18**, 1865-1875

127. Bae, S., Kim, S. Y., Jung, J. H., Yoon, Y., Cha, H. J., Lee, H., Kim, K., Kim, J., An, I. S., Kim, J., Um, H. D., Park, I. C., Lee, S. J., Nam, S. Y., Jin, Y. W., Lee, J. H., and An, S. (2012) *Cell research* **22**, 873-885

128. Cilenti, L., Ambivero, C. T., Ward, N., Alnemri, E. S., Germain, D., and Zervos, A. S. (2014) *Biochimica et biophysica acta* **1843**, 1295-1307

129. Cheung, W. Y. (1982) *Scientific American* **246**, 62-70

130. Cheung, W. Y. (1980) *Science* **207**, 19-27

131. Babu, Y. S., Sack, J. S., Greenhough, T. J., Bugg, C. E., Means, A. R., and Cook, W. J. (1985) *Nature* **315**, 37-40

132. Kretsinger, R. H., and Nockolds, C. E. (1973) *The Journal of biological chemistry* **248**, 3313-3326

133. Szebenyi, D. M., Obendorf, S. K., and Moffat, K. (1981) *Nature* **294**, 327-332

134. Sundaralingam, M., Bergstrom, R., Strasburg, G., Rao, S. T., Roychowdhury, P., Greaser, M., and Wang, B. C. (1985) *Science* **227**, 945-948

135. Herzberg, O., and James, M. N. (1985) *Nature* **313**, 653-659

136. Friedberg, F. (1990) *Protein sequences & data analysis* **3**, 335-337

137. Crivici, A., and Ikura, M. (1995) *Annual review of biophysics and biomolecular structure* **24**, 85-116

138. Rhoads, A. R., and Friedberg, F. (1997) *FASEB journal : official publication of the Federation of American Societies for Experimental Biology* **11**, 331-340

139. Cheney, R. E., and Mooseker, M. S. (1992) *Current opinion in cell biology* **4**, 27-35

140. Bahler, M., and Rhoads, A. (2002) *FEBS letters* **513**, 107-113

141. Houdusse, A., Silver, M., and Cohen, C. (1996) *Structure* **4**, 1475-1490

142. Wolenski, J. S. (1995) *Trends in cell biology* **5**, 310-316

143. Ho, Y. D., Joyal, J. L., Li, Z., and Sacks, D. B. (1999) *The Journal of biological chemistry* **274**, 464-470

144. Joyal, J. L., Annan, R. S., Ho, Y. D., Huddleston, M. E., Carr, S. A., Hart, M. J., and Sacks, D. B. (1997) *The Journal of biological chemistry* **272**, 15419-15425

145. Jang, D. J., Guo, M., and Wang, D. (2007) *J Proteome Res* **6**, 3718-3728

146. Klee, C. B., and Vanaman, T. C. (1982) *Advances in protein chemistry* **35**, 213-321

147. Contreras, L., Drago, I., Zampese, E., and Pozzan, T. (2010) *Biochimica et biophysica acta* **1797**, 607-618

148. Santo-Domingo, J., and Demaurex, N. (2010) *Biochimica et biophysica acta* **1797**, 907-912

149. Voccoli, V., and Colombaioni, L. (2009) *Brain research* **1252**, 15-29

150. Deshaies, R. J., and Joazeiro, C. A. (2009) *Annual review of biochemistry* **78**, 399-434

151. Budhidarmo, R., Nakatani, Y., and Day, C. L. (2012) *Trends in biochemical sciences* **37**, 58-65

152. Hochstrasser, M. (2006) *Cell* **124**, 27-34

153. Wenzel, D. M., and Klevit, R. E. (2012) *BMC biology* **10**, 24

154. Wang, M., and Pickart, C. M. (2005) *The EMBO journal* **24**, 4324-4333

155. Kim, H. C., and Huibregtse, J. M. (2009) *Molecular and cellular biology* **29**, 3307-3318

156. Badura-Stronka, M., Jamsheer, A., Materna-Kiryluk, A., Sowinska, A., Kiryluk, K., Budny, B., and Latos-Bielenska, A. (2010) *Clinical genetics* **77**, 141-144

157. Basel-Vanagaite, L., Dallapiccola, B., Ramirez-Solis, R., Segref, A., Thiele, H., Edwards, A., Arends, M. J., Miro, X., White, J. K., Desir, J., Abramowicz, M., Dentici, M. L., Lepri, F., Hofmann, K., Har-Zahav, A., Ryder, E., Karp, N. A., Estabel, J., Gerdin, A. K., Podrini, C., Ingham, N. J., Altmuller, J., Nurnberg, G., Frommolt, P., Abdelhak, S., Pasmanik-Chor, M., Konen, O., Kelley, R. I., Shohat, M., Nurnberg, P., Flint, J., Steel, K. P., Hoppe, T., Kubisch, C., Adams, D. J., and Borck, G. (2012) *American journal of human genetics* **91**, 998-1010

158. Budny, B., Badura-Stronka, M., Materna-Kiryluk, A., Tzschach, A., Raynaud, M., Latos-Bielenska, A., and Ropers, H. H. (2010) *Clinical genetics* **77**, 541-551

159. Flex, E., Ciolfi, A., Caputo, V., Fodale, V., Leoni, C., Melis, D., Bedeschi, M. F., Mazzanti, L., Pizzuti, A., Tartaglia, M., and Zampino, G. (2013) *Journal of medical genetics*

160. Froyen, G., Corbett, M., Vandewalle, J., Jarvela, I., Lawrence, O., Meldrum, C., Bauters, M., Govaerts, K., Vandeleur, L., Van Esch, H., Chelly, J., Sanlaville, D., van Bokhoven, H., Ropers, H. H., Laumonnier, F., Ranieri, E., Schwartz, C. E., Abidi, F., Tarpey, P. S., Futreal, P. A., Whibley, A., Raymond, F. L., Stratton, M. R., Fryns, J. P., Scott, R., Peippo, M., Sipponen, M., Partington, M., Mowat, D., Field, M., Hackett, A., Marynen, P., Turner, G., and Gecz, J. (2008) *American journal of human genetics* **82**, 432-443

161. Hwang, C. S., Sukalo, M., Batygin, O., Addor, M. C., Brunner, H., Aytes, A. P., Mayerle, J., Song, H. K., Varshavsky, A., and Zenker, M. (2011) *PloS one* **6**, e24925

162. Isrie, M., Kalscheuer, V. M., Holvoet, M., Fieremans, N., Van Esch, H., and Devriendt, K. (2013) *European journal of medical genetics* **56**, 379-382

163. Kishino, T., Lalande, M., and Wagstaff, J. (1997) *Nature genetics* **15**, 70-73

164. Matsuura, T., Sutcliffe, J. S., Fang, P., Galjaard, R. J., Jiang, Y. H., Benton, C. S., Rommens, J. M., and Beaudet, A. L. (1997) *Nature genetics* **15**, 74-77

165. Zou, Y., Liu, Q., Chen, B., Zhang, X., Guo, C., Zhou, H., Li, J., Gao, G., Guo, Y., Yan, C., Wei, J., Shao, C., and Gong, Y. (2007) *American journal of human genetics* **80**, 561-566

166. Zenker, M., Mayerle, J., Lerch, M. M., Tagariello, A., Zerres, K., Durie, P. R., Beier, M., Hulskamp, G., Guzman, C., Rehder, H., Beemer, F. A., Hamel, B., Vanlieferinghen, P., Gershoni-Baruch, R., Vieira, M. W., Dumic, M., Auslender, R., Gil-da-Silva-Lopes, V. L., Steinlicht, S., Rauh, M., Shalev, S. A., Thiel, C., Ekici, A. B., Winterpacht, A., Kwon, Y. T., Varshavsky, A., and Reis, A. (2005) *Nature genetics* **37**, 1345-1350

167. Tarpey, P. S., Raymond, F. L., O'Meara, S., Edkins, S., Teague, J., Butler, A., Dicks, E., Stevens, C., Tofts, C., Avis, T., Barthorpe, S., Buck, G., Cole, J., Gray, K., Halliday, K.,

Harrison, R., Hills, K., Jenkinson, A., Jones, D., Menzies, A., Mironenko, T., Perry, J., Raine, K., Richardson, D., Shepherd, R., Small, A., Varian, J., West, S., Widaa, S., Mallya, U., Moon, J., Luo, Y., Holder, S., Smithson, S. F., Hurst, J. A., Clayton-Smith, J., Kerr, B., Boyle, J., Shaw, M., Vandeleur, L., Rodriguez, J., Slaugh, R., Easton, D. F., Wooster, R., Bobrow, M., Srivastava, A. K., Stevenson, R. E., Schwartz, C. E., Turner, G., Gecz, J., Futreal, P. A., Stratton, M. R., and Partington, M. (2007) *American journal of human genetics* **80**, 345-352

168. Jung, S. Y., Malovannaya, A., Wei, J., O'Malley, B. W., and Qin, J. (2005) *Molecular endocrinology* **19**, 2451-2465

169. Matentzoglu, K., and Scheffner, M. (2008) *Biochemical Society transactions* **36**, 797-801

170. Williams, C. A., Beaudet, A. L., Clayton-Smith, J., Knoll, J. H., Kyllerman, M., Laan, L. A., Magenis, R. E., Moncla, A., Schinzel, A. A., Summers, J. A., and Wagstaff, J. (2006) *American journal of medical genetics. Part A* **140**, 413-418

171. Margolis, S. S., Sell, G. L., Zbinden, M. A., and Bird, L. M. (2015) *Neurotherapeutics : the journal of the American Society for Experimental NeuroTherapeutics*

172. Tomaic, V., and Banks, L. (2015) *Cell death & disease* **6**, e1625

173. Garcia-Gonzalo, F. R., and Rosa, J. L. (2005) *Cellular and molecular life sciences : CMLS* **62**, 1826-1838

174. Wang, M., Cheng, D., Peng, J., and Pickart, C. M. (2006) *The EMBO journal* **25**, 1710-1719

175. Jiang, J. H., Liu, Y. F., Ke, A. W., Gu, F. M., Yu, Y., Dai, Z., Gao, Q., Shi, G. M., Liao, B. Y., Xie, Y. H., Fan, J., Huang, X. W., and Zhou, J. (2014) *Hepatology* **59**, 2216-2227

176. Pan, S. J., Zhan, S. K., Ji, W. Z., Pan, Y. X., Liu, W., Li, D. Y., Huang, P., Zhang, X. X., Cao, C. Y., Zhang, J., Bian, L. G., Sun, B., and Sun, Q. F. (2015) *Scientific reports* **5**, 11066

177. Karbowski, M., Neutzner, A., and Youle, R. J. (2007) *The Journal of cell biology* **178**, 71-84

178. Nagashima, S., Tokuyama, T., Yonashiro, R., Inatome, R., and Yanagi, S. (2014) *Journal of biochemistry* **155**, 273-279

179. Braschi, E., Zunino, R., and McBride, H. M. (2009) *EMBO reports* **10**, 748-754

180. Benard, G., Neutzner, A., Peng, G., Wang, C., Livak, F., Youle, R. J., and Karbowski, M. (2010) *The EMBO journal* **29**, 1458-1471

181. Tang, F., Wang, B., Li, N., Wu, Y., Jia, J., Suo, T., Chen, Q., Liu, Y. J., and Tang, J. (2011) *PloS one* **6**, e24367

182. Narendra, D., Tanaka, A., Suen, D. F., and Youle, R. J. (2008) *The Journal of cell biology* **183**, 795-803

183. Neutzner, A., and Youle, R. J. (2005) *The Journal of biological chemistry* **280**, 18598-18603

184. Cohen, M. M., Leboucher, G. P., Livnat-Levanon, N., Glickman, M. H., and Weissman, A. M. (2008) *Molecular biology of the cell* **19**, 2457-2464

185. Leboucher, G. P., Tsai, Y. C., Yang, M., Shaw, K. C., Zhou, M., Veenstra, T. D., Glickman, M. H., and Weissman, A. M. (2012) *Molecular cell* **47**, 547-557

186. Narendra, D., Walker, J. E., and Youle, R. (2012) *Cold Spring Harbor perspectives in biology* **4**

187. Sugiura, A., Yonashiro, R., Fukuda, T., Matsushita, N., Nagashima, S., Inatome, R., and Yanagi, S. (2011) *Mitochondrion* **11**, 139-146

188. Benischke, A. S., Hemion, C., Flammer, J., and Neutzner, A. (2014) *Mitochondrion* **17**, 182-186

189. Ruggiano, A., Foresti, O., and Carvalho, P. (2014) *The Journal of cell biology* **204**, 869-879

190. Neutzner, A., Youle, R. J., and Karbowski, M. (2007) *Novartis Foundation symposium* **287**, 4-14; discussion 14-20

191. Basel-Vanagaite, L., Yilmaz, R., Tang, S., Reuter, M. S., Rahner, N., Grange, D. K., Mortenson, M., Koty, P., Feenstra, H., Farwell Gonzalez, K. D., Sticht, H., Boddaert, N., Desir, J., Anyane-Yeboa, K., Zweier, C., Reis, A., Kubisch, C., Jewett, T., Zeng, W., and Borck, G. (2014) *Human genetics*

192. Pedurupillay, C. R., Baroy, T., Holmgren, A., Blomhoff, A., Vigeland, M. D., Sheng, Y., Frengen, E., Stromme, P., and Misceo, D. (2015) *American journal of medical genetics. Part A* **167**, 657-663

193. Chahrour, M. H., Yu, T. W., Lim, E. T., Ataman, B., Coulter, M. E., Hill, R. S., Stevens, C. R., Schubert, C. R., Collaboration, A. A. S., Greenberg, M. E., Gabriel, S. B., and Walsh, C. A. (2012) *PLoS genetics* **8**, e1002635

194. Venhoranta, H., Pausch, H., Flisikowski, K., Wurmser, C., Taponen, J., Rautala, H., Kind, A., Schnieke, A., Fries, R., Lohi, H., and Andersson, M. (2014) *BMC genomics* **15**, 890

195. Roux, K. J., Kim, D. I., Raida, M., and Burke, B. (2012) *The Journal of cell biology* **196**, 801-810

196. Goellner, E. M., Grimme, B., Brown, A. R., Lin, Y. C., Wang, X. H., Sugrue, K. F., Mitchell, L., Trivedi, R. N., Tang, J. B., and Sobol, R. W. (2011) *Cancer research* **71**, 2308-2317

197. Trivedi, R. N., Wang, X. H., Jelezcova, E., Goellner, E. M., Tang, J. B., and Sobol, R. W. (2008) *Mol Pharmacol* **74**, 505-516

198. Fouquerel, E., Goellner, E. M., Yu, Z., Gagne, J. P., Barbi de Moura, M., Feinstein, T., Wheeler, D., Redpath, P., Li, J., Romero, G., Migaud, M., Van Houten, B., Poirier, G. G., and Sobol, R. W. (2014) *Cell reports* **8**, 1819-1831

199. Fang, Q., Inanc, B., Schamus, S., Wang, X. H., Wei, L., Brown, A. R., Svilar, D., Sugrue, K. F., Goellner, E. M., Zeng, X., Yates, N. A., Lan, L., Vens, C., and Sobol, R. W. (2014) *Nature communications* **5**, 5513

200. Svilar, D., Dyavaiah, M., Brown, A. R., Tang, J. B., Li, J., McDonald, P. R., Shun, T. Y., Braganza, A., Wang, X. H., Maniar, S., St Croix, C. M., Lazo, J. S., Pollack, I. F., Begley, T. J., and Sobol, R. W. (2012) *Molecular cancer research : MCR* **10**, 1580-1596

201. Tang, J. B., Goellner, E. M., Wang, X. H., Trivedi, R. N., St Croix, C. M., Jelezcova, E., Svilar, D., Brown, A. R., and Sobol, R. W. (2010) *Molecular cancer research : MCR* **8**, 67-79

202. Miedel, M. T., Zeng, X., Yates, N. A., Silverman, G. A., and Luke, C. J. (2014) *Methods* **68**, 536-541

203. Eng, J. K., Jahan, T. A., and Hoopmann, M. R. (2013) *Proteomics* **13**, 22-24

204. Gong, T. W., Huang, L., Warner, S. J., and Lomax, M. I. (2003) *Genomics* **82**, 143-152

205. Kelley, L. A., Mezulis, S., Yates, C. M., Wass, M. N., and Sternberg, M. J. (2015) *Nature protocols* **10**, 845-858

206. Goujon, M., McWilliam, H., Li, W., Valentin, F., Squizzato, S., Paern, J., and Lopez, R. (2010) *Nucleic acids research* **38**, W695-699

207. Larkin, M. A., Blackshields, G., Brown, N. P., Chenna, R., McGettigan, P. A., McWilliam, H., Valentin, F., Wallace, I. M., Wilm, A., Lopez, R., Thompson, J. D., Gibson, T. J., and Higgins, D. G. (2007) *Bioinformatics* **23**, 2947-2948

208. Trudeau, K. M., Gottlieb, R. A., and Shirihai, O. S. (2014) *Methods in enzymology* **547**, 21-38

209. Laker, R. C., Xu, P., Ryall, K. A., Sujkowski, A., Kenwood, B. M., Chain, K. H., Zhang, M., Royal, M. A., Hoehn, K. L., Driscoll, M., Adler, P. N., Wessells, R. J., Saucerman, J. J., and Yan, Z. (2014) *The Journal of biological chemistry* **289**, 12005-12015

210. Hernandez, G., Thornton, C., Stotland, A., Lui, D., Sin, J., Ramil, J., Magee, N., Andres, A., Quarato, G., Carreira, R. S., Sayen, M. R., Wolkowicz, R., and Gottlieb, R. A. (2013) *Autophagy* **9**, 1852-1861

211. Ferree, A. W., Trudeau, K., Zik, E., Benador, I. Y., Twig, G., Gottlieb, R. A., and Shirihai, O. S. (2013) *Autophagy* **9**, 1887-1896

212. Verdecia, M. A., Joazeiro, C. A., Wells, N. J., Ferrer, J. L., Bowman, M. E., Hunter, T., and Noel, J. P. (2003) *Molecular cell* **11**, 249-259

213. Damo, S. M., Feldkamp, M. D., Chagot, B., and Chazin, W. J. (2013) *Methods in molecular biology* **963**, 173-186

214. Jang, D. J., Ban, B., and Lee, J. A. (2011) *Molecules and cells* **32**, 511-518

215. Feldkamp, M. D., Yu, L., and Shea, M. A. (2011) *Structure* **19**, 733-747

216. Kim, D. I., Birendra, K. C., Zhu, W., Motamedchaboki, K., Doye, V., and Roux, K. J. (2014) *Proceedings of the National Academy of Sciences of the United States of America* **111**, E2453-2461

217. Rotin, D., and Kumar, S. (2009) *Nature reviews. Molecular cell biology* **10**, 398-409

218. Ikeda, F., and Dikic, I. (2008) *EMBO reports* **9**, 536-542

219. Kazlauskaite, A., Kondapalli, C., Gourlay, R., Campbell, D. G., Ritorto, M. S., Hofmann, K., Alessi, D. R., Knebel, A., Trost, M., and Muqit, M. M. (2014) *The Biochemical journal* **460**, 127-139

220. Wauer, T., Swatek, K. N., Wagstaff, J. L., Gladkova, C., Pruneda, J. N., Michel, M. A., Gersch, M., Johnson, C. M., Freund, S. M., and Komander, D. (2015) *The EMBO journal* **34**, 307-325

221. Wen, J. L., Wen, X. F., Li, R. B., Jin, Y. C., Wang, X. L., Zhou, L., and Chen, H. X. (2015) *PloS one* **10**, e0115622

222. Li, Y., Zhang, L., Zhou, J., Luo, S., Huang, R., Zhao, C., and Diao, A. (2015) *Cell proliferation* **48**, 338-347

223. Theivanthiran, B., Kathania, M., Zeng, M., Anguiano, E., Basrur, V., Vandergriff, T., Pascual, V., Wei, W. Z., Massoumi, R., and Venuprasad, K. (2015) *Science signaling* **8**, ra22

224. Coyaud, E., Mis, M., Laurent, E. M., Dunham, W. H., Couzens, A. L., Robitaille, M., Gingras, A. C., Angers, S., and Raught, B. (2015) *Molecular & cellular proteomics : MCP* **14**, 1781-1795

225. Huang, H., Tan, B. Z., Shen, Y., Tao, J., Jiang, F., Sung, Y. Y., Ng, C. K., Raida, M., Kohr, G., Higuchi, M., Fatemi-Shariatpanahi, H., Harden, B., Yue, D. T., and Soong, T. W. (2012) *Neuron* **73**, 304-316

226. Fischer, C., Kugler, A., Hoth, S., and Dietrich, P. (2013) *Plant & cell physiology* **54**, 573-584

227. Findeisen, F., Rumpf, C. H., and Minor, D. L., Jr. (2013) *Journal of molecular biology* **425**, 3217-3234

228. Lu, Q., Li, J., Ye, F., and Zhang, M. (2015) *Nature structural & molecular biology* **22**, 81-88

229. Wang, J., Peng, Q., Lin, Q., Childress, C., Carey, D., and Yang, W. (2010) *The Journal of biological chemistry* **285**, 12279-12288

230. Zhao, Y., Araki, S., Wu, J., Teramoto, T., Chang, Y. F., Nakano, M., Abdelfattah, A. S., Fujiwara, M., Ishihara, T., Nagai, T., and Campbell, R. E. (2011) *Science* **333**, 1888-1891

231. Wenzel, D. M., Stoll, K. E., and Klevit, R. E. (2011) *The Biochemical journal* **433**, 31-42

232. van Wijk, S. J., and Timmers, H. T. (2010) *FASEB journal : official publication of the Federation of American Societies for Experimental Biology* **24**, 981-993

233. Fiesel, F. C., Moussaud-Lamodiere, E. L., Ando, M., and Springer, W. (2014) *Journal of cell science* **127**, 3488-3504

234. Pierson, E., Consortium, G. T., Koller, D., Battle, A., Mostafavi, S., Ardlie, K. G., Getz, G., Wright, F. A., Kellis, M., Volpi, S., and Dermitzakis, E. T. (2015) *PLoS computational biology* **11**, e1004220

235. Baran, Y., Subramaniam, M., Biton, A., Tukiainen, T., Tsang, E. K., Rivas, M. A., Pirinen, M., Gutierrez-Arcelus, M., Smith, K. S., Kukurba, K. R., Zhang, R., Eng, C., Torgerson, D. G., Urbanek, C., Consortium, G. T., Li, J. B., Rodriguez-Santana, J. R., Burchard, E. G., Seibold, M. A., MacArthur, D. G., Montgomery, S. B., Zaitlen, N. A., and Lappalainen, T. (2015) *Genome research* **25**, 927-936

236. Rivas, M. A., Pirinen, M., Conrad, D. F., Lek, M., Tsang, E. K., Karczewski, K. J., Maller, J. B., Kukurba, K. R., DeLuca, D. S., Fromer, M., Ferreira, P. G., Smith, K. S., Zhang, R., Zhao, F., Banks, E., Poplin, R., Ruderfer, D. M., Purcell, S. M., Tukiainen, T., Minikel, E. V., Stenson, P. D., Cooper, D. N., Huang, K. H., Sullivan, T. J., Nedzel, J., Consortium, G. T., Geuvadis, C., Bustamante, C. D., Li, J. B., Daly, M. J., Guigo, R., Donnelly, P., Ardlie, K., Sammeth, M., Dermitzakis, E. T., McCarthy, M. I., Montgomery, S. B., Lappalainen, T., and MacArthur, D. G. (2015) *Science* **348**, 666-669

237. Mele, M., Ferreira, P. G., Reverter, F., DeLuca, D. S., Monlong, J., Sammeth, M., Young, T. R., Goldmann, J. M., Pervouchine, D. D., Sullivan, T. J., Johnson, R., Segre, A. V., Djebali, S., Niarchou, A., Consortium, G. T., Wright, F. A., Lappalainen, T.,

Calvo, M., Getz, G., Dermitzakis, E. T., Ardlie, K. G., and Guigo, R. (2015) *Science* **348**, 660-665

238. Consortium, G. T. (2015) *Science* **348**, 648-660

239. Escobar-Henriques, M., Westermann, B., and Langer, T. (2006) *The Journal of cell biology* **173**, 645-650

240. Okatsu, K., Iemura, S., Koyano, F., Go, E., Kimura, M., Natsume, T., Tanaka, K., and Matsuda, N. (2012) *Biochemical and biophysical research communications* **428**, 197-202

241. Chen, Y., and Dorn, G. W., 2nd. (2013) *Science* **340**, 471-475

242. Ye, Y., Shibata, Y., Yun, C., Ron, D., and Rapoport, T. A. (2004) *Nature* **429**, 841-847

243. Tresse, E., Salomons, F. A., Vesa, J., Bott, L. C., Kimonis, V., Yao, T. P., Dantuma, N. P., and Taylor, J. P. (2010) *Autophagy* **6**, 217-227

244. Ju, J. S., Fuentealba, R. A., Miller, S. E., Jackson, E., Piwnica-Worms, D., Baloh, R. H., and Weihl, C. C. (2009) *The Journal of cell biology* **187**, 875-888

245. Meyer, H. H., Wang, Y., and Warren, G. (2002) *The EMBO journal* **21**, 5645-5652

246. Ramadan, K., Bruderer, R., Spiga, F. M., Popp, O., Baur, T., Gotta, M., and Meyer, H. H. (2007) *Nature* **450**, 1258-1262

247. Watts, G. D., Wymer, J., Kovach, M. J., Mehta, S. G., Mumm, S., Darvish, D., Pestronk, A., Whyte, M. P., and Kimonis, V. E. (2004) *Nature genetics* **36**, 377-381

248. Le Ber, I., Van Bortel, I., Nicolas, G., Bouya-Ahmed, K., Camuzat, A., Wallon, D., De Septenville, A., Latouche, M., Lattante, S., Kabashi, E., Jornea, L., Hannequin, D., Brice, A., and French research Network on, F. F.-A. (2014) *Neurobiology of aging* **35**, 934 e935-936

249. Majounie, E., Traynor, B. J., Chio, A., Restagno, G., Mandrioli, J., Benatar, M., Taylor, J. P., and Singleton, A. B. (2012) *Neurobiology of aging* **33**, 209 e201-202

250. Kakizuka, A. (2008) *Biochemical Society transactions* **36**, 105-108

251. Rouiller, I., DeLaBarre, B., May, A. P., Weis, W. I., Brunger, A. T., Milligan, R. A., and Wilson-Kubalek, E. M. (2002) *Nature structural biology* **9**, 950-957

252. Li, G., Huang, C., Zhao, G., and Lennarz, W. J. (2012) *Proceedings of the National Academy of Sciences of the United States of America* **109**, 3737-3741

253. Beskow, A., Grimberg, K. B., Bott, L. C., Salomons, F. A., Dantuma, N. P., and Young, P. (2009) *Journal of molecular biology* **394**, 732-746

254. Ye, Y. (2006) *Journal of structural biology* **156**, 29-40

255. Kloppsteck, P., Ewens, C. A., Forster, A., Zhang, X., and Freemont, P. S. (2012) *Biochimica et biophysica acta* **1823**, 125-129

256. Hanzelmann, P., Buchberger, A., and Schindelin, H. (2011) *Structure* **19**, 833-843

257. Yeung, H. O., Kloppsteck, P., Niwa, H., Isaacson, R. L., Matthews, S., Zhang, X., and Freemont, P. S. (2008) *Biochemical Society transactions* **36**, 62-67

258. Heo, J. M., Nielson, J. R., Dephoure, N., Gygi, S. P., and Rutter, J. (2013) *Molecular biology of the cell* **24**, 1263-1273

259. Tran, J. R., Tomsic, L. R., and Brodsky, J. L. (2011) *The Journal of biological chemistry* **286**, 5744-5755

260. Stapf, C., Cartwright, E., Bycroft, M., Hofmann, K., and Buchberger, A. (2011) *The Journal of biological chemistry* **286**, 38670-38678

261. Heo, J. M., Livnat-Levanon, N., Taylor, E. B., Jones, K. T., Dephoure, N., Ring, J., Xie, J., Brodsky, J. L., Madeo, F., Gygi, S. P., Ashrafi, K., Glickman, M. H., and Rutter, J. (2010) *Molecular cell* **40**, 465-480

262. van Tijn, P., Verhage, M. C., Hobo, B., van Leeuwen, F. W., and Fischer, D. F. (2010) *Journal of neuroscience research* **88**, 2325-2337

263. van Tijn, P., de Vrij, F. M., Schuurman, K. G., Dantuma, N. P., Fischer, D. F., van Leeuwen, F. W., and Hol, E. M. (2007) *Journal of cell science* **120**, 1615-1623

264. Lindsten, K., de Vrij, F. M., Verhoef, L. G., Fischer, D. F., van Leeuwen, F. W., Hol, E. M., Masucci, M. G., and Dantuma, N. P. (2002) *The Journal of cell biology* **157**, 417-427

265. Fischer, D. F., van Dijk, R., van Tijn, P., Hobo, B., Verhage, M. C., van der Schors, R. C., Li, K. W., van Minnen, J., Hol, E. M., and van Leeuwen, F. W. (2009) *Neurobiology of aging* **30**, 847-863

266. Tan, Z., Sun, X., Hou, F. S., Oh, H. W., Hilgenberg, L. G., Hol, E. M., van Leeuwen, F. W., Smith, M. A., O'Dowd, D. K., and Schreiber, S. S. (2007) *Cell death and differentiation* **14**, 1721-1732

267. De Vrij, F. M., Sluijs, J. A., Gregori, L., Fischer, D. F., Hermens, W. T., Goldgaber, D., Verhaagen, J., Van Leeuwen, F. W., and Hol, E. M. (2001) *FASEB journal : official publication of the Federation of American Societies for Experimental Biology* **15**, 2680-2688

268. Braun, R. J., Sommer, C., Leibiger, C., Gentier, R. J., Dumit, V. I., Paduch, K., Eisenberg, T., Habernig, L., Trausinger, G., Magnes, C., Pieber, T., Sinner, F., Dengjel, J., van Leeuwen, F. W., Kroemer, G., and Madeo, F. (2015) *Cell reports*

269. Chan, N. C., Salazar, A. M., Pham, A. H., Sweredoski, M. J., Kolawa, N. J., Graham, R. L., Hess, S., and Chan, D. C. (2011) *Human molecular genetics* **20**, 1726-1737

270. Taylor, E. B., and Rutter, J. (2011) *Biochemical Society transactions* **39**, 1509-1513

271. Kim, N. C., Tresse, E., Kolaitis, R. M., Molliex, A., Thomas, R. E., Alami, N. H., Wang, B., Joshi, A., Smith, R. B., Ritson, G. P., Winborn, B. J., Moore, J., Lee, J. Y., Yao, T. P., Pallanck, L., Kundu, M., and Taylor, J. P. (2013) *Neuron* **78**, 65-80

272. Sparkman, O. D. (2000) *Mass spectrometry desk reference*, Global View Publishing, Pittsburgh, PA

273. Heist, E. K., and Schulman, H. (1998) *Cell calcium* **23**, 103-114

274. Anderson, K. A., and Kane, C. D. (1998) *Biometals : an international journal on the role of metal ions in biology, biochemistry, and medicine* **11**, 331-343

275. Westphal, R. S., Anderson, K. A., Means, A. R., and Wadzinski, B. E. (1998) *Science* **280**, 1258-1261

276. Anderson, K. A., Noeldner, P. K., Reece, K., Wadzinski, B. E., and Means, A. R. (2004) *The Journal of biological chemistry* **279**, 31708-31716

277. Chowdhury, D., Keogh, M. C., Ishii, H., Peterson, C. L., Buratowski, S., and Lieberman, J. (2005) *Molecular cell* **20**, 801-809

278. Chatr-Aryamontri, A., Breitkreutz, B. J., Oughtred, R., Boucher, L., Heinicke, S., Chen, D., Stark, C., Breitkreutz, A., Kolas, N., O'Donnell, L., Reguly, T., Nixon, J., Ramage, L., Winter, A., Sellam, A., Chang, C., Hirschman, J., Theesfeld, C., Rust, J., Livstone, M. S., Dolinski, K., and Tyers, M. (2015) *Nucleic acids research* **43**, D470-478

279. Sang, L., Miller, J. J., Corbit, K. C., Giles, R. H., Brauer, M. J., Otto, E. A., Baye, L. M., Wen, X., Scales, S. J., Kwong, M., Huntzicker, E. G., Sfakianos, M. K., Sandoval, W., Bazan, J. F., Kulkarni, P., Garcia-Gonzalo, F. R., Seol, A. D., O'Toole, J. F., Held, S., Reutter, H. M., Lane, W. S., Rafiq, M. A., Noor, A., Ansar, M., Devi, A. R., Sheffield, V. C., Slusarski, D. C., Vincent, J. B., Doherty, D. A., Hildebrandt, F., Reiter, J. F., and Jackson, P. K. (2011) *Cell* **145**, 513-528

280. Hildebrandt, F., Attanasio, M., and Otto, E. (2009) *Journal of the American Society of Nephrology : JASN* **20**, 23-35

281. Parisi, M. A., Doherty, D., Chance, P. F., and Glass, I. A. (2007) *European journal of human genetics : EJHG* **15**, 511-521

282. Salonen, R., and Paavola, P. (1998) *Journal of medical genetics* **35**, 497-501

283. Garcia-Caballero, A., Gadotti, V. M., Stemkowski, P., Weiss, N., Souza, I. A., Hodgkinson, V., Bladen, C., Chen, L., Hamid, J., Pizzoccaro, A., Deage, M., Francois, A., Bourinet, E., and Zamponi, G. W. (2014) *Neuron* **83**, 1144-1158

284. Falkenberg, M., Larsson, N. G., and Gustafsson, C. M. (2007) *Annual review of biochemistry* **76**, 679-699

285. Takamatsu, C., Umeda, S., Ohsato, T., Ohno, T., Abe, Y., Fukuoh, A., Shinagawa, H., Hamasaki, N., and Kang, D. (2002) *EMBO reports* **3**, 451-456

286. Metodiev, M. D., Lesko, N., Park, C. B., Camara, Y., Shi, Y., Wibom, R., Hultenby, K., Gustafsson, C. M., and Larsson, N. G. (2009) *Cell metabolism* **9**, 386-397

287. Kukat, C., Wurm, C. A., Spahr, H., Falkenberg, M., Larsson, N. G., and Jakobs, S. (2011) *Proceedings of the National Academy of Sciences of the United States of America* **108**, 13534-13539

288. Ekstrand, M. I., Falkenberg, M., Rantanen, A., Park, C. B., Gaspari, M., Hultenby, K., Rustin, P., Gustafsson, C. M., and Larsson, N. G. (2004) *Human molecular genetics* **13**, 935-944

289. Garrido, N., Griparic, L., Jokitalo, E., Wartiovaara, J., van der Bliek, A. M., and Spelbrink, J. N. (2003) *Molecular biology of the cell* **14**, 1583-1596

290. Kaguni, L. S. (2004) *Annual review of biochemistry* **73**, 293-320

291. Murphy, M. P. (2009) *The Biochemical journal* **417**, 1-13

292. Turrens, J. F., Alexandre, A., and Lehninger, A. L. (1985) *Archives of biochemistry and biophysics* **237**, 408-414

293. Yushchenko, D. A., Zhang, M., Yan, Q., Waggoner, A. S., and Bruchez, M. P. (2012) *Chembiochem : a European journal of chemical biology* **13**, 1564-1568

294. Friedberg, E. W., GC; Siede, W; Schultz, RA. (2006) *DNA repair and mutagenesis*, ASM Press, Washington, DC

295. Keimling, M., Deniz, M., Varga, D., Stahl, A., Schrezenmeier, H., Kreienberg, R., Hoffmann, I., Konig, J., and Wiesmuller, L. (2012) *FASEB journal : official publication of the Federation of American Societies for Experimental Biology* **26**, 2094-2104

296. Tang, J. B., Svilar, D., Trivedi, R. N., Wang, X. H., Goellner, E. M., Moore, B., Hamilton, R. L., Banze, L. A., Brown, A. R., and Sobol, R. W. (2011) *Neuro-oncology* **13**, 471-486

297. Sobol, R. W. (2012) *PLoS genetics* **8**, e1003086

298. Paddison, P. J., and Hannon, G. J. (2002) *Cancer cell* **2**, 17-23

299. McManus, M. T., and Sharp, P. A. (2002) *Nature reviews. Genetics* **3**, 737-747

300. Dykxhoorn, D. M., Novina, C. D., and Sharp, P. A. (2003) *Nature reviews. Molecular cell biology* **4**, 457-467

301. Schurmann, N., Trabuco, L. G., Bender, C., Russell, R. B., and Grimm, D. (2013) *Nature structural & molecular biology* **20**, 818-826

302. Fire, A., Xu, S., Montgomery, M. K., Kostas, S. A., Driver, S. E., and Mello, C. C. (1998) *Nature* **391**, 806-811

303. Elbashir, S. M., Harborth, J., Lendeckel, W., Yalcin, A., Weber, K., and Tuschl, T. (2001) *Nature* **411**, 494-498

304. Caplen, N. J., Parrish, S., Imani, F., Fire, A., and Morgan, R. A. (2001) *Proceedings of the National Academy of Sciences of the United States of America* **98**, 9742-9747

305. Izquierdo, M. (2005) *Cancer gene therapy* **12**, 217-227

306. Ullu, E., Djikeng, A., Shi, H., and Tschudi, C. (2002) *Philosophical transactions of the Royal Society of London. Series B, Biological sciences* **357**, 65-70

307. Yu, J. Y., DeRuiter, S. L., and Turner, D. L. (2002) *Proceedings of the National Academy of Sciences of the United States of America* **99**, 6047-6052

308. Paddison, P. J., Caudy, A. A., and Hannon, G. J. (2002) *Proceedings of the National Academy of Sciences of the United States of America* **99**, 1443-1448

309. Brummelkamp, T. R., Bernards, R., and Agami, R. (2002) *Science* **296**, 550-553

310. Javanbakht, H., Halwani, R., Cen, S., Saadatmand, J., Musier-Forsyth, K., Gottlinger, H., and Kleiman, L. (2003) *The Journal of biological chemistry* **278**, 27644-27651

311. Rubinson, D. A., Dillon, C. P., Kwiatkowski, A. V., Sievers, C., Yang, L., Kopinja, J., Rooney, D. L., Zhang, M., Ihrig, M. M., McManus, M. T., Gertler, F. B., Scott, M. L., and Van Parijs, L. (2003) *Nature genetics* **33**, 401-406

312. Mutamba, J. T., Svilar, D., Prasongtanakij, S., Wang, X. H., Lin, Y. C., Dedon, P. C., Sobol, R. W., and Engelward, B. P. (2011) *DNA repair* **10**, 1282-1293

313. Heid, C. A., Stevens, J., Livak, K. J., and Williams, P. M. (1996) *Genome research* **6**, 986-994

314. Semizarov, D., Frost, L., Sarthy, A., Kroeger, P., Halbert, D. N., and Fesik, S. W. (2003) *Proceedings of the National Academy of Sciences of the United States of America* **100**, 6347-6352

315. Wang, S., Sim, T. B., Kim, Y. S., and Chang, Y. T. (2004) *Current opinion in chemical biology* **8**, 371-377

316. Sirbu, B. M., and Cortez, D. (2013) *Cold Spring Harbor perspectives in biology* **5**, a012724

317. Jackson, S. P., and Bartek, J. (2009) *Nature* **461**, 1071-1078

318. Harper, J. W., and Elledge, S. J. (2007) *Molecular cell* **28**, 739-745

319. Hassa, P. O., Haenni, S. S., Elser, M., and Hottiger, M. O. (2006) *Microbiology and molecular biology reviews : MMBR* **70**, 789-829

320. Rulten, S. L., Fisher, A. E., Robert, I., Zuma, M. C., Rouleau, M., Ju, L., Poirier, G., Reina-San-Martin, B., and Caldecott, K. W. (2011) *Molecular cell* **41**, 33-45

321. Hottiger, M. O., Hassa, P. O., Luscher, B., Schuler, H., and Koch-Nolte, F. (2010) *Trends in biochemical sciences* **35**, 208-219

322. Almeida, K. H., and Sobol, R. W. (2007) *DNA repair* **6**, 695-711

323. Wang, M., Wu, W., Wu, W., Rosidi, B., Zhang, L., Wang, H., and Iliakis, G. (2006) *Nucleic acids research* **34**, 6170-6182

324. Robert, I., Dantzer, F., and Reina-San-Martin, B. (2009) *The Journal of experimental medicine* **206**, 1047-1056

325. Pears, C. J., Couto, C. A., Wang, H. Y., Borer, C., Kiely, R., and Lakin, N. D. (2012) *Cell cycle* **11**, 48-56

326. Mitchell, J., Smith, G. C., and Curtin, N. J. (2009) *International journal of radiation oncology, biology, physics* **75**, 1520-1527

327. Mansour, W. Y., Rhein, T., and Dahm-Daphi, J. (2010) *Nucleic acids research* **38**, 6065-6077

328. Couto, C. A., Wang, H. Y., Green, J. C., Kiely, R., Siddaway, R., Borer, C., Pears, C. J., and Lakin, N. D. (2011) *The Journal of cell biology* **194**, 367-375

329. Audebert, M., Salles, B., Weinfeld, M., and Calsou, P. (2006) *Journal of molecular biology* **356**, 257-265

330. Audebert, M., Salles, B., and Calsou, P. (2004) *The Journal of biological chemistry* **279**, 55117-55126

331. Alberts, B. (2009) *Science* **325**, 1319

332. Berridge, M. V., and Tan, A. S. (1993) *Archives of biochemistry and biophysics* **303**, 474-482

333. Kooistra, S. M., and Helin, K. (2012) *Nature reviews. Molecular cell biology* **13**, 297-311

334. Jones, L. J., Gray, M., Yue, S. T., Haugland, R. P., and Singer, V. L. (2001) *Journal of immunological methods* **254**, 85-98

335. Chi, P., Allis, C. D., and Wang, G. G. (2010) *Nature reviews. Cancer* **10**, 457-469

336. Goellner, E. M., Svilar, D., Almeida, K. H., and Sobol, R. W. (2012) *Current molecular pharmacology* **5**, 68-87

337. Shamma, A., Takegami, Y., Miki, T., Kitajima, S., Noda, M., Obara, T., Okamoto, T., and Takahashi, C. (2009) *Cancer cell* **15**, 255-269

338. Towbin, H., Staehelin, T., and Gordon, J. (1992) *Biotechnology* **24**, 145-149

339. McCabe, N., Turner, N. C., Lord, C. J., Kluzek, K., Bialkowska, A., Swift, S., Giavara, S., O'Connor, M. J., Tutt, A. N., Zdzienicka, M. Z., Smith, G. C., and Ashworth, A. (2006) *Cancer research* **66**, 8109-8115

340. Ame, J. C., Fouquerel, E., Gauthier, L. R., Biard, D., Boussin, F. D., Dantzer, F., de Murcia, G., and Schreiber, V. (2009) *Journal of cell science* **122**, 1990-2002

341. Jelezcova, E., Trivedi, R. N., Wang, X. H., Tang, J. B., Brown, A. R., Goellner, E. M., Schamus, S., Fornsaglio, J. L., and Sobol, R. W. (2010) *Mutation research* **686**, 57-67